

Physics and Ecology in the Marginal Ice Zone of the Fram Strait – a Robotic Approach

Dissertation

**Zur Erlangung des
Doktorgrades der Naturwissenschaften (Dr. rer. nat.)**

**Im Fachbereich der Geowissenschaften
der Universität Bremen**

vorgelegt von

Thorben Wulff

Gutachter:
1. Prof. Dr. Antje Boetius
2. Prof. Dr. Oliver Zielinski

Datum der Einreichung: 13.10.2015
Datum der Verteidigung: 21.12.2015

Per aspera ad astra

Durch Mühsal zu den Sternen

Für meine Eltern

Preface

This PhD thesis was written at the Department of Geosciences of the University of Bremen, Germany, and at the HGF-MPG Joint Research Group for Deep Sea Ecology and Technology of the Alfred Wegener Institute Helmholtz Centre for Polar and Marine Research (AWI) in Bremerhaven, Germany. Over the course of the thesis, funding was provided by the projects EUROFLEETS (contract number 228344) and ROBEX (contract number HA-304). The work has been carried out from December 2010 to June 2015. Data analyzed in this thesis were collected with AWI's Autonomous Underwater Vehicle (AUV) "PAUL" in the marginal ice zone of the Fram Strait – between Greenland and the Svalbard archipelago. The thesis includes data from the cruises ARK 25/2, ARK 26/2, and ARK 27/2 (R/V *Polarstern*), and the cruise MSM 29 (R/V *Maria S. Merian*).

The introduction focuses on general physical and ecological conditions in Marginal Ice Zones (MIZ). Physics of the MIZ include the complex interaction between ice and atmosphere, the interaction of the ice with ocean waves, heat and radiation budget as well as the exchange of CO₂.

Described ecologic features comprise the definition of different habitats in the MIZ and under the ice, biological productivity in the MIZ, and an overview on prominent species. Both the physical and the ecological section focus on the Arctic and a short overview on future trends with regard to the climate change is given.

This is followed by a detailed description of the Fram Strait, including a general description of its location and bathymetric features. The great importance of the Fram Strait is explained by its hydrography and cryosphere which strongly affect the entire Arctic.

The Fram Strait section closes with a detailed description of its ecology – with a special focus on the lower trophic levels.

The final subsection of the introduction illustrates basic technological characteristics of AUVs and of *PAUL* in particular. It also comprises a short overview on AUV deployments in the Arctic.

Subsequently, two short sections illustrate the objectives of this thesis and an outline of the included papers is given.

The main part consists of six research papers. The first four of these papers have a technical focus and describe design and development work necessary to deploy *PAUL* in the MIZ. All of these papers were published between 2010 and 2015 by ISI or peer-reviewed international journals. Of the two other manuscripts, one has a methodical / scientific background and one has a purely scientific background describing the first direct observations of front-related vertical water transports along an Arctic meltwater front. Both manuscripts have been submitted to international, peer-reviewed journals.

At the end of the thesis, a concluding section describes progresses and achievements with regard to the respective objective.

The thesis closes with a final section providing an outlook on open scientific questions and necessary technical developments. Here, AWI's future examination concept for the MIZ using various instruments and measuring platforms is introduced.

Table of Contents

Preface	IV
Abbreviations	VII
Definitions	VIII
Abstract	IX
Kurzfassung	XI
1 Introduction	1
1.1 Physics of the Marginal Ice Zone	1
1.2 Ecology of the Marginal Ice Zone	7
1.3 Study Area – Fram Strait	12
1.4 Autonomous Underwater Vehicles	21
2 Objectives	28
3 Publication Outline	29
4 First study (Manuscript I)	32
Development and Operation of an AUV-based Water Sample Collector	
5 Second Study (Manuscript II)	38
Biogeochemical Research with an Autonomous Underwater Vehicle: Payload Structure and Arctic Operations	
6 Third Study (Manuscript III)	59
Flying Drone for AUV Under-Ice Missions	
7 Fourth Study (Manuscript IV)	65
Correcting Navigation Data of Shallow Diving AUV in Arctic	
8 Fifth Study (Manuscript V)	74
Collecting Water Samples in the Arctic Marginal Ice Zone with AUV “PAUL”: Sample Safety, Sample Purity and Exemplary Results of Field Measurements	
9 Sixth Study (Manuscript VI)	100
Physical and Ecological Processes at a Moving Ice Edge in the Fram Strait as Observed with an AUV	

10	Conclusion.....	130
11	Outlook.....	137
	Final statement	144
	Acknowledgements.....	145
	References	146
	Appendix	157
	Versicherung an Eides statt.....	160

Abbreviations

ABS	Acrylonitrile Butadiene Styrene
ADCP	Acoustic Doppler Current Profiler
AUV	Autonomous Underwater Vehicle
AWI	Alfred Wegener Institute
CDOM	Colored Dissolved Organic Matter
CTD	Conductivity-Temperature-Depth Probe
DIC	Dissolved Inorganic Carbon
DOC	Dissolved Organic Carbon
DVL	Doppler Velocity Log
EGC	East Greenland Current
GPS	Global Positioning System
IDN	Inorganic Dissolved Nutrient
INS	Inertia Navigation System
LBL	Long Baseline System
MIZ	Marginal Ice Zone
NDE	Northeast Drift Event
PAR	Photosynthetically Active Radiation
PAUL	Polar Autonomous Underwater Vehicle
PCC	Payload Control Computer
PE	Polyethylene
POC	Particulate Organic Carbon
PTFE	Polytetrafluorethylene
PV	Potential Vorticity
PVDF	Polyvinylidene Fluoride
RAC	Return Atlantic Current
ROV	Remotely Operated Vehicle
SI	Symmetric Instability
SST	Sea Surface Temperature
SVS	Sound Velocity System
TA	Total Alkalinity
UAV	Unmanned Aerial Vehicle
USBL	Ultrashort Baseline System
WSC	West Spitzbergen Current

Definitions

Bottom / Water lock mode	Operational modes of an AUV depending on the vertical distance between vehicle and sea floor. When cruising close to the sea floor (max. distance approx. 100 m) the sea floor is acoustically tracked and provides a fixed reference so the vehicle can determine its true speed and travelled distance (Bottom lock mode). In contrast to this, the Water lock mode is established when the distance exceeds 100 m. Here the tracking signal is reflected by particles floating in the water column rather than the sea floor – resulting in reduced navigation accuracy as the vehicle is unable to determine its true speed.
Ekman layer	Term is used to define the depth of the water layers still affected by the wind. Thickness of this layer depends on wind conditions, sea surface roughness and the latitude.
Float maneuver	AUV maneuver with the vehicle shutting off its thruster and starts ascending due to its residual buoyancy. Maneuver is applied to collect high resolution data of the stratification of the water column.
Front	Surface boundary line between different water masses featuring abrupt changes in physical or chemical parameters.
Frontogenesis	Process creating or intensifying an ocean front.
GAPS:	Acoustic underwater tracking system by the French manufacturer iXBlue (Marly le Roi, France). System is able to track objects in up to 4,000 m distance.
HAUSGARTEN	Long term deep sea observatory located in the Fram Strait established in 1999. The observatory consists of 21 stations between 78.5 to 80 °N and 5 °W to 12 °E. Stations are annually visited by research vessels.
Marginal ice zone (MIZ):	Transition zone between solid ice and the open ocean. Portion of the ice that is still influenced by open ocean processes.
Tube	Term is used for the sample containers of <i>PAUL</i> 's water sample collector.

Abstract

The Polar marginal ice zones are characterized by the complex interaction of ocean, ice, and atmosphere. The associated physical processes take place on different spatial and temporal scales that shape the ecosystem at and underneath the ice. However, the influence of small scale physical processes on biological production is still poorly understood.

To investigate the ecologic relations at a marginal ice zone, an autonomous underwater vehicle was deployed. The vehicle was specifically equipped with instruments collecting physical, chemical, and biological data. Dives were conducted between 0 and 50 m water depth, thus covering the entire euphotic zone. Measurements of the vehicle were complemented by means of ship, satellite, and model based data. The vehicle was deployed between Greenland and the Svalbard archipelago; close to the Molloy Deep in the marginal ice zone of the Fram Strait.

The results of a dive at a meltwater front that was located several kilometers from the ice edge, indicated wind-driven, vertical transport processes in the water column. These processes featured meso- and submesoscale dimensions. The water column was divided into four different zones characterized by different biogeochemical parameters. The spatial distribution of these parameters (concentration of nitrate and chlorophyll *a*, oxygen saturation) was patchy; however a specific qualitative ratio was always maintained between the parameters. High chlorophyll *a* concentrations were associated with high oxygen saturation and low nitrate values (and vice versa).

The mesoscale transport process was caused by the wind-driven movement of an ice tongue 70 km in length.

The drift of the tongue entailed elevated nitrate levels at the surface (with respect to a similar dive from the previous year). However, no indications for an ecologic response such as increased production rates could be detected thus suggesting that upwelling has occurred shortly before the dive. Enhanced chlorophyll *a* concentrations in a 2 – 3 km wide “belt” along the front were caused by accumulation processes rather than by primary production.

Submesoscale transport processes were caused by wind interacting with the meltwater front and subsequently intensifying the front (frontogenesis). Frontogenetic processes led to water column instabilities and stimulated the formation of an ageostrophic secondary circulation (ASC). The ASC could be identified by upward and downward bulged isopycnals respectively. Additionally, submerging surface water masses could be identified by their chemical and biological signatures. The depth over which the ASC-related circulation penetrated was within the euphotic zone. Thus, the possible ecologic relevance of frontogenetic processes remained unclear.

In order to conduct these studies, biogeochemical instruments and supporting systems were integrated into the vehicle. In total, the vehicle is able to measure nine independent parameters (conductivity, temperature, pressure, concentration of nitrate, oxygen and CO₂, fluorescence of chlorophyll *a* and colored dissolved organic matter, and photosynthetically active radiation) and to collect up to 22 water samples. To record the data and to centrally provide the payload with electric power, a payload control computer was integrated into the vehicle. For data processing and correcting the vehicle's navigation data, newly developed

algorithms were applied. Thus, biogeochemical measurements were georeferenced as precise as possible.

Methodically, the float maneuver, with the vehicle repeatedly deactivating its thruster and slowly drifting towards the surface, was developed to investigate the stratification of the upper water column. Methods to handle the vehicle's small-volume water samples were also

investigated and suitable procedures were defined.

The first studies of this thesis describe the technical foundation of AUV operations focusing on ecological research in MIZs. Following this, the scientific results are presented. Reviewing the achievements of this thesis, open scientific questions and possible technological upgrades are presented in the Outlook section.

Kurzfassung

Die polaren Eisrandgebiete zeichnen sich durch ein komplexes Zusammenspiel zwischen Eis, Ozean und Atmosphäre aus. Die damit verbundenen physikalischen Prozesse, die sich auf unterschiedlichen räumlichen und zeitlichen Skalen abspielen, prägen das Ökosystem an und unter dem Eis. Insbesondere der Einfluss kleinskaliger physikalischer Prozesse auf die biologische Produktion ist bisher jedoch nur unzureichend verstanden.

Zur Untersuchung der ökologischen Zusammenhänge im Eisrandbereich kam ein autonomes Unterwasserfahrzeug zum Einsatz, das speziell für diesen Zweck mit physikalischen, chemischen und biologischen Instrumenten ausgestattet war. Die Tauchgänge wurden in Tiefen zwischen 0 und 50 m durchgeführt und deckten somit die euphotische Zone ab. Die Messungen des Fahrzeugs wurden durch Schiffs-, Satelliten- und Modelldaten ergänzt und in einen größeren Kontext gesetzt. Die Einsätze erfolgten zwischen Grönland und Spitzbergen; in der Eisrandzone der Framstraße, nahe des Molloy Deeps.

Tauchgänge an einer dem Eis vorgelagerten Schmelzwasserfront lieferten deutliche Hinweise auf sich überlagernde, windgetriebene, vertikale Transportprozesse die sich im meso- und submesoskaligen Bereich abspielten. Innerhalb der Wassersäule konnten vier Zonen identifiziert werden, die sich insbesondere anhand ihrer biogeochemischen Charakteristika voneinander unterschieden. Nitrat, Chlorophyll *a* und Sauerstoff waren ungleichmäßig in der Wassersäule verteilt, behielten jedoch ein typisches, qualitatives Verhältnis untereinander stets bei: Hohe Chlorophyll *a* Konzentrationen gingen einher mit hohen Sauerstoffsättigungs- und niedrigen Nitratwerten (und umgekehrt).

Der mesoskalige Transportprozess konnte auf die windgetriebene Drift einer ca. 70 km langen Eiszunge zurückgeführt werden. Die Drift hatte einen, im Vergleich zu einem ähnlichen Tauchgang der im Jahr zuvor durchgeführt wurde, erhöhten Nitratgehalt des Oberflächenwassers zur Folge. Eine unmittelbare biologische Reaktion in Form erhöhter Produktivität konnte zum Zeitpunkt des Tauchgangs jedoch nicht festgestellt werden, was eine grobe zeitliche Einordnung des Prozesses erlaubte. Eine im Tauchgebiet registrierte Ansammlung von Chlorophyll *a* in Form eines 2 – 3 km breiten „Gürtels“ entlang der Schmelzwasserfront war eher Folge vorangegangener Akkumulationsprozesse denn biologischer Produktion.

Im submesoskaligen Bereich führte die Einwirkung des Windes auf die Schmelzwasserfront zu Frontogeneseprozessen die in dieser Form erstmals an einer Schmelzwasserfront nachgewiesen werden konnten. Die Auswirkung der Frontogenese, der damit verbundenen Instabilität der Wassersäule und die Ausbildung einer ageostrophischen Zirkulation waren physikalisch durch Anhebung, bzw. Absenkung der Isopyknen zu erkennen. Absinkende oder aufsteigende Wassermassen konnten zudem an ihrer chemischen und biologischen Signatur erkannt werden.

Der Einfluss der Zirkulation blieb auf Tiefen innerhalb der euphotischen Zone beschränkt, so dass deren ökologische Relevanz zum derzeitigen Stand noch nicht abschließend geklärt ist.

Zur Durchführung der genannten Studien war der Aufbau einer biogeochemischen Nutzlast nötig. Insgesamt ist das Fahrzeug in der Lage neun unabhängige Parameter zu bestimmen

(Leitfähigkeit, Temperatur, Druck, Nitratgehalt, CO₂- und Sauerstoffkonzentration, Gelbstoff- und Chlorophyll *a*-Fluoreszenz, photosynthetisch aktive Strahlung) und bis zu 22 Wasserproben zu entnehmen. Um eine zentrale Datenaufnahme und Stromversorgung der Nutzlast zu erreichen wurde ein Nutzlastcomputer entwickelt und in das Fahrzeug integriert. Zur Prozessierung der Messdaten kommen neu entwickelte Korrekturalgorithmen zum Einsatz. Neben den Messdaten werden auch die Navigationsdaten des Fahrzeugs korrigiert um eine bestmögliche Georeferenzierung der Messwerte zu erreichen. Zur Erforschung der Wasserschichtung wurde das Float-Manöver entwickelt, bei dem das Fahrzeug wiederholt antriebslos zur Oberfläche

treibt und dabei hochaufgelöste Profile der Wassersäule aufnimmt. Des Weiteren wurden Methoden zur Prozessierung der kleinvolumigen Wasserproben des Fahrzeugs entwickelt.

In mehreren Studien werden zunächst die technischen Grundlagen erläutert, die den Einsatz des Fahrzeugs im Rahmen ökologischer Forschung im arktischen Eisrandbereich ermöglichten. Darauf aufbauend werden wissenschaftliche Ergebnisse und deren Interpretation dargelegt. In einem abschließenden Ausblick werden offene wissenschaftliche Fragen und mögliche technologische Erweiterungen des Fahrzeugs erläutert.

1 Introduction

1.1 Physics of the Marginal Ice Zone

Looking at Earth from space, the ice caps of the Polar Regions are one of the most distinctive features of our planet. In the north, the Arctic Ocean is covered by floating ice. In the south, continent Antarctica lies below an ice cover of several kilometers thickness. Although they look rather similar, these regions feature two completely different types of ice. The Antarctic ice shield is more similar to a glacier, with the ice being formed by compressed snow. The ice slowly flows towards the open ocean and eventually starts to float as soon as it reaches the ocean water. This type of ice is called shelf ice. In contrast, the ice of the Arctic Ocean consists of comparably thin ice floes created by freezing sea water. This thesis will focus on processes along Arctic sea ice covers and thus shelf ice will be disregarded.

About 3 – 6 % of the total surface area of the earth is covered with a seasonally changing ice cover (Comiso, 2003). Fig. 1-1 shows the ice cover of the northern hemisphere at its maximum and minimum extent. In the course of the climate change, especially the Arctic faces profound changes. The Arctic ice sheet in general tends to be smaller, thinner, and younger. From 1979 to 2010 the ice extent dropped from $7.2 \cdot 10^6$ km² to $4.9 \cdot 10^6$ km² (Stroeve et al., 2012). A record minimum of $3.4 \cdot 10^6$ km² was reached in 2012. Its peak winter thickness fell from 3.64 m in 1980 to 1.89 m in 2008 (Kwok & Rothrock, 2009b), with the greatest thickness losses in the eastern and central Arctic (Rothrock et al. 2003). In 1987, 57 % of the ice in the central Arctic was older than 5 years, whereas in 2007, this value dropped to 7 % (Maslanik et al. 2007).

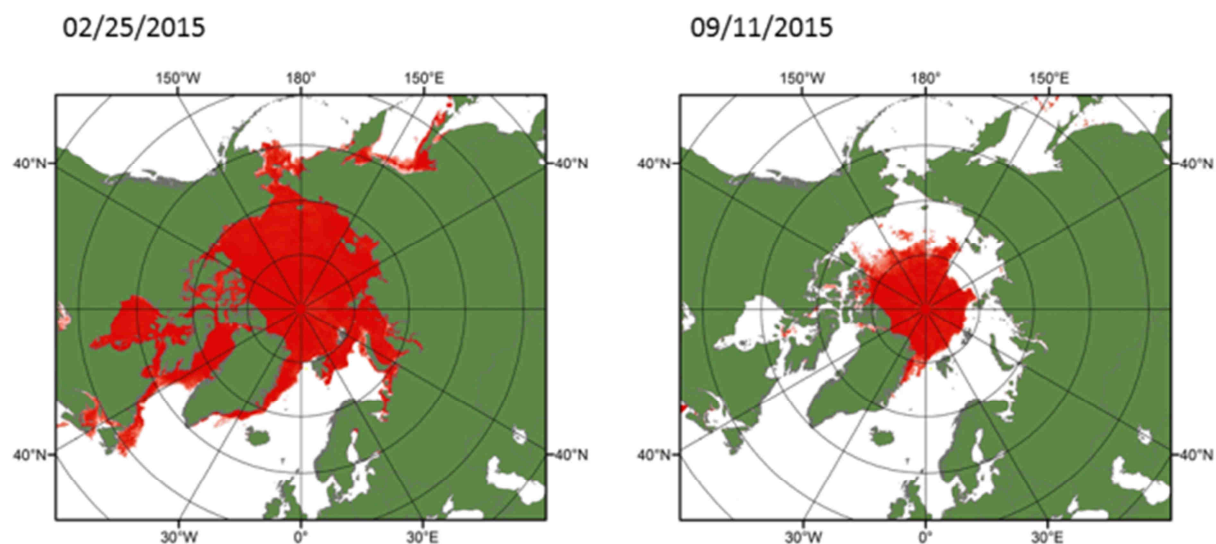


Fig. 1-1. Figures illustrating the annual change in Arctic sea ice (red) coverage. The edge of the ice is assumed to be the 10 % boundary line of the ice concentration. Left panel: Ice maximum of 2015 on February 25th. Right panel: Ice minimum of 2015 on September 11th.

This trend is superimposed by seasonal variations and regional characteristics. In the Bering Sea the ice edge retreats by over 1,000 km in summer to advance again during winter (Niebauer, 1988). The Chukchi Sea is ice covered in winter and becomes completely ice free in summer. Compared to these distances, the Fram Strait features a rather stationary ice edge (Smith et al., 1985). However, the ice edge's location has drastically changed over the past 15 – 20 years and western Fram Strait has become almost ice free during the last Arctic sea ice minima.

Rather than “ice edge”, the transition zone between ice and ocean is called Marginal Ice Zone (MIZ). This zone can feature different characteristics which make it difficult to find a uniform definition. The width of the MIZ can reach from just meters and an abrupt change between ice and water, to several hundred kilometers with the ice slowly fading towards the open ocean (Fig. 1-2).



Fig. 1-2. MIZ consisting of numerous ice floes creating a “gradual” transition between the ice and the ocean.

According to Dumont et al. (2011) the MIZ is the area of the ice edge that is still influenced by open ocean processes. Squire & Moore (1980) further divided the MIZ into three smaller subzones: 1) the edge zone, 2) the transition zone, 3) the interior zone.

The MIZ normally consists of ice floes with different sizes and shapes. Ice vortices illustrate the low cohesion and low shear viscosity which give rise to the high dynamic of a MIZ (Dumont et al., 2011). In contrast to the pack ice, which is normally considered to be a rather uniform material, the MIZ is highly heterogeneous and, for example due to stress communicated by floe-floe contact (Williams et al., 2011), difficult to model.

The properties of a MIZ depend on various factors and their appearances significantly vary with their location in the world ocean. In this section, physical processes and conditions generally applicable to all marginal sea ice zones are described (the MIZ of the Fram Strait, which was of special importance for this thesis is described in detail in section 1.3).

It is common to all MIZs that these zones represent regions where the influence of ocean, ice and atmosphere are in a permanent non-equilibrium (Niebauer, 1989). The most important water column-influencing processes emerging from this imbalance are (Barber et al., 2015): 1) Momentum exchange between atmosphere and ocean governed by the ice's surface roughness (Birbaum & Lüpkes, 2002, 2005), 2) interaction between ocean waves and ice including ice floe breaking and internal waves (Muench et al., 1983; Wadhams et al., 1988; Kohout & Meylan, 2008), 3) heat exchange (Perovich et al., 1989; Inoue et al., 2011), and 4) salt flux (McPhee et al., 2008). Further relevant processes are the ice's radiation budget (Nicolaus et al., 2012), the gas exchange with a special reference on CO₂ (Semiletov et al., 2007), and the ice-associated meltwater front as frontal systems are often baroclinically unstable and thus can stimulate mixing and transport processes (Lu et al., 2015).

1.1.1 Momentum exchange

In the presence of ice, the exchange of momentum between atmosphere and ocean is largely governed by the topography of the ice. Especially in a MIZ which usually features a highly inhomogeneous surface topography (alternating areas of ice and water), the surface drag can be high (Guest et al., 1995) and various processes such as upwelling can be stimulated in the water column. (Slagstad & McClimans, 2005). “Keel stirring”, caused by the drift of thick ice floes, was found to be an effective mixing mechanism also under heavy pack ice (Lemke & Manley, 1984). In general, older or multiyear ice (MYI) normally features higher drag coefficients than young and flat first year ice (FYI) (Fig. 1-3, Guest & Davidson, 1987). Additionally, the ice floes need to be (at least partly) moveable to effectively communicate wind stress to the water column. These conditions are more likely to be met in the MIZ than in the internal pack ice. For example Schulze & Pickart (2012) were able to measure the velocity of a jet at the shelf break of the Alaskan Beaufort Sea. The flow turned out to be strongest in the “partial ice season” – most likely

intensified by drifting ice floes.

Since the 1980s there have been several attempts to numerically simulate the MIZ’s and the water column’s response to atmospheric forcing (e.g. Niebauer, 1982; Fennel & Johannessen, 1998). Parameterization of the surface drag is crucial for modelling the MIZ, yet is still challenging (Lüpkes & Birnbaum, 2005; Gupta et al., 2014). Although results are dependent on numerous parameters and thus are extensive, the following rules that are related to momentum exchange, can be applied to all MIZs: 1) down-ice wind conditions (along the ice edge with the ice on the right, Fig. 1-4) are upwelling favorable, 2) a wind driven upwelling signature propagates when the ice moves, 3) the MIZ is compacted in down-ice wind conditions, 4) the MIZ diverges in off-ice or calm wind conditions.

1.1.2 Interaction with ocean waves

In the MIZ, the interaction between ocean waves and the ice is characterized by two main processes: 1) wave attenuation and 2) ice floe break-up due to dynamic stress (Williams et al., 2013).



Fig. 1-3. (Left) Exemplary image of a flat ice surface featuring small drag coefficients. (Right) Ice floe with a rough surface. These ice floes can communicate wind stress effectively and can emphasize mixing processes (“keel stirring”).

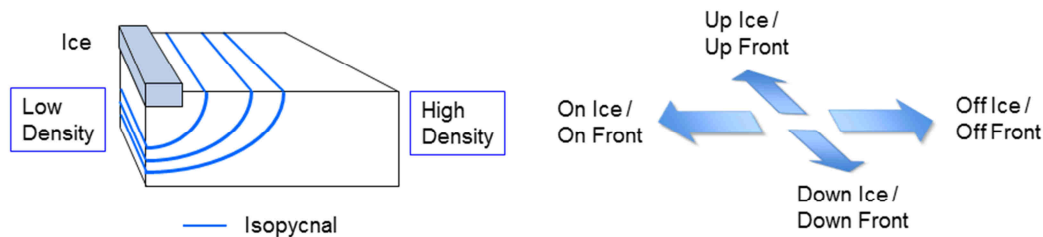


Fig. 1-4. (Left) Schematic illustration of physical properties at the ice edge: Melting ice creates a low density layer on the surface. Off the ice edge the isopycnals rise towards the surface, illustrating the horizontal density gradient at the meltwater front. (Right) Convention for naming wind directions relative to the ice edge / meltwater front on the northern hemisphere.

Break-up of the ice can directly affect the thermodynamic equilibrium of a MIZ as it can increase melting rates in summer (Steele, 1992) and can support the formation of new ice by opening up leads or rafting small floes in winter (Lange et al., 1989). If wave-induced stress is sufficient to break the ice cover, the average floe size is equal to half the dominant wave length (Williams et al., 2013).

The influence of ocean waves is not necessarily limited to the MIZ. Long-period waves (swell) can reach several hundred kilometers into the ice and can still cause ice fragmentation (Prinsenberg & Peterson, 2011). In contrast, short-period waves penetrate shorter distances into the ice and entail higher fragmentation rates (Squire & Moore, 1980). Thus, apart from the thickness of the ice and its mechanical properties, the peak period of the wave spectrum is one of the key factors determining the width of a MIZ (Williams et al., 2013).

1.1.3 Heat exchange and salt flux

Both heat and salt are two key components in a MIZ's thermodynamic system and thus they are described together. The oceanic heat flux can feature large regional differences.

For the Arctic basin it was shown that an oceanic heat flux (from the ocean to the ice) of about 2.6 W m^{-2} marks a critical threshold to keep the Arctic ice sheet in a stable equilibrium (Maykut & Untersteiner, 1971). In contrast to this value, an oceanic heat flux of 1600 W m^{-2} was reported by Perovich et al. (1989) in the MIZ of the Greenland Sea.

In terms of heat, ice reduces the energy exchange between the ocean and the atmosphere as it for example prevents wind driven convection over the ocean. However, in a MIZ the ice cover is usually not entirely closed but there are interstices between the floes. With regard to this partial coverage, heat can be exchanged between ocean and atmosphere directly and via heat transfer through the ice. In this respect, it is of high importance that ice is by no means uniform, but is considered to be a “mushy” layer (Feltham et al., 2006) – making it difficult to determine heat transfer rates. Additionally, the heat transfer between ice and atmosphere features both a conductive and a convective component. As stated by Lytle & Ackley, (1996), convection can occur when ice floes are covered by snow which forms a slush layer. The slush layer at the ice-snow interface can be formed by melting processes or, especially in the MIZ, by waves washing over the floes.

In this case, convection occurs when the slush layer freezes again and it might outperform conduction as primary heat transfer mechanism through the ice (Lytle & Ackley, 1996).

Apart from heat transfer through the ice, heat can also be transferred through open water areas between the floes. The interstices between the floes are comparable to leads (Smith & Morison, 1993). In winter the ocean loses large amount of both sensible and latent heat to the atmosphere through leads. Low atmospheric temperatures cool down the exposed water below its freezing point and thus new ice is formed. As the water freezes, salt is rejected from the ice matrix and a cold, high saline brine is created below the new ice. Due to its high density, the brine sinks and mixes with the underlying water. Thus, brine rejection and the related vertical mixing processes occur below these leads and keep the surface mixed layer growing down to a depth of 50 m and more (Peralta-Ferriz & Woodgate, 2015). Rising temperatures during the polar summer cause the ice to melt and lead to the release of low salinity melt water. Due to its low salinity the density is low as well, resulting in the melt water to lie upon the “normal” ocean water. The melt water layer can reach several meters in thickness. In this phase of the year, the water column at the surface features steep density gradients and a pronounced stratification.

1.1.4 Radiation budget

Another physical factor with ecologic relevance is the radiation budget of the ice. The structure of the ice, its thickness and additional parameters such as a snow layer on top of it determine the absorbency and reflectivity of the ice. Ice covered waters reflect about 65 % of the incoming radiation. In case of snow on top of the ice, this value rises to 80 – 90 % (Perovich et al.,

2002). As the incidence angle of the sunlight is flat in high latitudes, little light is available. Thus, light levels below the ice are generally low. Measurements by Nicolaus et al. (2007) showed that it is mainly light of 500 – 570 nm wavelength that penetrates through the ice.

The ice shield’s albedo changes significantly over the year. Due to rising temperatures in summer, melt water gathers in small depressions on the surface of the ice. This process has a positive feedback as these melt water ponds reflect less sunlight than the surrounding ice and start to warm up (Perovich et al., 2002) – eventually becoming “hot spots” on the ice that support melting processes. This “Ice-Albedo feedback” strongly accelerates the retreat of the ice edge in summer (Deser et al., 2000).

1.1.5 Gas / CO₂ exchange

A solid ice cover largely reduces the gas exchange between atmosphere and ocean. Although slightly permeable, results of Loose et al. (2011) suggest that ice related CO₂ exchange is almost negligible compared to the gas exchange occurring through open water. Exchange rates are further reduced by snow lying on the ice or ice layers formed by snow melting and refreezing (Nomura et al., 2010).

Thus, open water areas of the MIZ gain in importance as they expose cold water with enhanced gas solubility to the atmosphere (e.g. Volk & Hoffert, 1985). Apart from these well-known processes, recent studies indicate an enhanced CO₂ absorption for oceans covered by drifting sea ice, as it is encountered in the MIZ. However, mechanisms causing this increase (e.g. turbulence generated by ice drift, buoyancy flux or chemical enhancement) are still highly speculative and subject to current research efforts (Barber et al., 2015).

1.1.6 Investigation

The complexity, the time scale and the number of processes make it difficult to gather a holistic picture of a MIZ. Thus, apart from large-scale field research programs such as the multinational Marginal Ice Zone EXperiment (MIZEX) in the Fram Strait in 1983/84 or the current Marginal Ice Zone Program of the Office of Naval Research (ONR) in the Beaufort and Chukchi Sea, there have been attempts of modelling the MIZ. Gammelsrød et al. (1975) presented a model explaining ice-edge upwelling in 1975. In this model, up-ice wind conditions along a straight, stationary ice edge were assumed. The presence of the ice cover results in an uneven momentum transfer with the water of the ice free part being driven away from the ice.

Hence, a divergent zone is formed along the ice. The divergence is compensated by water upwelled from deeper layers. More sophisticated models which were developed in the following years (e.g. Niebauer, 1982; Røed & O'Brien, 1983; Sjøberg & Mork, 1985; Häkkinen, 1986) included moveable ice covers, variable ice coverage or the influence of the melt water. By adding these parameters, more possibilities for vertical transport processes induced by atmospheric forcing emerged (Fig. 1-5). More recent models indicate that down-ice wind conditions are more realistic and important for the evolution of vertical transport processes (e.g. Fennel & Johannessen, 1998). The latest sea ice models such as CSIM (latest version in June 2004) or CICE (latest version in 2015) also include melt water ponds or horizontal advection.

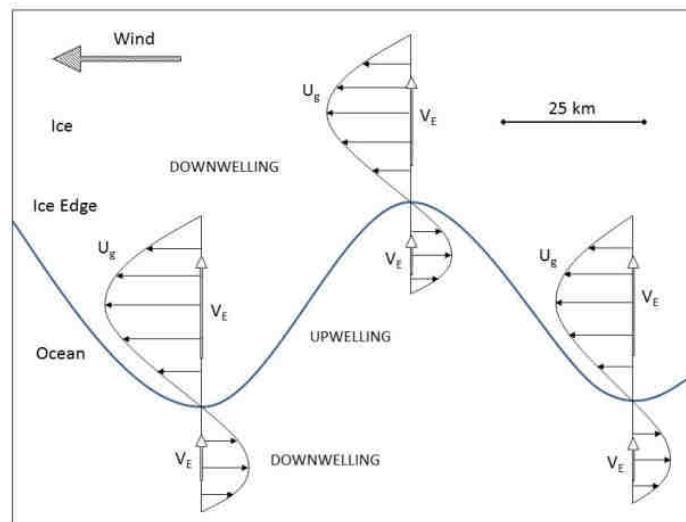


Fig. 1-5. Diagram modified after Häkkinen (1986) exemplarily illustrating the complex and small scale interaction between wind and a wavy ice edge. Regions featuring upwelling or downwelling are close together. U_E is the zonal water velocity due to wind. V_E is the meridional velocity vector due to the Ekman transport.

1.2 Ecology of the Marginal Ice Zone

1.2.1 Primary Production

Polar environments are shaped by extreme seasonality with six months of darkness as well as six months of permanent daylight. As for the entire polar region, ice related productivity is thus variable on a temporal scale.

On an annual scale, the availability of light controls the onset of the productive period (e.g. Cherkasheva et al., 2014). During the polar winter, sea water freezes and brine rejection causes deep vertical mixing – bringing up nutrients from deep water layers (e.g. Rudels et al., 1996; Popova et al., 2010). The absence of light prevents primary production and nutrients can accumulate. During this time, nutrient levels reach their annual maximum (e.g. nitrate: 12 μM in the Fram Strait or 20 μM in the Bering Sea, Niebauer, 1991). In spring, light levels rise and the ice retreats due to warmer temperatures. Nutrient laden surface water is exposed to sunlight – triggering the onset of a spring bloom (in the Arctic usually between March and May, Degerlund & Eilertsen, 2010).

Additionally, as stated by Smetacek & Nicol (2005), sea ice contains nutrients and trace elements (e.g. iron, Taylor et al., 2013) as well as seed organisms which are released into the ocean as soon as the ice melts (although data from the Hudson Bay provide little evidence for this hypothesis, Michel et al., 1993).

In summer, light availability still remains a crucial factor for biological production. An ice cover significantly reduces the amount of light available for photosynthesis (Smetacek & Nicol, 2005; Nicolaus et al., 2008; Slagstad et al., 2011). Below an ice cover, the euphotic zone, defined as the 1 % isolume of the surface PAR value (e.g. Lee et al., 2007), can be reduced considerably (Fig. 1-6) or photosynthesis can even be prevented completely due to low light levels. Consequently, Carmack et al. (2006) concluded that ice determines the timing of primary production by controlling the amount of sunlight penetrating into the water and nutrients control the amount of biomass being created.

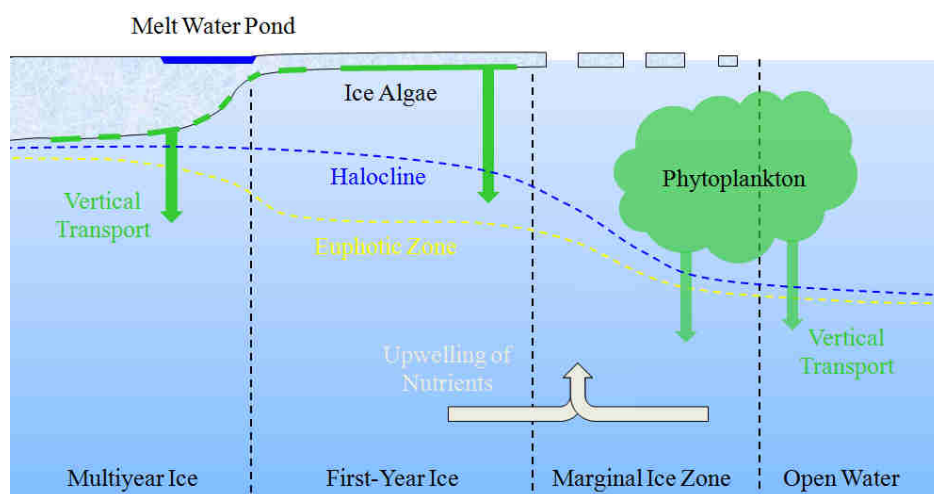


Fig. 1-6. Graphic depiction of major features of ice covered seas related to primary production. Figure modified after AMAP (2012).

Melting sea ice also releases large amounts of fresh water which has a lower density than “normal” ocean water. Consequently, the upper water column in the MIZ is highly stratified in summer. Although this stratification prevents phytoplankton from sinking and maintains it in an enhanced light regime, it can also keep the surface from being (re-)supplied with nutrients (Doney, 2006; Tremblay et al., 2015). Thus, ice edge phytoplankton blooms are a common feature of MIZs, yet they are transient – limited by the depletion of the winter accumulated nutrient inventory. Still, ice edge phytoplankton blooms can be extremely productive. Wassmann et al. (2006) reported an increase of the daily carbon flux in the MIZ of the southwestern Barents Sea from $12 \text{ mg C m}^{-2} \text{ d}^{-1}$ in pre-bloom conditions to $1800 \text{ mg C m}^{-2} \text{ d}^{-1}$ during a bloom event. To maintain high production rates over prolonged periods of time or to support blooms later than spring, nutrients must be provided actively. Processes such as for example wind induced ice edge upwelling or cyclonic eddies can transport nutrients to the surface. Niebauer (1991) stated that ice edge upwelling is of rather minor importance for providing nutrients for primary production and eddies appear to be of greater relevance. Especially eddies, which are active for 20 days or more as observed in Fram Strait (Johannessen et al., 1983), can provide nutrients for sufficient time periods to stimulate or prolong primary production.

1.2.2 Habitats and associated species

The entire ice-related environment can be divided into four different zones featuring different biogeochemical characteristics (Fig. 1-6): Multiyear ice, first year ice, marginal ice zone and the ice-influenced part of the open ocean.

Biological production below the multiyear pack ice is low (e.g. Dunbar, 1981) but it increases when the MIZ is approached (Smith, 1987; Hunt et al., 2002). For example, average annual carbon flux of the MIZ in the Barents Sea was determined to be about $100 \text{ g C m}^{-2} \text{ y}^{-1}$ compared to $60 \text{ g C m}^{-2} \text{ y}^{-1}$ in the ice covered parts (Wassmann et al., 2006).

Vertically, the marine ecosystem below the ice can be divided into different habitats which form two different systems. Following Gosselin et al. (1997), the ice itself, its lower side, and the ice-water interface form distinct habitats that belong to the “sympagic system”. The sympagic system encompasses organisms which are directly associated to the ice. One of the most abundant species of this system is *Melosira arctica*, an ice algae that forms large colonies attached to the lower side of the ice (Boetius et al., 2013). Gosselin et al. (1997) conducted a section from the Chuckchi Sea to the Eurasian Basin in the central Arctic and found pennate diatoms of the genera *Nitzschia* and *Navicula* to be dominant in the sympagic system (Fig. 1-7).

The water column below the ice represents another habitat and belongs to the “pelagic system”. Phytoplankton blooms in the pelagic system are normally dominated by centric diatoms of the genera *Chaetoceros* spp. and *Thalassiosira* spp. (Barber et al., 2015). Apart from this, frequently encountered species are pennate diatoms of the genus *Fragilariopsis* and the haptophyte *Phaeocystis pouchetii* (Fig. 1-8). As the results of the aforementioned studies do not necessarily represent the taxonomic conditions in the Fram Strait, a dedicated study is presented in section 1.3.

Below a solid ice cover, for example below the pack ice of the central Arctic, primary production by the sympagic ecosystem is of high relevance for the food web.

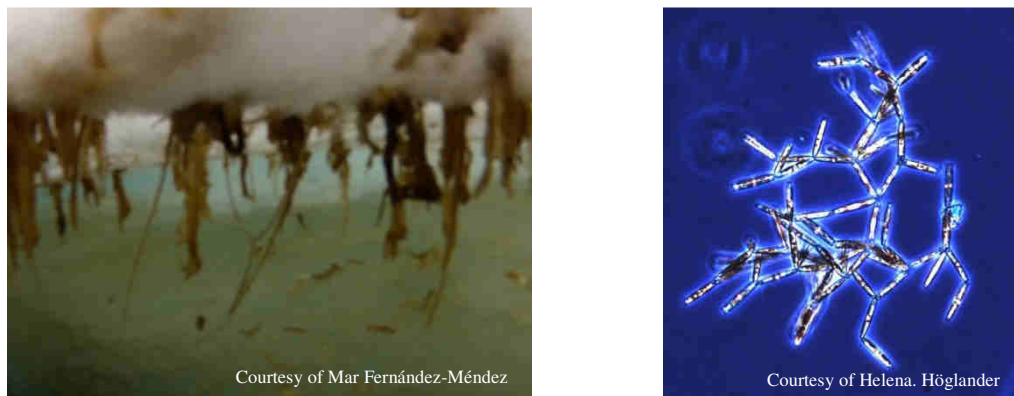


Fig. 1-7. Left panel: *Melosira arctica* forms large colonies that are attached to the lower side of the ice. Right panel: *Nitzschia frigida* as one prominent taxon of the genus *Nitzschia*.

As stated by [Boetius et al. \(2013\)](#), ice algae contributed to the overall primary production in the central Arctic by about 45 % in 2012. Results by [Fernández-Méndez et al. \(2015\)](#) even indicate a contribution of 60 % to the total primary production. With these algae sinking to the seafloor, they provide an important food source for benthic organisms and thus are closely associated to the benthic ecosystem. In contrast to this, the sympagic system's contribution to overall primary production in the MIZ is comparably small.

Ice algae related primary production is estimated to be about one or two magnitudes lower than phytoplankton related production ([Barber et al., 2015](#)). However, the bloom of the sympagic system occurs prior to the onset of the phytoplankton bloom and might also be related to the abundance of meltwater ponds acting as windows for light ([Falk-Petersen et al., 2000](#)).

Thus the sympagic bloom provides a food source for organisms of higher trophic levels when water column production is still negligible ([Arrigo et al., 2014](#)).

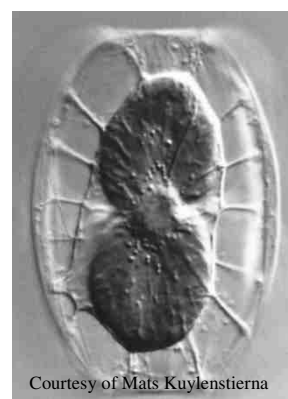
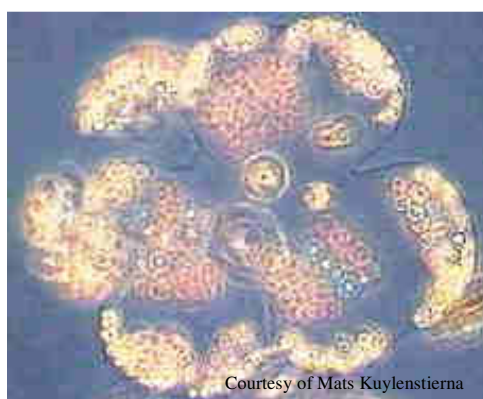


Fig. 1-8. Left panel: *Phaeocystis pouchetii* and right panel: *Thalassiosira hyaline* as two examples for planktonic taxons abundant in the pelagic system.

1.2.3 Higher trophic levels

Due to high primary production rates, enhanced biological activity in the MIZ can be found on all trophic levels. The sea-ice fauna can be divided into autochthonous (permanently ice associated) and allochthonous (temporarily ice associated) species. Autochthonous species include nematodes, turbellarians, rotifers and crustaceans (Gradinger & Ikävalko, 1998; Gradinger, 1999). Cracks and ridges in the ice, formed by waves deforming it, are inhabited by ice amphipods (Gradinger et al., 2010). Although amphipods are able to cover short distances through the water column for example to reach neighboring ice floes in the MIZ (Arndt & Lønne, 2002), species such as *Onisimus nanseni* (Fig. 1-9), *Gammarus wilkitzkii* or *Gammarocanthus loricatus* are considered to be autochthonous species (Lønne & Gulliksen, 1991).

Polar cod often feeds on ice and pelagic amphipods and thus has to be considered ice associated as well (Rand et al., 2013).

Top-predators in a MIZ include for example whales, polar bears (Arctic), and seals (Fig. 1-9, Stirling, 1997; Friedlaender, 2006).



1.2.4 Future development

The future Arctic will be characterized by less, younger and thinner ice with more meltwater ponds (Maslanik et al., 2007; Rösel & Kaleschke, 2012). In general, the loss of sea ice will entail a loss of autochthonous species.

As a consequence of thinner ice and numerous meltwater ponds, more light will penetrate through the ice and light levels will be sufficient to stimulate phytoplankton blooms below closed ice covers (Arrigo et al., 2012). In terms of space, thus the “productive zone” will move away from the MIZ towards ice covered areas – eventually restricting the access of organisms of higher trophic levels (e.g. seabirds) to secondary production related biomass (Barber et al., 2015). In terms of time, changes in the onset of the sympagic and the pelagic bloom will affect zooplankton grazers (Gosselin et al., 1997). A mismatch in timing might disrupt the Arctic food chain with negative effects for higher consumers (Søreide et al., 2010). However, the loss of ice and the freshening of the Arctic Ocean could also reduce nutrient availability and thus might limit phytoplankton growth – despite enhanced light levels (Lee et al., 2012).

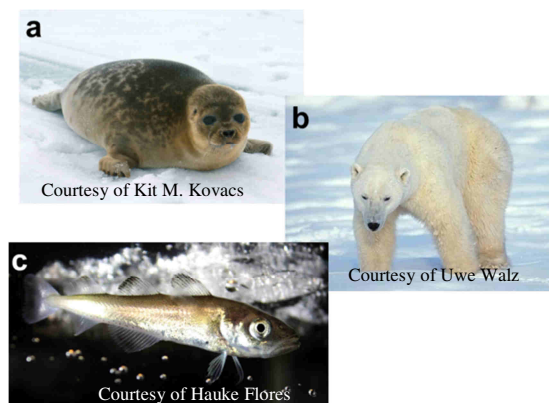


Fig. 1-9. Examples for higher trophic species in the MIZ. Left panel: Ice amphipod *Onisimus nanseni*. Right panel: Examples of top-predators in the MIZ: a) Ringed seal (*Phoca hispida*), b) Polar bear (*Ursus maritimus*), c) Polar cod (*Boreogadus saida*).

The question whether the future Arctic Ocean will tend to limit production via light or via nutrients cannot be answered yet ([Post et al., 2013](#)). At least in the Pacific sector of the Arctic, with its annually retreating and advancing ice masses covering large distances, phytoplankton biomass and primary production are assumed to increase in the future ([Wassmann et al., 2011](#)).

Furthermore, the trend towards thinner ice causes a reduction of pressure ridges in the MIZ which are crucial refuges for the sympagic fauna in times of increased ice melt in summer ([Gradinger et al., 2010](#)). Low sympagic biomass which has been recorded north of Svalbard since 2005 indicates that the sympagic community has already become reduced ([Barber et al., 2015](#)).

1.3 Study Area – Fram Strait

1.3.1 Location and Topography

The Arctic Ocean is enclosed by the Eurasian and the North American landmass. As a consequence, the central Arctic basin has only four relatively small connections to the world ocean (Fig. 1-10). One of the connections is the Bering Strait between Alaska and Russia. Another connection is the Davis Strait between Greenland and Canada. Additionally, there is the Barents Sea and the Fram Strait which both connect the central Arctic to the Atlantic Ocean. Compared to other parts of the Arctic Ocean the Fram Strait features some remarkable characteristics. In geographic terms, Fram Strait and Barents Sea are divided by the Svalbard

archipelago with the Fram Strait forming a 500 km wide “channel” between Svalbard and Greenland. In contrast to the other straits, the Fram Strait is comparably deep. The average depth of the Barents Sea is 230 m (Loeng, 1991). The Bering Strait reaches down to only 50 m (Shaffer, 1994). Davis Strait reaches greater depths, yet is separated from the central Arctic Ocean by the Canadian Arctic Archipelago – limiting the sill depth to 130 – 250 m (Niebauer, 1991). Fram Strait however has a sill depth of 2,300 m (Klenke & Schenke, 2002), thus representing the only deep water connection between the Arctic basin and the world ocean.

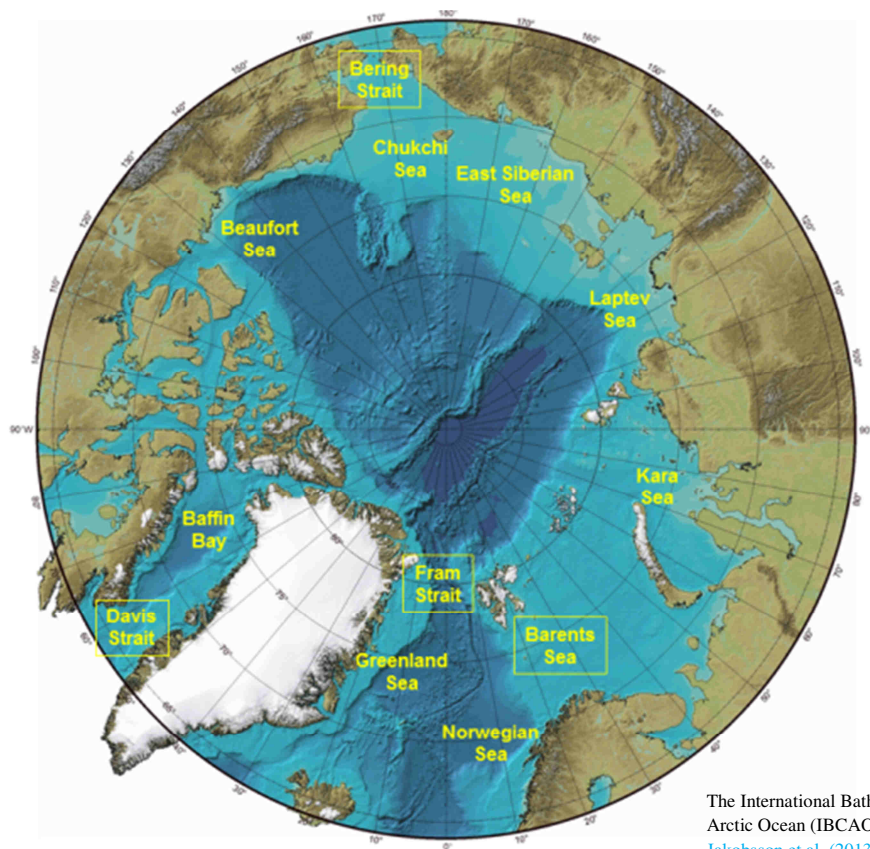


Fig. 1-10. Bathymetric chart of the Arctic Ocean and its most important marginal seas and straits. The four connections mentioned before are framed in yellow boxes (annotations in the chart were added by the author).

Generally, the topography of the Fram Strait is complex and shaped by extreme depth variations. At its western side, the continental margin rises steeply from 2,000 m to less than 500 m to form a wide, shallow plateau off the coast of Greenland. On its eastern side the continental slope is equally steep, yet the plateau off the coast of Svalbard is narrower. In the central Fram Strait some deep depressions such as the Molloy Deep, the deepest spot in the entire Arctic Ocean with 5,607 m (Thiede et al., 1990), can be found. Another prominent topographic feature is the Yermak Plateau northwest of Svalbard that reaches up to just 800 m below the water surface (Fig. 1-11).

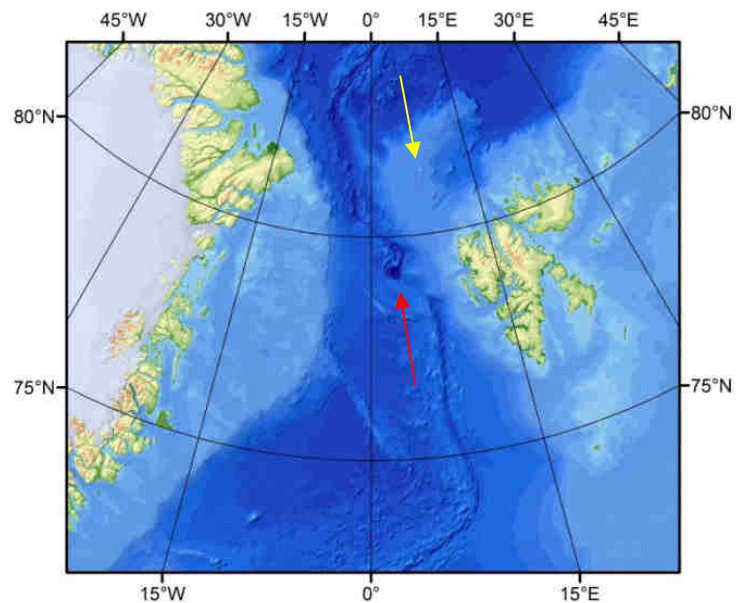


Fig. 1-11. Bathymetric chart of the Fram Strait with Greenland on the western side and the Svalbard archipelago in the east. Note the Molloy Deep which is marked with a red arrow in the center of the map. The Yermak Plateau is marked with a yellow arrow.

1.3.2 Hydrography

The Fram Strait plays an important role for the heat and mass exchange between the Arctic and the world ocean. Compared to the inflow of Pacific water through the Bering Strait, the net volume exchange through the Fram Strait is about 5 times larger (Coachman & Aagard, 1988; Roach et al., 1995; Fahrbach et al., 2001). Thus, Fram Strait handles about 75 % of the water exchange (Aagard & Greisman, 1975) between the Arctic and the world ocean.

The hydrographic regime of the Fram Strait features a complex pattern of water currents flowing in different directions in different depths. Rudels et al. (2005) identified twelve different water masses with different physical characteristics in the Fram Strait. However, on a large scale, the hydrographic regime is dominated by two major currents flowing in opposite directions (Fig. 1-12). In the eastern

Fram Strait, the warm West Spitzbergen Current (WSC), an extension of the Gulf Stream, flows in northward direction. In the western Fram Strait, the cold East Greenland Current (EGC) flows to the south along the Greenland continental shelf (Schlichtholz & Houssais, 1999). Based on field observations, Fahrbach et al. (2001) suggested a mean monthly southward water transport of 13.7 ± 1.7 Sv and a northward transport of 9.5 ± 1.4 Sv – resulting in a net southward water transport of 4.2 ± 2.3 Sv which is in the same order of magnitude as modelling results (Maslowski et al., 2004). Both currents feature cross-flow widths of about 100 km and are situated over the eastern and western slopes. The currents are separated by a 100 km wide region which is dominated by weak southwesterly currents. In this region, in the center of the Fram Strait, Atlantic water masses of the upper and intermediate layers recirculate to form the Return Atlantic Current (RAC) (Fahrbach et al., 2001).

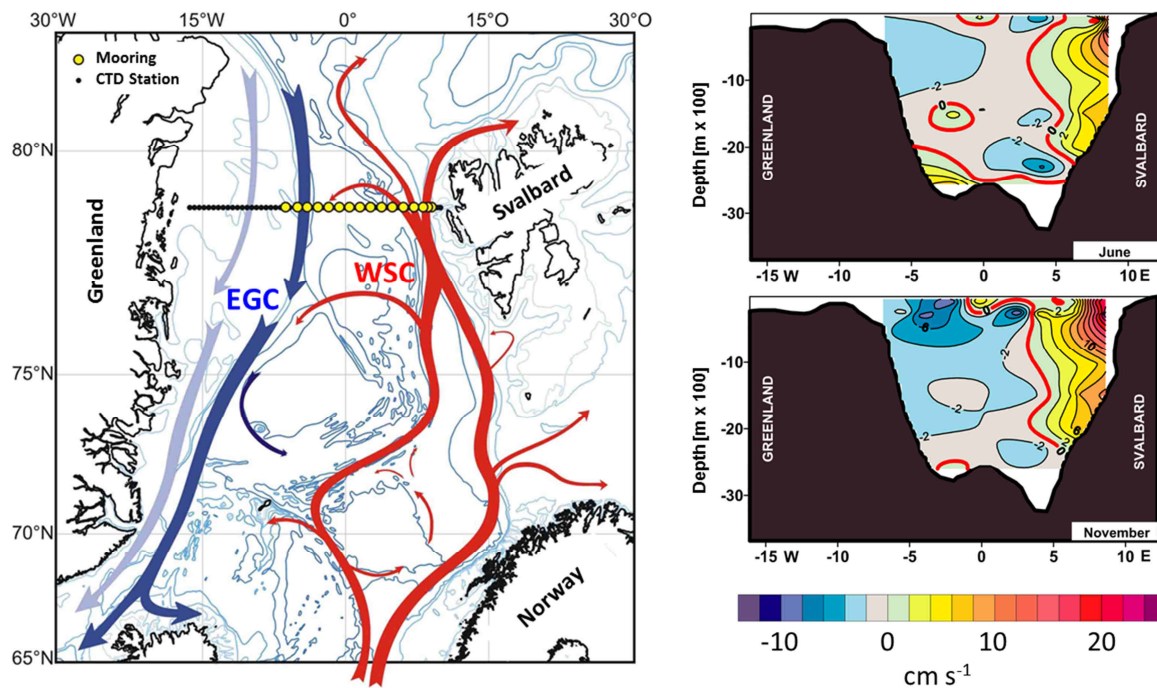


Fig. 1-12. Hydrography of the Fram Strait. Left panel: Cold East Greenland Current (EGC) and warm West Spitzbergen Current (WSC) flowing in opposite directions (Image by AWI and modified by the author). Right panel: Cross section through the Fram Strait along a meridional transect (black line, left panel) illustrates EGC and WSC by means of opposite flow velocities. Panel exemplarily shows conditions in June and November (Image from Hop et al., 2006).

However, Rudels et al. (2005) argued that waters of the RAC are interspersed by lenses of Arctic Atlantic Water and the RAC cannot be considered a real stream. Additionally, recirculation and interleaving between the two currents is characterized by an eddy field (Johannessen et al., 1987). These eddies most likely originate from instabilities within the WSC and the Norwegian Current (Gascard et al., 1988) as well as from atmospheric forcing (Manley et al., 1987; Jónsson et al., 1992). The EGC is dynamically stable and thus unable to generate eddies – suggesting that eddies are generated in the eastern Fram Strait and are advected with recirculating water masses.

The topography of the seafloor contributes to the complex hydrography as well. Vinje (1977) described an eddy located above the Molloy Deep for the first time. Since then, this cyclonic eddy of roughly 60 km diameter has frequently

been observed and it appears to be quasi-stationary in the Molloy Deep region (Wadhams & Squire, 1983; Bourke et al., 1987). Furthermore, transient eddies which appear to be generated in the vicinity of the MIZ frequently appear in the Fram Strait. These mostly cyclonic eddies with diameters of 10 – 40 km can extend to more than 500 m depth and have life times of at least 20 days (Johannessen et al., 1983; MIZEX Group, 1986).

Hydrographic data show a pronounced annual cycle in the Fram Strait. Depending on the month, the location of the meridional boundary line between the two currents varies between 5 °E and 3 °W (Hop et al., 2006). Volume transport of the WSC also changes over the year. Data of the period 1997 – 2010 show that a maximum of 8 Sv is reached in March and a minimum of 4.2 Sv is reached in July (Beszczynska-Möller et al., 2012).

In terms of flow velocity, the WSC reaches a first maximum of 40 – 50 cm s⁻¹ between January and March. Between May and July the flow velocities are weaker and reach a second maximum in August / September (20 cm s⁻¹). Flow velocities of the WSC decrease with depth and can turn southward at depths greater than 1,500 m (Hop et al., 2006). The EGC flow velocities are generally lower and less variant. An annual cycle is not clearly detectable. However, EGC-associated volume transport maxima of 19 – 24 Sv were reported to occur in December and spring (April – June) (Fahrbach et al., 2001). The core of the EGC is located in 200 m water depth and it is characterized by average flow velocities of 9 cm s⁻¹. Maximum velocities are observed at the surface between 2 °W and 6 °W (Fahrbach et al., 2001; Hop et al., 2006).

Along with the water, large amounts of heat are exchanged. Although the amount of exchanged heat greatly varies, reaching for example from a net northward transport of 6.0 TW in 1997/98 to 36.3 TW in 1998/99 (Schauer et al., 2004), water temperatures in the central and eastern part of the Fram Strait (east of 2° W) are above 1 °C at 250 m water depth throughout the year (Beszczynska-Möller et al., 2012).

Fram Strait represents the main heat source for the Arctic, handling about 90 % of the heat exchange between Arctic and the world ocean (Wadhams, 1983). Due to its depth, Fram Strait allows warm Atlantic water to transit into the Arctic at intermediate levels, and thus prevents the water from losing much energy to the atmosphere (Schauer et al., 2006; Maslowski et al., 2004). This is important as the upper 100 m of the WSC face a substantial heat loss of about 500 W m² in winter and 300 W m² in summer (Untersteiner, 1988). The heat transport into the Arctic is likely to increase in the future as rising temperatures of the deep water in Fram Strait have been observed (von Appen et al., 2015).

1.3.3 Cryosphere

A further specific feature of the Fram Strait is the prevailing ice conditions. Fram Strait represents the main passage for ice exiting the Arctic. Every year, about 10 % of the Arctic ice cover is lost due to year-around southward export through the Fram Strait with highest export rates in winter (Kwok et al., 2009a). Between Svalbard and Greenland, the ice forms a 300 to 450 km wide stream roughly overlaying the EGC and flowing southward while staying close to the coast of Greenland (Kwok et al., 2004). Drifting southward through Fram Strait, the ice encounters the warm water masses of the WSC and starts to melt. The two opposing processes, permanent ice export in the west and melting in the east cause the ice edge to stretch diagonally over the Fram Strait (Fig. 1-13).

The exported ice largely consists of multiyear ice (MYI). Tucker et al. (1987) reported that MYI comprises 72 % of the ice floes in the Fram Strait. Assuming MYI to be about 70 % thicker than first year ice (FYI), this corresponds to 84 % of the volume of the exported ice consisting of MYI. Applying backward trajectory analysis, the Laptev and East Siberian Sea could be identified as the predominant source regions of the ice (Fig. 1-14, Hansen et al., 2013). Ice formed in these two regions is usually exported via Fram Strait within three years. Ice originating from the Beaufort Sea is rarely exported through the Fram Strait, yet some ice on the westernmost part of the Fram Strait might originate from there. Compared to other Arctic marginal seas the ice edge “exhibits relatively little geographic movement” over the year (Smith et al., 1985). Although the ice shows only minor variations in its location, its interaction between the current system and eddies (either advected or generated in the MIZ as described by Johannessen et al., 1987) entails an “unsettled” behavior.

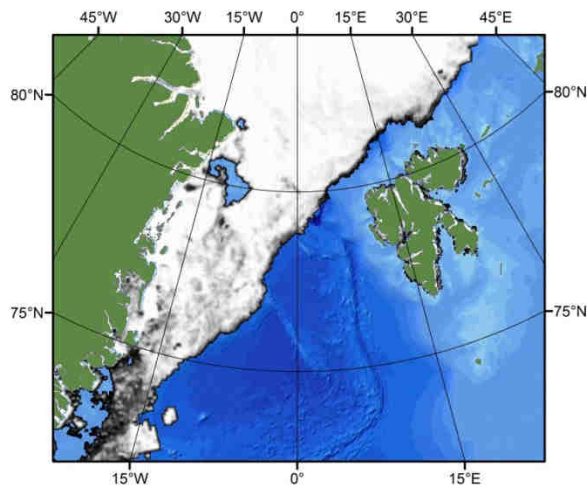


Fig. 1-13. Ice edge stretching diagonally over the Fram Strait on July 24th, 2013.

Large ice structures such as ice tongues which can extend several tens of kilometers from the main ice edge and drift on speeds comparable to a pedestrian, are a common phenomenon in this region (Wadhams & Squire, 1983). These extending ice structures can quickly fall under the influence of the WSC and thus melting rates along these structures can be elevated. For example in case of Atlantic water of 3 K above the freezing point being transported below the ice, melting rates were increased by a factor of ten compared to the interior of the pack ice (Johannessen et al., 1986).

Additionally, the ice volume flux is highly variable and so is the extent of the ice cover. For example, although most likely caused by anomalous winds in the early and mid-1990s (Polyakov et al., 2012), data of Kwok et al. (2004) for the period 1991 to 1999 indicate a maximum export of 3,363 km³ in 1994/95 and only 1,914 km³ in the following year. Generally, wind conditions and atmospheric forcing appear to have a large effect on the ice export rates.

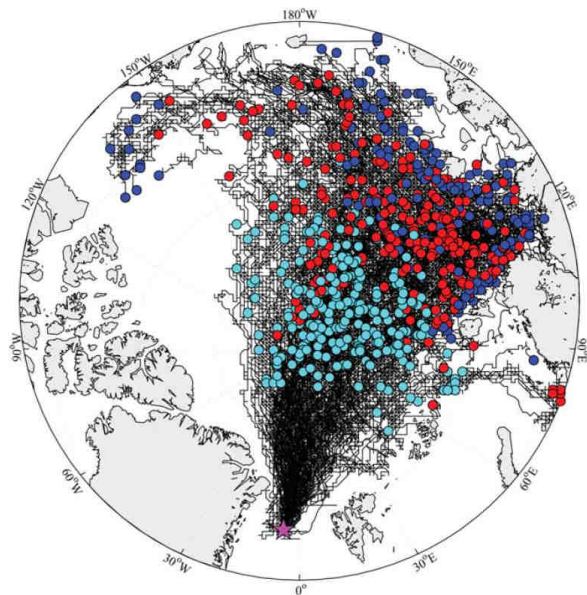


Fig. 1-14. Backwards trajectories for ice masses exported through the Fram Strait. The circles indicate the position of the ice 1 (cyan), 2 (red) and 3 years (purple) prior to the export (Image from Hansen et al., 2013).

Although the ice drift appears to be closely related to the underlying hydrography, particularly to the southward flowing EGC, this accounts to only one third of the total ice flux (Smedsrud et al., 2011). Van Engelen et al. (2013) suggested northerly winds (Greenland Sea Jet, GSJ) to maintain the ice export through the Fram Strait. Considering that most of the ice in the Fram Strait is assumed to be MYI featuring a rough surface topography and high drag coefficients, atmospheric forcing might significantly contribute to export processes (Smedsrud et al., 2011).

On a larger time scale, a long-term trend towards higher export rates can be observed. Kwok et al. (2004) reported an increase of the winter (October – May) ice area flux of 3,040 km² yr⁻¹ for the period 1978 – 2002. Particularly high export rates through the Fram Strait were also reported for the period 2005 – 2008 (Smedsrud et al., 2011).

At the same time there is a trend towards thinner ice. Ice thickness data from Hansen et al. (2013) for the period 1990 to 2011 show a multimodal

or at least bimodal thickness distribution (Fig. 1-15). These two modes represent FYI and MYI. According to Haas et al. (2010) the bimodal thickness distribution is typical for the Fram Strait in April as the ice stream contains a lot of new ice which was formed on leads. Consequently, ice with a maximum thickness of 1 m is abundant. The other mode can nowadays be seen at about 2 m thickness. Between 1990 and 2012 this second mode has moved from about 3 m to 2 m (Hansen et al., 2013). In general, the annual average of the monthly mean ice thickness in the Fram Strait stayed relatively constant until 2005, reaching thickness values of 2.8 ± 0.5 m. After the rather exceptional years 2005 – 2006 (thickness of 3.3 m) the thickness of the ice constantly declined and reached 2.0 m by 2011.

1.3.4 Ecology

(Due to the topic of this thesis, this section will focus on the lower trophic levels of the pelagic and sympagic system).

Although the Fram Strait is a rather small portion of the Arctic Ocean, it features various different habitats due to its complex hydrography and cryosphere. Primary production and consequently the entire food chain is affected by a number of key top-down (heterotrophic grazing) and bottom-up processes (ice cover, stratification, light availability, wind mixing, water transports) (Cherkasheva et al., 2014).

The temporal and spatial distribution of primary production in the Fram Strait is variable (Smith et al., 1987b).

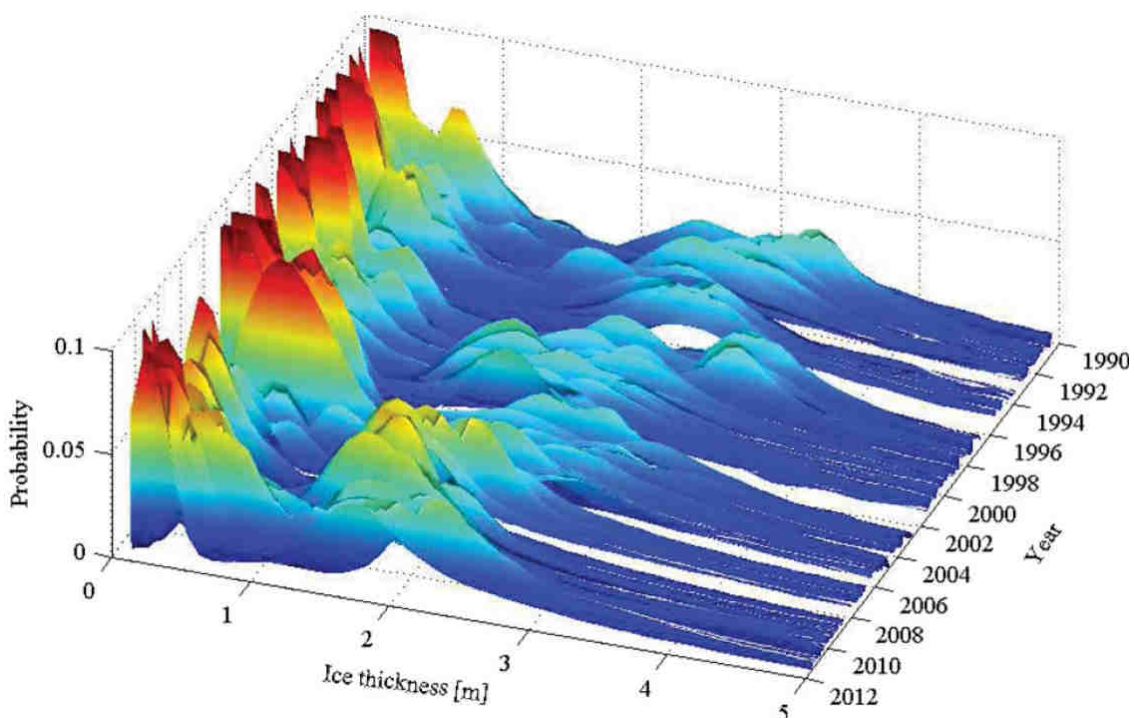


Fig. 1-15. Probability distribution of thicknesses (monthly averaged) of exported ice for the period 1990 – 2011 (Image from Hansen et al., 2013)

Characterized by the onset of the productive season, at least four different zones can be identified from east to west (Cherkasheva et al., 2014): 1) The Svalbard coastal region, 2) the open ocean, 3) the marginal ice zone, and 4) the western Fram Strait off the coast of Greenland. The beginning of the productive period propagates from east to west – starting in the Svalbard coastal region in April, then proceeds to the open ocean regions to start in May and finally begins as late as July or August off the coast of Greenland. Along with this seasonal productivity cycle there is an interannual trend towards later blooms. As described by Cherkasheva et al. (2014), most of the blooms since 2002 have been observed to occur in July.

The average annual primary production of the Fram Strait (open water) is estimated to be about $80 \text{ g C m}^{-2} \text{ yr}^{-1}$ (Hop et al., 2006; Richardson et al., 2005) with $50 - 60 \text{ g C m}^{-2}$ being produced in the period between May and August (Rey et al., 2000). The highest annual mean, yet also the highest variance can be observed in the marginal ice zone.

At least in the southern part of the Fram Strait, data by Cherkasheva et al. (2014) indicate a 30 % increase in bloom related carbon concentrations between 1998 and 2009 (annual average over the months April to August, percentage increase in relation to the mean value of 1998). Gradinger & Baumann (1991) showed that biological processes coincide with the hydrographic regime. In the MIZ, highest primary production rates occurred in water masses characterized by surface temperatures between $0 - 2 \text{ }^\circ\text{C}$. Cherkasheva et al. (2014) identified the stratification of the water column to be the most important factor for primary production in the Fram Strait's MIZ and the open ocean part – either induced by melting sea ice or solar warming. At the ice edge, eddies can be

generated which also affect biological processes and ultimately the entire food chain and export of biogenic matter (Lalande et al., 2011)

In general the biological productivity of the MIZ of the Fram Strait is low compared to MIZs of other parts of the Arctic Ocean (Niebauer, 1991). Primary production rates measured by daily carbon uptake are roughly four times lower than in the Bering Sea (Fram Strait: $1.7 \text{ g C m}^{-2} \text{ d}^{-1}$, Bering Sea: $6.6 \text{ g C m}^{-2} \text{ d}^{-1}$). The low productivity might be caused by lower nutrient levels. Maximum nitrate concentrations in the Fram Strait's MIZ are less than half as high as in the Bering Sea (Fram Strait: $12 \text{ } \mu\text{M}$, Bering Sea: $> 25 \text{ } \mu\text{M}$). Average Chlorophyll *a* levels in the Fram Strait's MIZ reach about $4 \text{ } \mu\text{g l}^{-1}$, whereas the Bering Sea exhibits about $22 - 25 \text{ } \mu\text{g l}^{-1}$ (Niebauer, 1991).

At the beginning of the growth season in March, ice algae on the underside of the ice, dominated by the diatom *Nitzschia frigida* (McMinn & Hegseth, 2004), largely account for primary production. For a short period of time, diatom species that are normally associated to pelagic phytoplankton blooms such as *Chaetoceros* spp., *Corethron criophilum*, *Proboscia alata*, *Rhizosolenia hebetate* and *Pseudo-nitzschia delicatissima* can also be found underneath the ice (McMinn & Hegseth, 2004). The subsequent spring phytoplankton bloom which occurs about one month later is usually dominated by the diatom species *Chaetoceros socialis*, *C. furcellatus*, *Thalassiosira nordenskiöldii*, *T. Antarctica*, *T. hyaline* and *Fragilariopsis oceanica* (McMinn & Hegseth, 2004; Richardson et al., 2005). Additionally, *Phaeocystis pouchetii* might occasionally be dominant, as intense open-water blooms were also observed between April and early May (Smith et al. 1991; McMinn & Hegseth, 2004).

Further abundant organisms belong to dinoflagellates and small pico- and nanoflagellates. Later in the year (June) *Phaeocystis pouchetii* can still be abundant, yet the phytoplankton community is increasingly dominated by the genera *Chaetoceros* spp., *Nitzschia* spp. and *Thalassiosira* spp. which become dominant in summer and autumn (Spies, 1987; Noethig et al., 2015). On an annual basis, diatoms account for about 50 % of the biomass produced in the northern North Atlantic Ocean (Bauerfeind et al., 1994; 2009).

It must be stated that species composition does not only vary with the season but also with the location and the depth. As Spies (1987) reported, there was a huge difference between the taxonomic assemblages of a station located within the EGC and a station that was influenced by Atlantic water masses. At the EGC, *Chaetoceros* spp. was dominant. In the Atlantic water masses, the diatom community was more diverse and nano- and microflagellates were abundant.

Long- term measurements of carbon export in the HAUSGARTEN area and in the eastern Fram Strait yielded that most of the produced organic matter is recycled in the upper water column (Bauerfeind et al., 2009). This confirmed the assumption of Hop et al. (2006) that only about 30 % of the annual primary production can be utilized by other organisms. Thus, 70 % “is recycled and/or made available for a carbon pathway involving small phytoplankton and small grazers, i.e. pico-, nano- and microzooplankton”. Due to the topic of this thesis and the amount of publications, higher trophic levels including zooplankton will only be discussed in brief.

Published information comprise 83 taxa of zooplankton (both holo- and merozooplankton) (Hop et al., 2006). Within this group, calanoid

copepods and other crustaceans of the two orders amphipoda and euphausiacea comprise about 45 % of all the recorded taxa in the Fram Strait (copepods: 24, amphipoda: 10, euphausiacea: 3) (Hop et al., 2006).

As the best studied taxa within the group of herbivorous copepods, the three *Calanus* species, *C. finmarchicus*, *C. glacialis*, *C. hyperboreus* are known to inhabit the upper 200 m of the water column in the period June to August (Hop et al., 2006). Starting in August, at least individuals of *C. hyperboreus* enter a dormant overwintering phase in great depth (in the Fram Strait: 2300 m, Auel et al., 2003). These three species account for about 66 – 75 % of the mesozooplankton standing stock in water depths between 0 and 50 m (Auel & Hagen, 2002). All species occur sympatrically (Auel et al., 2003). However, the different species appear to be strongly associated to specific water masses: *C. finmarchicus* to warmer Atlantic water of the WSC and the two other species to colder Arctic waters (Hop et al., 2006). *C. finmarchicus* enters the Fram Strait as it is transported with Atlantic water masses (Mumm et al., 1998). In contrast, *C. glacialis* inhabits Arctic shelf seas and *C. hyperboreus* prefers habitats over large ocean basins (Auel & Hagen, 2002).

Another important group of crustaceans are amphipods of which many are associated with the ice. In summer, amphipods seem to be the main grazers in the sympagic system (Werner & Auel, 2005), although Polterman (2001) stated that detritus is probably the more valuable food source. Studies showed that the abundance of the four most important autochthonous species (*Gammarus wilkitzkii*, *Apherusa glacialis*, *Onisimus glacialis* and *O. nansenii*) is associated to the structure of the overlying ice. In general, amphipod biomass below MYI is 10 – 100 times higher than below FYI (Lønne & Gulliksen, 1991a, b). This is of high importance as large

(and increasing) amounts of MYI are exported through the Fram Strait and thus the associated amphipod biomass is transported into the Greenland Sea. Estimates of the biomass flux are between $7 \cdot 10^5$ and $3.66 \cdot 10^6$ t yr⁻¹ (Lønne & Gulliksen, 1991b; Hop et al., 2006).

1.3.5 Investigation

The MIZ of the Fram Strait has been extensively investigated by two large multidisciplinary programs in the 1980s: MIZEX (Marginal Ice Zone Experiment) and CEAREX (Coordinated Eastern Arctic Experiment).

To conduct year-around measurements of different physical and ecological processes and the pelagic-benthic coupling in the Fram Strait, AWI has operated its long-term deep sea observatory HAUSGARTEN since 1999 (e.g. Soltwedel et al., 2009). The observatory consists of 21 stations which are arranged cross-shaped between 78.5 to 80 °N and 3 to 6 °E (Fig. 1-16). Stations which form the meridional part of this cross are installed along the 2,500 m

water depth contour line. The zonal stations are installed along 79 °N latitude. In the eastern Fram Strait this chain of stations begins in the Kongsfjord (Svalbard) in 250 m water depth, then proceeds westwards along the Vestnesa Ridge to the Molloy Deep station in 5,500 m water depth and rises into shallower waters in the western Fram Strait over the Greenland continental margin. Stations are annually visited by research vessels.

Instruments such as moorings, equipped with sediment traps and water current profilers, are operated year-around. On the sea floor, stand-alone systems such as for example lander systems to measure oxygen levels in the sediment are deployed. Apart from these long term investigations, remotely operated vehicles (ROVs) and AWI's autonomous underwater vehicle (AUV) "PAUL" are deployed. PAUL's main field of operation is the investigation of the upper water column, to a maximum depth of 600 m, in the MIZ. In conjunction with the benthic and pelagic data of the HAUSGARTEN stations, processes in the entire water column, from the surface to the sea floor, can thus be described.

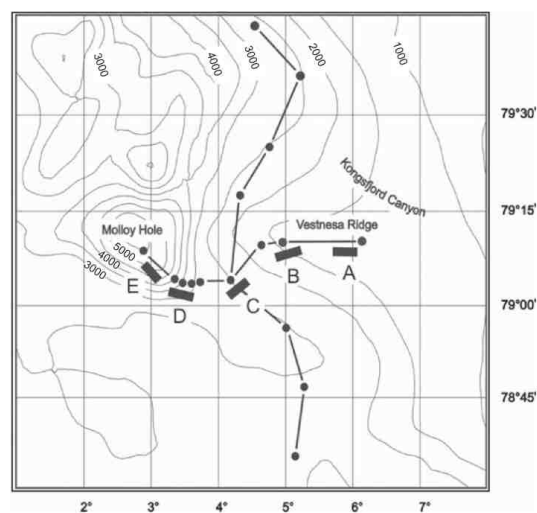


Fig. 1-16. Overview of the HAUSGARTEN observatory. Black bars marked A – E indicate locations of annually repeated sea floor observation transects (Image from Soltwedel et al., 2009).

1.4 Autonomous Underwater Vehicles

1.4.1 Early History

Autonomous underwater vehicles (AUVs) encompass a group of submersible robots with the capability to navigate and operate without human supervision thus making the requirement for a physical connection to a support vessel to transmit control signals unnecessary. Within the inventory of oceanographic instruments, AUVs represent a relatively young technology although the development of these vehicles began decades ago. Naval torpedoes can be considered the first “autonomous underwater vehicles” as they were able to maintain the course fired upon or, as in the case of the German naval torpedo “*Zaunkönig*” introduced in 1943, were even able to adjust their heading to pursue a sound source (noise of a ship’s propeller). The history of civilian AUVs began in 1957 when the Applied Physics Laboratory (APL) of the University of Washington started developing the Self Propelled Underwater Research Vehicle (*SPURV*, Fig. 1-17). Even this early generation vehicle’s operational range was approximately 40 km, depth rating was 3,000 m, and it was able

to communicate acoustically. *SPURV* was used for scientific purposes such as measuring the conductivity and temperature along isobaric lines. The first European attempt to build an AUV began in 1976 at IFREMER (Institut français de recherche pour l’exploitation de la mer) with the construction of “*Epaulard*” (Fig. 1-18). *Epaulard* had a depth rating of 6,000 m and provided images and bathymetric charts of the sea floor. As of 1990, the vehicle accomplished over 300 successful dives.

1.4.2 Technology

One of the main challenges in the development of AUVs was the navigation system. The vertical position (depth) can mostly be determined by using a pressure sensor while the horizontal plane (northings, eastings) of the AUV operates in an environment lacking spatial reference points to determine its own direction of motion and velocity.



Fig. 1-17. *SPURV* is being deployed.



Fig. 1-18. *Epaulard* on display in Toulon.

For the navigation system to have a baseline for georeferenced position (longitude, latitude), a GPS fix is necessary. Since electromagnetic waves are quickly absorbed by sea water, a GPS signal will no longer be obtainable once the vehicle has submerged resulting in a loss of a georeferenced position.

Dead reckoning using an Inertial Navigation System (INS) is the most accurate method to navigate in this environment without additional aiding. To implement this kind of navigation method, sensors need to measure the translational and rotational acceleration rates about all six degrees of freedom (Fig. 1-19).

AUVs are typically operated close to the sea floor. The sea floor represents a fixed reference the vehicles can track with a Doppler Velocity Log (DVL). In this so called “Bottom Lock Mode” the vehicles can determine their direction of motion and velocity relative to a fixed reference and thus significantly increase their navigation accuracy. Usually AUVs need to be within 100 m or less distance to establish bottom lock for navigational purposes. In case the distance between the vehicle and the sea floor exceeds the measurement range of the DVL, the vehicle is operated in the so called “Water Lock Mode”.

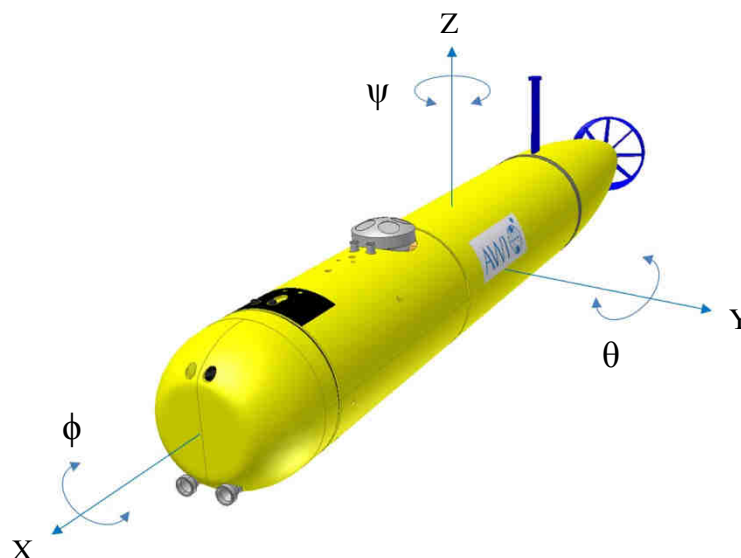


Fig. 1-19. Torpedo-shaped AUV with the six degrees of freedom: Three translational (X, Y, Z) and three rotational (ϕ , θ , ψ).

By measuring the acceleration rates and the exact time periods these accelerations appeared, the direction of motion, the velocity, and eventually the travelled distance can be calculated. This calculation is done by a vehicle for example every 0.1 s. From a known starting point, the current position of the vehicle can thus be determined by stringing together these small sections. In case of an AUV, the coordinates of the starting point are determined using GPS when the vehicle is still on the surface.

In contrast to measure its velocity relative to a fixed reference, the DVL provides the control computer with the vehicle velocity relative to the water. Since the water might move itself, the navigation accuracy degrades in this mode of operation.

As DVL tracking works with propagation times of acoustic signals through water, it is necessary to know about the sound velocity. Either a sound velocity sensor (SVS) or a conductivity, temperature and depth probe (CTD) to measure

the sound velocity is a crucial part of every AUV navigation system.

In summary, an AUV's navigation system consists of five core components; the INS, GPS, vehicle depth, sound speed, and velocity. The inertial navigation system uses the inputs of the GPS receiver to determine the precise georeferenced location of the vehicle while on the surface, the pressure sensor for vehicle depth, a CTD or SVS for sound velocity measurements, and the DVL for the velocity of the vehicle.

Apart from these basic components of the navigation system, additional navigational aids have been developed over the years for AUVs. One of the older solutions is to provide a vehicle with a fixed reference frame by deploying transponders either on the seafloor or within the water column as navigational reference points; this is referred to as a Long Baseline Network (LBL). This is one method to create an acoustic array in which the AUV can accurately navigate. Another option to support the vehicle's navigation is to track the vehicle with an Ultrashort Baseline (USBL) system. These systems are easy to handle as no transponders have to be deployed on the seafloor.

Instead of providing the vehicle with an acoustic array, USBL systems can be used to track the vehicle. After it is resiliently located, the determined position is transmitted to the vehicle via acoustic communication.

Furthermore, the sensory equipment of the vehicles can allow autonomous and quasi-intelligent reactions on unexpected mission scenarios. Standardly, many vehicles are equipped with sensors, such as sonars that form an Obstacle Avoidance System (OAS). Improved control algorithms provide AUVs with increased problem-solving abilities and mark another step towards real autonomy. An impressive example of a successful execution of different control algorithms, that eventually saved a vehicle from being lost, is one dive of the British AUV "Autosub 3" (Fig. 1-20) of the National Oceanography Centre (NOC) below the Pine Island Glacier (PIG) in 2009 (McPhail et al., 2009). In 60 km distance to the ice edge the vehicle ran into an ice cavern. While attempting to get out of that cavern it collided with the ice several times. After 30 minutes, an emergency descent behavior was triggered and executed autonomously – eventually freeing *Autosub3* from the cavern with minor damages.



Courtesy of the National Oceanography Centre (NOC)

Fig. 1-20. Autosub3 of the NOC is being recovered.

1.4.3 AUVs in the Arctic

Due to the missing physical connection to a support vessel, plans to deploy AUVs in ice covered seas developed early. In 1972, the “Unmanned Arctic Research Submersible” (UARS) became the first vehicle to operate below Arctic sea ice (Francois & Nodland, 1972). Using an upward looking sonar system, the vehicle mapped the lower side of the ice. In 1992, convection processes along ice leads were investigated using the “Autonomous Conductivity Temperature Vehicle” (ACTV, Morison & McPhee, 1998). Starting in 1992, Canada began developing the long-range vehicle “*Theseus*” which was supposed to lay glass fiber cables. In 1996, this 12 m long and 9.6 t heavy vehicle laid 175 km of glass fiber cable during one single deployment below Arctic sea ice at 85.5 °N (Ferguson et al., 1999). Further deployments below the ice took place in 1998 (Hayes & Morison, 2002), in 2001 (Wadhams et al., 2004, McEwen et al., 2005), in 2004 (Wadhams et al., 2006) and 2007. In 2007, within the framework of project “Arctic Gakkel Vents” (AGAVE), the two vehicles “*PUMA*” and “*JAGUAR*” of the Woods Hole Oceanographic Institution (WHOI) accomplished the deepest dives below the ice with 4,062 m (Kunz et al., 2008). The first under ice mission of AWI’s *PAUL* was conducted in the Fram Strait in 2010 (Wulff et al., 2010).

1.4.4 AWI’s Polar Autonomous Underwater Laboratory (*PAUL*)

With the particular goal of conducting missions in polar seas, *PAUL* was purchased in 2003 by AWI (Fig. 1-21). *PAUL* is based on a 21’’ class vehicle of the American manufacturer Bluefin Robotics Corporation (Quincy, Massachusetts, USA). The torpedo-shaped vehicle has a depth rating of 3,000 m and an operational range of 70 km. Vehicles manufactured by Bluefin Robotics are designed in modular sections. These sections allow the vehicle to be adjusted to the respective mission scenario (e.g. by swapping sections) and they also allow the vehicle to vary in length. In its initial design of 2003, *PAUL* was 3.2 m long. After a total reconstruction of the vehicle in 2011, *PAUL* is now 4.3 m long and weighs roughly 500 kg. The payload section is cylindrical in shape, about 1 m long and 0.5 m in diameter. The outer hull of the vehicle represents a hydrodynamic housing, yet it is not a pressure hull. Openings in the hull allow water to flood the vehicle’s interior as soon as it enters the water. Due to this reason all instruments installed in *PAUL* need to be pressure resistant. *PAUL*’s navigation system consists of the five basic components mentioned before (Table 1-1). *PAUL* does not have any other systems for obstacle avoidance and is also not able to track the lower side of the ice. Since the DVL is orientated to face the seafloor, it cannot be used to calculate the vehicle velocity relative to the ice. The relatively simple navigation equipment of the vehicle caused some trouble as, for this thesis, the AUV-project had a biological and geochemical focus. Additionally, the measurements were supposed to be done in the marginal ice zone (MIZ) which is an extremely risky environment for AUV operations.

Table 1-1Components of *PAUL*'s navigation system.

Instrument	Type of device	Manufacturer
INS	KN-5053	Kearfott (Little Falls, New Jersey, USA)
Pressure sensor	Digiquartz	Paroscientific (Redmond, Washington, USA)
GPS receiver	Ashtech DG-14	Trimble Navigation (Sunnyvale, California, USA)
CTD	SBE 49 FastCAT	Sea Bird Electronics (Bellevue, Washington, USA)
DVL	WH Navigator	Teledyne RDI (Poway, California, USA)

Due to the availability of light, biological and related chemical processes are closely tied to the water surface. As a consequence, *PAUL* had to approach the ice without an obstacle avoidance system by just a few meters in order to collect the necessary measurements in the desired area. Rapidly drifting ice floes that can move above the surface point and with no means of detection by the vehicle, pose a threat as well. Additionally, shallow dive missions in the Fram Strait, where the average water depth is 2,500 m, result in the vehicle operating in an environment out of range for the DVL to acquire bottom lock. Having the INS dependent on water velocities rather than bottom track velocities reduces the navigation accuracy. Supporting the vehicle with a LBL system was not an option, as the MIZ is an extremely dynamic region. Although the geographic position of the ice edge remains relatively constant throughout the year, some parts of the ice can achieve drift speeds of $1.5 \text{ km}\cdot\text{h}^{-1}$ (Lehmenhecker & Wulff, 2013). Deploying a LBL network is time consuming and thus the position of the ice edge several hours later would have to be estimated.

Practically, this task is unfeasible in the MIZ and the French USBL system "GAPS" (iXBlue, Marly le Roi, France) was used to track the vehicle. Tracking of *PAUL* was possible to a maximum range of 2 – 3 km. However, *R/V Polarstern* turned out to be a very noisy ship – making it impossible to establish acoustic communication to the vehicle and transmit position updates.

For these reasons, there were significant inherent risks of a total loss associated with deploying *PAUL* in the Arctic MIZ.

As one of few vehicles worldwide, *PAUL*'s sensory equipment is designed to investigate biological and geochemical questions. At first, a water sample collector was installed in 2008 / 2009 (Fig. 1-22). The sample collector is able to gather 22 samples of 220 ml each. Within the framework of this thesis, the payload was expanded by various sensors and data storage and power supply of the entire payload was centralized. The last deployment of *PAUL* to provide data for this thesis dates back to 2013. The payload included the sensors given in Table 1-2.

Table 1-2

 Scientific payload of *PAUL* as of summer 2013

Parameter	Type of device	Manufacturer
Conductivity	SBE 49FastCAT	Sea Bird Electronics (Bellevue, Washington, USA)
Temperature		
Pressure		
Dissolved Oxygen	SBE 43	Sea Bird Electronics (Bellevue, Washington, USA)
Nitrate	Deep SUNA	Satlantic (Halifax, Canada)
PAR	PAR-log-s	Satlantic (Halifax, Canada)
Chlorophyll <i>a</i>	C7-c	Turner Designs (Sunnyvale, California, USA)
CDOM	C7-u	Turner Designs (Sunnyvale, California, USA)
pCO ₂	HydroC CO2	Contros (Kiel, Germany)
Sample Collector	<i>Prototype</i>	AWI

When putting together the sensors of the payload, great attention was dedicated to the issue of data fusion. Especially the possibility to combine in-situ measurements (sensors) with ex-situ analyses (water samples) should be taken advantage of (Fig. 1-23). Water samples can be used for ground truthing purposes, or, in conjunction with sensor data, they can also be used to gain new information.

For example, the marine carbonate system can be described completely when the data of the pCO₂ sensor is combined with water sample analysis to measure total alkalinity (TA) or the concentration of dissolved inorganic carbon (DIC). Additionally, water samples can also be used to investigate phytoplankton communities and other parameters which are not measurable in-situ yet.

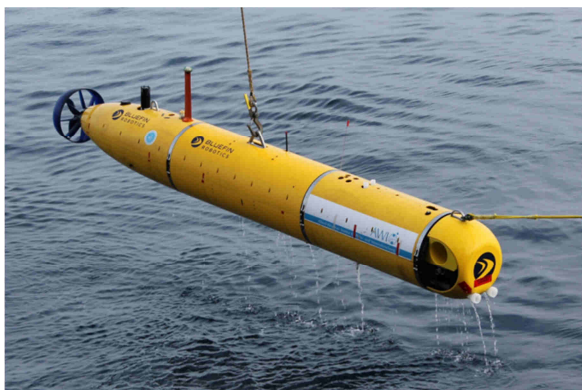

Fig. 1-21. *PAUL* is being recovered

Fig. 1-22. *PAUL*'s payload section. Note the white tubes which are the containers of the sample collector.

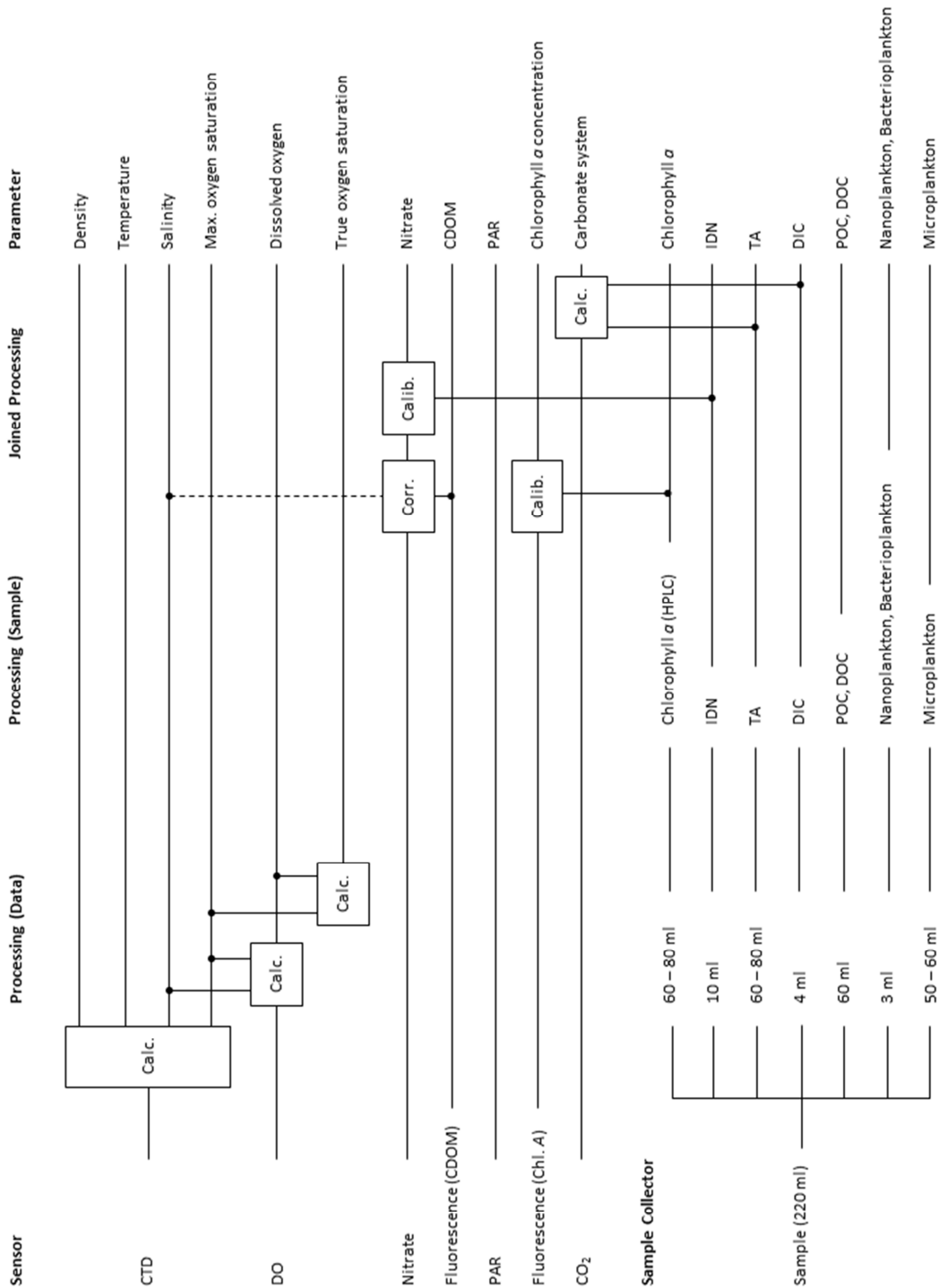


Fig. 1-23. Diagram illustrating measurable parameters and instrument fusion within the payload of *PAUL*. Instrument fusion includes calculating derived parameters (Calc.), calibration of sensor data using samples (Calib.) and correcting data by applying independent parameters (Corr.).

2 Objectives

Major uncertainties in understanding the physical and ecological properties of MIZs are related to the structure of the uppermost meters of the water column. Roughly to a depth of ~15 m, this part of the water column is strongly stratified due to melt water input and it interacts directly with the ice and the atmosphere. This fine stratification is normally destroyed by a ship's hull – especially by icebreakers having a heavy hull and large draft. As a consequence, there is a lack of field observations and the fine structure of the water column and small scale (submesoscale) processes along the ice edge are hardly known. There is even less knowledge about the ecological effects that are stimulated by these physical preconditions. Accumulation of phytoplankton along the ice edge is known in principal; however, the small scale distribution along and under the ice still needs to be investigated in detail. The MIZ is known for high rates of biological activity, yet what are the physical processes governing primary production and how do they interfere?

An AUV is able to collect data in this sensitive environment with only little disturbance. Marine science largely benefits from the speed and spatial resolution of such a vehicle's measurements. Compared to former investigations with ship bound CTDs, AUV mounted sensors provide high resolution data within a few hours.

Although the possibility to collect valuable data is of course meaningful, this is countered by the risk for the AUV. From a merely technological point of view, biogeochemical research in general is a challenging field for an AUV. The field comprises numerous parameters – making it necessary to integrate an extensive payload. The vehicle has to operate close to the water surface to stay in the euphotic zone. Thus, depending on the water depth, the vehicle is unable to establish bottom lock mode and faces reduced navigation accuracy. For this reason, certain tolerances have to be allowed for when defining the vehicle's dive track. Missions under or in the vicinity of ice are of particular complexity, as malfunctions or programming errors always involve the risk of a total loss of the vehicle. The vehicle's surface point has to be defined carefully in order to keep a safe distance from the ice. As there might be hours between programming the vehicle and actual surfacing, the location of the ice at the end of the dive needs to be extrapolated. Thus, information about the drift of the ice is needed. Acoustic tracking and communication systems reduce the risk of a total loss. However, their performance degrades in the MIZ environment as the strong stratification of the water column interferes with sound propagation and thus reduces the range of these systems.

Summarizing this, the objectives of this thesis can be listed as follows:

Objective I

1. Scientific: Identification of key physical, chemical and biological parameters that define the productivity of the MIZ
2. Technological: Review, testing and integration of existing biogeochemical sensors.

Objective II

1. Scientific: Study of ecologically relevant meso- and submesoscale transport processes in the MIZ.
2. Technological: Development of methods to resolve the surface water stratification.

3 Publication Outline

Study I: Development and Operation of an AUV-based Water Sample Collector

Thorben Wulff, Sascha Lehmenhecker, Ulrich Hoge
Sea Technology, 2010: 51(12), 15-19

The study describes the development of a water sample collector and its first operation below Arctic sea ice. During this very first under ice dive of AWI's AUV in summer 2010, the vehicle covered about 4 km under the ice and collected a total number of 18 samples which were analyzed with regard to dissolved organic carbon and phytoplankton species.

The sample collector was built by T. Wulff within the framework of his master thesis. The control electronics were developed by S. Lehmenhecker. During the PhD, a previously existing extension concept was realized by T. Wulff and the number of sample containers was doubled to 22. The under ice dive was conducted by the authors with support of Kimberly Shurn (Bluefin Robotics). The manuscript was written by T. Wulff.

Study II: Biogeochemical Research with an Autonomous Underwater Vehicle: Payload Structure and Arctic Operations

Thorben Wulff, Sascha Lehmenhecker, Eduard Bauerfeind, Ulrich Hoge, Kimberly Shurn, Michael Klages
IEEE, 2013: OCEANS-Bergen, 2013 MTS/IEEE, 1-10
doi: 10.1109/OCEANS-Bergen.2013.6608043

The study focuses on the integration of sensors and supporting systems into the AUV to measure biogeochemical parameters. The article describes the entire payload, its structure, the sensors, and supporting systems in the vehicle. Steps towards data correction and methods to calibrate sensors with the vehicle's water samples are presented. Additionally, the "Float" maneuver which was developed to investigate the surface micro-stratification is introduced in this article. Results of Arctic campaigns of 2011 and 2012 are shown, with both datasets include under ice data.

As the integration of new instruments exceeded the vehicle's ability to provide space, power, data storage capacity and buoyancy, its payload section was completely redesigned in 2011. Design work and buoyancy calculations were done by T. Wulff who was also responsible for manufacturing the parts. Data recording and power supply were centralized in the form of the newly developed Payload Control Computer. Hardware design was done by T. Wulff. The software was developed by S. Lehmenhecker. Testing the float maneuver was done by T. Wulff. E. Bauerfeind contributed to scientific dive planning. M. Klages is the initiator of the AUV-project and provided funding. The manuscript was written by T. Wulff and contributions were received by all co-authors.

Study III Flying Drone for AUV Under-Ice Missions

Sascha Lehmenhecker, Thorben Wulff

Sea Technology, 2013: 54(2), 61-64

The study describes the development and operation of a remotely controlled multicopter (“hexacopter”) which was deployed to observe the drift of an ice edge. The hexacopter carried a GPS receiving / transmitting unit and landed on the ice. While standing on the ice it was constantly sending its own position. Additionally, it measured Photosynthetically Active Radiation (PAR). In the study, two Arctic deployments of 5.5 hours duration each are described.

The hexacopter was developed, built and flown by S. Lehmenhecker. It was deployed in the framework of a study which was planned by T. Wulff. The manuscript was written by both authors.

Study IV Correcting Navigation Data of Shallow Diving AUV in Arctic

Uwe Wulff, Thorben Wulff

Sea Technology, 2015: 56(3), 27-30

The study describes a software filter specifically developed to merge vehicle navigation data and tracking data of the USBL system GAPS. The filter is applied in data post processing and eliminates unrealistic tracking results (e.g. reflection of sound at different water layers can cause error in acoustic positioning). The remaining tracking data are used to correct the vehicle navigation – providing resilient georeferencing for the payload data.

Development of the basic idea of the algorithm and programming was done by U. Wulff. Field studies to provide navigation and tracking data were planned and conducted by T. Wulff. The data were processed by U. Wulff. The manuscript was written by T. Wulff.

**Study V Collecting Water Samples in the Arctic Marginal Ice Zone with AUV “PAUL”:
Sample Safety, Sample Purity and Exemplary Results of Field Measurements.**

*Thorben Wulff, Eduard Bauerfeind, Jonas Hagemann, Christiane Hasemann, Boris P. Koch,
Sascha Lehmenhecker, Mascha Wurst, Michael Klages*

Submitted to *Methods in Oceanography* in April 2015

The study describes design features and techniques of the water sample collector to protect the samples from being contaminated. Different methods of sample processing are investigated in detail. Results showed that laboratory materials such as filters, hoses or syringes can affect the composition of a sample. Tests were conducted for nitrate, nitrite, ammonium, silicate, phosphate, and dissolved organic carbon (DOC). Finally, results of field measurements of the mentioned parameters are presented and compared with literature data.

The study was planned and mainly conducted by T. Wulff. Substantial support to develop suitable sample processing methods was provided by E. Bauerfeind, J. Hagemann, and S. Lehmenhecker. DOC data (field and laboratory data) were provided by B.P. Koch and M. Wurst. Statistical calculations were conducted by C. Hasemann. M. Klages is the original initiator of the AUV-project and provided funding. The manuscript was written by T. Wulff with particular support of B.P. Koch.

**Study VI Physical and Ecological Processes at a Moving Ice Edge in the Fram Strait as
Observed with an AUV**

Thorben Wulff, Eduard Bauerfeind, Wilken-Jon von Appen

Submitted to *Deep Sea Reseracht Part I: Oceanographic Research* in October 2015

This study describes physical and ecological conditions in the vicinity of a 70 km long ice tongue. The AUV provided high resolution data of the melt water front. The results indicate vertical transport processes in the water column which are related to the presence of the front and atmospheric forcing. At a melt water front, these processes have not been described before. Along with this, ecologic tracers such as chlorophyll *a* showed a highly inhomogeneous distribution – proving the complex and rapid interaction between physics and ecology in the marginal ice zone. Environmental data such as satellite images, wind data, and ship bound measurements are applied to provide the bigger context.

The study was planned and conducted by T. Wulff with the support of AWI’s AUV team. Data interpretation in a biological context was done by T. Wulff and E. Bauerfeind. Analyzing data against a physical background was conducted by T. Wulff and W.-J. v. Appen. The manuscript was written by T. Wulff with support of both co-authors.

4 First study (Manuscript I)

Development and Operation of an AUV-based Water Sample Collector

Thorben Wulff^{a, *}, Sascha Lehmenhecker^a, Ulrich Hoge^a

^a) AWI – Alfred Wegener Institute Helmholtz Centre for Polar and Marine Research
HGF-MPG Joint Research Group for Deep Sea Ecology and Technology
Am Handelshafen 12, 27570 Bremerhaven, Germany

^{*}) Corresponding Author
Tel: +49 (0) 471 4831 2045
Fax: +49 (0) 471 4831 1776
Mail: Thorben.wulff@awi.de

Published by Sea Technology in December 2010 (Sea Technology, 51(12), 15–19)

(An Abstract is normally not included in Sea Technology Publications. It was added in the thesis to achieve a consistent formatting.)

4.1 Abstract

To investigate ecological processes in the sea, both biological and chemical oceanography are dependent on the availability of water samples – although numerous relevant parameters are measurable *in-situ* due to improvements in sensor technology. Ship-based sample collector systems such as CTD rosettes are common instruments on research vessels. An autonomous underwater vehicle (AUV) represents a more “exotic” platform for a water sample collector. The Alfred Wegener Institute for Polar and Marine Research (AWI) in Bremerhaven, Germany, operates an AUV of the type Bluefin-21 in polar seas. In this study, the development of a sample collector system, integrated in AWI’s AUV and able to collect 22 samples with an overall volume of 4.8 liters, is described. The design of the device allowed for the cleanliness requirements of different analysis methods. For verification purposes, operational results of a dive of summer 2010 are presented. During this particular dive, the AUV conducted its very first mission below Arctic sea ice and collected samples successfully.

4.2 Introduction and Preconditions

Within the frame of the German Arctic expedition ARK XXV/2 (June 30th – July 29th, Fram Strait), the Alfred Wegener Institute for Polar and Marine Research (AWI) accomplished its first under-ice mission with its Autonomous Underwater Vehicle (AUV). The vehicle, of the type Bluefin-21, was deployed from the German research icebreaker R/V *Polarstern*. Apart from various sensors, the payload includes a newly developed water sample collector which gathered samples under the ice.

The Alfred Wegener Institute in Bremerhaven, Germany has owned an AUV of the US manufacturer Bluefin Robotics (Boston, Massachusetts) since 2003 (Fig. 4-1). For the AWI, operating an AUV is of special interest since this kind of vehicle is able to operate without a physical connection to a mother ship. This particular feature enables this vehicle type to dive in ice covered areas and thereby open up totally new possibilities for Polar research. Against this backdrop the decision to develop a water sample collector for the Bluefin-21 vehicle was taken at the AWI in spring 2008. Actual work on the system began in September 2008.

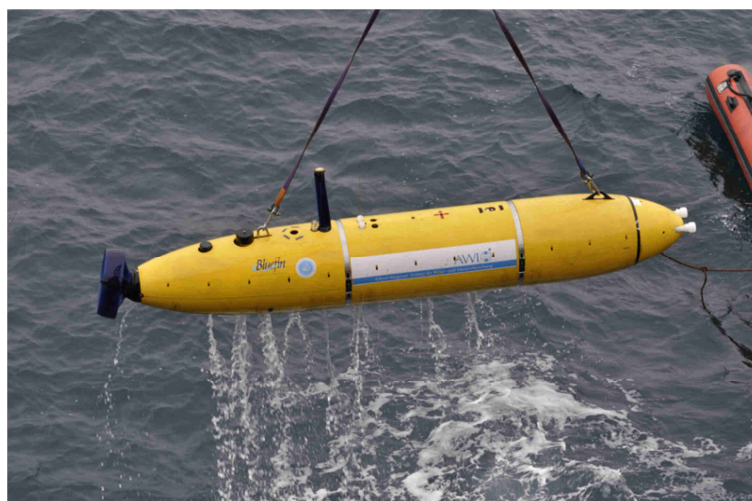


Fig. 4-1. The AUV is being recovered after accomplishing a dive in the Arctic Ocean.

Basic Preconditions

From the beginning, scientists of different specialist disciplines were involved in the development. The goal was to build a sample collector that meets the requirements of various research fields and is therefore versatile.

In order to gather a large number of samples, each sample has to be as small as possible, but big enough to meet the demands of different analytical methods. As it turned out the best possible compromise was a sample volume of 200 – 250 ml each.

Due to purity criteria the material selection was limited to such an extent that eventually only advanced materials, like the plastics Polytetrafluoroethylene (PTFE) and Polyvinylidene fluoride (PVDF) or the stainless steel 1.4571 (ASTM/AISI: 316Ti, UNS: S31635), were allowed to be used for parts with contact with the samples. As the hull of the AUV consists of Acrylonitrile butadiene styrene (ABS), water that might have been into contact with the hull must also be classified as “probably contaminated”. Consequently, inlet openings to the sample collector have to be positioned in front of the AUV. In addition to the scientific requirements, the operating conditions also have to be taken into account. The amount of available space and the carrying capacity of an AUV is limited. As a consequence, the design of the sample collector had to follow the principle “compact and lightweight”.

The interior of the Bluefin-21 vehicle, including the payload section, is flooded completely. For this reason, during a dive, the sample collector is exposed to the environmental conditions (e.g. pressure).

Operations in polar areas can entail very low temperatures. Although the temperature of the water seldom falls below $-1.8\text{ }^{\circ}\text{C}$, longer downtimes on deck, with significant lower air temperatures, might cause a much stronger

cooling of the device. The use of cold resistant components was therefore just as mandatory as to be vigilant about tolerances and free spaces to allow thermal expansion.

4.3 Methodology

For safety reasons the AUV is trimmed to be a little less dense than water. Since it does not have a diving tank it only dives dynamically. That means that the AUV constantly has to push itself below the surface with the aid of its thruster and, as a consequence, moves forward. This forward movement causes a dynamic pressure which is sufficient to press water into the interior of the vehicle; therefore pumps to suck in water are obsolete. Thus, the intention was to integrate a flow channel into the AUV which is interrupted by a magazine with a number of sample containers (Fig. 4-2). This magazine is the actual sample collector. Similar to the functional principle of a revolver, the sample containers (in further text: “sample tubes” or “tubes”) are arranged in a rotatable drum magazine and one particular tube is positioned in front of the feed line (the barrel in a revolver). In a continuous process driven by the motion of the AUV, water enters the feed line, flows through the sample tube and leaves the AUV through a drainage pipe. If the drum magazine is turned one tube further, this has a double effect: On the one hand the rotation positions a new tube in front of the feed line and on the other hand, the rotation triggers a closure mechanism in that particular tube, which had previously been placed in front of the feed line, and closes both ends of the tube. By this, a section of the water flow is “cut” and isolated as a sample.

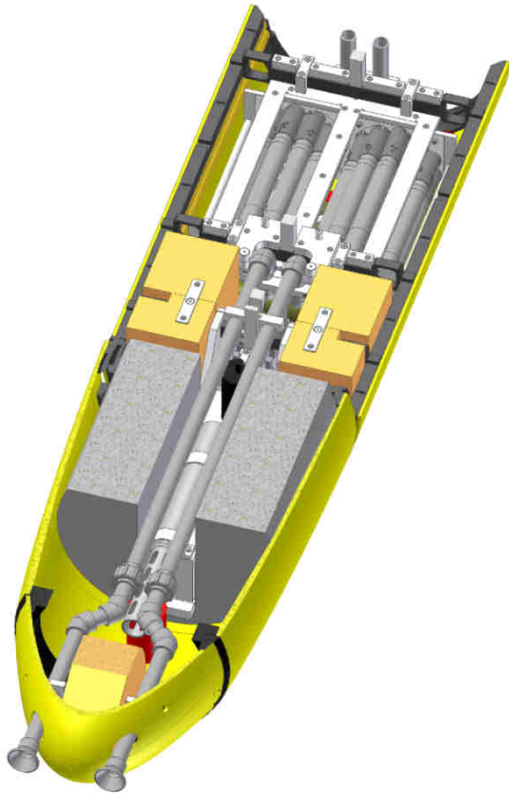


Fig. 4-2. CAD model of the sample collector inside the Bluefin-21 AUV. Both drum magazines are fully loaded with sample tubes.

The sample collector contains a total number of 22 sample tubes with a volume of 220 ml each. These tubes are mounted in two separate magazines. Each one of the two magazines has its own feed line, drainage pipe and drive motor. The motor is attached to the sample collectors' front and back side respectively. The integration of two independent magazines minimizes the risk of a total failure of the sample collector and the space in the payload section is used more efficiently than with one magazine. The inlet openings of the two feed lines are situated in front of the nose cone of the AUV and are visible in the form of two funnels.

The feed lines then lead through the battery section of the vehicle before they are finally attached to the sample collector. The feed lines including the funnels consist entirely of PVDF. The openings of the drainage pipes are visible on top of the payload section right in front of the blue GPS antenna (Fig. 4-1).

The Sample Tubes

The functional principle of the sample tubes is pretty similar to the principle of Niskin bottles. The interior of both ends of the tube are shaped conically so that female tapers are formed. These female tapers serve as counterparts for two cones ("locking-cones") which are interconnected by a tension spring. Prior to a dive the two locking-cones are lifted from their tapers and fixed at special suspension points inside the tube. When the drum magazine rotates, small levers, which are a part of the closure mechanism, release the locking cones from their suspension points. The force of the tension spring pulls the cones into the tapers and thus closes both ends of the tube.

Another central component of every sample tube is the moveable end cap. This end cap is adjustable, to a range of 10 ml, and therefore the overall length of the tube is flexible. A pressure spring below the cap produces a counteracting force if tube and cap are tried to be pushed together. When the sample tubes are mounted in the drum magazine (Fig. 4-3) they move in between two Teflon®-coated slide plates. The distance between these two plates is chosen so that the tubes cannot extend to their maximum length. Hence, the pressure spring is constantly compressed and the ends of the tubes are steadily pressed on the slide plates. When positioned in front of the feed line, this contact pressure seals the transition point between tube and feed line; an important precondition to ensure that only "clean" water can enter the sample tube.



Fig. 4-3. During preparation for the next dive the sample tubes are being inserted.

4.4 Results

During expedition ARK XXV/2 twelve dives were accomplished between July 2nd and July 21st. Unfortunately, frequently occurring fog strongly handicapped the work so eventually only one (and AWI's very first) under ice mission could be accomplished. The scientific goal of this particular mission was to measure biological parameters that have an influence on phytoplankton. Therefore, in addition to the sample collector, a sensor for photosynthetically active radiation (PAR), a fluorescence sensor and a CTD probe were sent along with the AUV.

The under ice mission was executed in the western Fram Strait (78° 49,74' N; 03° 49,89' W) on July 21st and led the AUV about two kilometers under the ice. The vehicle was deployed 800 m in front of the ice edge and transited to the ice in a depth of 20 m. 300 m in front of the ice edge it descended to its actual mission depth which was at 27 m.

In this depth the vehicle was expected to hit the fluorescence maximum, which represented the most interesting water layer for this mission. Water samples were taken in discrete time intervals of 90 s each. The process of taking samples was launched by a pressure sensor that identified the intended depth of 27 m. After reaching the turning point, the AUV returned to a pre-programmed position and was picked up by R/V *Polarstern*. After the vehicle had been recovered, the water samples were immediately given to scientists to be prepared for conservation. For that the tubes were taken out of the sample collector, stored in special transport containers and brought into the laboratory within few minutes. Due to the much stronger incident of light on the surface, the samples were darkened with an opaque film during tube-dismounting. According to a pre-developed procedure the samples were then divided into several fractions and preserved in the cold stores of R/V *Polarstern*.

4.5 Conclusion and Future Prospects

In the course of the expedition the functional principle of the sample collector, as well as its design, has delivered a good performance in practice. Even though the analysis of the samples is not yet finished there are no indications for malfunctions or major construction faults that might endanger the purity of the samples. The handling of the sample tubes and working in the laboratory proved to be simple and safe.

AUV operations during ARK XXV/2 demonstrated the great potential of the combination of an AUV and a sample collector, with biological research potentially gaining a large benefit from this in future missions. For the foreseeable future there still is a large number of analysis methods that cannot be replaced by sensors and in-situ measurements. Therefore gathering sample material is a fundamental part of scientific work.

For the same number of samples a team of scientists would have had to go on the ice and drill holes in order to gain access to the water below. For Arctic sea ice this might be difficult and time-consuming, yet feasible. In the case of shelf ice, with several hundred meters thickness, this method reaches its limits. Although it already has been done, these drilling sites remain isolated spots. For large scale investigations AUV-based systems remain the only access to the unknown world that lies under the ice.

4.6 Acknowledgement

The authors want to thank Kimberley Shurn and Ted Allison from Bluefin Robotics, as they played an important role in the successful outcome of the AUV operations during ARK XXV/2.

5 Second Study (Manuscript II)

Biogeochemical Research with an Autonomous Underwater Vehicle: Payload Structure and Arctic Operations

Thorben Wulff^{a, *}, Sascha Lehmenhecker^a, Eduard Bauerfeind^a, Ulrich Hoge^a,
Kimberly Shurn^b, Michael Klages^c

^a) AWI – Alfred Wegener Institute Helmholtz Centre for Polar and Marine Research
HGF-MPG Joint Research Group for Deep Sea Ecology and Technology
Am Handelshafen 12, 27570 Bremerhaven, Germany

^b) Bluefin Robotics Corporation
Quincy, Massachusetts 02169, USA

^c) Sven Lovén Center for Marine Sciences
University of Gothenburg
451 78 Fiskebäckskil, Sweden

^{*}) Corresponding Author
Tel: +49 (0) 471 4831 2045
Fax: +49 (0) 471 4831 1776
Mail: Thorben.wulff@awi.de

5.1 Abstract

In modern polar marine research, Autonomous Underwater Vehicles (AUV) gain increasing importance due to their ability to take on high risk or time-consuming tasks in the harsh physical environment of the polar seas. They represent a relatively new group of robots that can investigate large areas in all three dimensions without the direct need of human surveillance. The most common objective for these vehicles that are currently operated worldwide is to gather sonar data and create high-resolution maps of the sea floor. A relatively new task is their deployment within the framework of water column studies dealing with the investigation of biogeochemical processes in the open sea or in ice-covered areas.

The Alfred Wegener Institute for Polar and Marine Research (AWI) in Bremerhaven, Germany, operates a 21-inch class AUV of the American manufacturer Bluefin Robotics (Quincy, Massachusetts) named *PAUL*. The main objectives of the herein described AUV project at AWI are the investigation of biogeochemical processes in the surface water and to analyze the stratification of the upper water column in the marginal ice zone as well as the dynamic interaction between ice and ocean. For this reason, since 2008, *PAUL* has been equipped with a number of biogeochemical sensors (e.g. Nitrate, Oxygen, Fluorescence, etc.) and a newly designed water sample collector all specified for operations in icy waters.

In the course of several Arctic expeditions onboard the *R/V Polarstern*, the vehicle was deployed in the Fram Strait close to the AWI deep sea observatory HAUSGARTEN.

In a first series of diving trials in ice covered areas, the first mission under ice accomplished by *PAUL* occurred at the HAUSGARTEN site in summer 2010.

Here, the description of the vehicle, the mode of operations and especially the structure of the payload is detailed. The payload development process took advantage of complementary instruments: combining data of different sensors with water samples. The samples allow data to be obtained for parameters that cannot be measured in situ, for example the amount of microscopic plankton, and in addition, they can also be used for validation purposes. For example, by measuring the amount of chlorophyll *a* in distinct samples, the flow-through chlorophyll *a* fluorometer of the AUV can be calibrated. This provides more accurate values than a calibration with laboratory standards. Results of such measurements gathered from 2010 to 2012 (ARK 25/2 – ARK 27/2, *R/V Polarstern*) are presented exemplarily for the scientific use of the vehicle.

Additionally, a description will be given for the new technologies that were developed (remotely operated flying drones, GPS tracking of the ice edge) the new procedures (vehicle tracking, special dive maneuvers) introduced into the AUV project in order to acquire a comprehensive picture of the physical and biogeochemical conditions of the pelagic environment assessed. These steps were mandatory, not only to ensure the safety of the vehicle, but also to be able to place the measured data into the greater context of challenges in understanding the dynamics of ice-covered seas.

5.2 Introduction

The Alfred Wegener Institute for Polar and Marine Research (AWI) in Bremerhaven, Germany is one of three institutes in Germany that operates an Autonomous Underwater Vehicle (AUV) to pursue scientific objectives. The Center for Marine Environmental Sciences of the University of Bremen (MARUM) and the GEOMAR Helmholtz Center for Ocean Research in Kiel are the other institutes that also operate AUVs for scientific reasons. The general goals of these institutions differ - with the AWI focusing on investigations in the Polar Regions. With the particular goal of operations in high latitudes, a 21-inch class AUV from the American manufacturer Bluefin Robotics (Quincy, Massachusetts) was acquired in 2003 and named *PAUL*. Since 2008, the entire AUV project at AWI has focused on the investigation of the upper water column, the micro layers in the marginal ice zone, and the analysis of biogeochemical processes close to the surface.

The surface water layers of the oceans differ from the deeper water masses by the abundance of light and the gas exchange with the earth's atmosphere. As a consequence, photosynthetic primary production is exclusively tied to the upper water column. Organic particles that have been formed at the surface sink to the sea floor and then serve as an energy source for benthic life; thus connecting the upper and deeper water layers. With a certain time delay, surface bound processes are reflected on the sea floor. In the polar oceans, the ice coverage represents a unique variable that influences environmental conditions from sea surface to the bottom of the ocean. The low water temperatures of the polar oceans support the solubility of gases, but with a solid ice cover on top of the water, the gas exchange with the atmosphere is reduced to almost zero. Ice reduces the transmission of light

and thus decreases primary production rates. However, at the same time, the stable summer stratification of the surface water, a direct result of the melting of ice, is the reason for the high biological productivity of the marginal ice zone. The stratification and the consequences have already been investigated in the 1980's for example by [Smith et al. \(1984\)](#) or [Niebauer et al. \(1989\)](#). These kinds of effects, which are partly in competition to each other, make the Arctic Ocean a spatially and temporarily dynamic environment. Additionally, questions as to stratification and productivity of ice-covered seas gain even more importance against the background of climate change and a fast changing Arctic. The most visible consequence of the climate change is the dramatic sea ice retreat that could be observed in the last decades. The loss of sea ice causes fundamental changes in the Arctic habitat as it was described for example by [Arrigo et al. \(2008\)](#). AUVs offer the possibility to observe these processes in a very efficient way. Travelling at relatively high speeds, these vehicles can collect data from various locations within a short matter of time, thus providing an almost synoptic, three dimensional picture of the environment ([Brierly et al., 2002](#)). As there is no direct physical connection to a support vessel, these vehicles can also operate in regions almost inaccessible by traditional methods. As a consequence, one of the key requirements is reliable navigation of these vehicles under ice. Although there have been a number of attempts, with some groups achieving remarkable success, for example the *Autosub* missions of the National Oceanography Center in Southampton in 2009 ([McPhail et al., 2009](#)), these kind of missions still remain a challenge. Since 2009, *PAUL* has accomplished four cruises into the Arctic.

In order to study the biogeochemical interrelations in the marginal ice zone, five still relatively short missions were conducted below the ice. All Arctic missions were conducted in the Fram Strait between Svalbard and Greenland. This region is of high scientific interest as this strait represents the only deep water connection between the Arctic basin and the Earth's oceans (Perkin & Lewis, 1984). Starting in 1999, AWI has managed its deep sea observatory HAUSGARTEN in this area and the AUV project at AWI aims at connecting surface water data to benthic data which are regularly gathered at the HAUSGARTEN site.

5.3 The Vehicle

A 21-inch class AUV from the American manufacturer Bluefin Robotics serves as a carrier vehicle (Fig. 5-1). This class of torpedo-shaped vehicles is rated to a maximum depth of 3,000 m (the latest model has a 4,500 m depth rating) and has an outer diameter of 53.3 cm (= 21 inches).



Fig. 5-1. PAUL is being recovered. The float at the nose section is jettisoned.

The vehicles are divided into sections that are exchangeable according to their respective mission. Due to this modular design and desired payload, the length of a vehicle varies. In the current configuration, PAUL has an overall length of 4.3 m. The tail section contains the Main Vehicle Computer (MVC), communication and tracking systems, and the thruster. The thruster is a single gimbaled ducted thruster that moves horizontally and vertically with the aid of linear drives. Apart from the thruster, the vehicle does not have any other control equipment such as rudders that have the potential to be damaged if the vehicle surfaced between ice floes.

The centre section of the vehicle houses the batteries. This particular section currently contains three batteries with a possibility to use a maximum of six batteries. Each battery has a

capacity of 1.5 kWh allowing the vehicle to travel a distance of approximately 70 km. Additionally, the battery section also provides the central single lift point of the vehicle and the emergency ascent drop weight is installed here. The vehicle's payload section is located forward of the battery section and is described in detail in this paper. The foremost section is the nose section containing a jettison-able float with an attached recovery line.

The vehicle's navigation system is a Kearfott Inertial Navigation System (INS) of the type KN-5053 and is aided by the following sensors:

- Teledyne RDI: Workhorse Navigator Doppler Velocity Log (DVL) with 300 kHz.
- Paroscientific Inc.: Digiquartz pressure sensor (4,000 m).
- Thales Navigation: Ashtech DG-14 GPS receiver.
- Sea Bird Electronics SBE 49 FastCat Conductivity, Temperature and Depth probe is used to provide an in-situ sound profile to support DVL measurements.

The outer hull of the AUV forms a hydrodynamic efficient housing, and also allows for each section to be free flooded.

Consequently, every scientific instrument integrated in the payload section is directly exposed to environmental conditions like pressure and cold temperatures. Thus, every instrument has to be protected by an individual pressure hull. The weight of these pressure hulls can sum up to a large part of the payload's total weight – reducing the valuable interior volume of the vehicle as this weight has to be compensated by buoyancy modules.

With respect to the objectives of the project, namely investigating the upper water column, the maximum operation depth of the payload was defined to be at 600 m. This limitation made it possible to use lighter instruments with thinner pressure hull walls and less dense (= more efficient) buoyancy foam as the foam does not have to withstand high pressure. The 600 m depth rating is merely valid for the current and herein described payload section. As the vehicle consists of different sections that can easily be exchanged, the rest of the vehicle remained equipped with 3,000 m rated buoyancy modules. Thus, after a quick reconfiguration that only involves the payload section, the vehicle is able to cover its full operational range again.

5.4 The Payload Section

5.4.1 Sensors

The number of sensors needed to capture every biogeochemical parameter fairly exceeds the vehicle's payload capacity. Therefore it is necessary to define certain expressive

parameters and to integrate the respective sensors. The currently integrated instruments and the measurable parameters are as shown in [Table 5-1](#).

Table 5-1
Parameters measurable *in-situ* by PAUL

Parameter	Instrument	Description
Nitrate	Satlantic SUNA Deep Nitrate sensor	The amount of nitrate in the water is measured by the absorption of ultraviolet (UV) light (190 - 370 nm) following the basic principle of Johnson & Coletti (2002) .
Dissolved Carbon Dioxide (CO ₂)	Contros HydroC CO ₂ Sensor	Using a semi permeable membrane, CO ₂ molecules are extracted from the sea water and channeled into a measuring chamber. Here the amount of CO ₂ is determined using a Nondispersive Infrared Sensor (NDIR).
Dissolved Oxygen (DO)	Sea Bird SBE 43 (Version: SBE 43-2a)	The sensor's functional principle is based on a Clark Electrode. In order to minimize the response time a profiling configuration sensor (membrane thickness: 0.5 mm) is used.
Conductivity, Temperature and Depth probe (CTD)	Sea Bird SBE 49 FastCat (Version: SBE 49-1f)	The CTD is both a part of the scientific payload and of the vehicle navigation system. The SBE 49 was chosen as it has a short response time and is thus suitable for fast moving platforms like an AUV.
Colored Dissolved Organic Matter (CDOM)	Turner Designs C7 "U"	For CDOM this fluorometer works with an excitation wavelength of 325 nm and a detected emission wavelength of 470 nm.
Chlorophyll a (Chl. a)	Turner Designs C7 "C"	For chlorophyll a, this fluorometer works with an excitation wavelength of 465 nm and a detected emission wavelength of 696 nm.
Photosynthetically Active Radiation (PAR)	Satlantic PAR Sensor (Version: PAR-log-s)	As the AUV project includes missions below sea ice a logarithmic sensor is integrated in the vehicle to make use of its high resolution capabilities at low PAR values.

Data recording and power supply is centrally managed by the vehicle's Payload Control Computer (PCC) which was specifically designed for that purpose. The PCC is based on a VIA Pico ITX mainboard equipped with a 1 GHz VIA C7 processor running on an optimized version of Microsoft Windows XP®. Signals of the sensors are transmitted to the PCC in the form of analog signals. Data are digitalized by a 13 bit analog-digital converter and saved on a solid state hard disk.

5.4.2 Water Sample Collector

As some parameters cannot be measured in situ yet, the vehicle carries a water sample collector. AUV based water sample collectors are rather special payload components and operated by just a small number of institutions. Apart from the AWI, the Monterey Bay Aquarium Research Institute (MBARI, Monterey, USA) developed a sample collector called GULPER for one of their vehicles (Bird et al., 2007). The sample collector from AWI was an in-house development that was put into service in July 2009 (R/V *Polarstern*). With the aid of the sample collector the vehicle is able to collect a maximum of 22 water samples with a total volume of 4.8 l. The volume of each sample is 220 ml. To provide the sample collector with water, the forward movement of the vehicle and the resulting dynamic pressure in front of its nose is used. Funnels that stick out of the vehicle's nose channel the water into pipes and direct it into the vehicle's payload section. The actual sample containers work similar to Niskin bottles and are made of polyvinylidene fluoride (PVDF) to meet high purity standards of various biogeochemical analyses. The functional principle of the sample collector is described more detailed in (Wulff et al., 2010).

5.4.3 Data Fusion

One of the primary objectives while designing the payload section was to make use of complementary instruments. A common example for data fusion is the interaction between a CTD and a DO sensor. A Parameter such as salinity is derived from the CTD data and is necessary to calculate the oxygen content and the current oxygen saturation (Sea Bird Electronics Application No. 64, 2012). Also, by using CTD data, temperature dependent effects on the absorption spectrum of bromide ions, which absorb UV-light at a similar range as nitrate and thus interfere with the nitrate measurement, can be compensated (Zielinski et al., 2007; Sakamoto et al., 2009). One "special" feature of *PAUL* is the possibility to combine sensor data with the data of simultaneously taken water samples. Apart of providing material for investigations that can only be carried out with samples (e.g. amount of micro plankton), the samples are also used for a ground truth and calibration purposes. During the two cruises HE-377 (R/V *Heincke*, April 2012) and ARK 27/2 (R/V *Polarstern*, July 2012), the following parameters have been determined using AUV water samples: Total Alkalinity (TA), Dissolved Inorganic Carbon (DIC), Inorganic Dissolved Nutrients (IDN) and Chlorophyll *a* (Chl *a*).

Derived from the TA and DIC values, the partial pressure of CO₂ can be calculated following Zeebe & Wolf-Gladrow (2001) and the CO₂ sensor data can be verified by an independent source. As for the CO₂ sensor, the nitrate value can also be verified using the samples. Within the framework of the IDN analysis, the amount of the four different nutrients ammonium, phosphate, silicate, and nitrate is determined by default. Thereby, a ground truth for the nitrate sensor is done automatically. Unlike the processes mentioned before, measuring the

amount of chlorophyll *a* is not only important for signal verification but to calibrate the signals of the chlorophyll *a* fluorometer. As the fluorescence response of phytoplankton is not constant but varies with species (SooHoo et al., 1986) and due to the Kautsky effect (Büchel & Wilhelm, 1993), quantitative chlorophyll *a* measurements can only be achieved after an in-situ calibration of the instrument (Earp et al., 2011).

5.4.4 Structural Set-up

According to the torpedo shape of the vehicle the payload section is cylindrically shaped as well. The length of the section is 1,015 mm and the inner diameter is 520 mm. The section can be separated into a lower and upper half shell. The water sample collector represents the largest single instrument in the payload section. It has some special requirements distinguishing it from the sensors. The most important difference is that the sample collector needs to be easily accessible as the samples have to be processed in the ship's laboratories as soon as possible after the vehicle has been recovered. Additionally, the sample collector is passively flushed – using only the dynamic pressure in front of the vehicle as it cruises. In order to optimize the flow rate in the supply pipes, it is an asset to keep the pipes as short as possible meaning the position of the sample collector needed to be as close to the vehicle's front end as possible. These two basic requirements of the sample collector, accessibility and position, were important boundary conditions for the further design work. The design of the payload section can be seen in Fig. 5-2 and Fig. 5-3. In front of the sample collector the DO sensor, the CDOM sensor and two supply pumps are positioned. Located above the sample collector, the CO₂ and



Fig. 5-2. Payload section during ARK 27/2 prior to a dive. The sample containers are already installed.

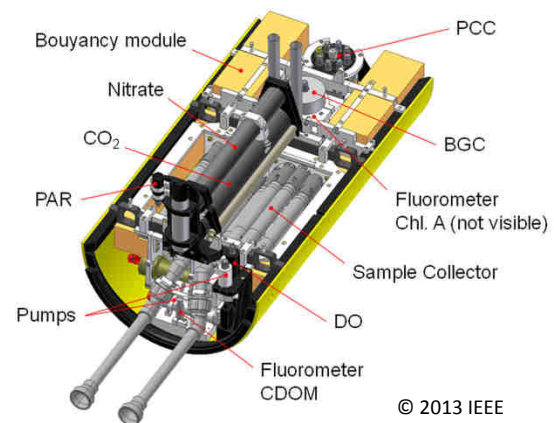


Fig. 5-3. Computer-aided design model of the payload section.

the nitrate sensor are both supplied with water via a shared water circuit for their integration. In addition to that, the PAR sensor is positioned above the sample collector in an upward looking configuration. Behind the sample collector, the chlorophyll *a* fluorometer and the PCC are integrated.

To be able to integrate instruments on short notice, for example instruments that come from external partners, the payload section has an exchangeable module. This module consists of a plastic box which can be inserted into the payload section like a drawer.

Below the module the outer skin of the vehicle has an opening to provide instruments with a direct access to the water. The module has a base area of 189 x 153 ml; the available volume is approximately 7.3 l. The first external user instrument which took advantage of this possibility was the BioGeoChemical Module (BGC) of the Max Planck Institute for Marine Microbiology in Bremen, Germany, during two cruises in 2012.

All structural parts of the payload section consist of lightweight polyethylene (PE). With an average density of $0.98 \text{ g}\cdot\text{cm}^{-3}$ this material

contributes to the vehicle's overall buoyancy. The actual buoyancy modules are made of microballoon based synthetic foams of the type TG-24 manufactured by Trelleborg Offshore, UK. The buoyancy modules have an average density of $0.385 \text{ g}\cdot\text{cm}^{-3}$ and are approved for a maximum water depth of 2,000 m. This depth rating largely covers our field of interest (max. 600 m depth) but at the same time it allows us to extend the mission depth in the future.

The currently available buoyancy reserve within the payload section is approximately 160 N.

5.5 Ice and Vehicle Tracking

Currently, unattended AUV missions in the open water column, particularly below ice are considered to be high risk. Additionally, navigation errors, which inevitably occur during missions in the open water column, can only be corrected when the vehicle is constantly tracked. When diving under ice, tracking the ice drift and the ice edge's orientation are also critical issues – not just to ensure the safety of the vehicle but also to support the scientific interpretation of the AUV data.

To track the vehicle under water the Ultra Short Baseline (USBL) system “GAPS” of the French manufacturer iXBlue (Marly le Roi, France) is used. According to manufacturer information the maximum range of this system is 4,000 m in all directions ([iXSea GAPS Carbon V1 User Guide, 2010](#)). Considering the particular objective to conduct shallow missions in the upper water column, it is of particular interest that GAPS covers an operating field of 200°. Thus it is possible to track objects close to the surface although the transducer is positioned underneath a ship.

Tracking of the ice is done by Global Positioning System (GPS) based tracking units which are deployed on the ice. These units determine their own position using GPS and transmit it via radio communication. By deploying at least two of these units it is possible to observe the ice edge's orientation. In 2012, during ARK 27/2, a remotely controlled flying drone was deployed on the ice for the first time to send position updates and collect PAR data ([Lehmenhecker & Wulff, 2013](#)).

All tracking signals are centrally displayed on the operators screen. Aside of the AUV and the ice, the ship itself and the boat which is used for recovery are put on display as well. Thus the operator can easily overlook the entire mission and can for example guide the recovery team to the vehicle in case of foggy conditions. Additionally the operators screen is broadcasted onto the bridge of the ship – making the communication with the ship's command safe and easy.

5.6 Float Maneuver / Data Correction

5.6.1 Float maneuver

At the beginning of 2012 a new maneuver was introduced into AWI's AUV project in order to investigate the micro stratification of the upper water column: The "Float"-maneuver. This maneuver takes advantage of the approximately 30 N residual buoyancy of the vehicle. As the vehicle reaches a specific position it stops the thruster and starts a slow ascent towards the surface, allowing the sensors to record a detailed vertical cast of the respective location. When the vehicle reaches a specific depth it reactivates the thruster and descends again to transit to the next Float location. Several Float maneuvers in a particular area can provide a detailed three dimensional picture of the investigated water volume. The first tests of the Float maneuver were conducted in March 2012 at the Bluefin Robotics test site onboard the R/V *Resolution*. The maneuver was further analyzed during the cruise HE-377 in the North Sea in April 2012 (R/V *Heincke*). First scientific operations in polar waters and under ice were accomplished in July 2012 during expedition ARK 27/2 in the Fram Strait. Unfortunately, during the under ice dives, the payload battery suffered a partial power loss and some data was lost. The Float maneuver combines three major advantages:

1. As the vehicle ascends slowly, it achieves a fine resolution of the water column. *PAUL*'s typical ascent velocities are between 10 and 20 $\text{cm}\cdot\text{s}^{-1}$. As the data recording frequency is 1 Hz, the vertical resolution is 10 to 20 cm as well.
2. As R/V *Polarstern* is an icebreaker, she has a heavy hull and a relatively large draft of approximately 12 m. Thus, at least to this

depth, one can assume that the fine stratification of the uppermost meters of the water column is destroyed and data derived from ship bound measurements do not necessarily represent correct environmental conditions. In contrast to that, *PAUL* crosses the water layers smoothly and causes as few disturbances as possible.

3. Due to the higher risk for the vehicle, missions below the ice are conducted within the GAPS tracking range. As the vehicle ascends almost vertically during the Floats, the distance to the support ship remains almost the same. Thus, compared to an undulating manner of driving, a bigger number of vertical casts can be recorded without leaving the GAPS tracking range.

5.6.2 Data Correction

Initially the term "micro layers" is not related to a specific size scale. In 1993 [Cowles & Desiderio \(1993\)](#) emphasized the need for sub-1-meter resolution and ultimately achieved a vertical resolution of 2 cm with their Rapid Sampling Vertical Profiler (RSVP). Using an AUV (and other instruments) and applying the three criteria defined by [Dekshenieks et al. \(2001\)](#) to identify thin phytoplankton layers, [Ryan et al. \(2008\)](#) detected layers with a minimum thickness of 1 m in the Monterey Bay. The scientific requirements defined *PAUL* to achieve a comparable resolution. In order to detect layers of that size and precisely correlate the measurement data of the different sensors, it is necessary to provide every parameter with an accurate depth stamp. As the depth sensor is positioned in the rear of the vehicle but the

payload section is at the front end, for example a relatively small pitch angle can cause a significant depth error.

5.6.2.1 Depth correction

To be able to calculate an exact depth stamp for every parameter, the position of the “sampled spot” relative to the vehicle’s depth sensor has to be known. In the case of sensors that protrude out of the vehicle into the water, the sampled spot was defined to be the sensitive surface of the instrument. In the case of sensors that are connected to a pumped water circuit, the sampled spot is the position of the water inlet at the vehicle. Measuring these positions, with the depth sensor of the vehicle as the point of origin, result in individual position vectors for every parameter. Depending on the pitch and roll angle of the vehicle and using rotation matrices these vectors can be rotated into their real orientation. Rotations in a three-dimensional space about an arbitrary axis can be described by the following matrix (Tsai & Lenz, 1989):

$$R_{\vec{n}}(\alpha) = \begin{pmatrix} n_x^2 t + r & n_x n_y t - n_z s & n_x n_z t + n_y s \\ n_x n_y t + n_z s & n_y^2 t + r & n_y n_z t - n_x s \\ n_x n_z t - n_y s & n_y n_z t + n_x s & n_z^2 t + r \end{pmatrix} \quad (1)$$

Where n_x , n_y , n_z represent the Cartesian components of the unit vector of the rotation axis \vec{n} . With α being the angle of the rotation, the variables r , s and t stand for:

$$r = \cos \alpha \quad (2)$$

$$s = \sin \alpha \quad (3)$$

$$t = (1 - \cos \alpha) \quad (4)$$

As pitch and roll movements are two independent transformations with different

angles and about different axes, two separate matrices have to be created. With the axes and angle convention given in Fig. 5-4 and may \vec{u} represent the position vector of one sensor, \vec{u}'' this position vector in its real orientation and \vec{x}' the unit vector of the vehicle’s longitudinal axis rotated by the pitch angle, this leads to the equation:

$$\vec{u}'' = (u_x'', u_y'', u_z'')^T = R_{\vec{x}'}(\phi) \cdot (R_{\vec{y}}(\theta) \cdot \vec{u}) \quad (5)$$

It is to be mentioned that the heading of the vehicle is disregarded. Thus the first rotation (pitch) is assumed to be around the global y-axis with its unit vector $\vec{y} = (0, 1, 0)^T$.

As it is only the vertical component of the rotated position vector \vec{u}'' which is necessary for correcting the depth, it follows:

$$depth_{corr} = depth_{raw} + u_z'' \quad (6)$$

Based on these equations each sensor has an individual depth stamp.

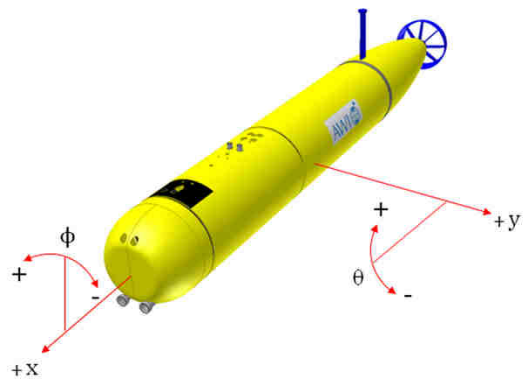


Fig. 5-4. Orientation of axes and angles used for depth correction.

5.6.2.2 Correction of PAR data

As the PAR measurement is an irradiance measurement and the PAR sensor is equipped with a cosine collector, the inclination of the sensor causes a shift in the data.

According to [Kirk \(1994\)](#), at a certain depth one can assume that most of the light in the water travels downwards. Thus, the inclination of the sensor with respect to the vertical is decisive for data correction. The real orientation of the sensor, represented by the normal vector of the sensor's sensitive surface (\vec{p}), can be calculated using rotation matrices like [Eq. 1](#). The inclination angle can be derived from the scalar product of the vertical vector \vec{z} and the direction vector of the PAR sensor \vec{p} .

Within a tolerance limit of 5° for the inclination angle following [Sturesh et al. \(2012\)](#), this yields to:

$$PAR_{corr} = \left(\frac{\vec{p} \cdot \vec{z}}{|\vec{p}| \cdot |\vec{z}|} \right)^{-1} \cdot PAR_{raw} \quad (7)$$

5.6.2.3 Correction of pump time delay

Some sensors in the vehicle are operated with a flow cell and thus are connected to a pumped water circuit. Depending on the flow rate and the volume of the respective supply line, a certain delay occurs in the sensor signal. For this reason, flow meters of the type 300-010 manufactured by Titan Enterprises Ltd. are installed in the supply lines. Unfortunately these devices are neither watertight nor pressure resistant. However, using silicone, they can be sufficiently sealed to measure the flow rate at the surface. Although the flow meters' electronics is destroyed when the vehicle starts a deeper dive, the devices remain in the supply lines so that the previously determined flow rate is not changed. In the flow meters, the flow rate is measured using a free-running paddle wheel spinning on a sapphire axis. Revolutions of that wheel are counted by a magnetic encoder. Although the flow meter is used in conditions way beyond its specifications as soon as the vehicle dives and might face pressure induced stress, the assumption is, the flow meter does not cause any changes in the flow rate as the paddle wheel is mechanically decoupled.

Based on the volume of the respective supply line and the measured flow rate at surface conditions, the signal delay is calculated for every parameter.

5.7 Results

Dividing the entire dive into separate mission phases has turned out to be advantageous. In the first phase the vehicle executes a number of Floats in a specific area to analyze the water column structure. In the second phase of the dive the vehicle dives down and starts taking water samples either in a constant depth or at different depth levels in ascending order. As the samples are collected during the last phase of the dive, they remain onboard the AUV for as short as possible before being processed and conserved in shipboard laboratories. When diving in the open water (no ice), the different phases of the dive are programmed within one single mission file. In the case of dives under or close to the ice edge, the unpredictable ice drift poses a serious risk to the vehicle as the preprogrammed surface point could be covered by ice. The individual phases of the dive are thus separated in short mission files of 1 – 2 h. After the vehicle completed a specific phase, it surfaces and allows the position, calculated by the INS, to be corrected via GPS and then waits for the next dive file. With these short missions the operator is able to adapt the dive plan according to the observed ice drift.

5.7.1 Open Water

Dive No. 3 of the expedition ARK 27/2 exemplarily represents one of *PAUL*'s open water dives (Fig. 5-5). The red circles represent positions where the vehicle took water samples. Fig. 5-6 shows the raw signal of the chlorophyll *a* fluorometer and the sample derived amount of chlorophyll *a*, both represented versus mission time of dive No. 3. The fluorometer was subsequently calibrated using these data and

additional data of one prior dive. The calibration curve is shown in Fig. 5-7.

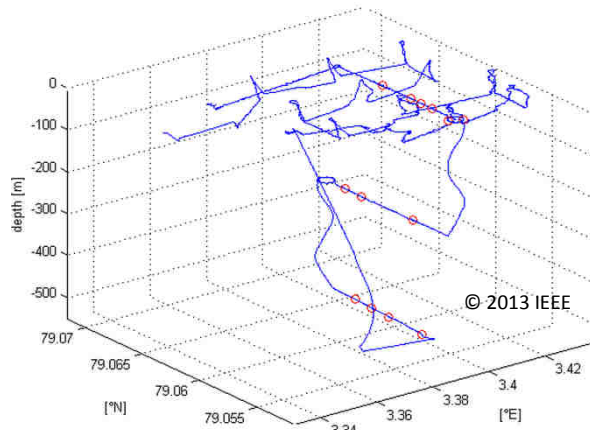


Fig. 5-5. Track of dive No. 3 (ARK 27/2).

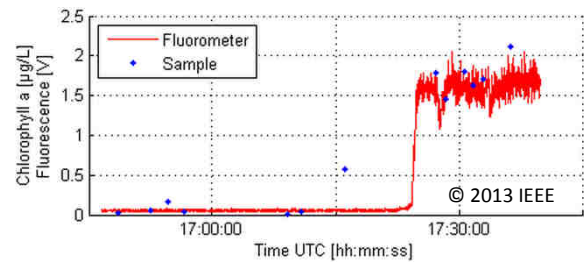


Fig. 5-6. Raw Fluorescence signal and sample derived chlorophyll *a* content versus UTC time (dive No. 3, ARK 27/2).

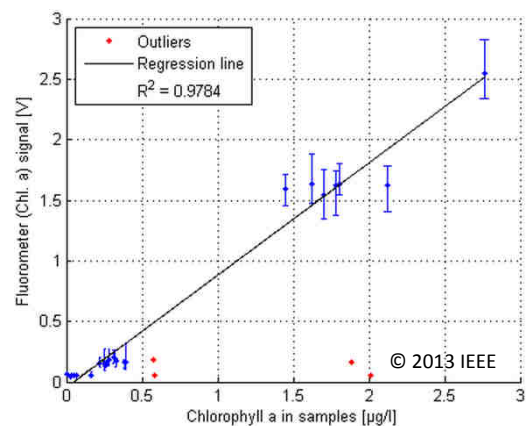


Fig. 5-7. Chlorophyll *a* calibration curve. The error bars represent the fluorometer values within +/- 5 s around the time the sample was taken. The blue dots represent the average values of these intervals.

Based on this calibration, the chlorophyll *a* distribution during the Float phase of dive No. 3 can be seen in Fig. 5-8. Data like nitrate (Fig. 5-9) or dissolved oxygen (Fig. 5-10) can be presented accordingly and show the expected correlations. Phytoplankton, indicated by the chlorophyll *a* value, produces oxygen and consumes nitrate as a nutrient. Thus, high chlorophyll *a* concentrations go along with low nitrate values and high dissolved oxygen values.

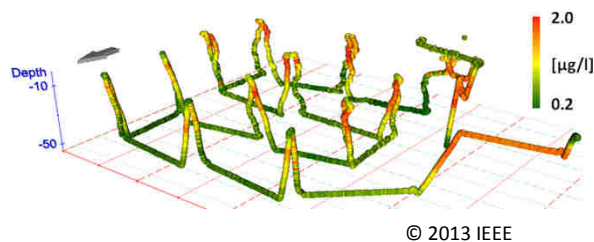


Fig. 5-8. Chlorophyll *a* distribution [$\mu\text{g}\cdot\text{l}^{-1}$] Float phase, dive No. 3.

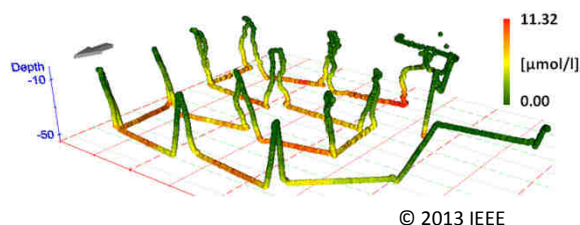


Fig. 5-9. Nitrate distribution [$\mu\text{mol}\cdot\text{l}^{-1}$] Float phase, dive No. 3.

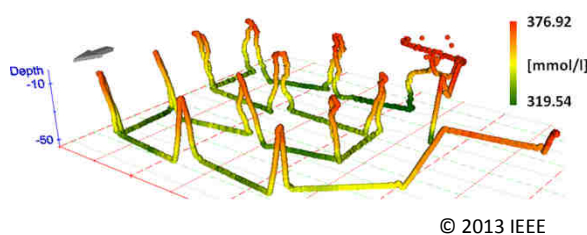


Fig. 5-10. Dissolved Oxygen [$\text{mmol}\cdot\text{l}^{-1}$] Float phase, dive No. 3.

5.7.2 B. Under Ice

The first two under ice dives, which *PAUL* accomplished in 2010 and 2011 respectively, were very similar (Fig. 5-11 and Fig. 5-12). As in the graphs before, the red circles indicate positions where the vehicle took water samples. Both missions were conducted at a constant depth of 27 m (2010) and 20 m (2011) and led the vehicle to a turning point about 2 - 2.5 km away from the ice edge. Both missions were accomplished under fast moving sea ice with a drift velocity of 1 - 1.5 $\text{km}\cdot\text{h}^{-1}$. The evolutions of the ice fields were observed using satellite images days before the dive. During both dives a horizontal light profile, which shall exemplarily be shown here, was obtained using the PAR sensor.

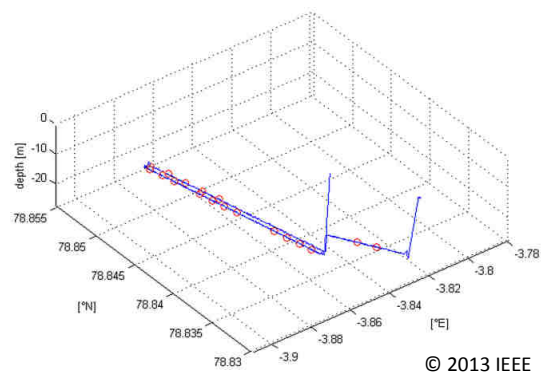


Fig. 5-11. Track of the very first under ice dive in 2010. After a short time at a depth of 20 meters the vehicle descended to the actual mission depth of 27 meters.

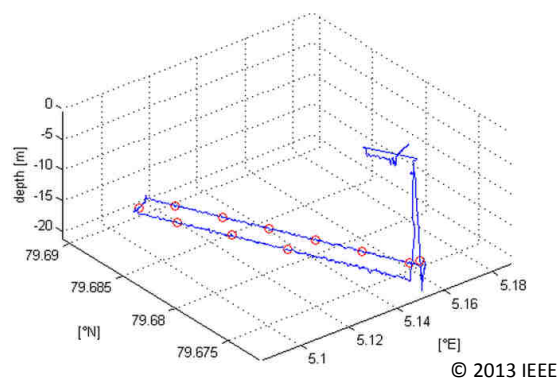


Fig. 5-12. Track of the under ice dive in 2011. The dive had to be aborted after half of the intended mission time. Thus the number of samples is relatively small.

Although the inbound and the outbound tracks are located close to each other, there is a time mismatch in between them. As the ice moves during the dive it makes no sense to merge the PAR data of the inbound and outbound track into one single profile. Instead of that, Fig. 5-13 and Fig. 5-14 exclusively show the light profiles of the respective inbound track.

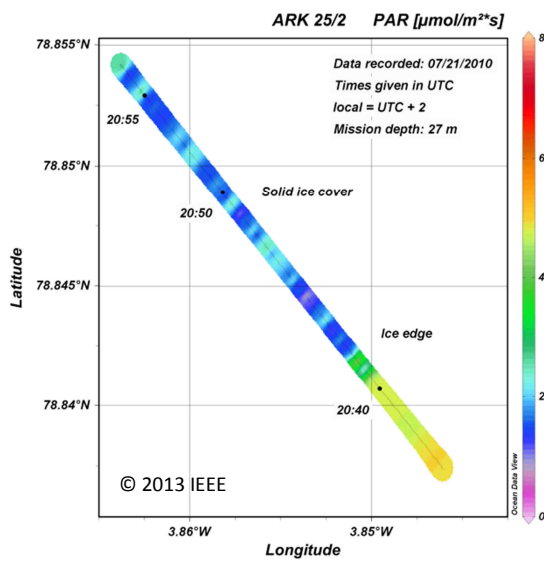


Fig. 5-13. Horizontal light profile (PAR) of the 2010 under ice dive.

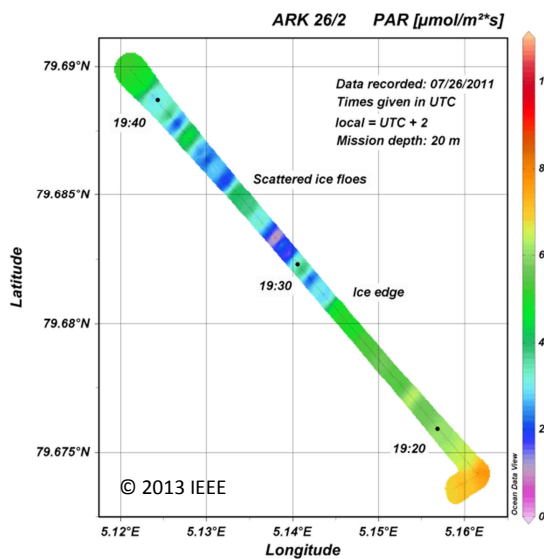


Fig. 5-14. Horizontal light profile (PAR) of the 2011 under ice dive. Notice the different PAR values below a solid ice cover and below a field of scattered ice floes.

In the framework of the Arctic expedition ARK 27/2 the Float maneuver was executed under ice for the first time. During dive 4A (July 24th 2012) the AUV started the Floats at a depth of 50 m and it approached the ice by a minimum distance of 10 m. In Fig. 5-15 and Fig. 5-16 the red and black lines indicate the positions of the ice edge at the beginning of the dive (red) and at the end of the dive (black), respectively. The positions were determined using the GPS tracking system mentioned in section 5.5.

Unfortunately, the power supply of the payload failed at the end of the dive, causing a severe data loss in the PCC. However, the data of the vehicle's CTD, which are shown in Fig. 5-15 and Fig. 5-16, and the position data of the water samples could be saved.

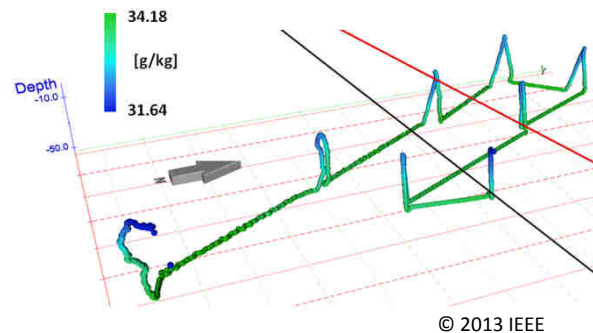


Fig. 5-15. Absolute salinity along the track of dive 4A. Notice the reduced salinity due to fresh water layers as the vehicle approaches the ice.

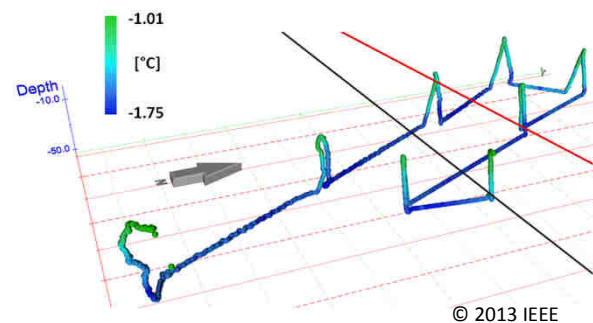


Fig. 5-16. Conservative Temperature along the track of dive 4A.

Comparing the Float data of an open water dive (dive No. 3) and the Float data of an under ice dive (dive No. 4A), the impact of melting sea ice on the water column below is clearly visible. Fig. 5-17 shows that the different water masses can be clearly distinguished by absolute salinity and density.

Dive No. 3 was conducted in an area influenced by the West Spitsbergen Current (WSC). Along the west coast of Spitsbergen, the WSC transports relatively warm and salty water from the Atlantic Ocean to the Arctic. In contrast, the data of dive 4A clearly show much fresher and lighter water, which is a result of melting sea ice.

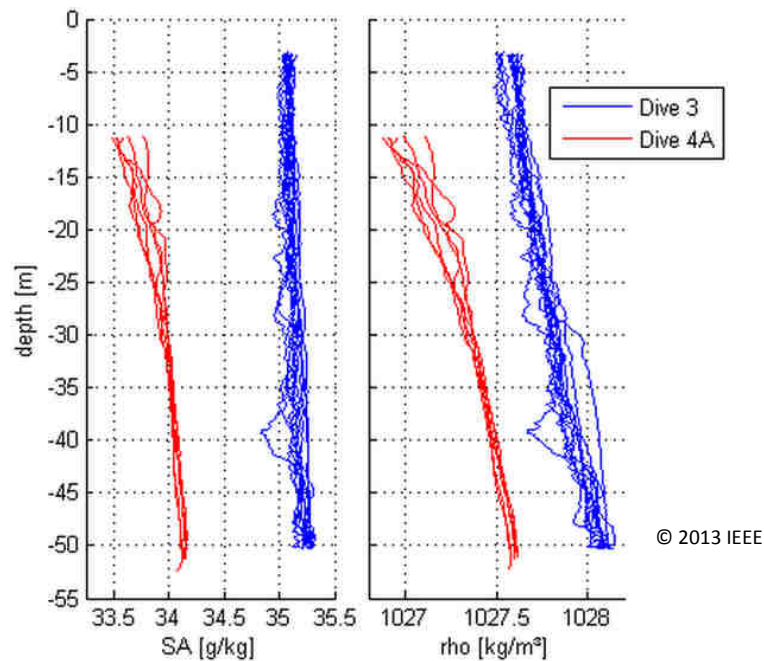


Fig. 5-17. Float profiles clearly show the difference between ice-influenced (Dive 4A) and purely Atlantic (Dive 3) water masses.

5.8 Discussion

Conducting water column operations with robots like AUVs entail technological challenges to every kind of vehicle. Starting at an altitude of approximately 130 m, *PAUL* is able to “see” the sea floor with the DVL and determine its exact velocity. When diving in the open water column without bottom lock for the DVL, the stationary reference is missing and navigation accuracy decreases. One option to provide the vehicle with a stationary reference is to deploy a Long Baseline (LBL) acoustic positioning system. However, the deployment of an array of transponder beacons is time-consuming and difficult to accomplish in a dynamic environment like the marginal ice zone. In contrast to that, USBL systems like GAPS can easily be operated from a ship. Using these systems, it is also possible to compensate navigation errors by detecting the vehicle’s position and transmitting position updates. However, the range of USBL systems is limited due to their relatively high tracking frequency. Additionally, the *R/V Polarstern* turned out to be a very noisy ship – making it almost impossible to establish a stable acoustic communication with the vehicle. Thus, staying in the range of the tracking system is not just for safety reasons but also to be able to subsequently correct the positioning data.

The first operations using the Float maneuver showed encouraging results. As no dynamic problems occurred and as the maneuver, to the current state of knowledge, does not significantly influence the vehicle’s navigation system, the Float maneuver can be expected to be used in future cruises as well. It has to be mentioned that all Floats which have been conducted to the present day, took approximately 4 to 4.5 min in average. The Float maneuvers started in 50 m depth and ended close to the surface. This might be sufficient to investigate the upper water

column, yet it has not been analyzed how longer Float phases influence the vehicle’s navigation system.

Especially while the vehicle is slowly ascending from the Float maneuver, it delivers high resolution data with an accurate depth stamp. However, the quality of the data can be further improved. Of particular interest are the data of the CO₂ and nitrate sensor. In the case of the CO₂ sensor the correction method proposed by [Fiedler et al. \(2013\)](#) is to be implemented in the future. In the case of the nitrate sensor the transmission of the sensor data via an analog signal reduces the data quality. As the analog signal does not contain any information about the recorded absorption spectra, the correction methods for bromide ions and CDOM ([Sakamoto et al., 2012](#), [Zielinski et al., 2011](#)) are currently not applicable. Although the SUNA nitrate sensor offers a special sea water mode, which makes the sensor using internal proxies to estimate bromide induced errors, there are some uncertainties remaining in the signal.

The data loss of the two under ice dives 4A and 4B during expedition ARK 27/2 is tragic as these dives represented one rare chance to combine physical and biochemical measurements from below the ice. Nevertheless, these dives demonstrated the enormous benefit marine research can derive from these kinds of AUV operations. Three dimensional imaging of the sensor data offers the possibility to quickly recognize correlations. As a final step of data imaging, there is currently work on software tools to interpolate in between the Floats and thus representing the data not just three dimensional, but volumetrically. This visualization method will provide the most intuitive impressions of what really happens in the oceans’ uppermost meters.

5.9 Acknowledgment

In the past four years the AUV project was supported by a large number of people. The contribution of Antje Boetius, Oliver Zielinski and Frank Wenzhöfer should be particularly highlighted here as they decisively influenced the scientific orientation of the AUV project. Also, the authors would like to specially thank Uwe Wulff, a retired mathematician who set up an entirely new basis for AUV data processing and management. We thank Bluefin Robotics for their repeated support and especially Will O'Halloran who initially came up with the idea of a floating vehicle. The project has largely profited from the contribution and help of Jonas Hagemann, Thomas Soltwedel, Normen

Lochthofen, Ilka Peeken, Michael Schlüter, Roi Martinez, Torben Gentz, Jana Hölscher, Kristin Hardge, Adam Mara, Kai-Uwe Ludwichowski and the professional support of the crews of R/V *Heincke* and R/V *Polarstern*.

Part of the scientific payload was developed with the financial support of the European Commission's 7th Framework Program (Research Infrastructures) EUROFLEETS (Contract No. 228344). Additionally, the financial contribution of the Institut français de recherche pour l'exploitation de la mer (Ifremer) for the development of the water sample collector is gratefully acknowledged.

5.10 References

- Arrigo K.R., van Dijken G., Pabi S., (2008). “*Impact of a shrinking ice cover on marine primary production*”, *Geophys. Res. Lett.*, 35(19).
- Bird L.E., Sherman A., Ryan J., (2007). “*Development of an active, large volume, discrete seawater sampler for autonomous underwater vehicles*”, In *Oceans 2007*, Conference Publication, IEEE, 1-5
- Brierly A.S., Fernandes P.G., Brandon M.A., Armstrong F., Millard N.W., McPhail S.D., Stevenson P., Pebody M., Perrett J., Squires M., Bone D.G., Griffiths G., (2002). “*Antarctic Krill under sea ice: Elevated abundance in a narrow band just south of ice edge*”, *Science*, 295(5561), 1890-1892
- Büchel C. & Wilhelm C., (1993). “*In vivo analysis of slow chlorophyll fluorescence induction kinetics in algae: progress, problems and perspectives*”, *Photochem. Photobiol.*, 58(1), 137-148
- Cowles T.J. & Desiderio R.A., (1993). “*Resolution of biological microstructure through in situ fluorescence emission data: an oceanographic application using optical fibres*”, *Oceanography*, 6(3), 105-111
- Deksheniaks M.M., Donaghay P.L., Sullivan J.M., Rines J.E.B., Osborn T.R., Twardowski M.S., (2001). “*Temporal and spatial occurrence of thin phytoplankton layers in relation to physical processes*”, *Mar. Ecol.-Prog. Ser.*, 223, 61-71
- Earp A., Hanson C.E., Ralph P.J., Brando V.E., Allen S., Baird M., Clementson L., Daniel P., Dekker A.G., Fearn P.R.C.S., Parslow J., Strutton P.G., Thompson P.A., Underwood M., Weeks S., Doblin M.A., (2011). “*Review of fluorescent standards for calibration of in situ fluorometers: recommendations applied in coastal and ocean observing programs*”, *Opt. Express*, 19(27), 26768-26782
- Fiedler B., Fietzek P., Vieira N., Silva P., Bittig H.C., Körtzinger A., (2013). “*In situ CO₂ and O₂ measurements on a profiling float*”, *J Atmos. Ocean. Tech.*, 30(1), 112-126
- Johnson K.S., Coletti L.J., (2002). “*In situ ultraviolet spectrophotometry for high resolution and long-term monitoring of nitrate, bromide and bisulfide in the ocean*”, *Deep-Sea Res. Pt. I*, 49(7), 1291-1305
- Kirk J.T.O., (1994). “*Light and photosynthesis in aquatic ecosystems*”, 2nd Edition., p. 113, ISBN 0 521 45353 4
- Lehmenhecker S. & Wulff T., (2013) “*Flying drone for AUV under-ice missions*”, *Sea Technology*, 54(2), 61-64
- McPhail S.D., Furlong M.E., Pebody M., Perrett J.R., Stevenson P., Webb A., White D., (2009). “*Exploring beneath the PIG ice shelf with the Autosub3 AUV*”, In *Oceans 2009 – Europe*, Conference Publication, IEEE, 1-8
- Niebauer H.J. & Smith W.O., (1989) “*A numerical model of mesoscale physical-biological interactions in the Fram Strait marginal ice zone*”, *J. Geophys. Res.*, 94(C11), 16151-16175
- Perkin R.G., Lewis E.L., (1984). “*Mixing in the West Spitsbergen Current*”, *J. Phys. Oceanogr.*, 14(8), 1315-1325

- Ryan J.P., McManus M.A., Paduan J.D., Chavez F.P., (2008). “*Phytoplankton thin layers caused by shear in frontal zones of a coastal upwelling system*”, Mar. Ecol.-Prog. Ser., 354, 21-34
- Sakamoto C.M., Johnson K.S., Coletti L.J., (2009). “*Improved algorithm for the computation of nitrate concentrations in seawater using an in situ ultraviolet spectrophotometer*”, Limnol. Oceanogr., 7(1), 132-143
- Smith W.O., Baumann M.E.M., Wilson D.V., Aletsee L., (1987). “*Phytoplankton biomass and productivity in the marginal ice zone of the Fram Strait during summer 1984*”, J. Geophys. Res., 92(C7), 6777-6786
- SooHoo J.B., Kiefer D.A., Collins D.J., McDermid I.S., (1986). “*In vivo fluorescence and absorption spectra of marine phytoplankton: I. taxonomic characteristics and responses to photoadaptation*” J. Plankton Res., 8(1), 197-214
- Suresh T., Talaulikar M., Desa E., Matondkar S.G.P., Kumar T.S., Lotlikar A., (2012). “*A simple method to minimize orientation effects in a profiling radiometer*” Mar. Geod., 35(4), 441-454
- Tsai R.Y. & Lenz R.K., (1989). “*A new technique for fully autonomous and efficient 3D robotics hand/eye calibration*”, Transactions on Robotics and Automation, IEEE, 5(3), 345-358
- Wulff T., Lehmenhecker S., Hoge U., (2010). “*Development and Operation of an AUV-based Water Sample Collector*”, Sea Technology, 51(12), 15-19
- Zeebe R.E. & Wolf-Gladrow D., (2001). “*CO₂ in seawater: equilibrium, kinetics, isotopes*”, Elsevier Oceanography Series, 65, p. 4
ISBN: 0 444 50946 1
- Zielinski O., Fiedler B., Heuermann R., Körtzinger A., Kopiske E., Meinecke G., Munderloh K., (2007). “*A new nitrate continuous observation sensor for autonomous sub-surface applications: Technical design and first results*” Oceans 2007 – Europe, Conference Publication, IEEE, 1-5
- Zielinski O., Voß D., Saworski B., Fiedler B., Körtzinger A., (2011). “*Computation of nitrate concentrations in turbid coastal waters using an in situ ultraviolet spectrophotometer*”, J. Sea Res., 65(4), 456-460

6 Third Study (Manuscript III)

Flying Drone for AUV Under-Ice Missions

Sascha Lehmenhecker^{a,*}, Thorben Wulff^a

^a) AWI – Alfred Wegener Institute Helmholtz Centre for Polar and Marine Research
HGF-MPG Joint Research Group for Deep Sea Ecology and Technology
Am Handelshafen 12, 27570 Bremerhaven, Germany

*) Corresponding Author
Tel: +49 (0) 471 4831 1349
Fax: +49 (0) 471 4831 1776
Mail: Thorben.wulff@awi.de

Published by Sea Technology in February 2013 (Sea Technology, 54(2), 61-64)

(An Abstract is normally not included in Sea Technology Publications. It was added in the thesis to achieve a consistent formatting.)

6.1 Abstract

Since 2010, the Autonomous Underwater Vehicle (AUV) of the Alfred Wegener Institute Helmholtz Centre for Polar and Marine Research has accomplished several missions in the Arctic Marginal Ice Zone (MIZ). To minimize the risk of deployments in the MIZ, detailed information on the drift of the ice is needed. Thus, the ice edge needs to be marked using GPS receiving / transmitting units. To facilitate this process a radio controlled hexacopter was developed that lands on the ice, determines its position via GPS and constantly transmits it to a support vessel. Additionally, the hexacopter measures the intensity of the incoming Photosynthetically Active Radiation (PAR). In this study, the design of the hexacopter and its functional principles are described. As soon as it touches down on the ice, the hexacopter switches to a hibernation mode to save energy. Results of two separate Arctic deployments, each of 5.5 hours duration, are presented.

6.2 Introduction and Preconditions

Starting in 2010, the Alfred Wegener Institute (AWI) has deployed a Bluefin Robotics Corp. (Quincy, Massachusetts) Bluefin-21 AUV in several dives under Arctic sea ice. All dives were conducted close to AWI's deep-sea observatory, HAUSGARTEN, which is located west of the Svalbard Archipelago in the ice-margin zone of the Fram Strait.

Since the ice-margin zone is a highly dynamic environment, it is crucial to track the position of the ice edge to define the AUV's mission parameters. In 2011, a GPS-based tracking system was developed to mark the ice edge and to observe the ice drift before and during an under-ice dive.

However, deploying the transmitters on the ice turned out to be risky and time-consuming. To facilitate the deployment of the tracking system on the ice, a remotely controlled flying drone was developed for polar operations.

Basic Conditions

The major goal was to design a vehicle able to carry a GPS transmitter along with other instruments onto the ice and back without using, for example, a rigid inflatable boat (RIB) for deployment. Conceptual plans considered the flying drone as a transporter that deploys instruments on the ice and then flies back to the ship. After completing all the measurements, the drone would return and recover the instruments from the ice. However, fog and the ice drift could cause difficulties in finding the location again.

Thus, it was decided the drone would land on the ice and stay there to act as a GPS transmitter. Along with the GPS transmitter, a sensor for photosynthetically active radiation (PAR) would be integrated to measure light on the ice and represent a surface reference for the AUV's PAR sensor. As AUV dives may take up to 10 hours, an operational time of 14 hours on the ice was considered to be mandatory for the drone.

6.3 Methodology

Preliminary tests conducted with a four-engine drone, or quadcopter in harsh conditions such as crosswinds proved reduced in-flight stability compared to a six-engine drone concept, or hexacopter. A hexacopter can also lift larger weights than a quadcopter of the same size and offers bigger safety reserves. For example, a hexacopter is able to compensate for the stability

problems caused by an engine failure, whereas a quadcopter would suffer an uncorrectable thrust imbalance and most likely a crash.

The hexacopter's mainframe consists of an aluminum frame with six arms arrayed radially outward from a center point (Fig. 6-1). The arms are made of square tubes (15 mm by 15 mm) and have a length of 350 mm each. At the center point, the entire electronics of the hexacopter is mounted in a lightweight carbon structure. For insulation, the hexacopter is protected by a 3 cm thick Styrofoam hull. Only the ends of the aluminum arms and the PAR sensor stick out of the hull. Additionally, the insulation offers sufficient buoyancy to make the hexacopter float in case of a crash or an emergency landing.

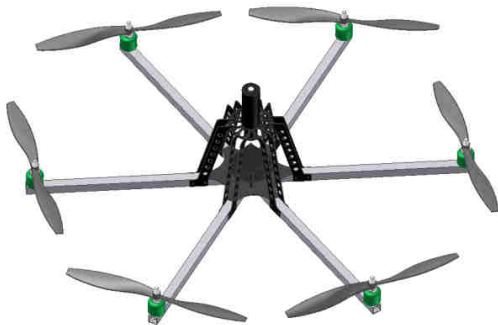


Fig. 6-1. A computer-aided design model of the hexacopter.

For visibility reasons, the outer hull of the hexacopter is painted in bright orange. Only a vertical line at the rear side of the hexacopter and the upper side of the hull are painted in black. With the black line, the pilot can determine the hexacopter's orientation. The black topside of the hull is to minimize the reflection of incoming sunlight so that the PAR sensor measures the downward radiation flux exclusively.

Six brushless motors with a shaft power of 110 W are mounted at the end of the arms and

point upwards. All motors have 12-inch-by-4.5-inch fixed-pitch propellers. With this propeller size and the engines running at a maximum speed of 10,000 revolutions per minute, the thrust of the hexacopter is approximately 47 N. As the hexacopter itself weighs about 3 kg, or 29 N, the remaining 18 N can be used for dynamic flight control. Roll, pitch and yaw rate of the hexacopter are controlled exclusively via motor speed. A microcontroller processes the control commands of the pilot and the data of an onboard gyro to provide stable maneuverability throughout the flight. The hexacopter is remotely controlled by a radio transmitter operating at a frequency of 35 MHz.

The hexacopter's payload includes a GPS receiver, a UHF transmitter to broadcast the GPS position to the ship (869 MHz, 500 mW), a Satlantic LP (Halifax, Canada) PAR-LOG-S sensor and a data logger for the PAR data. In contrast to the position data, the PAR data are not transmitted via UHF but stored internally. The measurement interval of the position, as well as the interval of the PAR measurement, is 1 Hz. The hexacopter's power supply consists of three Hacker Motor GmbH (Ergolding, Germany) TopFuel LiPo 30C-LIGHT 4,000 mAh 3S lithium polymer batteries, with 11.1 V, 45 Wh and an overall nominal capacity of 12 Ah. Two of the batteries (8 Ah) are assigned to the engine circuit, providing power for flight electronics and engines.

With an average power consumption of 32 A during flight, the hexacopter is able to fly for about 15 minutes. One battery (4 Ah) is assigned to the payload circuit, providing power for the GPS receiving-transmitting unit, the PAR sensor and its data logger. To extend the endurance of the hexacopter, an energysaving sleep mode was implemented.

In this mode, flight electronics, which normally consume up to 0.4 A in standby, are almost entirely switched off and only the payload circuit remains powered.

As lithium polymer cells are commonly known to react quite sensitively at low temperatures, and as the hexacopter's interior is not actively heated, the batteries had to be tested in cold conditions. Cooling the cells down to -4°C resulted in a 10 % capacity loss, which was defined as tolerable. Additionally, after spending several hours on the ice and with its cells entirely cold, the hexacopter has to take off from the ice again, forcing the cells to cope with high currents of up to 68 amperes during launch phase. Tests with the hexacopter at temperatures of -7°C proved the currents to be unproblematic.

6.4 Results

Initial Arctic deployment of the hexacopter took place in the Fram Strait in July 2012 during expedition ARKXXVII/ 2 using the R/V *Polarstern* (Fig. 6-2).

In order to mark the ice edge and prepare an under-ice dive of AWI's Bluefin-21 AUV, the hexacopter was deployed at a position close to $79^{\circ} 50' \text{ N}$ and $3^{\circ} 40' \text{ E}$. The ice field consisted of fast moving, different-sized, separate ice floes. *Polarstern's* radar was used to determine the general orientation of the ice edge and to find suitable floes to mark the field.

Eventually, the hexacopter lifted off from *Polarstern's* stern deck and landed on the ice within sight range. An additional GPS transmitter was deployed using an RIB 1 km further east to clearly mark the ice edge's orientation. With *Polarstern* leaving the area, the hexacopter started to transmit its position and gather PAR data. Meanwhile, the AUV was deployed and the inertial navigation system alignment procedure was started, giving the operator time to observe the ice drift and adjust the AUV's mission file accordingly.

After two dives in the ice-margin zone and a total mission time of about 3.5 hours submerged, the AUV was recovered and *Polarstern* approached the position of the hexacopter.



Fig. 6-2. The hexacopter on the ice edge in the Arctic.

When the hexacopter came into sight, it was woken up from sleep mode and flown back to *Polarstern*. It landed back safely on the vessel after having spent 5.5 hours on the ice. Waking up the hexacopter from its sleep mode and lifting off from the ice were carried out without any problems. During a second deployment on the following day, the hexacopter logged another 5.5 hours on the ice. The maximum distance between the hexacopter and *Polarstern* while still receiving a signal was 3 km. The hexacopter drifted to the southwest following a heading of

roughly 247 degrees at an average speed of about $1 \text{ km}\cdot\text{h}^{-1}$ (Fig. 6-3).

The orientation of the ice edge was almost 90 degrees, with the ice in the north. Data acquisition with the PAR sensor worked flawlessly. As it was a day with scattered clouds, the PAR diagram showed the expected spikes and dips, with a smooth decline towards the evening. Nevertheless, due to the polar day, the PAR values remained relatively stable throughout the day.

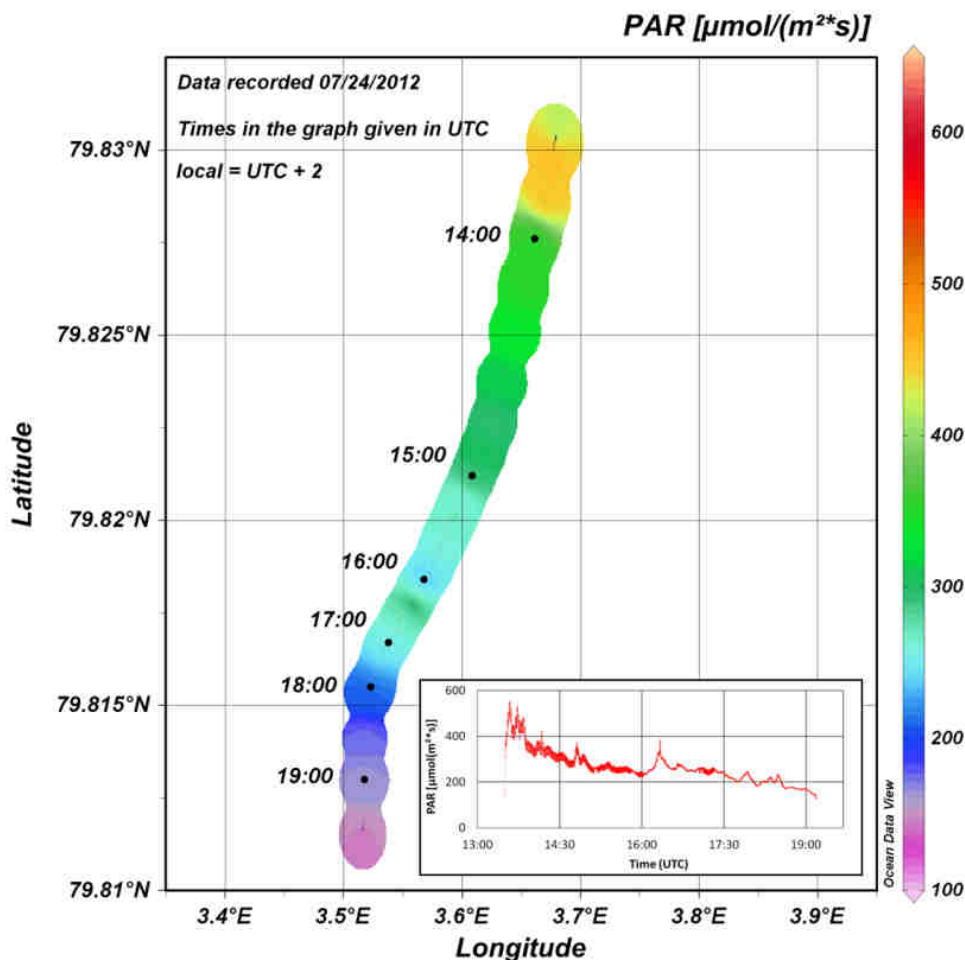


Fig. 6-3. Map showing the hexacopter's drift and the development of PAR values over time.

6.5 Future Prospects

The hexacopter is a platform that could be useful to all kinds of experiments. By marking the ice edge and conducting PAR measurements, expedition ARK-XXVII/2 demonstrated only one way that marine operations could benefit from flying drones. The plan is to enlarge the working range of the hexacopter significantly with, for instance, camera controlled flights, improved communication abilities and more autonomy via an automatic homing system.

At least for 2013, the scientific payload will remain the same. However, the type of PAR sensor will be changed from one with logarithmic output to a sensor with linear output (Satlantic's PAR-LIN-S). Within the range of the measured PAR values, which were relatively high on the surface of the ice, a linear sensor offers a higher resolution, whereas a logarithmic PAR sensor is used on AWI's AUV to make use of its high resolution at low PAR values.

Additionally, since PAR sensors are equipped with a cosine collector, the inclination of the hexacopter with respect to the sun is important. Especially as the hexacopter is operated in high latitudes where the sun remains low above the horizon, the resulting error caused by a tilted and moving sensor, for example, due to waves under the ice, is relatively big. To correct the data, the inclination angles of the hexacopter (taken from its gyro) and its orientation (using the compass) will be logged in the future.

6.6 Acknowledgments

The authors would like to thank Kimberly Shurn of Bluefin Robotics for her valuable assistance in feeding the signals of various GPS transmitters into Bluefin's AUV Dashboard control software.

7 Fourth Study (Manuscript IV)

Correcting Navigation Data of Shallow Diving AUV in Arctic

Uwe Wulff, Thorben Wulff^{a, *}

^{a)} AWI – Alfred Wegener Institute Helmholtz Centre for Polar and Marine Research
HGF-MPG Joint Research Group for Deep Sea Ecology and Technology
Am Handelshafen 12, 27570 Bremerhaven, Germany

^{*}) Corresponding Author
Tel: +49 (0) 471 4831 2045
Fax: +49 (0) 471 4831 1776
Mail: Thorben.wulff@awi.de

Published by Sea Technology in March 2015

(Sea Technology, 56(3), 27-30.)

(An Abstract is normally not included in Sea Technology Publications. It was added in the thesis to achieve a consistent formatting.)

7.1 Abstract

Operations in the open water column can significantly reduce the navigation accuracy of an autonomous underwater vehicle (AUV). If the vehicle conducts shallow dives, the sea floor can be out of range for the AUV's tracking systems. Lacking of this fix reference, the vehicle exclusively depends on its inertia navigation system (INS) which inevitably entails a certain drift. The Alfred Wegener Institute Helmholtz Centre for Polar and Marine Research (AWI) in Bremerhaven, Germany, conducts shallow missions with its Bluefin-21 AUV below Arctic sea ice. To georeference the measurements exactly, the AUV's navigation data need to be corrected.

Here, an algorithm correcting the navigation data via the tracking results of the ultra short baseline (USBL) system "GAPS" is presented. Based on careful analyses, filter criteria could be defined to eliminate unrealistic tracking results. In a four-step process the remaining tracking results are used to correct the vehicle's navigation data. Results of the correction algorithm are exemplarily depicted using the data of a dive which was conducted in summer 2012 in the Arctic. During this dive, a new maneuver that makes the vehicle float freely was executed for the first time under ice. Navigation accuracy was strongly degraded, making this particular dive a good demonstration object for the algorithm.

7.2 Introduction and Preconditions

In 2008, the Alfred Wegener Institute Helmholtz Center for Polar and Marine Research (AWI) in Bremerhaven, Germany, started refocusing its robotic exploration program in the Arctic. Since then, under the general term of “Biogeochemical Research,” a Bluefin-21 AUV from Bluefin Robotics (Quincy, Massachusetts) has been deployed to investigate, for example, primary production and the distribution of nutrients in the Arctic marginal ice zone. The vehicle is equipped with various sensors and a water sample collector. Its main site of operation in the Arctic has been the Fram Strait between Svalbard and Greenland where the AWI has run the permanent deep-sea observatory HAUSGARTEN since 1999.

Here, we describe a correction algorithm used during post-processing of the vehicle’s navigation data. Using position data of an external tracking system, this algorithm reconstructs the actual dive track of the AUV and provides reliable navigation data to georeference scientific measurements accurately.

Basic Preconditions

The majority of biogeochemical processes in the sea are closely related to the uppermost meters of the water column. Concerning the distribution of biogeochemical parameters, the Arctic marginal ice zone features high spatial variability in small areas. In order to investigate these steep gradients correctly, the assigning of the measurements to reliable navigation data is crucial. However, operating in these conditions entails a number of problems for the vehicle, as it has to navigate close to the surface, and thus, depending on the respective water depth, it might be unable to establish bottom tracking with its Doppler velocity log (DVL).

As a consequence, the vehicle will not have a reference to determine its exact velocity and heading.

AWI’s AUV also conducts “Float maneuvers” that place an additional burden on the vehicle’s navigation system. During this maneuver the thruster of the AUV is deactivated, making it behave like a float and record a high-resolution vertical profile of the water column as it ascends. Due to the missing “bottom lock” and the Float maneuver, the navigation accuracy is reduced.

External tracking systems can improve the quality of AUV navigation data. It is common to use long baseline (LBL) networks to support the navigation of a vehicle, although the exact deployment of the acoustic beacons is a time-consuming operation. In a fast-changing environment such as the Arctic marginal ice zone, with the ice achieving drift speeds of $1.5 \text{ km}\cdot\text{h}^{-1}$ and more, these kinds of operations are difficult to carry out. Although they have a smaller range, ship-bound ultrashort baseline (USBL) systems, which can be operated with less effort, can be used alternatively.

Since 2011, AWI has used the USBL system “GAPS” from iXBlue (Marly le Roi, France) to track the vehicle. According to iXBlue, this system offers a tracking range of 4,000 m distance in every direction and an opening angle of 200° . Thus, the system can still track objects close to the surface, although the transducer is positioned underneath a ship’s hull. GAPS provides both the geographical position and the depth of a tracked object.

The AUV itself is equipped with a KN-5053 INS manufactured by Kearfott (Little Falls, New Jersey).

Additional sensors for navigation include a downward-looking Workhorse DVL operating at 300 kHz (Teledyne RD Instruments, Poway, California), a 4,000 m depth-rated Digiquartz pressure sensor (Paroscientific, Redmond,

Washington), a DG-14 GPS receiver (Thales Navigation, San Dimas, California) and an SBE 49 FastCAT CTD probe to determine sound velocities (Sea-Bird Electronics, Bellevue, Washington).

7.3 Methodology

In summer 2012 there was relatively little experience with the Float maneuver, and the optimal dive settings had not been found yet. Thus the deviations that occurred during the dives were relatively big and well-suited for testing the correction algorithm. In this article, the correction algorithm is explained at an exemplary dive (AWI number: PS80/187-2) during Arctic expedition ARK 27/2 in July 2012 (R/V *Polarstern*). It represents the first mission in which the Float maneuver was conducted below Arctic sea ice. During this mission the Float maneuver was executed between 50 and 10 m depth. Maximum horizontal distance between the vehicle and R/V *Polarstern* was approximately 2 km.

An analysis of the data shows the high consistency of the AUV data. In terms of vehicle speed and heading, all consecutive positions are realistic. Position updates are calculated in steady intervals without any interruptions. In this case the vehicle updated its position every 0.1 s. However, after a mission is accomplished and the vehicle is back on the surface, an unrealistic “jump” appears in the navigation data. As soon as the vehicle is on the surface it determines its position via GPS and corrects its INS-based navigation data accordingly. Plotting these raw data on a map, this correction process occurs as an apparent gap, or jump, in the track. In contrast, analyzing the GAPS acoustic tracking data results in a different picture. Density shifts in the water column can refract sound waves and can cause tracking errors or even a complete loss of signal (LOS). Due to this, the GAPS data show less consistency than the vehicle data. However, when the vehicle is on the surface and receives a GPS signal, both the vehicle and the GAPS data match remarkably

well. As GPS is a reliable positioning source it can thus be concluded that GAPS is reliable as well, but outliers need to be removed.

One particular feature of the GAPS data became important during the development of the algorithm. As previously mentioned, GAPS also calculates the depth of a tracked object. Obviously unrealistic positions frequently go along with depth values that seem to be unrealistic as well. In contrast to the position data, the parameter “depth” can be compared to a reliable source that is permanently available during the dive: the depth sensor of the vehicle. Due to the close correlation described before and assuming that the AUV’s depth sensor is correct, a comparison of the two depth data sets (GAPS + AUV) can serve as a filter criterion to identify outliers in the GAPS position data.

The entire correction process can be divided into four different phases that gradually yield an improvement of the result.

7.3.1 Phase 1

In phase one (Index: PI), only the raw AUV data (Index: $P0$) are processed (Fig. 10-1). The function of the algorithm is exemplarily depicted by correcting the latitude value. The difference between the last INS-determined position ($AUV_{Lat\ INS}$) and the first GPS-determined position ($AUV_{Lat\ GPS}$) roughly represents orientation and extent of the spatial drift the INS experienced during the dive. For this first phase of the correction process, a constant drift of the INS and therefore a linear increase of the navigation error are assumed.

Thus, with N_{total} representing the total number of navigation updates exclusively based on the INS

and $N_{total}(t)$ representing the number of AUV navigation updates at a time t , this yields to:

$$AUV_{Lat P1}(t) = AUV_{Lat P0}(t) + \left[N_{total} \cdot \frac{\Delta Lat_{GPS-INS}}{N_{total}} \right] \quad (1)$$

variates, d_1 represents the shallower value and d_2 the deeper value. With two filter coefficients and the damping exponent x , the tolerance scale z_{tol} can be expressed as:

$$z_{tol} = d_1 \cdot (\varphi_A \cdot (\varphi_B)^x - 1) \quad (2)$$

$$\text{with} \quad x = \frac{\log(d_1)}{\log(2)} \quad (3)$$

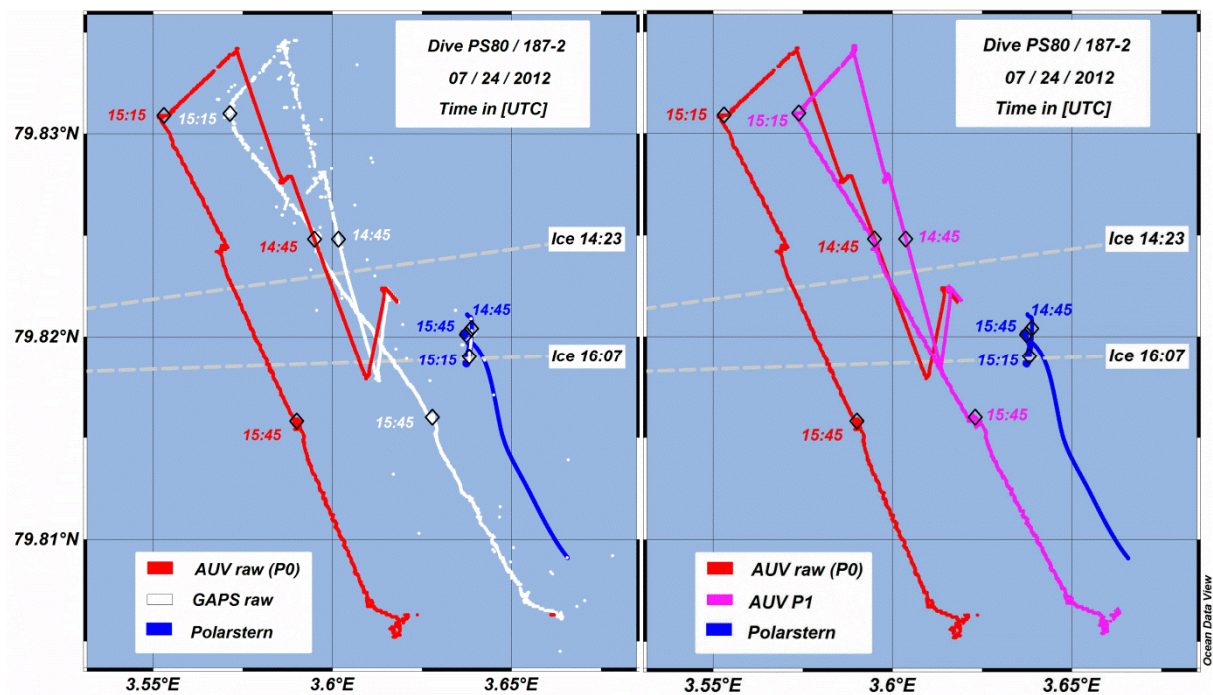


Fig. 10-1. Raw data of the AUV and GAPS (left) and phase one AUV data (right).

7.3.2 Phase 2

In phase two (Index: $P2$), the algorithm starts processing the GAPS data and removes outliers. It takes advantage of the close correlation between unrealistic position and depth values, which was described before. Derived from the GAPS and AUV depth data, a tolerance scale z_{tol} is defined to identify outliers in the GAPS data set.

For every time step, two different depth values (GAPS + AUV) are available. In this pair of

The first filter coefficient defines the initial extent of the tolerance scale. The second filter coefficient with the damping exponent restricts the size of z_{tol} , which otherwise would increase with depth.

The tolerance scale z_{tol} represents the maximum difference between the two depth values d_1 and d_2 . If the difference of a specific pair exceeds the respective value of z_{tol} , the associated GAPS position is considered to be invalid and thus ignored in the further process. In this particular case the two filter coefficients had the values 5.0

and 0.9, respectively. Using this method, a relatively coarse filter, which is unable to eliminate outliers completely, is applied to the data. For this particular dive, roughly 75 % of the GAPS data was accepted as valid.

minimal number of elements within these sequences is given by the variable n_s .

The last elements of each of these sequences are used to calculate a weighted average—pushing the calculated position towards the more reliable end of the sequence.

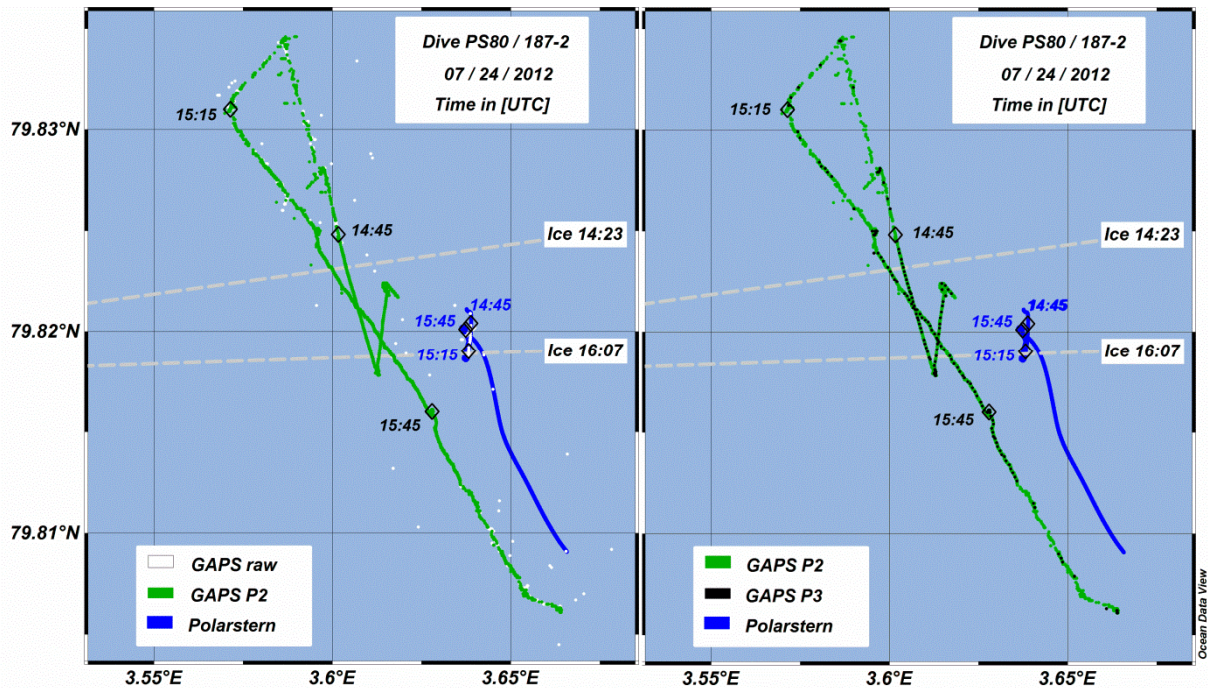


Fig. 10-2. Raw GAPS data overlaid by phase two data (left) and phase three “knots” (right).

7.3.3 Phase 3

In phase three of the correction process (Index: $P3$), the algorithm determines locations that the AUV “most likely” passed during the dive (Fig. 10-2). Following the naming convention used for spline functions, these special locations are further referred to as “knots.” In order to identify these knots, the basic assumption was that the longer a period of consecutive tracking results is not interrupted by an LOS, the more reliable the position data are. For this reason, the algorithm looks for sequences with a certain minimal number of consecutive tracking results (elements) from the set of valid GAPS data. The

The number of elements included in this weighted average is specified by variable n_A . In order to define a time stamp for the knots, they are assigned to the recording time of the last element of the respective sequence. A depth is defined by selecting the respective depth value of the AUV (AUV_{depth}). For a time T_x that represents the recording time of the last element of a sequence, the knot (K_{P3}) can now be described in all four dimensions (Eq. 4).

$$K_{P3}(T_x) = \begin{pmatrix} K_{Lat P3}(T_x) \\ K_{Lon P3}(T_x) \\ AUV_{depth}(T_x) \\ T_x \end{pmatrix} \quad (4)$$

Here, 15 elements were applied to n_s to identify sequences. The weighted average was calculated using the last five elements (n_A). For this dive, the number of knots was only 4 % of the valid GAPS data. These knots are considered to be locations at which the AUV was de facto.

7.3.4 Phase 4

In the fourth and final phase of the correction process (Index: $P4$), the preliminarily corrected AUV data of phase one are merged with the phase three knots derived from GAPS (Fig. 10-3). As the number of knots is relatively small compared to the number of AUV navigation data points, the track of the vehicle between the knots has to be approximated.

As in phase one, a linear increase of the navigation error is assumed and a similar approach to correct it can be applied.

By means of the time stamp, particular positions of the AUV P1 data set can be assigned to knots and can be relocated onto them. These particular positions in the P1 data set are further referred to as “fixpoints”. This cuts the P1 dataset into sections with a fixpoint representing the beginning of each section. Maintaining their original orientation and length, every section and the associated fixpoint are moved via parallel translation until the fixpoint is located on its respective knot. The algorithm calculates the error (distance and orientation) between a knot and the last position of the previous section. According to the assumed linear increase of the navigation error, this measured error is then distributed on the elements of the section - rotating the section around its fixpoint and stretching it until it bridges the space between two consecutive knots. Using this approach from knot to knot, the entire track of the vehicle can be reconstructed piecemeal.

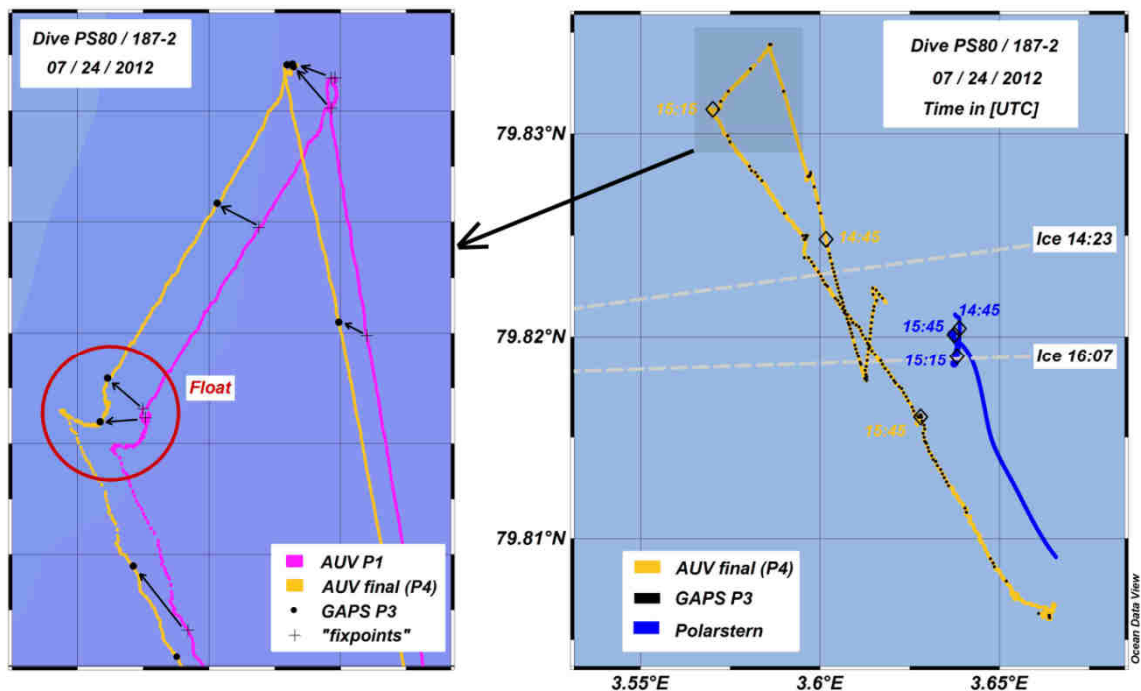


Fig. 10-3. Relocation of “fixpoints” onto time-synchronous knots during phase four (left) and the final result after the entire correction process (right).

7.4 Discussion

The correction algorithm described in this article is an attempt to merge the advantages of two error-containing sources for navigation data, so that the result is a reliable reconstruction of the actual AUV track. However, it is to be mentioned that the result does not represent the “absolute truth.” Changing the coefficients, the algorithm can be adjusted, thus, like in any other statistical method, there is some uncertainty remaining in the result. Additionally, physical parameters that have an influence on sound propagation in water (density, temperature, salinity) are highly variable in the Arctic marginal ice zone. These conditions restrict the performance of every acoustic tracking system. Taking this into account and considering that the vehicle operated close to an ice cover, GAPS performed very well.

Considering the navigation error that occurred during this exemplary dive (PS80/187-2), correction methods are necessary to gather resilient scientific data during these kinds of AUV missions. It is clear to see that the algorithm tremendously improves the quality of the navigation data. Meanwhile the navigation errors due to the Float maneuver have been minimized. However, as the vehicle still conducts missions without bottom lock, deviations in navigation data did not vanish completely. For this reason, the herein described algorithm is used by default at AWI.

7.5 Acknowledgments

The authors would like to thank Ulrich Hoge (AWI) for installing and operating GAPS on R/V *Polarstern* and Normen Lochthofen (AWI) for his support in handling GAPS raw data. Additionally, the authors would like to thank James Kinsey from Woods Hole Oceanographic Institution (WHOI) for a very interesting meeting in Bremen in April 2013, which ultimately resulted in a big improvement of the algorithm.

8 Fifth Study (Manuscript V)

Collecting Water Samples in the Arctic Marginal Ice Zone with AUV “PAUL”: Sample Safety, Sample Purity and Exemplary Results of Field Measurements.

Thorben Wulff^{a, *}, Eduard Bauerfeind^a, Jonas Hagemann^a, Christiane Hasemann^a, Boris P. Koch^{a, b},
Sascha Lehmenhecker^a, Mascha Wurst^a, Michael Klages^c

^a) AWI – Alfred Wegener Institute Helmholtz Centre for Polar and Marine Research
HGF-MPG Joint Research Group for Deep Sea Ecology and Technology
Am Handelshafen 12, 27570 Bremerhaven, Germany

^b) University of Applied Sciences Bremerhaven
An der Karlstadt 8, 27568 Bremerhaven, Germany

^c) Sven Lovén Centre for Marine Sciences
University of Gothenburg
Kristineberg 566, 451 78 Fiskebäckskil, Sweden

*) Corresponding Author
Tel: +49 (0) 471 4831 2045
Fax: +49 (0) 471 4831 1776
Mail: Thorben.wulff@awi.de

Submitted to Methods in Oceanography in April 2015

8.1 Abstract

Autonomous Underwater Vehicles (AUVs) have evolved to valuable and reliable instruments in modern oceanography and are operated in the framework of versatile scientific questions. The Alfred Wegener Institute Helmholtz Centre for Polar and Marine Research (AWI) in Bremerhaven, Germany, has used its Bluefin-21 AUV “*PAUL*” (Polar Autonomous Underwater Laboratory) over the past years primarily to investigate oceanographic and biogeochemical processes in the Arctic Ocean. Part of *PAUL*’s payload is a water sample collector which was developed at AWI and has been in service since summer 2009. Laboratory tests were carried out to investigate potential contamination of the water samples due to the intrusion of unsuitable water: i) water from the interior of the AUV which might intrude as a sample is being taken or ii) water intrusion into a closed container due to external overpressure. To test this, the containers (“tubes”) were exposed to different stress scenarios such as static or pulsating external overpressure. Additionally, it was tested whether the chemical composition of a sample might be affected by the sample collector (e.g. due to substances which might leach out of the sample collector’s materials or the laboratory equipment used for sample processing).

Different methods to extract the samples from the tubes were investigated. The tests were conducted with particular regard to the seawater-chemical parameters relevant for *PAUL*’s current field of application involving nutrients (nitrate, nitrite, silicate, phosphate, ammonium) and dissolved organic carbon. Test results proved that only negligible amounts of water (< 0.1 % of the sample volume) entered the tubes after closing - although they encountered external overpressure. Chemical modifications also remained small, yet slight changes in the samples’ composition could be observed after spending 18.5 h inside the tubes. The test results were used to derive correction values. Finally, exemplary results from AUV field operations, which *PAUL* partly accomplished under ice, are presented and compared with literature data. Data comparison showed a high level of conformity to known nutrient and DOC distribution patterns. The scientific usability of the sample collector was confirmed. However, *PAUL*’s results also indicated small-scale variations at an ice edge for example for DOC which have not been reported yet. This study thus illustrates the scientific value of high resolution sample collection via an AUV.

8.2 Introduction

Autonomous Underwater Vehicles (AUVs) gained increasing attention in the oceanographic research community. They increase the efficiency and flexibility of scientific explorations and allow investigations that cannot be accomplished by conventional methods. AUVs can operate below solid ice covers and operate with minimal environmental interference. The growing number of scientific parameters that can be measured by *in-situ* sensors parallels the fast evolution of autonomous robots in marine research. However, various detection methods have not been replaced by *in-situ* technology yet and marine scientists will further rely on the availability of water samples.

Despite their scientific value, sample collectors are a relatively uncommon payload on AUVs. Only a few institutions worldwide have conducted AUV-based sample return missions. The Monterey Bay Aquarium Research Institute (Moss Landing, California, USA) operates the “Gulper” water sampling system on the Dorado class vehicles (Bird et al., 2009). The National Oceanography Centre (Southampton, UK) deployed an “AquaLAB” sample collector with the Autosub2 AUV (Dodd et al., 2006).

The Alfred Wegener Institute Helmholtz Centre for Polar and Marine Research (AWI) in Bremerhaven, Germany installed an in-house developed sample collector as part of the scientific payload of its Bluefin-21 AUV “PAUL” (Fig. 8-1, Bluefin Robotics Corporation, Quincy, Massachusetts, USA).

PAUL’s main field of operation during the past few years has been the investigation of biogeochemical processes in the Arctic marginal ice zone (MIZ).

The oceanographic parameters within the MIZ (e.g. nutrient concentrations) are characterized by a very high spatial variability (e.g. Niebauer & Smith, 1989) which in turn may have a tremendous impact on the biological productivity. To resolve these steep gradients with a fast moving platform such as an AUV, sampling devices that collect samples almost instantly are mandatory – leading to the specific design of AWI’s sample collector.

The functional principle of the AWI sample collector is described in its European and American patent specifications (Wulff & Sauter, 2013 and 2012) and in a previous article (Wulff et al., 2010).



Fig. 8-1. PAUL is being recovered after a dive (left). PAUL’s payload section (right). The sample collector is marked with a red arrow.

This article describes the validation of AWI's sample-collector according to physical and chemical parameters. The tightness of the sample containers was tested under different stress scenarios. Experiments were conducted to assess sample purity as monitored by inorganic

dissolved nutrients (IDN: nitrate, nitrite, silicate, phosphate and ammonium) and dissolved organic carbon (DOC). Finally, the article will give exemplary results of field operations for these parameters.

8.3 Methods

8.3.1 The Sample Collector

In brief, the basic design of *PAUL*'s sample collector consists of two separate drum magazines each equipped with eleven sample containers. Similar to the functional principle of a revolver, these containers are successively positioned in front of a feed line. Water enters the system through funnels protruding from *PAUL*'s nose section (Fig. 8-2). The forward movement of the AUV provides a steady water supply of the sample collector so that pumps are not required.

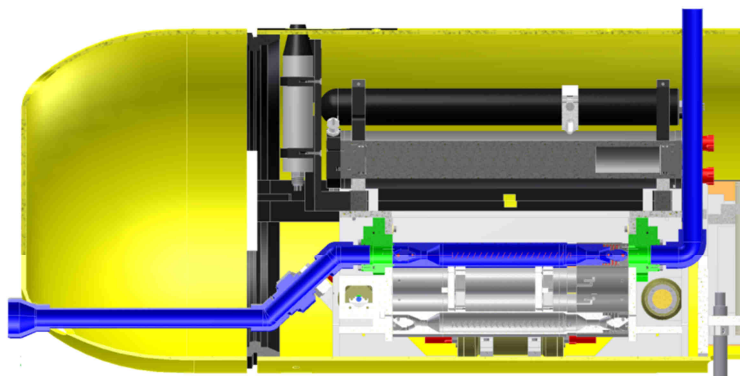


Fig. 8-2. Cross section through *PAUL*'s payload section showing the entire water path (blue).

The sample containers (“tubes”, Fig. 8-3, PMK Kunststoffverarbeitung, Geisingen Gutmadingen, Germany) are comparable to Niskin bottles. The tubes are inserted into the sample collector with open ends and the particular tube that is positioned in front of the feed line is constantly flushed with water prior to sampling. Both ends of each tube can be closed by two locking cones which are interconnected by a tension spring. For taking a sample, the locking

cones are released from their fixations, thus “cut” the water flow and enclose water in the tube. Each tube provides a maximum sample volume of 220 ml, sufficient to conduct a series of standard laboratory analyses. For sample extraction, each tube has one opening to drain the water and one opening for venting. Luer Lock adapters can be attached to the openings to ensure gastight withdrawal of the sample using a syringe. In case of analyses of less sensitive parameters, the tubes can be emptied by simply opening one of the locking cones. During sampling, the water is in contact with four different materials, specifically selected by their physico-chemical characteristics. The funnels of the water inlet, the feed lines and the tubes consist of Polyvinyliden fluoride (PVDF). A few structural parts are made of Polytetrafluoroethylene (PTFE) and the tension spring is of stainless steel (316Ti).

All sealing components (O-rings) are made of ethylene propylene diene monomer rubber (EPDM), a synthetic rubber well known for its chemical resistance.

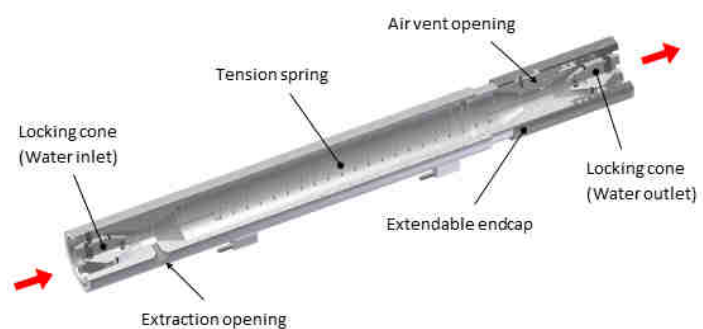


Fig. 8-3. Cutaway model of one of the sample containers (“tube”).

The total surface area of each material which is in contact with the sample is given in Table 8-1. As the water stays in the feed line for seconds but might remain in the tubes for hours, this table is divided into short and long term contact.

Table 8-1

Contact surfaces within the sample collector.

Material	Color Code in Fig. 8-2	Short term contact (Feed line) [cm ²]	Long term contact (Tube) [cm ²]
PVDF		615.9	297.1
316Ti		6.7	42.6
EPDM	--	18.1	2.3
PTFE		102.4	--

8.3.2 Physical contamination

During its missions, the vehicle's interior is completely flooded with seawater. As this water might have come into contact with various substances and materials in the interior of the vehicle, it is unsuitable as sample material. Therefore, it was tested whether this water can intrude into the tubes and contaminate the sample ("physical contamination").

The present study focuses on the two following scenarios, which had been identified as the most likely ones:

1. Water intrusion through leakages along the tube's front end when it is positioned in front of the feed line and water flows through it.
2. Water intrusion through the sealing of a closed tube.

The first scenario was experimentally tested using dyed water and a true to scale acrylic glass model of the tubes. This model was submersed in a tank and connected to a water reservoir. A water flow of approx. 0.8 m s⁻¹ was generated

inside the model – representing the expected flow velocity through the tubes during real AUV missions. To validate the continuous tightness of the sealings of the tubes, the tubes were exposed to different stress cases in a pressure tank.

This included i) equal internal and external pressure for 17, 30 and 135 hours, ii) static external overpressure of 2 bar for 35 minutes and iii) ten pulses of 2 bar external overpressure (30 seconds duration per pulse) within 9 minutes. An overpressure of 2 bar was applied as the greatest recorded inaccuracy in the vehicle's depth control system was 5 m below a pre-programmed mission depth. Thus, 2 bar (corresponding to 20 m water depth) represent a more severe case. The tests for scenarios ii) and iii) were repeated four times under identical conditions.

During the tests, six randomly chosen tubes were filled with ultrapure water (Milli-Q[®], Millipore Corporation, Billerica, Massachusetts, USA). The pressure tank was filled with potassium chloride (KCl) solution (2.224 mol l⁻¹). Water intrusion was quantified by measuring changes of the electrical conductivity of the MQW in the tubes. KCl was used due to its high molar conductivity (Vanýsek, 1999) and as electrostatic effects influencing electrical conductivity of the solution (Onsager and Fuoss, 1932) are well described.

The relation between the molar conductivity Λ and the electrolyte concentration c is given by (Lind et al., 1959):

$$\Lambda = 149.93 - 94.65\sqrt{c} + 58.74c \cdot \log c + 198.4c \quad (1)$$

Based on the relation between molar conductivity, electrolyte concentration and measured conductivity κ , Eq. 1 can be transformed. It follows:

$$\kappa = 149.93c - 94.65\sqrt{c^3} + 58.74c^2 \cdot \log c + 198.4c^2 \quad (2)$$

with κ in [$\mu\text{S}\cdot\text{cm}^{-1}$] and c in [$\text{mol}\cdot\text{l}^{-1}$].

The experiments were conducted under realistic temperature conditions of 5 °C. As electrical conductivity in aqueous salt solutions is temperature dependent and literature values are given for 25 °C, samples were warmed up prior to conductivity measurements (conductivity meter: GMH 3430, Greisinger electronic, Regenstauf, Germany). Accuracy of the conductivity measurements was $\pm 0.5\%$ of the measurement value plus $\pm 0.3\%$ of the adjusted measuring range (here: 0 – 200 or 0 – 2,000 $\mu\text{S}\cdot\text{cm}^{-1}$). Minimal accuracy of the device was $\pm 2\ \mu\text{S}\cdot\text{cm}^{-1}$, which here translates into an uncertainty of $\pm 1.3\cdot 10^{-3}$ ml of intruded KCl solution ($\pm 6\cdot 10^{-4}\%$ of a tube's volume).

8.3.3 Chemical Contamination

Potential contamination due to for example leaching compounds (“chemical contamination”) during sampling or sample extraction was assessed by the analysis of IDN and DOC. Different methods of sample extraction were investigated.

Following symbols represent the experimental steps:

-  Emptying the respective vessel
-  Emptying the tube using a hose adapter consisting of:
 - Custom made screw-in adapter, steel Ti316
 - Tygon[®] hose (Compagnie de Saint-Gobain, La Défense, France)
 - Rotilabo[®] hose connector with Luer lock, female (Carl Roth, Karlsruhe, Germany)
- All components were carefully rinsed first with MQW, then with sample material.
-  Usage of a sterile 50 ml syringe with rubber sealing: (Omnifix, Braun Melsungen AG, Melsungen, Germany)
-  Usage of a sterile 50 ml syringe without rubber sealing: (HSW, Henke – Sass, Wolf GmbH, Tuttlingen, Germany)
-  Filtration via 0.7 μm glass microfiber filter (GF/F, pre-combusted at 550 °C for 12 hours) in a polycarbonate filter holder (13 mm, Cole Parmer, Vernon Hills, Illinois, USA)
-  Screw cap container (250 ml, polypropylene, Sarstedt AG & Co., Nuembrecht, Germany)

To determine the impact of the different components involved in collecting and processing the samples, the sample was divided into fractions (Fig. 8-4). Every fraction consisted of three subsamples in case of IDN and four subsamples in case of DOC. Both IDN and DOC tests were conducted with two randomly chosen tubes – thus providing a total number of six data points per fraction for IDN and eight data points per fraction for DOC.

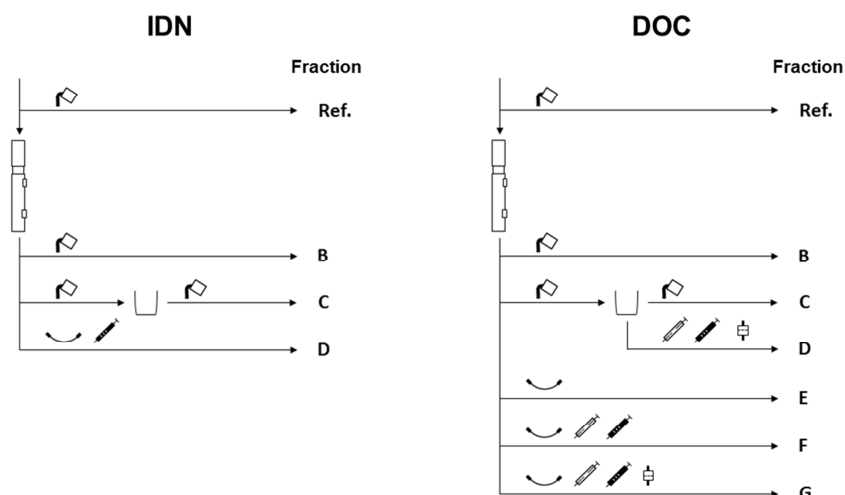


Fig. 8-4. Flow charts for each experimental step to elucidate potential chemical contamination of the water samples. Letters represent the sample nomenclature for inorganic dissolved nutrients (IDN, left) and dissolved inorganic carbon (DOC, right).

8.3.4 Analyses of inorganic dissolved nutrients

For each investigation, the first fraction represents the reference value (Ref.). This fraction was taken from the reservoir before the tubes were filled with water. Likewise, fraction B was taken directly from the tube to detect possible contaminations due to the storage of the water in the tube. For this reason, fraction B was poured out of the tube into the analysis vial – avoiding contact to any other material. All further fractions were extracted with different methods and laboratory equipment. In case several laboratory instruments (e.g. syringe + filter) were necessary for a method, the available water volume was further split into fractions to identify potential contamination arising from each single processing step. For example, comparing DOC values of fractions F and G, the contamination caused by the filtration conducted in G could be measured.

To test for chemical contaminations of IDN samples, the tubes were filled with water from the North Sea (NSW) as IDN values are well documented for this particular area (e.g. Brockmann & Kattner, 1997). Prior to the test, NSW was autoclaved for 4 h at 99 °C and filtered (0.2 µm pore size) to exclude biological activity and remove microorganisms. The water remained in the tubes for 18.5 h which exceeded usual storage time by far. To simulate the dive and normal working procedures, all substances and materials were cooled to 5 °C. Subsamples were collected in plastic vials (pre-rinsed with sample water) and stored at -20 °C.

NSW samples were colorimetrically measured for inorganic nutrients (QuAAtro SFA Analyzer, Seal Analytical, Southampton, UK) using standard methods (Table 8-2). To determine the average relative measuring accuracies of the methods, 15 technical replicates were used for each of the parameters. The detection limits are according to values stated by Seal Analytical Ltd..

Table 8-2

Detection methods and analytical thresholds for inorganic nutrients determined for North Sea water (detailed descriptions are available from Seal Analytical Ltd.).

Parameter	Method (Seal Analytical Registration Number)	Detection limit [$\mu\text{mol l}^{-1}$]	Rel. Accuracy [%]
Silicate	Q-066-05 Rev. 3	0.02	2.27
Phosphate	Q-064-05 Rev. 4	0.004	3.23
Nitrate	Q-068-05 Rev. 6	0.03	1.67
Nitrite	Q-070-05 Rev. 4	0.01	13.98
Ammonium	Q-080-06 Rev. 2	0.01	--

8.3.5 Analyses of dissolved organic carbon

DOC determinations were conducted with two tubes, which were either filled with MQW as a blank or with Antarctic surface water (ASW). The water remained in the tubes for 18.5 hours at 5 °C. For each fraction, subsamples were filled into pre-cleaned (10 % hydrochloric acid, 12 h) high-density polyethylene (HDPE) bottles and immediately stored at -20 °C.

DOC was determined by high temperature catalytic oxidation and subsequent non-dispersive infrared spectroscopy and chemiluminescence detection (TOC-VCPN by Shimadzu, Kyoto, Japan). After each batch of five samples one reference standard (DOC-DSR, Hansell Research Lab, University of Miami, US), one MQW blank and one potassium hydrogen phthalate standard were measured. The detection limit was 7 $\mu\text{mol C l}^{-1}$, the accuracy was 5 %.

8.3.6 Statistical Methods

In order to detect outliers in the measurement data, two different methods were applied. In case of a small sample size ($n < 7$), which was inappropriate for statistical methods, measurement data that differ more than 1.5 times

from the standard deviation of the arithmetic mean, were considered as outliers.

Additionally, some outliers could also clearly be identified visually. For sample numbers ≥ 7 the Normal distribution was checked prior to applying an outlier test (Shapiro & Wilk, 1965). If necessary a logarithmic transformation was applied to achieve a Normal distribution. Outliers in these data sets were detected using the Grubbs' test (Grubbs, 1969).

All statistical analyses were accomplished using the software STATISTICA by StatSoft (Hamburg, Germany).

8.3.7 Satellite Data

Within this study, satellite derived measurements of the euphotic depth (ED) and sea ice concentration data are used. ED measurements originate from NASA's earth observation satellite "Aqua". Data are available via the "GIOVANNI" platform of the Goddard Earth Sciences Data and Information Services Center (Acker & Leptoukh, 2007).

Sea ice concentration data are provided by the Ocean and Sea Ice Satellite Application Facility (OSI-SAF), which is part of the EUMETSAT network (Eastwood et al., 2011). Charts showing ED or the sea ice concentration are generated using Ocean Data View (Schlitzer, 2015).

8.4 Results

8.4.1 Physical Contamination

8.4.1.1 “Ram Pressure Sealing”

The transition point between the feed line and the tube is sealed with a compression spring integrated below the extendable endcap (see Fig. 8-3). This spring constantly presses the front end of the tube onto the feed line. To achieve a true hermetic sealing, the tubes have an additional sealing principle.

The front side of each locking cone (Fig. 8-5 a, yellow arrows) is flat and positioned perpendicular to the direction of the water flow (“flow deflector plate”). Thus, the hydrodynamic drag of this component, along with the resistance of the female taper behind the cone, is relatively high. If water flows through the tube, this drag generates a dynamic pressure which increases the total pressure inside the tube’s front end. Notches which have intentionally been carved into the front end of the model (Fig. 8-5 b, yellow arrows) simulated a poor sealing between feed line and tube. In the test, red dyed water flowed through the model (Fig. 8-5 c).

As can be seen from Fig. 8-5 c, streaks of dye leaked outwards through the notches at the tube’s front end (yellow arrows). This showed the elevated pressure level inside the tube. As a consequence of the elevated pressure level inside the tube, water would rather flow out of the tube than flowing in. Thus, the internal overpressure secures the transition point between feed line and tube.



Fig. 8-5a. Locking cone with deflector plates (yellow arrows).



Fig. 8-5b. Acrylic glass model with locking cone inside.

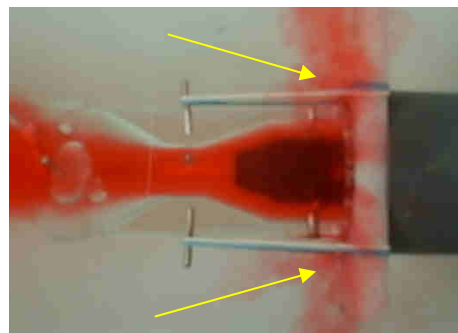


Fig. 8-5c. Model during verification tests. Streaks of dye leaking outwards are marked with yellow arrows.

8.4.1.2 Tightness of the tubes

The tests showed that static external overpressure (Fig. 8-6 b) (2 bar, 35 minutes) caused the largest intrusion of KCl solution into the tubes. Including all possible measurement uncertainties, a maximum volume of 0.22 ml leaked into the tubes, which is equal to 0.1 % of a tube's total inner volume (220 ml). Apart from this maximum, the average intruded volume for this scenario was usually below 0.1 ml or 0.05 % of a tube's volume. Both for equal external and internal pressure (Fig. 8-6 a) and for the scenario of pulsating external overpressure (Fig. 8-6 c), the maximum intruded volumes were below 0.04 ml or 0.02 % of a tube's total sample volume (complete list of results see Appendix). However, the tests also indicated a

considerable variance between the intruded water volumes. For example, considering an average water volume of 0.03 ml that entered the tubes in the “static external overpressure”-scenario (average of the grey bars, Fig. 8-6 b) the maximum value of 0.22 ml is more than seven times higher. This variance is basically explained by the fact that the exact position of the locking cones is only partially determined by the female tapers serving as the cones' mountings. In a closed tube, the cones are primarily fixated by their O-rings. However, due to its flexibility, rubber provides only limited guidance for a component, potentially resulting in a slightly inaccurate cone alignment and minimal leakages. Likewise, small scratches on the sealing surface could also cause leakages but their influence would be detectable as a repetitive offset.

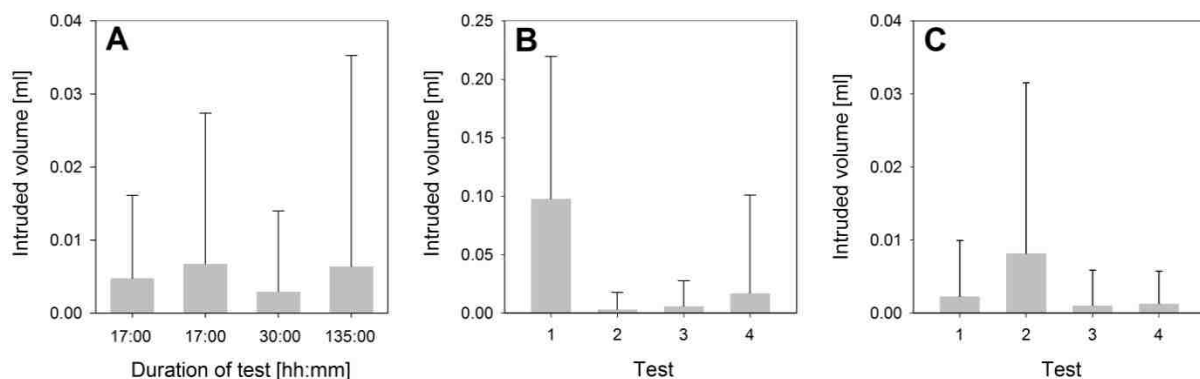


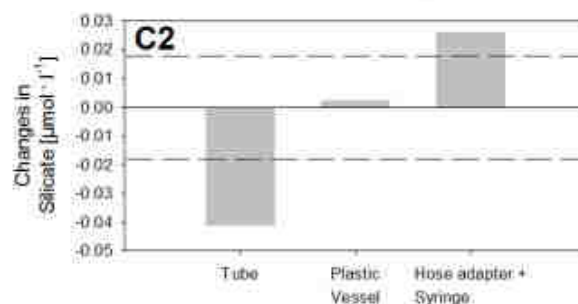
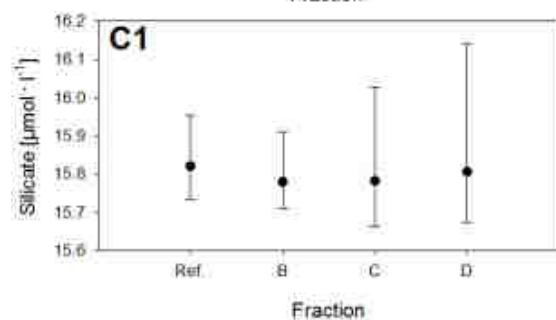
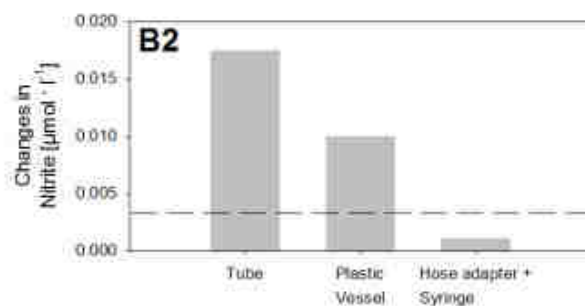
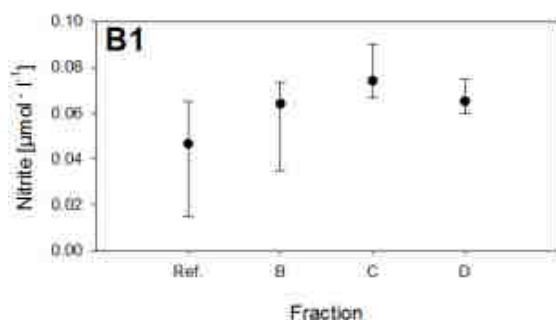
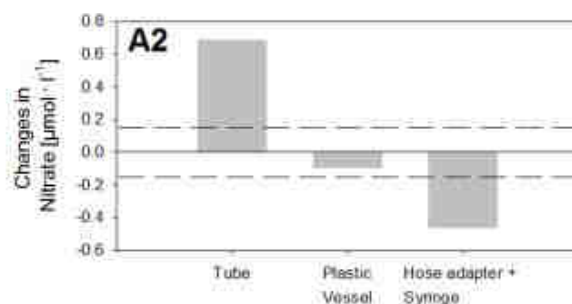
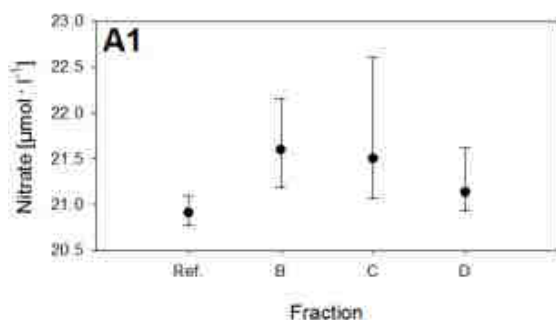
Fig. 8-6. a) Intruded volume at equal internal and external pressure and different test durations, b) static external overpressure and c) pulsating external overpressure. Grey bars represent average values of six individual measurements. Error bars indicate maximum intruded volume for the respective test.

8.4.2 Chemical Contamination

8.4.2.1 Inorganic dissolved nutrients

For all parameters except ammonium, influences of the sample collector and subsequent processing steps were detectable (Fig. 8-7). For each parameter, the tubes' influence was larger than the measurement uncertainties and thus, although small, it had to be taken into account. In some cases other components also seemed to affect the parameter concentrations. Due to the hose adapter and the syringe, the nitrate level was decreased by $0.46 \mu\text{mol l}^{-1}$ (approx. 2.2 %),

whereas the silicate value was increased by $0.26 \mu\text{mol l}^{-1}$ (approx. 0.2 %). The plastic vessel used during the sample extraction process slightly increased the nitrite concentration. As the measurement uncertainty for ammonium was unknown, the measurement error was not quantifiable. For the tested concentration range, correction values given in Table 8-3 can compensate the error by simple summation or subtraction.



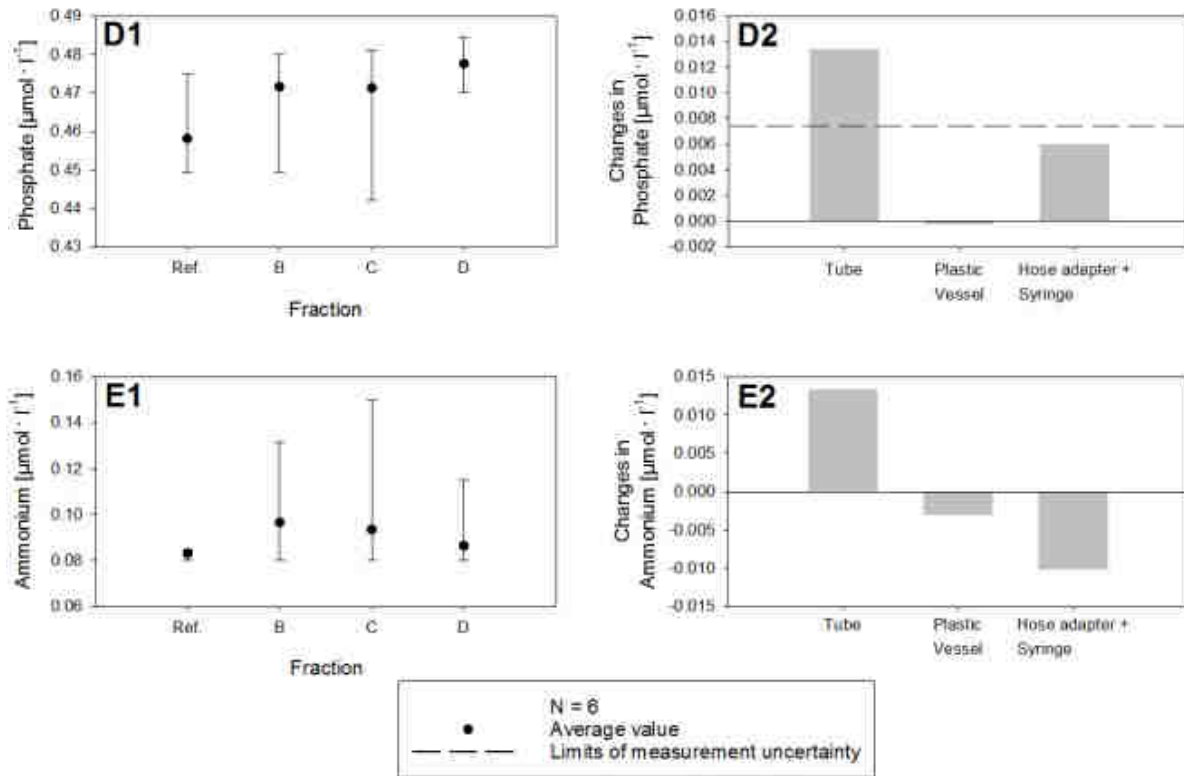


Fig. 8-7. Average values of IDN parameters using NSW after 18.5 hours retention time for the different fractions (left). Error bars indicate maximum and minimum values. Influence of different components on respective parameter (right).

Table 8-3
Correction values for IDN measurements.

	Correction values [$\mu\text{mol l}^{-1}$]		
	Tube	Plastic vessel	Hose adapter + syringe
Nitrate	-0.69		+0.46
Nitrite	-0.02	-0.01	
Silicate	+0.04		-0.26
Phosphate	-0.01		

8.4.2.2 Dissolved organic carbon

Using MQW for DOC investigations resulted in very low concentration values. Although many changes occurred close to or even below the detection limit some influences seemed to emerge. Compared to the reference fraction, the tests indicated an increase of DOC concentrations for fractions D, F and G (Fig. 8-8 a). In contrast, fractions B, C and E featured the smallest difference to the reference value. Therefore, the syringes were identified as the main source of contamination (Fig. 8-8 b). The hose adapter did not have any influence on DOC. Thus, at least for the particular length used in the experiments (10 cm), using Tygon® hoses proved to be non-critical. The effects of the tube and the filter appeared to act in opposite directions.

While the tube caused a small increase, the concentration of DOC was slightly reduced by the filter. Repeating the trial with ASW (Fig. 8-9) provided quantifiable data to derive correction values. Investigations using ASW indicated the same trends as for MQW – with syringes being the strongest source of contamination with an increase of $2.6 \mu\text{mol}\cdot\text{l}^{-1}$ DOC. However, also the tube itself ($+1.5 \mu\text{mol}\cdot\text{l}^{-1}$ DOC) and the filters ($+1.6 \mu\text{mol}\cdot\text{l}^{-1}$ DOC) slightly contribute to a contamination of the sample. As the correction values for IDN parameters, the correction values given in Table 8-4 are meant to compensate the contamination by simple summation or subtraction and thus are only valid for the investigated concentration range.

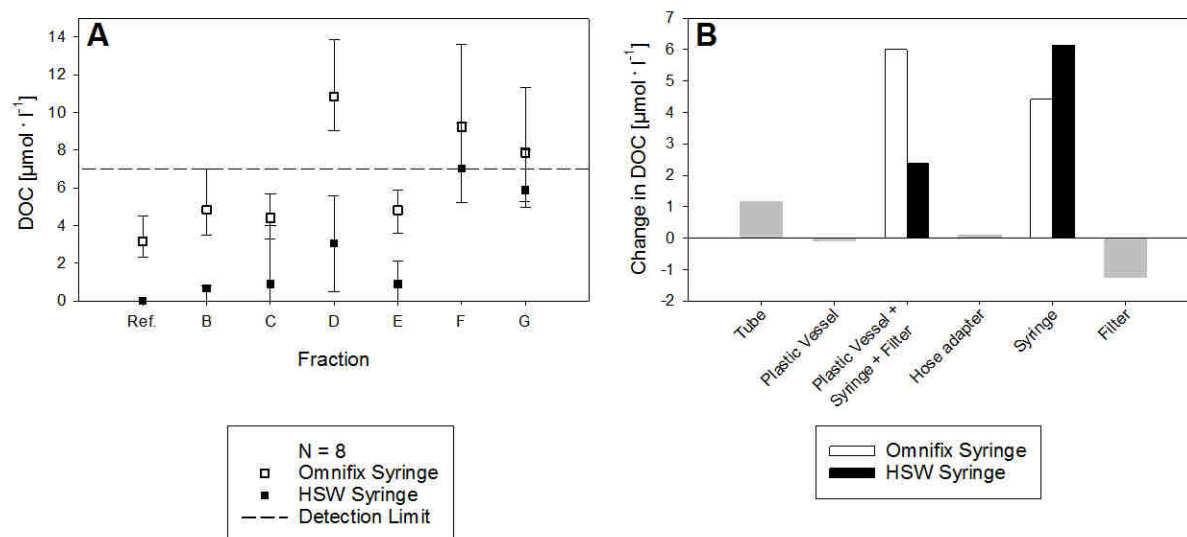


Fig. 8-8. Results of the DOC investigation using MQW after 18.5 hours retention time in the tubes. a) Average DOC values of the respective fractions. b) Influence of the different components on the DOC value.

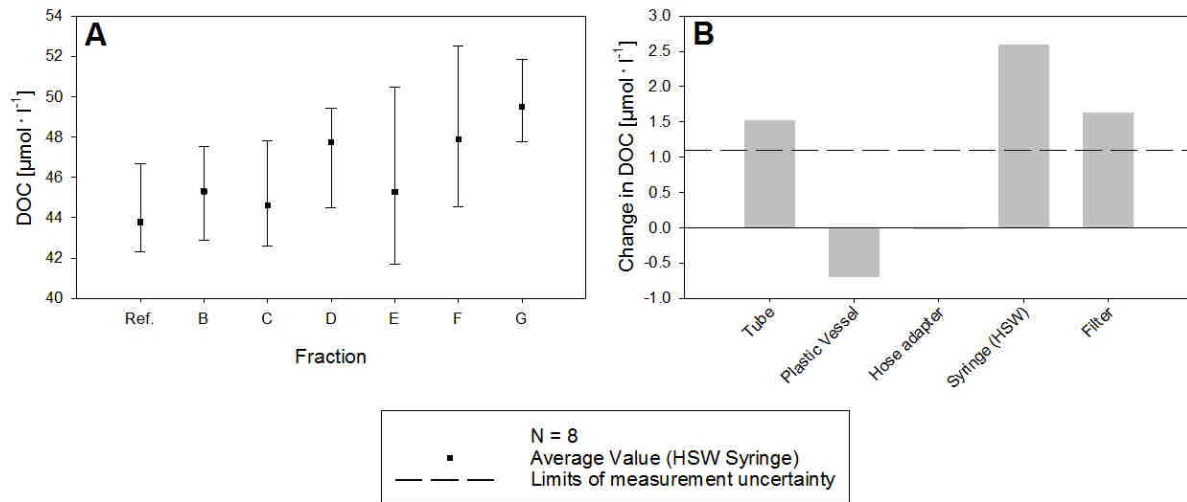


Fig. 8-9. Results of the DOC investigation using ASW after 18.5 hours retention time in the tubes. a) Average DOC values of the respective fractions. b) Influence of the different components on the DOC value.

Table 8-4

Correction values for DOC measurements.

	Correction values [$\mu\text{mol l}^{-1}$]				
	Tube	Plastic vessel	Hose adapter	Syringe (HSW)	Filter
DOC	-1.5			-2.6	-1.6

8.5 AUV Field Operations

Although laboratory tests can verify the water collector's general suitability for scientific purposes, newly developed devices also need to prove their feasibility in the field. For this reason, exemplary results of field operations accomplished in 2010 (expedition ARK 25/2, R/V *Polarstern*, Fram Strait) and 2012 (expedition ARK 27/2, R/V *Polarstern*, Fram Strait) are presented. These results are compared with literature data.

8.5.1 Operations with analyses of inorganic dissolved nutrients

During expedition ARK 27/2, on R/V *Polarstern* in summer 2012, PAUL accomplished two dives between Svalbard and Greenland on July 20th and July 22nd 2012 (in the further text named Dive 12-1 and Dive 12-2, Fig. 8-10 a). A total number of 27 samples were collected at depths between 550 and 15 m and analyzed for inorganic nutrients. Using the vehicle's CTD probe the investigated water bodies of these two dives could clearly be identified as Atlantic water by means of average temperature and salinity (Dive 12-1: 3.4 ± 2.6 °C / 35.1 ± 0.09 PSU and Dive 12-2: 3.0 ± 2.5 °C / 35.0 ± 0.07 PSU).

Warm and Cold Atlantic Water (AWw + AWc) according to Schlichtholz & Houssais, 2002).

An additional dive in the marginal ice zone was accomplished on July 24th in 2012 (Dive 12-3, Fig. 8-10 a) advancing roughly two kilometers under the sea ice. PAUL collected 14 samples which were analyzed for inorganic nutrients. In contrast to the previous two missions, samples were collected at a constant depth of 20 m. Salinity and temperature data of the vehicle showed that Polar water masses were sampled, confirming that two Arctic habitats with different characteristics (Atlantic and Polar) were investigated during these three deployments (Dive 12-3: -1.6 ± 0.06 °C / 33.5 ± 0.07 PSU. Polar Water (PW) according to Schlichtholz & Houssais, 2002).

In the context of nutrient data, the euphotic depth (ED) provides additional information on biological activity. Although the ED is not necessarily connected to the location of the nutricline, it indicates the depth down to which nutrients could have been consumed due to primary production prior to the dives. Thus, the ED served as a proxy, at which depth a clear change of the IDN parameters could be expected. According to satellite measurements the ED was located at 15 – 30 m water depth (Fig. 8-10 b).

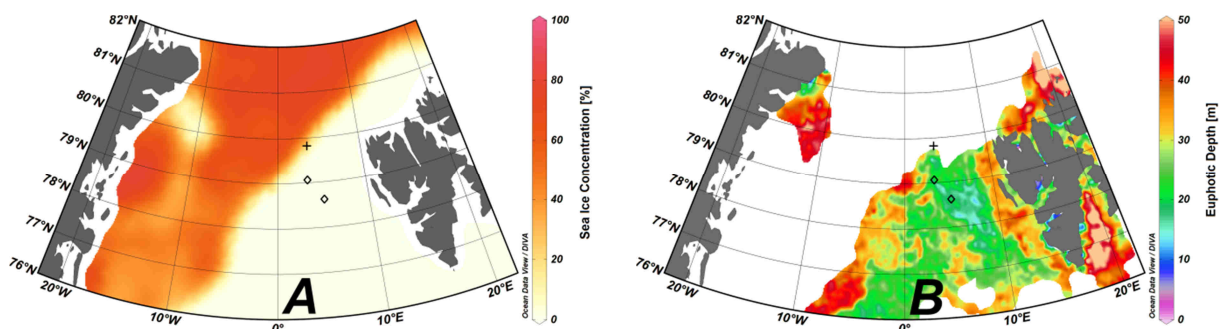


Fig. 8-10. a) Location of PAUL's deployments in the Fram Strait in 2012. Open water dives 12-1 and 12-2 (diamonds) and under ice dive 12-3 (crosses). Background colors represent average sea ice concentration at the day of the under ice mission. b) Average euphotic depth between July 11th and July 18th – the 7-day period just prior to the deployments.

The analytical results of the water samples and the different inorganic nutrients (Fig. 8-11) clearly showed a characteristic depth distribution for the different parameters during summer. While all parameters remained on a relatively constant level below 300 m water depth, biological processes caused a steep decrease of all nutrients above 50 m water depth. These profiles are also consistent with the satellite derived location of the euphotic depth. Between 15 and 30 m water depth, all values showed the strongest changes. Ammonium and nitrite, which are produced by heterotrophic bacteria, had a characteristic maximum at approx. 50 m water depth. The maximum ammonium concentration at 50 m water depth is in accordance with previous studies (Kattner & Becker, 1991).

A direct quantitative comparison between *PAUL*'s data and the data published by Kattner & Becker (1991) (especially Station 103, as it was the closest station to *PAUL*'s dive locations) showed a high level of conformity for nitrate, phosphate and ammonium. Additionally, nitrate, silicate and phosphate values were further confirmed by more recent data (Bauerfeind et al., 2014).

Comparing the dives, silicate is the only parameter that showed significant differences between open water and under ice values. These differences may be due to different ways of biological silicate cycling in the two habitats. Other parameters remained relatively constant between the individual missions.

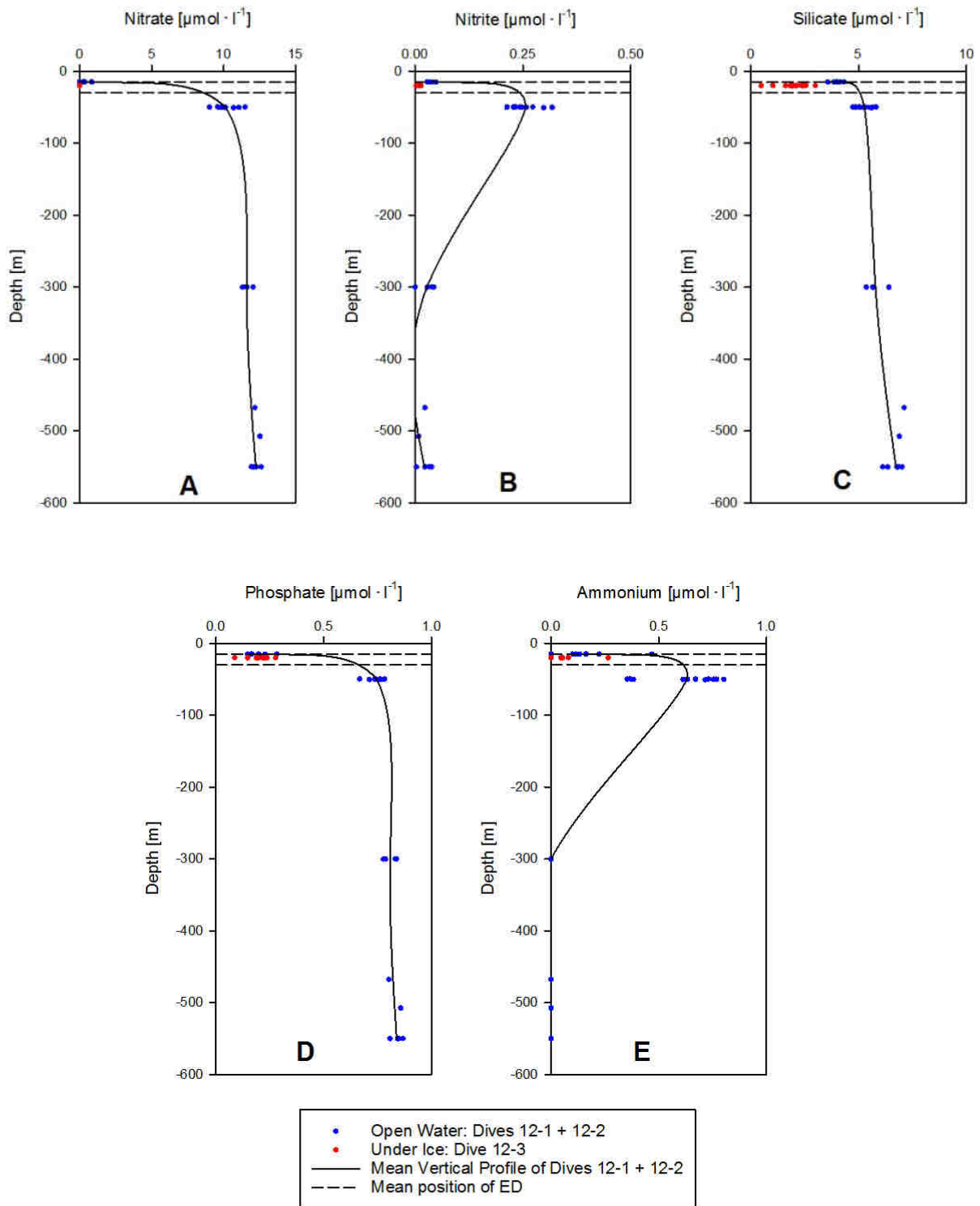


Fig. 8-11 a – e. Vertical distribution of nutrients as measured by PAUL in the Fram Strait in July 2012.

8.5.2 Operations with analyses of dissolved organic carbon

In 2010, in the framework of the Arctic expedition ARK 25/2 on R/V *Polarstern*, *PAUL*'s sample collector was used to gather sample material for DOC investigations for the first time. Additionally, *PAUL* accomplished its very first under-ice mission (July 21st 2010, Dive 10-2, Fig. 8-12) which led the vehicle approximately two kilometers beyond the ice edge. As *PAUL* had accomplished an open water dive some days before (July 8th 2010, Dive 10-1, Fig. 8-12), this provided an opportunity to compare the DOC values of two different environments. In the course of these two dives, 34 samples were collected – with 19 samples during the open water dive and 15 samples from below the ice. All samples were extracted from the tubes using syringes and thus respective correction values were applied.

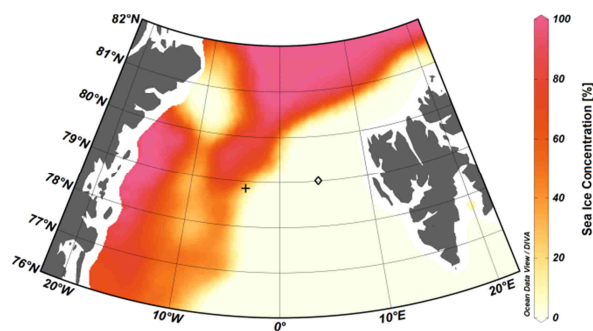


Fig. 8-12. Locations of *PAUL*'s deployments in the Fram Strait in 2010. Open water dive 10-1 (diamond) and under ice dive 10-2 (cross). Background colors represent average sea ice concentration at the day of the under ice mission.

Temperature and salinity data of the vehicle's CTD showed that *PAUL* crossed Atlantic water masses during Dive 10-1 (5.2 ± 0.16 °C / 35.2 ± 0.02 PSU) and Polar water masses were

crossed during Dive 10-2 (-1.7 ± 0.01 °C and 33.7 ± 0.03 PSU). For comparison purposes, the water masses were classified according to a system which assigns characteristic DOC values to Arctic and North Atlantic water masses (Amon et al., 2003). DOC concentrations were higher under ice than in open waters (Fig. 8-13). However, as there was a slight depth difference between the two dives and as an increase of DOC with decreasing depth is common in this region, they cannot be compared directly. Nevertheless, the relatively high average DOC concentrations of $90 \mu\text{mol}\cdot\text{l}^{-1}$ was in agreement with data obtained earlier from Polar water masses in this region (Amon et al., 2003). The high DOC concentrations can be attributed to the influence of water masses originating from the central Arctic Ocean which are known to be comparably rich in DOC.

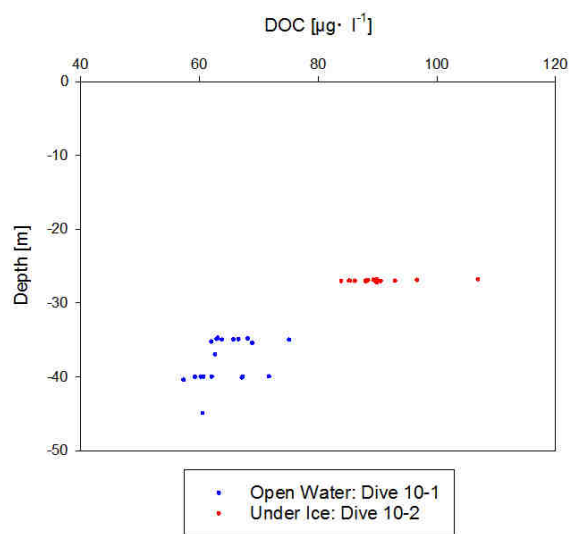


Fig. 8-13. Vertical distribution of DOC as measured during two dives in the Fram Strait in 2010.

In the region of Dive 10-2 two major currents originating from the central Arctic region, the East Greenland Current (EGC) and the Polar Front Current (PFC), merge with the Return Atlantic Current (RAC, Schlichtholz and Houssais, 1999).

During the under ice dive, 22 samples were collected with 15 being analyzed for DOC. These samples were collected along a 3 km long track line, providing an unprecedented horizontal resolution of 200 m per sample. Within these 3 km the DOC values varied between 85 and 107 $\mu\text{mol l}^{-1}$. Due to the high horizontal resolution and as the samples were collected within just 30 minutes, *PAUL*'s data indicated small-scale variations of DOC. The high resolution illustrates how valuable the use of AUVs is if it comes to 2D or 3D mapping of crucial environmental data.

8.6 Conclusion

Physical contamination

The “Ram Pressure Sealing” works as expected and it successfully prevents water from inside the AUV from penetrating into the tubes. It ensures that only “clean” water from the feed line is taken as a sample. Additionally, the internal overpressure in the front part of the tube is most likely higher than assumed. Preliminary results of a computer fluid dynamics (CFD) model, which was not part of this investigation, showed that a flow velocity of 0.8 m s^{-1} , is exceeded during real AUV missions. Thus the ram pressure sealing principle would be even more effective.

Exposing the tubes to two bar external overpressure resulted in a maximum intruded water volume of 0.22 ml, which is equal to 0.1 % of the internal volume of a tube and as such negligible. However, vehicle operators are required to ensure that the samples are collected in an ascending order to avoid the tubes encounter external overpressure at all.

In general, the risk for physical contamination is negligibly small and the samples can be considered safe.

Chemical Contamination

With respect to chemical contaminations, tube materials and sample processing are more critical than expected. Measured contaminations were low yet sometimes outside uncertainty limits of the respective detection method and thus they must not be ignored.

To avoid possible contaminations, it is advantageous to keep the number of laboratory devices and materials with contact to the sample small. However, especially on vessels, where the ambient air can contain various different substances, isolating and protecting the sample must be one of the key objectives.

8.7 Acknowledgements

In contrast to a possible systematic contamination due to laboratory equipment, the input of unknown substances from the air is most likely not correctable. Syringes represent a closed and protective containment and provide maximum safety. Additionally, they make it possible to determine the extracted volume exactly.

Within the framework of this article, correction values could be determined for the different parameters. However, it cannot be ruled out yet that these values vary with the concentration of the respective parameter or with the respective retention time of the sample in its tube. At this point further research efforts have to be undertaken.

Field Operations

Acquired oceanographic data matched well with published measurements. IDN and DOC values are within realistic and expected levels – showing that applied procedures for sample handling and analysis are correct. *PAUL*'s measurements also indicate small-scale variability which have not been observed before, likely because classical methodologies (e.g. ship bound CTD rosette) could not achieve the spatial and temporal resolution of AUV supported ocean sampling. For this reason, the investigation of biochemical processes and the fine-scale distribution of substances with biological relevance are key questions of AWI's AUV project and as such crucial part of current research efforts.

We would like to thank Uwe Wulff who constantly improves our data processing abilities, Kimberly Shurn as a highly skilled AUV engineer and Mandy Kiel and Dieter Janssen for assistance in DOC analyses. Anja Terbrüggen and Kai-Uwe Ludwichowski are acknowledged for IDN analyses. We also would like to thank the crew of the research vessels R/V *Polarstern* and the Bluefin Robotics Corporation for their valuable assistance and professional support of our AUV project. We also acknowledge the anonymous reviewers for their helpful comments.

The investigations described in this article were accomplished within the framework of the Helmholtz Alliance “Robotic Exploration of Extreme Environments – ROBEX”. *PAUL*'s scientific payload was partly funded with the financial support of the European Commission's 7th Framework Program (Research Infrastructure) “EUROFLEETS” (Contract No. 228344).

8.8 Appendix

Table 8-5

Results of conductivity measurements for testing the tightness of the tubes at
i) equal internal and external pressure.

A	No	Conductivity before test [$\mu\text{S cm}^{-1}$]	Conductivity after test [$\mu\text{S cm}^{-1}$]	Concentration of KCl in the tube [mol l^{-1}]	Volume of intruded KCl solution [ml]
17 h	1	0.9	0.9	0.000000	0.000
	2	0.9	6.7	0.000039	0.007
	3	0.9	6.1	0.000035	0.007
	4	0.9	0.7	0.000000	0.000
	5	0.9	2.9	0.000013	0.002
	6	0.9	10.9	0.000067	0.013
17 h	1	1.8	5.0	0.000021	0.004
	2	1.8	7.8	0.000040	0.008
	3	1.8	19.9	0.000121	0.023
	4	2.4	2.3	0.000000	0.000
	5	2.4	4.3	0.000013	0.002
	6	2.4	5.5	0.000021	0.004
30 h	1	6.1	5.5	0.000000	0.000
	2	6.1	7.2	0.000007	0.001
	3	6.1	13.3	0.000048	0.009
	4	1.2	1.2	0.000000	0.000
	5	1.2	2.2	0.000007	0.001
	6	1.2	6.0	0.000032	0.006
135 h	1	1.1	2.0	0.000006	0.001
	2	1.1	26.2	0.000167	0.031
	3	1.1	3.5	0.000016	0.003
	4	1.3	0.9	0.000000	0.000
	5	1.3	3.0	0.000011	0.002
	6	1.3	2.0	0.000005	0.001

Table 8-6

 Results of conductivity measurements for testing the tightness of the tubes at
 ii) static external overpressure.

B	No.	Conductivity before test [$\mu\text{S cm}^{-1}$]	Conductivity after Test [$\mu\text{S cm}^{-1}$]	Concentration of KCl in the tube [mol l^{-1}]	Volume of intruded KCl solution [ml]
Test 1	1	1.0	316.0	0.002103	0.208
	2	1.0	6.7	0.000038	0.004
	3	1.0	325.0	0.002163	0.214
	4	1.2	1.7	0.000003	0.000
	5	1.2	1.4	0.000001	0.000
	6	1.2	245.0	0.001627	0.161
Test 2	1	1.5	2.1	0.000004	0.000
	2	1.5	25.1	0.000157	0.016
	3	1.5	4.5	0.000020	0.002
	4	1.7	2.0	0.000002	0.000
	5	1.7	2.5	0.000005	0.001
	6	1.7	2.3	0.000004	0.000
Test 3	1	2.4	5.3	0.000019	0.002
	2	2.4	40.5	0.000254	0.025
	3	2.4	13.8	0.000076	0.008
	4	2.7	3.3	0.000004	0.000
	5	2.7	3.9	0.000008	0.001
	6	2.7	3.8	0.000007	0.001
Test 4	1	2.9	5.7	0.000019	0.002
	2	2.9	151.9	0.000994	0.098
	3	2.9	3.2	0.000002	0.000
	4	3.4	3.4	0.000000	0.000
	5	3.4	3.5	0.000001	0.000
	6	3.4	6.2	0.000019	0.002

Table 8-7

Results of conductivity measurements for testing the tightness of the tubes at
iii) ten pulses of 2 bar external overpressure (30 seconds duration) within nine minutes.

C	No.	Conductivity before test [$\mu\text{S cm}^{-1}$]	Conductivity after test [$\mu\text{S cm}^{-1}$]	Concentration of KCl in the tube [mol l^{-1}]	Volume of intruded KCl solution [ml]
Test 1	1	4.2	4.5	0.000002	0.000
	2	4.2	12.7	0.000057	0.006
	3	4.2	15.3	0.000074	0.007
	4	4.2	4.2	0.000000	0.000
	5	4.2	4.9	0.000005	0.000
	6	4.2	4.6	0.000003	0.000
Test 2	1	5.0	17.0	0.000080	0.008
	2	5.0	48.8	0.000292	0.029
	3	5.0	20.8	0.000105	0.010
	4	5.0	5.2	0.000001	0.000
	5	5.0	5.4	0.000003	0.000
	6	5.0	7.3	0.000015	0.002
Test 3	1	6.2	6.4	0.000001	0.000
	2	6.2	7.4	0.000008	0.001
	3	6.2	11.1	0.000033	0.003
	4	7.4	7.6	0.000001	0.000
	5	7.4	8.8	0.000009	0.001
	6	7.4	9.2	0.000012	0.001
Test 4	1	7.4	12.1	0.000031	0.003
	2	7.4	7.9	0.000003	0.000
	3	7.4	10.0	0.000017	0.002
	4	7.9	8.1	0.000001	0.000
	5	7.9	8.5	0.000004	0.000
	6	7.9	11.2	0.000022	0.002

8.9 References

- Acker, J.G. & Leptoukh, G., (2007). „*Online Analysis Enhances Use of NASA Earth Science Data*”, Eos, Trans. AGU, 88(2), 14 – 17.
- Aminot, A. et al., (2009). “*Nutrients in Seawater Using Segmented Flow Analysis*, In: *Practical Guidelines for the Analysis of Seawater*”, CRC-Press, Boca Raton, USA, 2009, pp. 148. ISBN: 978-1-4200-7306-5
- Amon, R.M., Budéus, G., Meon, B., (2003). “*Dissolved organic carbon distribution and origin in the Nordic Seas: Exchanges with the Arctic Ocean and the North Atlantic*”. J. Geophys. Res.-Oceans (1978–2012), 108(C7).
- Bauerfeind, E., Kattner, G., Ludwichowski, K.U., Nöthig, E.M., Sandhop, N., (2014). „*Inorganic nutrients measured on water bottle samples at HAUSGARTEN during POLARSTERN cruise ARK-XXIII/2*”, Alfred Wegener Institute, Helmholtz Centre for Polar and Marine Research, Bremerhaven.
- Bird, L.E., Sherman, A., Ryany, J., (2007). “*Development of an Active, Large Volume, Discrete Seawater Sampler for Autonomous Underwater Vehicles*”, IEEE, OCEANS 2007, 1 – 5.
- Brockmann, U. H. & Kattner, G., (1997). „*Winter-to-summer changes of nutrients, dissolved and particulate organic material in the North Sea*”, Deutsche Hydrografische Zeitschrift, 49(2-3), 229-242.
- Dodd, P.A., Heywood, P.R., Pebody, M., (2006). “*Collection of Water Samples from an Autonomous Underwater Vehicle for Tracer Analysis*”. J. Atmos. Oceanic. Technol., 23(12), 1759 – 1767.
- Eastwood, S., Larsen, K.R., Lavergne, T., Nielsen, E., Tonboe, R., (2011). “*Global Sea Ice Concentration Reprocessing, Product User Manual*”, Product OSI-409, Document Version 1.3, The EUMETSAT Network of Satellite Application Facilities – Ocean and Sea Ice (OSI SAF). Available at: http://osisaf.met.no/docs/pum_seaicereproc_s2_v1p3.pdf
- Grubbs, F. E., (1969). “*Procedures for detecting outlying observations in samples*”, Technometrics, 11(1), 1-21.
- Kattner, G. & Becker, H., (1991). “*Nutrients and Organic Nitrogenous Compounds in the Marginal Ice Zone of the Fram Strait*”, J. Marine. Syst., 2(3), 385 – 394.
- Lind, J.E., Zwolenik, J.J., Fuoss, R.M., (1959). „*Calibration of Conductance Cells at 25° with Aqueous Solutions of Potassium Chloride*”. J. Am. Chem. Soc., 81(7), 1557 – 1559.
- Niebauer, H. J. & Smith, W. O., (1989). „*A numerical model of mesoscale physical-biological interactions in the Fram Strait marginal ice zone*”, J. Geophys. Res.-Oceans (1978–2012), 94(C11), 16151-16175.
- Onsager, L. & Fuoss, R.M., (1932). “*Irreversible Processes in Electrolytes. Diffusion, Conductance, and Viscous Flow in Arbitrary Mixtures of Strong Electrolytes*”, J. Phys. Chem., 36(11), 2689 – 2778.
- Schlichtholz, P. & Houssais, M. N., (1999). „*An inverse modeling study in Fram Strait. Part I: dynamics and circulation*”. Deep-Sea Res. Pt. II, 46(6), 1083-1135.
- Schlichtholz, P. & Houssais, M.N., (2002). „*An Overview of the $teta - S$ Correlation in Fram Strait based on the MIZEX 84 data*”, Oceanologia, 44(2), 243 – 272.

- Schlitzer, R., (2015). *Ocean Data View*, <http://odv.awi.de>, 2015
- Shapiro, S. S. & Wilk, M. B., (1965). “*An analysis of variance test for normality (complete samples)*”, *Biometrika*, 52(3), 591-611.
- Vanýsek, P., (1999-2000). “*Ionic Conductivity and Diffusion at Infinite Dilution*”. in: Lide, D.R., Ed., *CRC Handbook of Chemistry and Physics*, 80th ed., CRC Press, Boca Raton, pp. 5-94.
- Wulff, T. et al., (2010). “*Development and Operation of an AUV-based water sample collector*”. *Sea Technology*, 51(12), 15–19.
- Wulff, T. & Sauter, E., (2012). “*Water Sampling Device*”, US Patent Application Publication US2012/0096958A1, 13 pages.
- Wulff, T. & Sauter, E., (2013). “*Water Sampling Device*”. European Patent EP2449358B1, 20 pages.

9 Sixth Study (Manuscript VI)

Physical and Ecological Processes at a Moving Ice Edge in the Fram Strait as Observed with an AUV

Thorben Wulff^{a, *}, Eduard Bauerfeind^a, Wilken-Jon von Appen^a

^a) AWI – Alfred Wegener Institute Helmholtz Centre for Polar and Marine Research
HGF-MPG Joint Research Group for Deep Sea Ecology and Technology
Am Handelshafen 12, 27570 Bremerhaven, Germany

^{*}) Corresponding Author
Tel: +49 (0) 471 4831 2045
Fax: +49 (0) 471 4831 1776
Mail: Thorben.wulff@awi.de

Submitted to Deep Sea Research Part I: Oceanographic Research in October 2015

9.1 Abstract

The marginal ice zone and the meltwater front of a moving ice edge in the Fram Strait were investigated with an Autonomous Underwater Vehicle (AUV). The AUV was equipped with physical and biogeochemical sensors to study the complex interaction between physical processes and ecological responses along the ice edge. The AUV covered two cross-front sections of 9 km length each and recorded high resolution vertical profiles of the physical and biogeochemical properties between 0 and 50 m water depth and at a horizontal station spacing of 800 – 1,000 m. In both physical and biogeochemical terms, the measurements revealed a complex structure of the water column. The distribution of phytoplankton and nutrients was highly inhomogeneous. Chlorophyll *a* concentrations of $5 \mu\text{g l}^{-1}$ were detected at the frontal interface in a small corridor just 2 – 4 km wide and only 5 m deep.

Nutrients at the surface were depleted, yet, compared to previous studies of this region, were still present in the euphotic zone. Below the euphotic zone, nitrate concentrations of $8 \mu\text{mol l}^{-1}$ and oxygen saturation values of 100 % resulted in a “dome-like” pattern – suggestive of vertical transport processes. Based on these measurements, four different zones featuring individual biogeochemical characteristics could be identified in the cross-front sections. The atmospheric forcing and the evolution of the ice cover contributed to the complexity of the water column. Large scale upwelling as well as more localized upwelling and downwelling events seem to have occurred. Furthermore, frontogenesis likely contributed to vertical water movements at the meltwater front. All of the processes had an effect on the ecological conditions along the observed ice edge.

9.2 Introduction

It is well known that the ice cover plays a key role in biological processes in Polar Regions. At the same time, especially the Arctic ice cover is changing rapidly and accurate models including ecologic parameters are necessary to predict future developments. Against this background, understanding physics and ecology of marginal ice zones (MIZ) is of particular interest as these are highly productive regions.

According to [Dumont et al. \(2011\)](#) the MIZ is the portion of the ice cover which is affected by open ocean processes. It can further be divided into three subzones: 1) the edge zone which is closest to the open water, 2) the transition zone, and 3) the interior zone ([Squire & Moore, 1980](#)). In a MIZ, the interaction between ocean, ice and atmosphere creates an extremely dynamic environment in both physical and ecological terms ([Wassmann & Reigstad, 2011](#); [Cherkasheva et al., 2014](#)). Filaments, eddies or other signatures indicating dynamic transport processes are common features in the water column of MIZs.

In the Arctic, the Fram Strait is a region that exhibits particularly dynamic interactions between ocean and ice. The Fram Strait features some bathymetric anomalies such as the Molloy Deep (5607 m, [Thiede et al., 1990](#)) and a complex hydrography. The hydrographic regime is dominated by the northward flowing warm West Spitsbergen Current (WSC) in the east ([Beszczynska-Möller et al., 2012](#)) and the southward flowing cold East Greenland Current (EGC) in the western Fram Strait ([de Steur et al., 2009](#)). Every year, roughly 10 % of the Arctic ice cover leaves the central Arctic via this strait ([Kwok et al., 2009](#)).

Along with the tendency of the Molloy Deep area to generate eddies ([Smith et al., 1984](#); [Quadfasel et al., 1987](#); [Bourke et al., 1987](#)) these features lead to a “lively” ice edge, with structures such as ice tongues extending far away from the main edge. These ice tongues frequently encounter warm Atlantic water ([Wadhams & Squire, 1983](#); [Johannessen et al., 1992](#); [Johannessen et al., 1994](#)). Melting rates along these structures can be elevated – reaching maximum values of 40 cm bottom ablation per day for water 3 K above the freezing point ([Josberger, 1987](#)), compared to 1 – 2 cm d⁻¹ in the interior of the pack ice ([Johannessen et al., 1987](#)).

Freshwater released by melting sea ice creates a pronounced meltwater front. Processes at these fronts such as vertical and horizontal transports can occur when they interact with atmospheric forcing and meanwhile modern technologies such as Gliders and Autonomous Underwater Vehicles (AUV) are available to conduct high resolution, synoptic measurements. Hence, chances are fairly good to unravel processes in these highly dynamic regions ([Lee et al., 2012](#); [Zhang et al., 2013](#); [Zhang et al., 2015](#)). As a result of ageostrophic secondary circulations (ASC), [Thomas & Lee \(2005\)](#) were able to detect and simulate strong up and downwelling along frontal systems associated with Symmetric Instability (SI, [Haine & Marshall, 1998](#); [Thomas et al., 2013](#)). Forced SI occurs if wind sets up an Ekman transport towards the front and the convergence causes water from the dense side of the front to be pushed over less dense water. Mixing processes to compensate this imbalance and restore marginal stability can drive an ASC.

Resulting from these dynamic physical conditions, ecologic conditions are dynamic as well. Below an ice cover, the availability of sunlight limits primary production (Smith et al., 1987b; Nicolaus et al., 2012). Due to limited production, nutrients are preserved and nutrient laden surface water can suddenly be exposed to sunlight when the ice retreats – inducing a phytoplankton bloom along the ice edge. This bloom is further supported by melting processes and the resulting stratification of the upper water column. The stratification can prevent phytoplankton from sinking and thus keep it in the suitable light regime of the euphotic zone (Niebauer & Alexander, 1985; Doney, 2006). On the other hand, the stratification can also prevent nutrients from being upwelled. Thus, phytoplankton blooms can be transient events, terminated by nutrient depletion if the water column is not mixed.

Direct observations of the MIZ are difficult to achieve and there have been several attempts of modelling this region. Based on a theoretical model Gammelsrød et al. (1975) predicted wind driven upwelling along ice edges. Among others, Niebauer (1982), Røed & O'Brien (1983) and Fennel & Johannessen (1998) included ice melting and ice drift as further parameters. Eventually, ecological features such as the distribution of nutrients, the activity of grazers or self-shading by high phytoplankton standing stocks were added to numerical models (e.g. Niebauer, 1991; Slagstad & McClimans, 2005; Wassmann et al., 2006; Skogen et al., 2007; Slagstad, 2011). Field studies mainly focusing on physical processes or physico-biological interactions at the ice edge have been conducted for example by Buckley et al. (1979) and

Johannessen et al. (1983) north of Svalbard, by Niebauer & Alexander (1985) in the Bering Sea, in the Barents Sea (Wassmann, 2002) or within the framework of the Marginal Ice Zone Experiment (MIZEX) program in the entire Fram Strait and Greenland Sea (MIZEX Group, 1986). Recently, also Gliders were used to study the MIZ for example as part of the Marginal Ice Zone Program of the Office of Naval Research (ONR) (Lee et al., 2012).

In the framework of project HAUSGARTEN, the Alfred Wegener Institute Helmholtz Centre for Polar and Marine Research (AWI) in Bremerhaven, Germany, has conducted year-around investigations on the pelagic-benthic coupling in seasonal ice covered areas of the Fram Strait since 1999 (e.g. Bauerfeind et al., 2009). Deployments of AWI's AUV "PAUL" are part of the pelagic observation program and are particularly assigned to investigate the interaction between physical and ecological processes in the MIZ (Nihoul (1986) used the term "Ecohydrodynamics"). The vehicle can conduct its missions while only slightly disturbing the environment. Hence, it can resolve the delicate structure of the upper meters of the water column which is normally destroyed by a vessel's draft during shipboard investigations.

This study focusses on one of PAUL's dives which took place in the MIZ of a large ice tongue in the Fram Strait in summer 2013. In the methods and data part, the AUV and its mission are described as well as other environmental data used. The following section describes the physical conditions and associated physical processes in the MIZ. Based on these physical measurements, the ecological response of the system is discussed.

9.3 Methods and Data

9.3.1 AUV “PAUL”

“PAUL” is based on a 21-inch vehicle of the American manufacturer Bluefin Robotics (Quincy, Massachusetts, USA). The torpedo-shaped vehicle is 4.3 m long, it weighs approx. 400 kg and has an operational range of 70 km. Considering its intended mission types, namely shallow missions, the original depth rating of 3,000 m was limited to 600 m. Since 2009, PAUL has regularly been operated in the MIZ of the Fram Strait (Wulff et al., 2013). During the 2013 Arctic campaign, PAUL’s scientific payload consisted of different sensors and a water sample collector (Table 9-1).

For this particular campaign, the water samples were only used to calibrate the nitrate sensor and to convert the fluorometer’s analog signals to

chlorophyll *a* concentrations (Wulff et al., 2010; Wulff et al., 2015, submitted). To determine nitrate concentrations, 8 ml of each water sample were stored at -20 °C and later measured colorimetrically using a QuAatro SFA Analyzer (Seal Analytical, Southampton, UK). After the subsample was taken for nitrate analysis, the rest of each sample (~180 ml) was filtered onto Whatman GF/F filters (25 mm diameter, 0.7 µm nominal pore size) to determine chlorophyll *a* concentrations. The filters were stored at -20 °C, until treatment by an ultrasonic device and chlorophyll *a* extraction into 90 % acetone. Chlorophyll *a* content of this solution was measured with a calibrated TD-700 Laboratory Fluorometer (Turner Designs, Sunnyvale, California, USA) (Edler, 1979; Evans et al., 1987).

Table 9-1

Scientific instruments of PAUL in the 2013 Arctic campaign.

Parameter	Type of device	Manufacturer
Conductivity	SBE 49FastCAT	Sea Bird Electronics (Bellevue, Washington, USA)
Temperature		
Pressure		
Dissolved Oxygen	SBE 43	Sea Bird Electronics (Bellevue, Washington, USA)
Nitrate	Deep SUNA	Satlantic (Halifax, Canada)
PAR	PAR-log-s	Satlantic (Halifax, Canada)
Chlorophyll <i>a</i>	C7-c	Turner Designs (Sunnyvale, California, USA)
CDOM	C7-u	Turner Designs (Sunnyvale, California, USA)
pCO ₂	HydroC CO2	Contros (Kiel, Germany)
Sample Collector	Prototype	AWI

9.3.2 AUV Operations

PAUL was deployed by the German research vessel “*Maria S. Merian*” (in further text: “*Merian*”) as part of the Arctic expedition MSM 29 (Wenzhöfer et al., 2014). The dive that this study focusses on, the third dive of the expedition, started at 8:30 PM on July 2nd and ended at 2:25 AM on July 3rd.

The dive area was localized using satellite imagery and observing the evolution of the ice cover. On a smaller scale, the dive area was further localized using temperature, salinity and fluorescence recordings obtained by *Merian*’s flow system. Navigating relative to the ice edge, *Merian* could determine the position and orientation of the meltwater front which *PAUL* was supposed to cross during the mission.

The dive area was at 78.76 °N and 5.15 °E at the southeast edge of a large ice tongue (Fig. 9-1). The mission itself consisted of two 9 km long

sections perpendicular to the meltwater front. The two sections were ~1 km apart with the eastern section being the first to be occupied by *PAUL*. Along the sections, *PAUL* conducted several “float” maneuvers where it shut down its thruster, drifted towards the surface with 10 – 20 cm s⁻¹ vertical speed and recorded a high resolution vertical profile of the water column (Wulff et al., 2013). Each float started in 50 m water depth. In open water, *PAUL* reactivated its thruster at 3 m water depth, still drifting further up for another 2 m. If there was the risk of encountering ice floes, the thruster was reactivated at 7 m depth, with *PAUL* peaking at 5 m. In total, 22 Floats were conducted during the entire mission resulting in a horizontal station spacing of 800 – 1,000 m (Fig. 9-1). For this study, only data recorded during the floats were used. In order to accurately georeference the measurements, *PAUL*’s navigation data needed to be corrected.

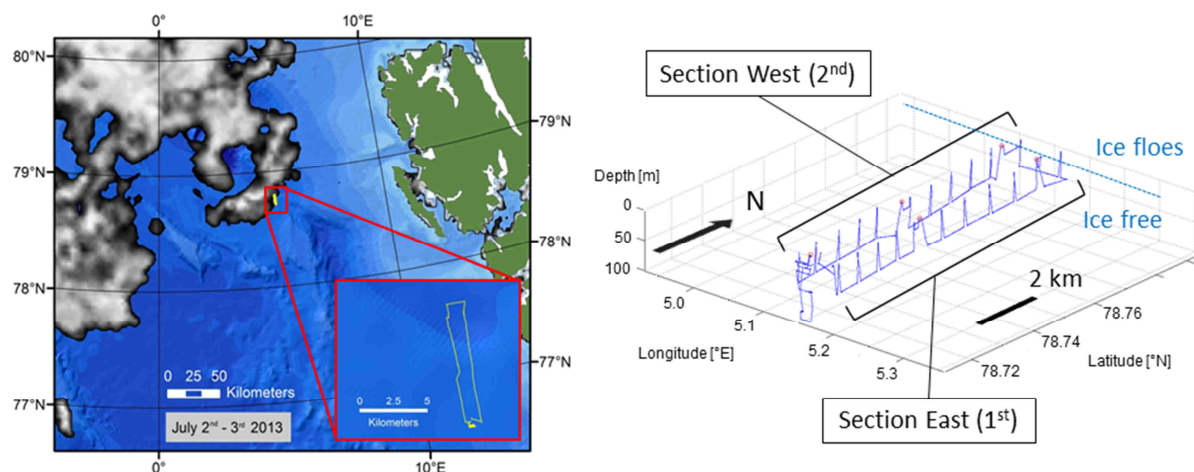


Fig. 9-1. Left panel: *PAUL*’s dive (yellow) at the southeast edge of the ice tongue on July 2nd and 3rd 2013. Green: Svalbard, blue: bathymetry, Grey: ice concentration on July 2nd dive according to data of satellite GCOM-1 “Shizuku”. The inset shows a detail view of the dive. Right panel: the dive in detail showing the two sections. Floats can be seen as spikes along the track. The northernmost part of the dive took place in an area with scattered ice floes.

As shallow AUV missions in the Molloy Deep area entail distances of several thousand meters between the vehicle and the seafloor, the vehicle's Doppler Velocity Log (DVL) was unable to establish seafloor tracking. Thus, *PAUL* missed a fixed reference to support its Inertial Navigation System (INS) and the navigation accuracy was degraded. Consequently, the Ultra Short Baseline (USBL) System "GAPS" of the French manufacturer iXBlue (Marly le Roi, France) was used to track the vehicle from the ship. After the dive, *PAUL*'s navigation data were corrected applying the tracking data and the correction algorithm described by [Wulff & Wulff \(2015\)](#).

9.3.3 Environmental data

Ice cover from satellite data

The dynamics of the ice was monitored using data of the Advanced Microwave Scanning Radiometer 2 (AMSR2) instrument onboard the Japanese earth observation satellite GCOM-W1 "Shizuku". Data were processed by the Institute of Environmental Physics at the University of Bremen (Bremen, Germany) and were downloaded from:

http://www.iup.uni-bremen.de:8084/amsr2data/asi_daygrid_swath/n3125/2013/jul/Svalbard/.

Derived ice charts have a spatial resolution of 3.125 km and a temporal resolution of 24 h ([Sprenn et al., 2008](#)). The ice edge is defined as the 10 % ice concentration boundary line. To determine the orientation of the ice edge relevant for this study, a boundary with a distance of the 1st mode baroclinic Rossby radius was introduced around *PAUL*'s dive path. The intersections between the ice and this boundary

were used to determine the orientation of the ice edge.

Salinity, Temperature and Chlorophyll a from Merian's underway system

Near-surface measurements were taken by *Merian's* clean seawater facility. In a permanently flushed measuring chamber a thermometer SBE 38 and a thermosalinograph SBE 45 (both manufactured by Sea Bird Electronics) were used to gather temperature and salinity information. An ECO FLNTU fluorometer by WetLabs (Philomath, Oregon, USA) was used to measure the chlorophyll *a* fluorescence in the chamber. The water inlet of the system was positioned ~6 m below the water line.

Wind data from a reanalysis

Velocity and direction of the wind was determined using model data of the "Modern-Era Retrospective Analysis for Research and Applications" (MERRA) ([Rienecker et al., 2011](#)) as provided by the GIOVANNI platform ([Acker & Leptoukh, 2007](#)).

http://gdata1.sci.gsfc.nasa.gov/daac-bin/G3/gui.cgi?instance_id=MERRA_HOUR_3D

The spatial resolution of the grid is 1.25° x 1.25° and the temporal resolution is 3 h. Since the surface wind speed is of interest for this study, only the 1,000 hPa pressure level was analyzed. Shipboard wind measurements served as reference values to allow a ground truthing of the MERRA data. Most data points were within a tolerance limit of +/- 30° for the wind direction and +/- 2 m s⁻¹ for the wind speed. The local wind conditions in the study area were determined by averaging the velocities and directions of the four MERRA grid points edging

PAUL's area of operation. In this study, the wind direction is given in relation to the ice edge or the meltwater front respectively (Fig. 9-2).

The depth of the wind-influenced layer depends on the turbulence level and type in the upper water column which is typically parameterized with an eddy viscosity A_Z . The thickness of the Ekman layer (Ekman, 1905) can then be expressed as

$$D_E = \sqrt{\frac{2\pi^2 \cdot A_Z}{\bar{\rho}_D \cdot f}} \quad (1)$$

Here $\bar{\rho}_D$ is the average potential density of a water body and f is the Coriolis parameter.

Water Currents

To obtain data on water current velocities, a 75 kHz Acoustic Doppler Current Profiler (ADCP) of the type Ocean Surveyor (Teledyne RD Instruments, San Diego, California, USA) was operated onboard *Merian*. ADCP profiles were recorded between 23 and 335 m water depth and the profiles consisted of 39 Bins with a cell size of 8 m each. For this study, ADCP data recorded 3 h after *PAUL*'s dive were used. Post Processing was conducted applying a MATLAB® software package, developed by

GEOMAR (Kiel, Germany) to process RDI-ADCP data [T. Fischer, personal communication]. Due to an unknown error and although data of the ship's Motion Reference Unit (MRU) as well as GPS data were fed into the system, the first bins seemed to be influenced by *Merian*'s motions. As three casts with the ship's CTD were conducted during the ADCP measurements, these three positions offered "reference points" where the ship stood still and ADCP data were not influenced. It turned out that above 60 m water depth, ADCP data with *Merian* moving and data with *Merian* standing still showed significant differences. Thus, for this study, all ADCP data above 60 m water depth were neglected.

Surface Irradiation

Surface irradiation in the wavelength range of 400 – 700 nm (Photosynthetically Active Radiation, PAR) was constantly measured with a shipboard radiometer. By comparing these surface data with *PAUL*'s PAR data, the euphotic depth (ED) could be determined. Conventionally the threshold value to define the lower boundary of the euphotic zone is set at the depth where 1 % of the surface PAR value is present (e.g. Lee et al., 2007).

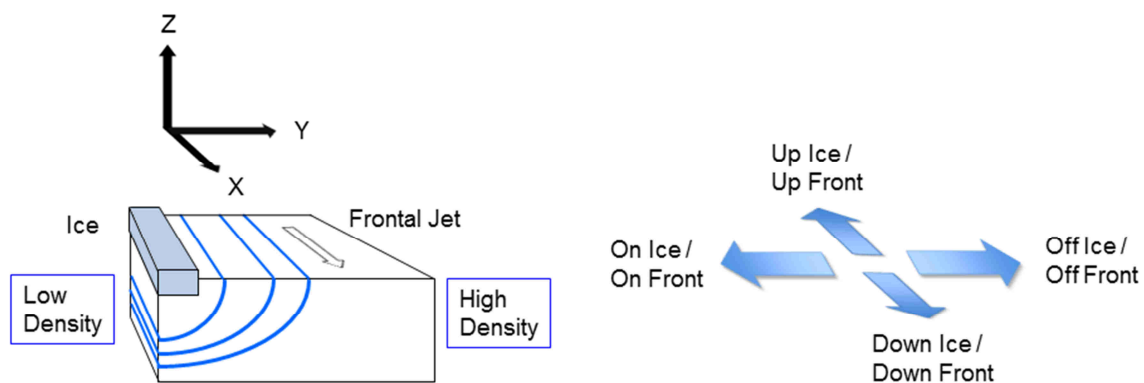


Fig. 9-2. Naming convention to define orientations and directions for this study.

9.4 Results and Discussion

9.4.1 Physical Conditions in the MIZ

Before turning our attention to the sections measured by the AUV, we first describe the physical conditions at the dive site from auxiliary data.

9.4.1.1 Environmental data

Environmental data considered in this study date back one week prior to the dive (observation started on June 25th 2013). To provide a coherent picture of the measurements and to bring them into temporal relationship, data are contextualized in a single figure (Fig. 9-3).

Ice cover

From June 25th onwards, an ice tongue could be observed which rose from the main ice edge south of the Molloy Deep area into southern direction (Fig. 9-3 b, c, d). Between June 25th and June 28th this ice tongue drifted to northeast. During this “Northeast Drift Event” (NDE), the southern tip of the ice tongue travelled 70 km in 72 h. Due to a slight rotation of the tongue, the western flank travelled only 60 km in the same time. After the NDE, the ice tongue remained at its geographical site, yet changed its shape. Between June 28th and June 29th a second and smaller ice tongue becomes visible just west of the Molloy Deep. The Molloy Deep itself remained ice free. Over the following days both tongues slowly advanced to the south. On July 2nd the tongue in the east suddenly drifted several kilometers to southwest, so both tongues formed an almost closed ring around the Molloy Deep. On this particular day, *PAUL* was

deployed at the southeast edge of the eastern tongue. On the day after the dive the eastern tongue abruptly retreats several kilometers northward. In contrast to that, the western tongue kept drifting to south. Satellite based measurements of the Sea Surface Temperature (SST) showed that the ice tongues encountered water temperatures of 2 – 5 °C, with a maximum on July 3rd. *Merian*'s radar systems indicated that the ice field at *PAUL*'s study area consisted of numerous ice floes of different sizes and with different surface textures.

Meltwater front

The formation of a meltwater front was associated with the ice edge. Beginning with June 25th, the front was crossed several times by *Merian* and on July 1st, 2nd and 3rd the orientation of the front was determined by crossing it within short periods of time at different locations. The front was orientated zonally with the meltwater in the north (Fig. 9-3 e). On July 2nd and 3rd the front was crossed 6 times within 12 hours. In this time the front drifted ~1.1 km northward (2.5 cm s⁻¹).

Data of three different cross-front sections (Crossing A, B and C, Fig. 9-4), which were occupied by *Merian* on July 1st and 2nd, revealed differences in the intensity of the front. Data of crossings A and C showed a relatively smooth transition between Atlantic and Polar water. In contrast, a sharp bend can be noticed in the temperature and salinity graphs of crossing B (at 3 km) and the graph is curved in a convex manner. This can be interpreted as a strong horizontal gradient with contour lines on the surface lying closer to each other than in crossings A and C (Fig. 9-3 f).

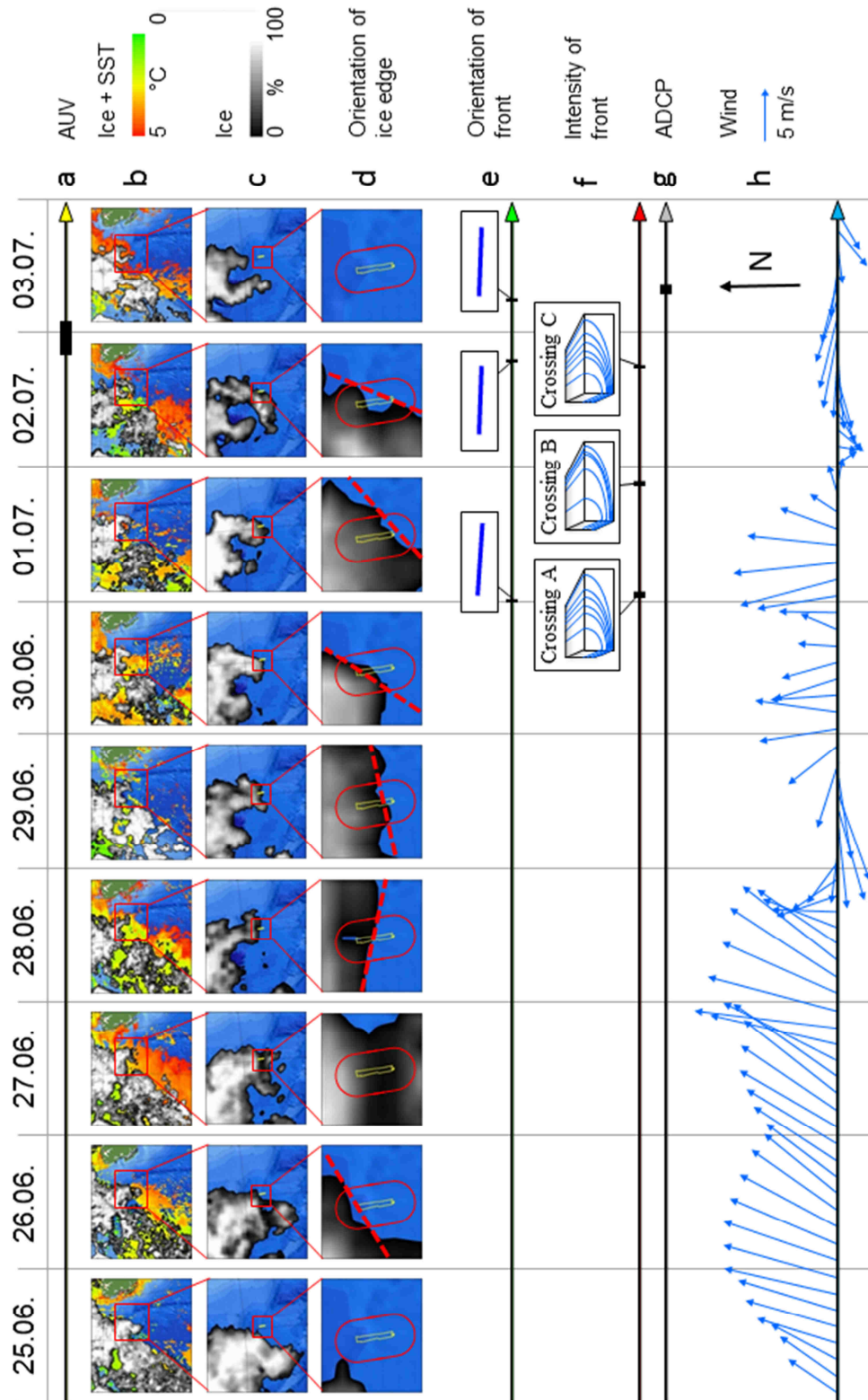


Fig. 9-3. Chronologic sequence of the different investigations and the evolution of relevant features from June 25th to July 3rd. a) AUV dive on July 2nd / 3rd. b) Large scale (W x H: 570 km x 500 km) evolution of the ice edge and sea surface temperatures. c) Medium scale (W x H: 180 km x 155 km) evolution of the ice edge and ice concentration. d) Small scale (W x H: 27 km x 25 km) view of the ice and 1st mode baroclinic Rossby radius around PAUL's dive path. Broken red line illustrates orientation of the ice edge. e) Orientation of the meltwater front as measured by *Merian*. f) Qualitative illustration of the cross-front density gradient (intensity of front) as measured by *Merian*. g) Time frame of ADCP measurements and h) Wind speed and direction.

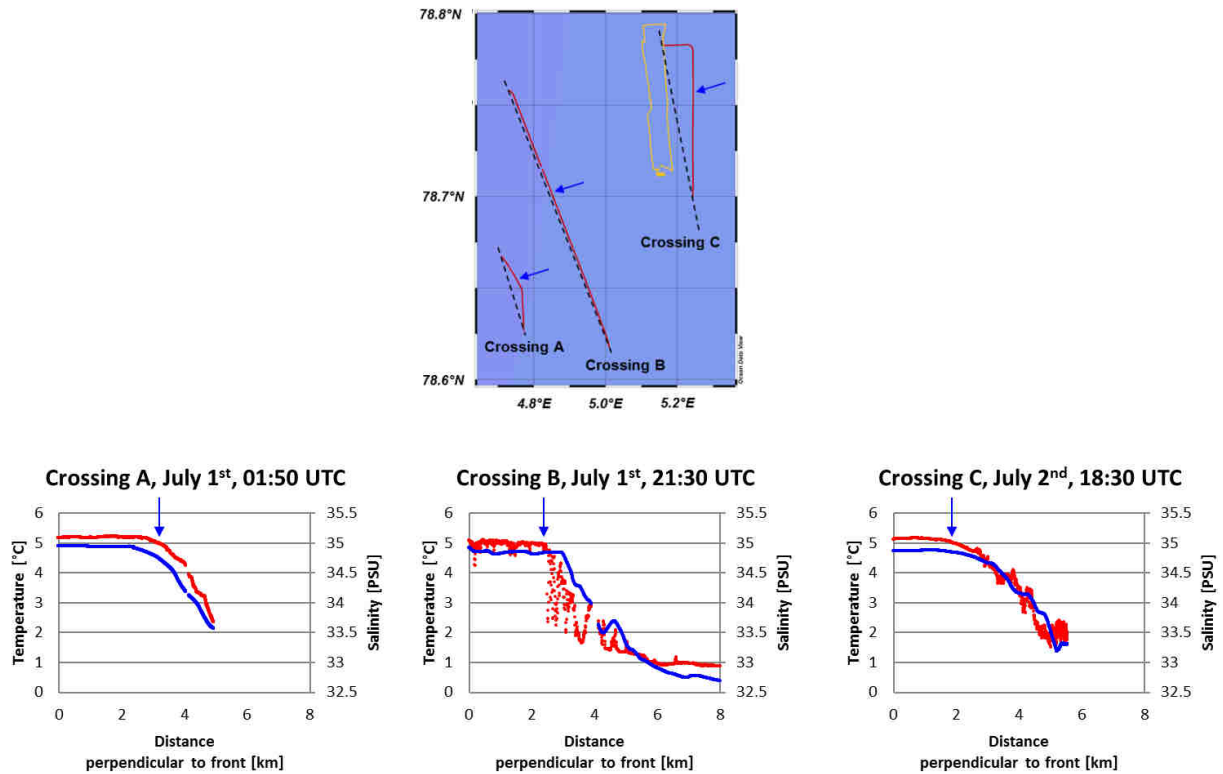


Fig. 9-4. Upper panel: locations of the three crossings (red tracks) used in this study in relation to *PAUL*'s dive (yellow). The broken black lines indicate projection planes perpendicular to the front. Lower panels: temperature (red) and salinity (blue) profiles as recorded by *Merian*'s flow through system and projected onto the respective planes. The blue arrows mark the front. The left side of the profile corresponds to the southern tip of each crossing.

Currents

A cross-front ADCP profile, which was recorded 3 hours after *PAUL*'s dive (Fig. 9-3 g), showed westward velocities of $\sim 0.1 \text{ m s}^{-1}$ between 60 and 100 m water depth (Fig. 9-5). As the front was orientated almost zonally, this corresponds to a geostrophically balanced down-front water flow. Further in the south (Fig. 9-5), the current is $\sim 0.1 \text{ m s}^{-1}$ southward. Regarding the orientation of the front, this corresponds to an off-front current.

Wind

The investigated time frame was dominated by southerly or southwesterly winds (Fig. 9-3 h). Short phases of easterly winds were only observed on June 29th, July 2nd and July 3rd. For these easterly wind events, the average wind

speed was 5.5 m s^{-1} (max. 8.7 m s^{-1} , min. 1.8 m s^{-1}). For the rest of the time the average wind speed was 8.5 m s^{-1} (max. 13.6 m s^{-1} , min. 2.1 m s^{-1}). The different orientations of the ice edge and meltwater front resulted in wind conditions not being identical for these two features – however they always had a common wind component. For example, the easterly wind event on July 2nd resulted in down-front yet on-ice wind conditions.

An Ekman layer of 70 m depth would result from an eddy viscosity of about $40 \text{ kg m}^{-1} \text{ s}^{-1}$ which is similar to what has been inferred (Schmidt, 1917; Neumann & Pierson, 1966) for wind velocities of $\sim 9 \text{ m s}^{-1}$. This wind velocity is consistent with values recorded during the investigated time frame. Due to lower wind speeds during the easterly wind events, the Ekman layer may have been shallower (40 m) during these events.

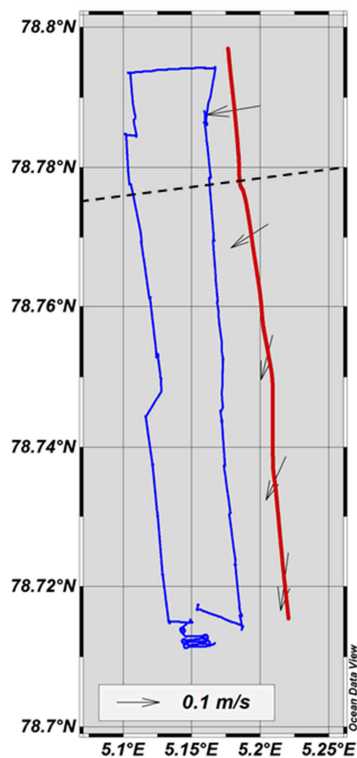


Fig. 9-5. Merian's ADCP section (red) in relation to PAUL's dive (blue). ADCP data were recorded about 3 h after PAUL's dive. Arrows indicate the average flow direction and speed of the water between 60 and 100 m depth. The broken black line represents the front. With increasing distance from the front the flow rotates from down-front to off-front. The speed is about 0.1 m s^{-1} .

9.4.1.2 AUV sections

PAUL was deployed in about 5 km distance to the ice-associated meltwater front. As measured by *PAUL*, the meltwater layer consisted of modified Atlantic water featuring lower temperatures and lower salinities compared to the Atlantic water masses it overlaid (Fig. 9-6). The Atlantic water masses had an average salinity of ~ 35 PSU and a temperature of $4.2 - 5.3 \text{ }^\circ\text{C}$. In the meltwater layer itself, water temperatures dropped below $1 \text{ }^\circ\text{C}$ and salinity values reached a minimum of 33 PSU.

The AUV sections are shown in Fig. 9-7. Beginning at a section distance of $x = 6 \text{ km}$, the meltwater layer can be seen as a water body of 15 m thickness. It extended to the north. Isopycnals around the meltwater layer run close to each other and show the strong stratification of the water column in this area. An area at around $x = 2 \text{ km}$ and 25 – 30 m water depth is noticeable as isopycnals have an increased vertical separation and the water column is less stratified from the surface to 50 m water depth (Fig. 9-7 cW/cE). Other areas with low buoyancy frequencies can be recognized at $x = 6 - 8 \text{ km}$ (section west) and $x = 4 - 6 \text{ km}$ respectively (section east). However, these areas do not reach to the surface but peak at around 30 m depth.

The meltwater front between isopycnals of 26.8 and 27.4 kg m^{-3} exhibits steep horizontal gradients and thus is likely subject to fast instabilities such as symmetric instability (Thomas et al., 2013). Away from the front, the water column is stable with respect to symmetric instability.

Except for minor variations the two sections are very similar in their hydrographic structures and can almost be considered symmetrical.

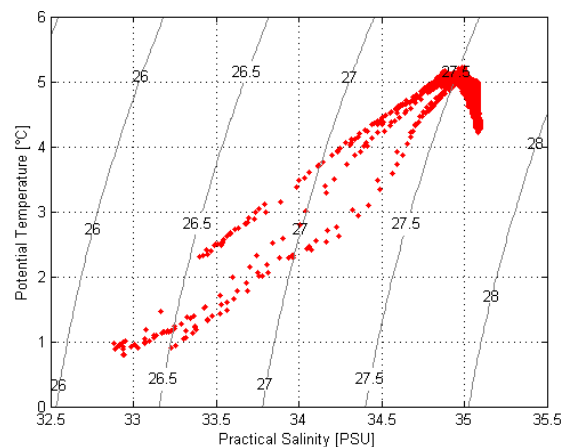


Fig. 9-6. T-S diagram of the AUV data showing physical properties of the investigated water masses. Grey contour lines represent isopycnals. Values conglomerate at about 35 PSU and $4.2 - 5.3 \text{ }^\circ\text{C}$. Modified Atlantic water representing the meltwater layer is visible at < 35 PSU.

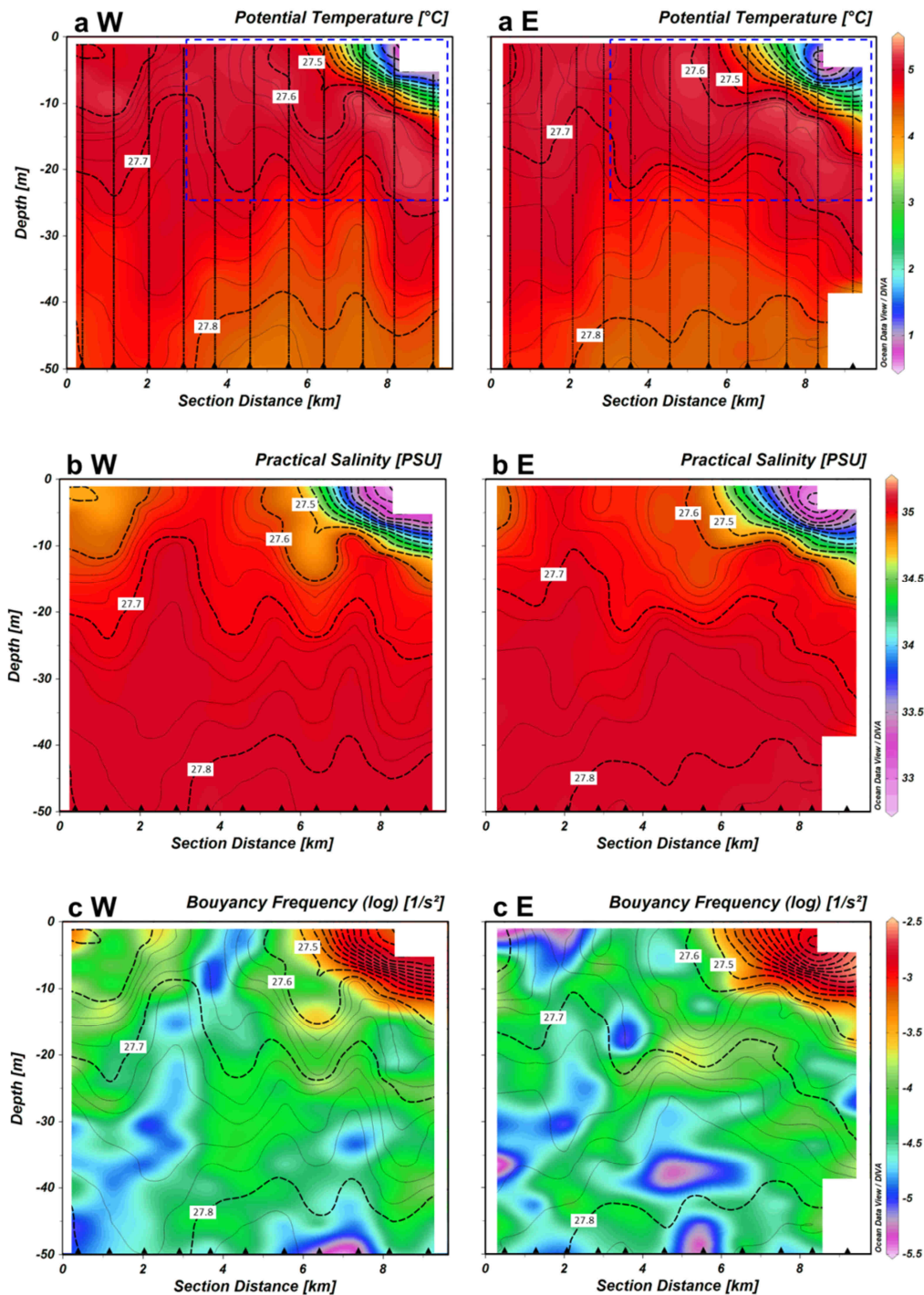


Fig. 9-7. Sections showing the physical data recorded by *PAUL*. From top to bottom: a) potential temperature, b) practical salinity, and c) stratification ($\log(N^2)$). Left column showing results for section west (W), right column for section east (E). Section west and east according to Fig. 9-1. A section distance of $x = 0$ km corresponds to the southern (ice free) end of the sections. Figures aW/aE and bW/bE contain the following isopycnals: Broken black lines represent an increment of 0.1 kg m^{-3} . For $\sigma_\theta > 27.6 \text{ kg m}^{-3}$, an increment of 0.02 kg m^{-3} is indicated by thin black lines. Black triangles at the bottom of each section show positions of the float maneuver (additionally illustrated by vertical lines in the potential temperature plot). The broken blue rectangle in the potential temperature plot depicts the boundaries of a detail view used in Fig. 9-9.

9.4.2 Physical Processes in the MIZ

9.4.2.1 Wake Upwelling

Numerical models illustrated that atmospheric forcing can cause various physical processes in MIZs. Among others, upwelling processes that can emerge along drifting ice edges interacting with down ice wind conditions were investigated by Fennel & Johannessen (1998). In their “case Johannessen” an ice edge consisting of a solid ice cover and a field of ice floes with a width of the 1st mode baroclinic Rossby radius (~5 km) in front of it encounters down ice wind conditions. Momentum transfer between wind and ocean is assumed to be largest below the ice floes. In the model, the ice retreats at a constant speed of 10 cm s⁻¹. After ~20 h of excitation ($ft = 10$, applied to PAUL’s dive site at 79° N), an upward bulging of the isopycnals of 5 – 10 m could be detected (Fennel & Johannessen, 1998). The upwelling signature was visible to 100 m depth. It propagated with the ice, yet it also remained present along the path of the moving ice. Consequently the ice left a large area of upwelled water in its wake.

In addition to that, not only the presence of ice but also variations in its spatial distribution can lead to pycnocline changes when the system is affected by down ice wind conditions. Taking variations in the ice concentration at scales of tens of kilometers along a straight ice edge, for example the model of Häkkinen (1986) generated pycnocline anomalies of +9 m. The size of the anomalies was found to be related to the size of the supporting ice cover variation. For cover variations perpendicular to the ice edge and reaching from 20 - 80 % within 20 km distance, the resulting upwelling signature along the ice edge was 25 km wide after 1.5 days of excitation ($ft = 18.5$) at wind speeds of 12 m s⁻¹

(Häkkinen, 1986). In case of a wavy ice edge the anomaly was even more emphasized.

Applied to the present study, down ice, upwelling favorable wind conditions along the 70 km long western flank of the ice tongue were observed in the period from June 25th – 28th and June 30th – July 1st with wind speeds of 6 – 10 m s⁻¹. The northeast drift event (NDE, June 25th – 28th) matches with this time frame. If a constant drift of the western flank is assumed, this equals 23 cm s⁻¹ which is roughly in agreement with the speed of the ice edge in the model of Fennel & Johannessen (1998). Satellite images indicated a wavy ice edge during this period. Ice cover variations are detectable, yet spatial and temporal resolutions of the images are too coarse to clearly follow the evolution of the ice cover. However, if stochastic distribution of the ice is assumed, conditions similar to the model of Häkkinen (1986) are not unlikely.

Upwelling along the western flank could have resulted from both processes. Due to the drift of the ice, signatures of vertical transport propagated over a large distance and leave an area of upwelled water behind (Fig. 9-8). We suggest that these signatures which were formed along the western flank of the ice tongue eventually also affected PAUL’s later diving site.

9.4.2.2 Frontogenesis

Most studies investigating physical processes initiated by atmospheric forcing have focused on the influence of the ice itself. Apart from the ice edge however, frontal systems can also generate vertical transports and thus need to be taken into account as well. As it was shown along the Kuroshio Current (Thomas & Lee, 2005; Clayton et al., 2014) or the Gulf Stream (Thomas et al., 2013), down front wind conditions can cause an intensification of a front (frontogenesis).

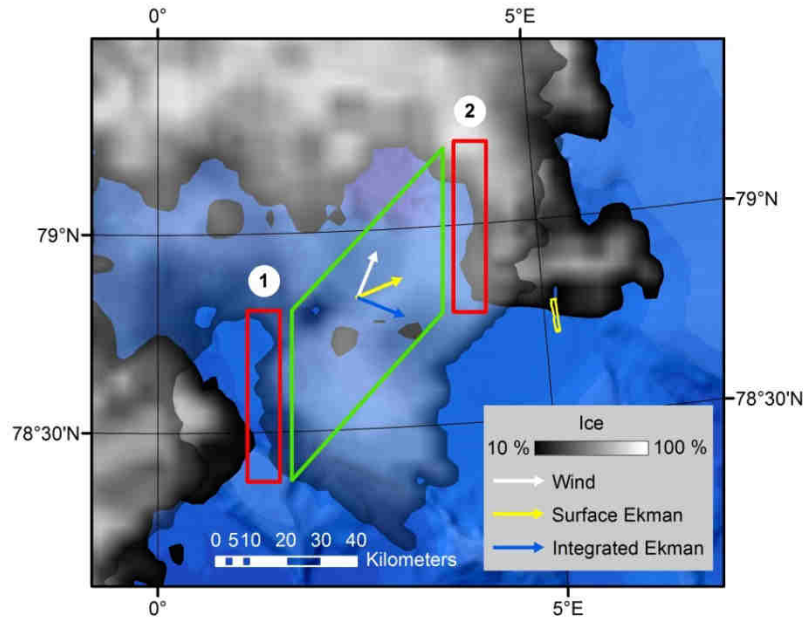


Fig. 9-8. Ice conditions on June 25th (transparent grey top layer) and on June 28th overlaying a bathymetric chart of the Molloy Deep region. *PAUL*'s dive is indicated by the yellow rectangle at the edge of the ice tongue. The white arrow shows the predominant wind direction of 22° for this time frame. Wind speed was 6 – 10 m s⁻¹. The meridional western flank of the ice tongue is highlighted in a red rectangle (1: June 25th, 2: June 28th). In the green area, water was upwelled due to the flank's drift.

Frontogenesis is a stepwise process that involves the generation of ageostrophic secondary circulations (ASC) with downwelling on the dense side of the front and upwelling along the frontal interface (Thomas & Lee, 2005). The characteristic cross-front width of an ASC is defined as the distance between the upwelling or downwelling branches of two neighboring circulating cells (L_0 , Thomas & Lee, 2005).

$$L_0 = \frac{4H\sqrt{-q_{ml}}}{f^2} \quad (4)$$

Here, H is the depth of the mixed layer, f is the Coriolis parameter and q_{ml} is the potential vorticity (PV) in the mixed layer defined by

$$q_{ml} = N_{ml}^2 f^2 - M_{ml}^4 \quad (5)$$

$$q_{ml} = \frac{-g}{\rho_0} \frac{\partial \rho}{\partial z} f^2 - \left(\frac{g}{\rho_0} \frac{\partial \rho}{\partial y} \right)^2 \quad (6)$$

Here, N_{ml}^2 is the vertical stratification (buoyancy frequency) in the mixed layer and M_{ml}^2 is the horizontal stratification. The earth's gravity is given by g and ρ and ρ_0 represent the density of the water and the density of a reference layer respectively.

The structure of the water column close to the meltwater front indicates the presence of ongoing upwelling and downwelling processes. Isopycnals are bulged upwards at section distances of $x = 5 - 6$ km and $7 - 8$ km (section west) and at $x = 4 - 5$ km and 7 km (section east) (Fig. 9-9). In this region, the water column structure suggests a horizontal density gradient of $\sim 4 \cdot 10^{-4}$ kg m⁻³ m⁻¹ and a vertical gradient of $\sim 7 \cdot 10^{-2}$ kg m⁻³ m⁻¹ along the sections shown in Fig. 9-9. Applying these values and assuming a mixed layer depth of 30 m and a reference layer density of 1027 kg m⁻³ in Eq. 4 leads to a cross front width of the ASC of 2,800 to 5,800 m, which is consistent with the observations. Both sections cross the same ASC that has a cross-front width of about 3,000 m.

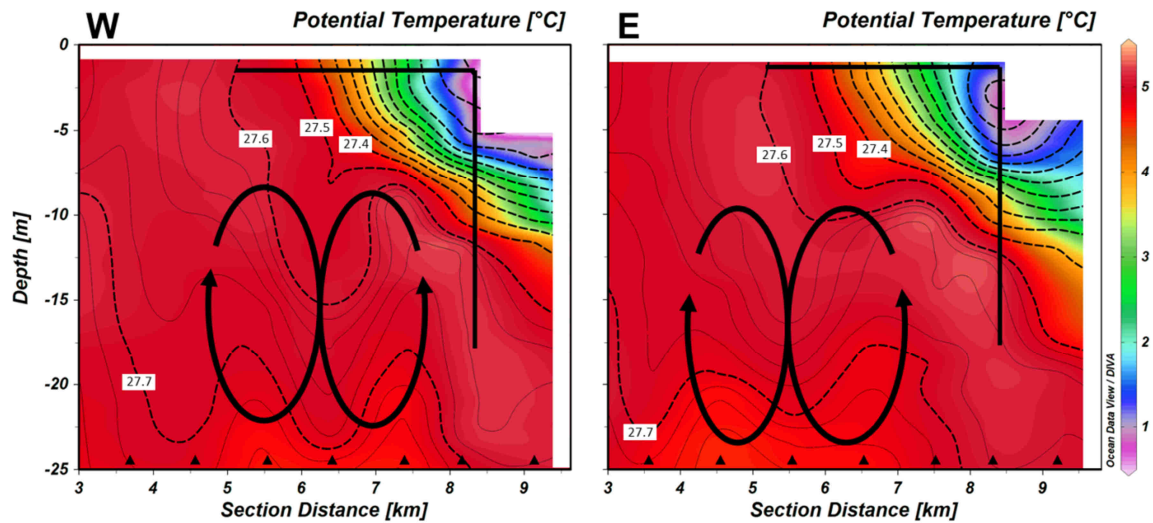


Fig. 9-9. Potential temperature and isopycnals at the frontal interface (detail view from Fig. 9-7 aW/aE). Left panel, western section. Right panel, eastern section. Black arrows illustrate the position and sense of rotation of the ASC-related upwelling / downwelling cells. Black lines represent sections over which the vertical and horizontal gradient was measured to calculate L_0 . The increment of the isopycnals is the same as in Fig. 9-7. Black triangles at the bottom of each section show positions of the float maneuver.

However, it needs to be stated that equations are quite unstable in this region and results of Eq. 6 are close to 0. Minor variations in the parameters are sufficient to change a cell's diameter significantly or even make Eq. 4 unsolvable.

At a greater distance from the front, at section distances of 2 – 4 km (Fig. 9-7 aW/aE), the isopycnals indicate another upwelling area above 25 m water depth. Although no associated downwelling branch is visible, it can be speculated that this structure represents the upwelling part of another cell.

Frontogenetic processes quickly affect the water column. Results of a numerical study (Thomas & Lee, 2005) which was conducted for ~12 m Ekman depth, revealed the formation of upwelling and downwelling areas within 1 – 1.5 inertial periods (wind stress: 0.1 N m^{-2} and atmospheric buoyancy flux: $6.3 \cdot 10^{-8} \text{ m}^2 \text{ s}^{-3}$). Considering the parameter regime of our study (dive site at 78.76°N), 1 – 1.5 inertial periods correspond to 12 – 18 h. During the 2013 Arctic campaign, down front wind conditions were

recorded as well (July 2nd, prior to the dive). These winds prevailed for only a short period of time, yet the duration exceeded 12 h. In addition to that, horizontal density gradients at the meltwater front were significantly steeper than in case of past investigations at the Kuroshio Current (Thomas & Lee, 2005; Clayton et al., 2014) or the Gulf Stream (Thomas et al., 2013). As a result, the horizontal Ekman buoyancy flux is huge, equivalent to several 10s of thousands W m^{-2} surface heat loss, whereas normal huge storm events would lead to a maximum of $1,000 \text{ W m}^{-2}$ in open water, disregarding processes associated with sea ice. Thus, ASCs could cause high vertical velocities along a meltwater front.

It is regrettable that the upper 60 m of ADCP data must be neglected due to an unknown and uncorrectable error. Due to the missing velocity data, important parameters could not be calculated. Since no flight model exists for PAUL (as it does for gliders), attempts to calculate water velocities by means of the spatial drift PAUL encountered during the individual

floats remained unsuccessful as well. Thus, u_g which is the horizontal alongfront velocity of the geostrophic flow is undetermined in the following equation to define the two-dimensional PV of the geostrophic flow (Thomas & Lee, 2005):

$$q_g = N^2 \left(f^2 - f \frac{\partial u_g}{\partial y} \right) - M^4 \quad (7)$$

With increasing distance to the front, the water current rotated from a down-front flow to an off-front flow (Fig. 9-5). Thus, the gradient of the horizontal alongfront velocity is negative ($\partial u_g / \partial y < 0$). Assuming water currents between the surface and the depth of the meltwater layer (0 – 15 m) are comparable to the flow pattern shown in Fig. 9-5, this would increase the vertical stability term in Eq. 7. However, cross-front density gradients are huge – making low PV values, including negative PV, likely. Since the AUV did not measure water currents, the PV could not be computed directly. Low PV values would, however, be indicative of the action of symmetric instability and ASCs which would subduct water with PV ~ 0 (marginal stability).

9.4.3 Ecological Response

9.4.3.1 Generally Elevated Nitrate Values

In both sections of the dive, PAUL detected widespread nitrate concentrations of $4 \mu\text{mol l}^{-1}$ in less than 10 m water depth. In comparison to investigations which have been conducted in the same region and the same season, these surface nitrate concentrations appear to be generally elevated (e.g. in comparison to Kattner & Becker, 1991: $0 - 2 \mu\text{mol l}^{-1}$ between 0 – 30 m depth, Smith et al., 1985: $0 - 1 \mu\text{mol l}^{-1}$ between 0 – 30 m depth; Smith, 1987a: $0 - 3 \mu\text{mol l}^{-1}$ in the euphotic zone; Bauerfeind et al., 2014: $0 - 5 \mu\text{mol l}^{-1}$ between 0 – 20 m depth). This observation is further supported by data of a similar dive PAUL accomplished in the same region (15 km further south) and season (17 days later) in summer 2012. In 2012 the water column showed a “classic” pattern with the nutricline following the lower boundary of the euphotic zone in a depth of about 25 m (Fig. 9-10).

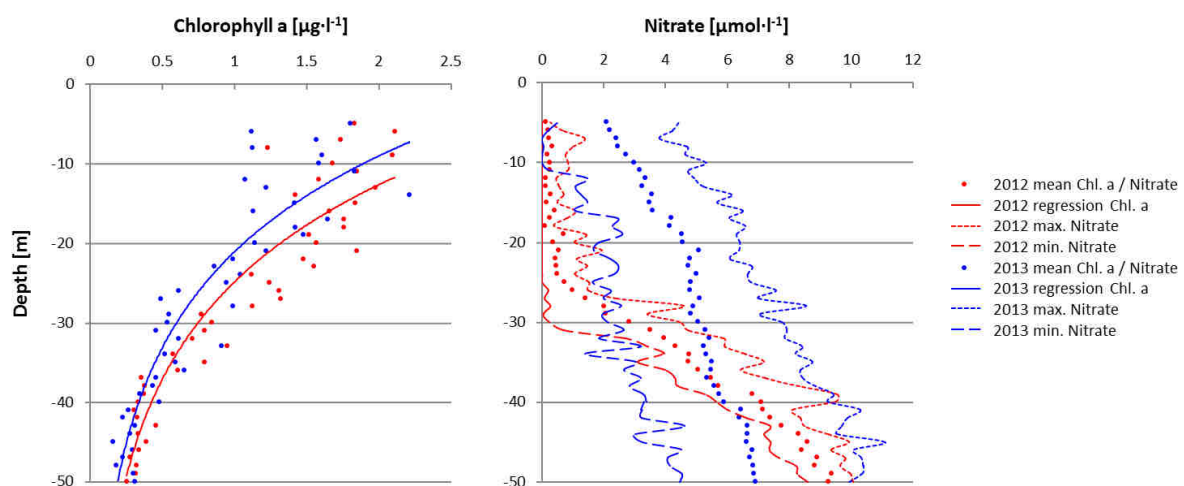


Fig. 9-10. Comparison between the AUV dives of 2012 (not ice-associated) and 2013 (in the MIZ). Left panel: average chlorophyll *a* concentrations fitted by logarithmic curves. Chl. *a* distributions were almost identical. Right panel: average nitrate concentrations. For averaging, data of all Float maneuvers of the respective dive (2012: 9 Floats, 2013: 22 Floats) were averaged for depth intervals of 1 m.

Above the nutricline, nitrate concentrations were low ($< 1 \mu\text{mol l}^{-1}$). Below that depth, nitrate concentrations rose quickly – reaching $10 \mu\text{mol l}^{-1}$ in 50 m water depth. In contrast to this, average nitrate levels of 2013 reached $2 \mu\text{mol l}^{-1}$ at the surface and no indications for a nutricline could be found. Additionally, the values show higher variance in 2013. The vertical distribution and amount of chlorophyll *a* of 2012 and 2013 is almost identical – indicating that phytoplankton has not adapted to enhanced nutrient availability in 2013 yet. Thus we conclude that an associated upwelling event occurred prior to the AUV dive, probably within a few days. The main difference between the dives of 2012 and 2013 was the absence of ice in 2012. In 2012 the ice was over 90 km away and the water column was unaffected by ice or meltwater related processes. It thus seems that the exceptionally high nitrate concentrations of 2013 were caused by large scale upwelling processes occurring in the vicinity of the drifting ice tongue (see “Wake Upwelling”). This conclusion is consistent with the drift of the ice tongue – especially the NDE which lasted until June 28th (four days prior to PAUL’s dive). Although the area affected by the drifting ice tongue is about 25 km further west (Fig. 9-8), we suggest that large scale upwelling along the western flank of the ice tongue also affected PAUL’s diving site.

9.4.3.2 Biogeochemical Zones

One of the most prominent features in the biogeochemical sections is an area with high concentrations of chlorophyll *a* close to the surface directly at the meltwater interface at $x = 4 - 5$ km (Fig. 9-11 aW/aE). Here, chlorophyll concentrations reached $4 - 5 \mu\text{g l}^{-1}$. A second area with elevated chlorophyll

concentrations ($2 - 3 \mu\text{g l}^{-1}$) is noticeable at the interface of the front at $x = 6$ km, reaching down to ~ 20 m. In a third area at $x = 1 - 2$ km chlorophyll concentrations of $1 - 1.5 \mu\text{g l}^{-1}$ could be measured to a maximum depth of 50 m (likely even deeper). This is remarkable as the euphotic depth (ED) was determined to be at 27 ± 7 m depth (Fig. 9-11 aW/aE).

Elevated chlorophyll *a* concentrations go along with low nitrate concentrations and high rates of oxygen saturation (Fig. 9-11 bW/bE and cW/cE) indicating growing phytoplankton populations. In areas of highest chlorophyll concentrations at the surface, nitrate was hardly detectable whereas the water was supersaturated with oxygen (120 %) due to ongoing primary production. Chlorophyll rich water masses below the euphotic zone at $x = 1 - 2$ km also feature this characteristic ratio of low nitrate concentrations and high oxygen saturation values.

The three parameters oxygen saturation, nitrate and chlorophyll *a* concentration illustrate another prominent feature of the sections across the meltwater front: Centered at $x = 4$ and $8 - 9$ km in section west and at $x = 3$ and 8 km at section east, “dome-like” structures of high nitrate concentrations are present (Fig. 9-11 bW/bE). These domes are ~ 2 km wide and rise from 50 to 30 m water depth. Compared to surface conditions, the domes are characterized by a reverse ratio of the biogeochemical parameters with low chlorophyll *a* and oxygen saturation values, yet high nitrate concentrations. Within the domes, chlorophyll *a* could not be detected and nitrate reached a maximum of $10 - 12 \mu\text{mol l}^{-1}$. Oxygen saturation values were reduced compared to surface values, but still reached 100 %. At the frontal interface, at about $x = 6$ km and $0 - 20$ m depth, it can be seen that gradients in nitrate and oxygen saturation are almost parallel to isopycnals.

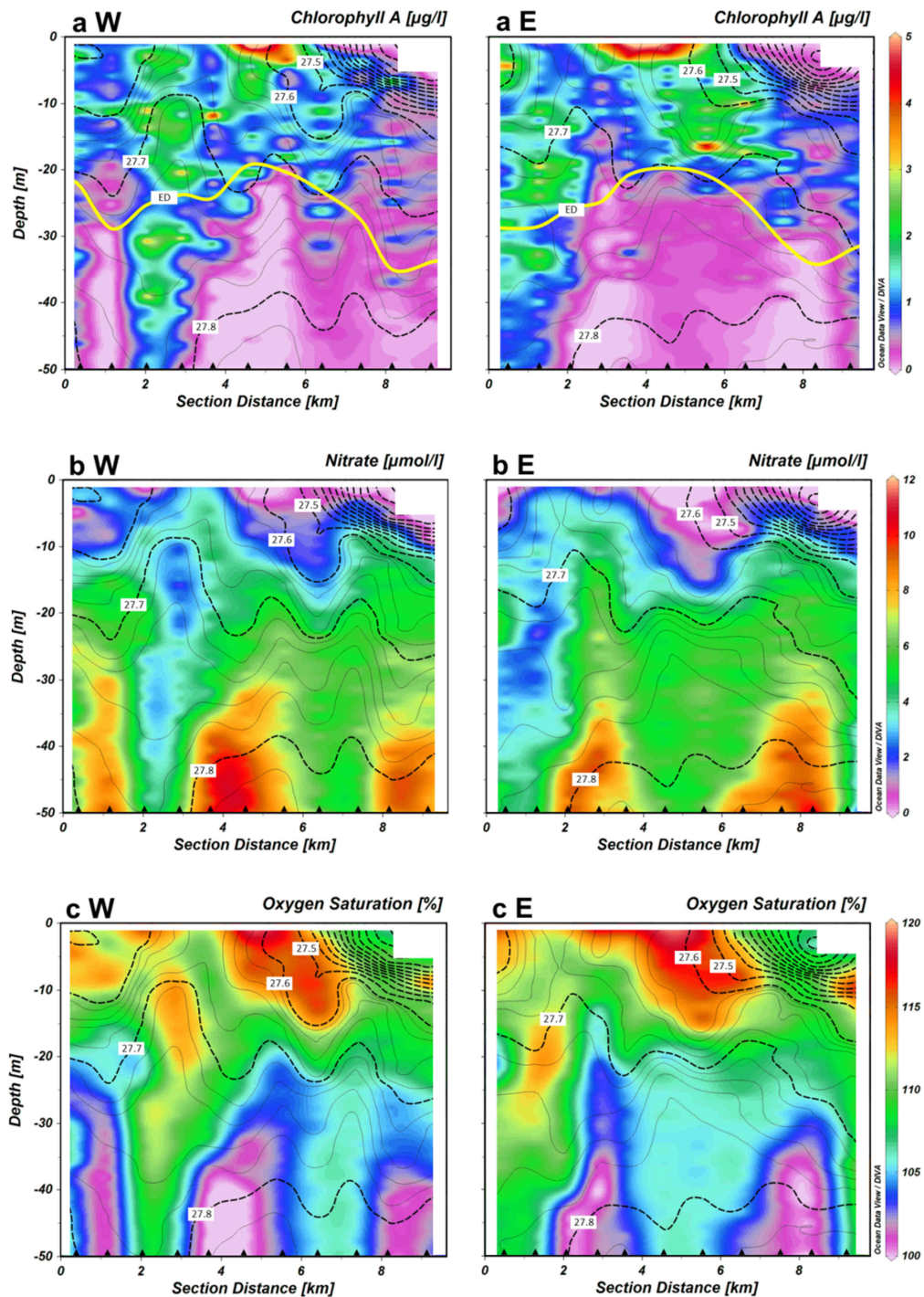


Fig. 9-11. Sections showing biogeochemical data recorded by *PAUL*. a) chlorophyll *a*, b) nitrate, and c) oxygen saturation. For reference, the sections contain the same isopycnals as in Fig. 9-7. Left column shows results for section west (W), right column for section east (E). Section west and east according to Fig. 9-1. A section distance of $x = 0$ km corresponds to the southern (ice free) end of the sections. Black triangles at the bottom of each section indicate positions of the float maneuvers. The yellow line (ED) in the chlorophyll *a* plots represents the euphotic depth.

In contrast, this relation between isopycnals and biogeochemical parameters cannot be detected for the domes. The domes are clearly visible in the biogeochemical parameters, yet they cross the contour lines of the physical parameters.

All described structures cannot be identified in the CDOM distribution (not shown). In general, CDOM values equaled between 0.5 – 0.6 ppb quinine sulfate (QS). Within the meltwater layer, values dropped to 0.45 ppb QS.

The almost symmetric picture of the two sections in the hydrographic properties is also seen in the biogeochemical data. Except for the domes the biogeochemical parameters correspond to the physical parameters. Although PAUL's data reach down to only 50 m, we expect the structures to continue into greater depth.

Based on PAUL's results, 4 different biogeochemical zones could be identified in each of the sections. In Fig. 9-12 these zones are marked showing chlorophyll *a* concentrations for reference. The black rectangle frames the chlorophyll *a* maximum at the surface. This zone will further be referred to as the “accumulation zone”. Below, the “subduction zone” which includes the area of elevated chlorophyll *a* concentrations below the meltwater layer, is marked with a red rectangle. In the south of each section the yellow rectangle marks the “low stratification zone”: a narrow belt of elevated chlorophyll *a* concentrations that reach down below the euphotic zone. Finally, the blue rectangles indicate the “domes”.

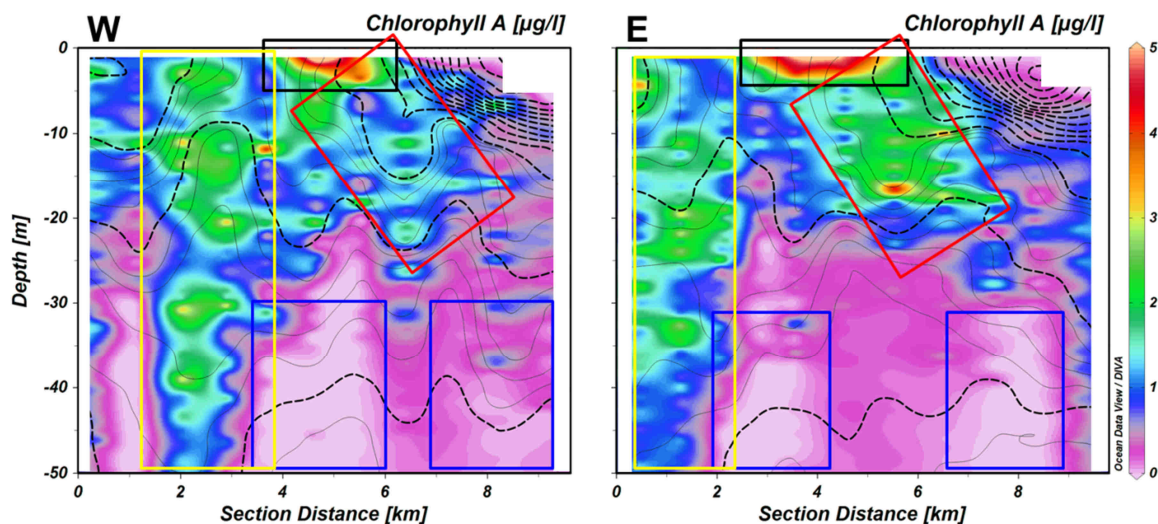


Fig. 9-12. The four different biogeochemical zones: The accumulation zone (black), the subduction zone (red), the low stratification zone (yellow) and the domes (blue) are shown relative to the chlorophyll *a* distribution. Left figure: section west. Right figure: section east.

Accumulation and Subduction Zone

It is an obvious question how the high chlorophyll *a* concentrations in the accumulation zone, located directly along the meltwater layer to a depth of 5 m, were formed (Fig. 9-12: black rectangle). Measurement errors can be excluded as the existence of that zone was confirmed by several independent measurement parameters (e.g. oxygen saturation, nitrate concentration). In addition to that, the ED is elevated by about 7 m below this zone. This can be explained by turbid water due to high phytoplankton concentrations. Estimating the amount of nitrate necessary to produce this amount of phytoplankton with a C/Chl ratio of 100 – 200 g g⁻¹ according to Smith & Sakshaug (1990) and a C/N ratio of 6.7 mol mol⁻¹ (Redfield, 1963; Sterner et al., 2008) results in a nitrate requirement of 5 – 10 μmol l⁻¹ to explain the chlorophyll *a* concentration. As the dive was conducted at the beginning of July, several months after the Arctic plankton bloom in spring (between March and May, e.g. Degerlund & Eilertsen, 2010), the maximum nitrate concentrations encountered in the study region at that time were between 0 – 3 μmol l⁻¹ (at 5 m depth). Hence, although nitrate concentrations were not totally depleted, it is unlikely that it has grown at that spot but is the product of recent upwelling and accumulation processes at the meltwater interface. Accumulation of plankton at frontal systems is a known feature which besides physical processes is also affected by the ability of phytoplankton organisms to regulate its buoyancy (e.g. Smayda et al., 1970; Skreslet, 1988; Franks, 1992; Acuna et al., 2010; McManus and Woodson, 2012; Prairie et al., 2013; Arrieta et al., 2015).

Furthermore, the subduction zone (Fig. 9-12: red rectangle) which is considered to be the downwelling branch of an ASC-related upwelling / downwelling cell seems to be

strongly connected to the accumulation zone. The downward displaced density contour lines are consistent with an ongoing downward vertical motion on the denser side of the front with phytoplankton being actively transported into deeper regions (Fig. 9-7 aW/aE: $x = 6$ km, 15 m depth). The buoyancy frequency and the oxygen saturation values in the subduction zone are also increased compared to the surrounding water (buoyancy frequency approx. $10^{-3.5}$ s⁻² in contrast to 10^{-4} s⁻² and 117 % oxygen saturation in contrast to 107 %, Fig. 9-7 cW/cE and Fig. 9-11 cW/cE). This can be explained by a plume of stratified surface water which was submerged at the denser side of the front.

The existence of the two zones and wind data give rise to the following scenario: The meltwater front was orientated zonally from July 1st onwards (Fig. 9-3 e). Assuming the front was also orientated zonally on June 30th, on front wind conditions dominated for 48 hours (Fig. 9-3 h). Due to surface Ekman transport, on front wind conditions caused an intensification of the front as it was recorded by Merian in the evening of July 1st (Fig. 9-3 f), and, at the same time, phytoplankton was accumulated along the frontal interface. In the morning of July 2nd, wind conditions turned to down-front – eventually stimulating a frontogenetic ASC. Starting on July 2nd, the upwelling / downwelling cell of the ASC, situated at $x = 7$ km and 12 – 15 m water depth, partly eroded the accumulation zone from below and transported phytoplankton into deeper regions. We propose that species or individuals with a slightly smaller positive buoyancy were advected with the water along the isopycnals to greater depth. This would explain the intermediate chlorophyll *a* concentrations in the subduction zone (red rectangle). Conversely, phytoplankton with stronger positive buoyancy would remain in the lower density surface layer as the water's density slightly increases upon

subduction and isolation from diurnal heating and wave breaking induced bubble input. This could explain the apparent decoupling of the phytoplankton transport from the water flow. That is, the phytoplankton is not purely advected like a passive tracer such as oxygen or nitrate and other dissolved substances. This is the only scenario by which we can explain the vastly higher chlorophyll *a* concentration in the accumulation zone (Fig. 9-12: black rectangle). Unfortunately, the proposed scenario cannot be tested with the available data as PAUL's water samples were not analyzed with respect to plankton composition. However, qualitative analyses of plankton net samples from the upper 20 m taken in the vicinity of the ice edge after the dive revealed that colonies of *Phaeocystis sp.* dominated. Alternatively, some phytoplankton may be adapted to stay at the surface. There may also be differences in the exact level of positive buoyancy between different species or individuals of a species.

Low Stratification Zone

With regard to the physical parameters, the low stratification zone (Fig. 9-12: yellow rectangle) is characterized by isopycnals with extended vertical distance. This phenomenon had been detected before (see Johannessen et al. (1983), their Fig. 15, section X, at $x = 18$ km and 10 – 18 m depth), but the evolution of that feature had not been discussed. As observed during the AUV dive, chlorophyll *a* has been submerged to at least 50 m well below the euphotic depth in this zone. Thus, it was not formed at that depth, yet must have encountered active vertical transport. The course of the isopycnals and submerged chlorophyll *a* suggests that a downwelling event might have been superimposed by a smaller upwelling event. Although a specific downwelling event could not be identified, it can be speculated that upwelling

was caused by frontogenetic processes on July 2nd. The upwelling event lasted shorter and its impact remained limited to the uppermost meters – causing the isopycnals to move further apart.

Another option to explain this structure is the presence of a filament which was crossed by PAUL's dive. Filaments can be related to frontogenetic processes and high vorticity filaments can be associated to significant vertical water transports (Lapeyre & Klein, 2006; Legal et al., 2007). However, as PV values cannot be determined, this approach remains speculative.

Domes

The domes (Fig. 9-12: blue rectangles) could indicate individual upwelling events. However, the dome-like structure could also result from downwelled surface water, in the region between the domes.

Taking the $8 \mu\text{mol l}^{-1}$ nitrate concentration contour line to mark the domes, it can be seen that the tips of the domes reach up to ~35 m water depth (Fig. 9-13). In 2012, the water contains similar amounts of nitrate at ~35 – 40 m (Fig. 9-10) and various other studies also reported comparable nitrate distributions (e.g. $8 \mu\text{mol l}^{-1}$ nitrate in Smith et al., 1985: 50 ± 15 m depth; Smith, 1987a: 50 ± 15 m depth; Kattner & Becker, 1991: between 40 – 50 m depth). This makes the domes less exceptional than the space between them.

Compared to the domes, the space between them features slightly increased oxygen saturation values and chlorophyll concentrations. In contrast to this, nitrate concentrations are reduced (Fig. 9-11 bW/bE). This indicates that the water originated from the surface or at least from a layer within the euphotic zone. In addition, salinity values are lower in the space between the domes than within them (Fig. 9-13 W: $x = 6 - 8$ km and E: $x = 4 - 6$ km).

9.5 Conclusion

As salinity is unaffected by biological processes and as it is exchanged slowly, it can be considered the most stable parameter of the entire system, clearly marking displaced water masses. However, isopycnals do not show any sign of downwelling between the domes.

We suggest that the domes do not represent individual upwelling events but they are relicts of the former stratification of the water column. Thus the domes are a negative imprint of a previous process that formed the gaps between them.

Within the framework of this study, an AUV conducted physical and biogeochemical investigations at the meltwater front of a moving ice edge. Occupying two transects of 9 km length each, the vehicle collected data on salinity, temperature, density, oxygen saturation, PAR intensity, nitrate and chlorophyll *a* concentrations between the surface and 50 m water depth. Subsequently, four zones with different biogeochemical characteristics could be identified. Using satellite and ship bound data, the results of the dive were put into a larger context and processes which might have caused the evolution of the observed structures are discussed.

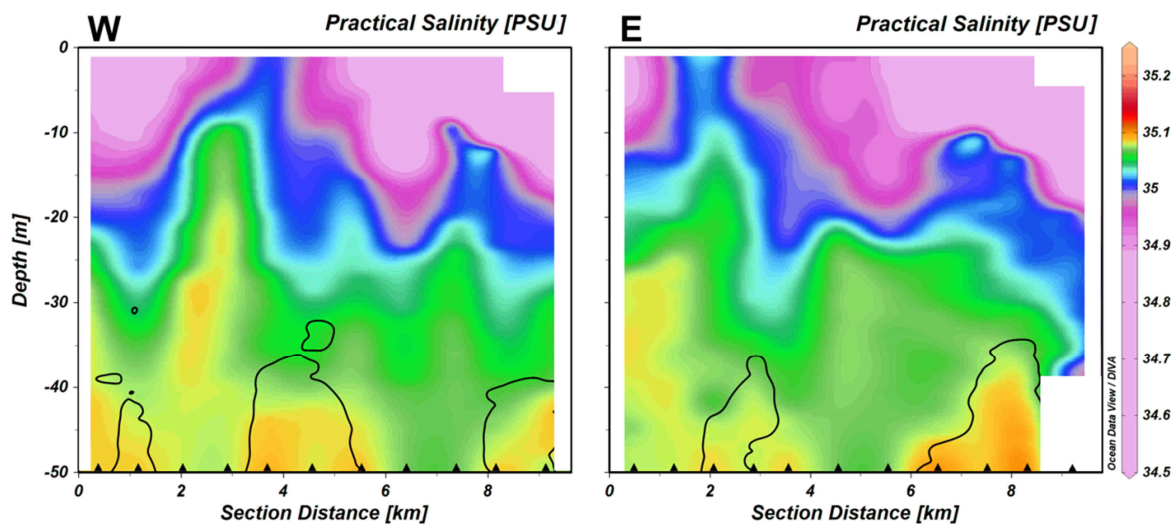


Fig. 9-13. Salinity profiles with modified colorbar settings to make reduced salinity values between the domes visible. The domes are indicated by the $8 \mu\text{mol l}^{-1}$ nitrate contour lines (black lines). Black triangles mark float positions along the track. Left figure, section west. Right figure section east.

The processes described in this study take place on different spatial and temporal scales. The four different biogeochemical zones (accumulation zone, subduction zone, low stratification zone, and the domes) resulted from small scale processes which quickly affect the water column (smaller than the 1st mode baroclinic Rossby radius of ~5 km and faster than one inertial period of ~12 h). The accumulation and subduction zone were formed by surface convergence and a frontogenetic ASC. The main difference between previous studies and *PAUL*'s investigations is the depth of the front. Previous field studies confirming the findings of [Thomas & Lee \(2005\)](#) were conducted at systems where the frontal structures were deeper than the Ekman layer (e.g. at the Kuroshio Current by [Thomas & Lee \(2005\)](#) or along the Gulf Stream by [Thomas et al. \(2013\)](#)).

Thus, the entire momentum of the wind affected the front in the form of the integrated Ekman transport. The herein described meltwater front only reached to 15 m depth and the depth of the Ekman layer was estimated to be about 40 m during the down-front wind event on July 2nd. As a consequence, only the momentum close to the surface is communicated to the front ([Lee & Eriksen, 1996](#)). The depth of the front might also limit the ecologic relevance of frontogenetic processes. As the depth of the front determines the depth over which the ASC penetrates, a shallow front entails shallow ASCs as well. Frontogenetic upwelling and downwelling events might thus be confined to the euphotic zone and the nutrient concentrations would remain unchanged.

In contrast to the accumulation and subduction zone, processes which formed the low stratification zone and the domes remained speculative. As *PAUL*'s data provided just a short and small glimpse of the entire dynamics of the MIZ, the evolution of these structures could

not be traced back to a specific event. Quantifying these processes and predicting their impact on larger areas, maybe even on the MIZ of the entire Fram Strait is not possible yet. Consequently, there is no reason to doubt the conclusion of [Niebauer \(1991\)](#) stating that ice edge upwelling plays a minor role for biologic stimulation compared to eddy-driven upwelling or nutrient laden surface water being suddenly exposed to sunlight due to a retreating ice edge.

The situation is different in the case of a drifting ice tongue. Due to their drift, such ice structures have the potential to trigger extensive vertical transport processes. Depending on their respective shape, these structures feature edges with different orientations. Assuming an idealized rectangular ice tongue, reaching several tens of kilometers from the main ice edge and its marginal zone consisting of scattered ice floes, there are three edges offering three different possibilities for down ice, upwelling favorable wind conditions (of course at the same time it offers the same number of opportunities for downwelling favorable wind conditions). The ice tongue extends far from the main ice field so that internal ice stress does not affect the tongue's drift. Down ice wind conditions generate ice edge upwelling and at the same time, cause an up-ice Ekman transport. Thus the ice is constantly pushed away from the region where it has just caused upwelling, leaving behind an upwelling signature that gets wider with the drift of the ice ([Fennel & Johannessen, 1998](#)).

Additionally, as investigated numerically by [Häkkinen \(1986\)](#), variations in the ice concentration can also cause upwelling processes along an ice edge when forced by down-front winds. If a stochastic distribution of ice floes is assumed within the ice tongue, it is not unlikely that there are variations in the ice cover that are comparable to the scenario given in [Häkkinen \(1986\)](#). Eventually, this process might add to the

9.6 Acknowledgements

previously described upwelling due to a drifting ice tongue. Hence, every larger ice tongue with its drift predominantly driven by the wind may entail a region with upwelled water masses in its wake. If this upwelling is accompanied by an increased nutrient availability, it depends on the residence time and growth rate of phytoplankton in the water column to what extent this can be used for primary production. Especially for the eastern Fram Strait, this is an interesting question as ice tongues are a common feature there.

Apart from this, the impact of the meltwater front on vertical transport processes should be the subject of future research efforts. With respect to frontogenetic processes, the lack of water current data between the surface and 60 m water depth represented a major setback for this study. As a consequence, parameters indicating the stability of a water column (PV) could not be computed. However, *PAUL*'s measurements represent the first observations of frontogenetic processes and associated vertical transports at a meltwater front. This is of particular interest, as two independent systems, the ice and the front, both capable of stimulating vertical transports, are present in the confined area of a MIZ. The application of the theory of frontogenesis on meltwater fronts and the combined impact of ice and front related processes on the ecology of MIZs needs to be refined in the future.

The analysis revealed steep gradients and a patchy distribution of different parameters, emphasizing the necessity for high resolution data. Clayton et al. (2014) pointed out that alternative observation methods, namely operations with specifically equipped AUVs, are required “to fully understand the bio-physical dynamics” at frontal systems.

The authors would like to thank Sascha Lehmenhecker and Jonas Hagemann for their technical work and support on AUV *PAUL*. We would like to thank Kristin Hardge and Kai-Uwe Ludwichowski (both AWI) for their help with processing *PAUL*'s water samples and Tim Fischer (GEOMAR) for his help with processing *Merian*'s ADCP data. The achievements of Michael Klages, who initiated the entire AUV project at AWI in 2002, are gratefully acknowledged. Thanks are also due to all people involved in the Arctic cruise of *Merian* in June / July 2013 (MSM 29) – especially the ship's crew for excellent support and accommodation. AMSR-2 data were supplied by the GCOM-W1 data providing service, Japan Aerospace Exploration Agency (JAXA).

9.7 References

- Acuña, J. L., López-Alvarez, M., Nogueira, E., & González-Taboada, F. (2010). *Diatom flotation at the onset of the spring phytoplankton bloom: an in situ experiment*. *Mar. Ecol.-Prog. Ser.*, 400, 115-125.
- Acker, J. G., & Leptoukh, G. (2007). *Online analysis enhances use of NASA earth science data*. *Eos, Trans Amer Geophys Union*, 88(2), 14-17.
- Arrieta J., Barreira A., Tuval I. (2015) *Microscale Patches of Nonmotile Phytoplankton*. *Phys. Rev. Lett.* 114,128102-1 -128102-5.
- Bauerfeind, E., Nöthig, E. M., Beszczynska, A., Fahl, K., Kaleschke, L., Kreker, K., Klages, M., Soltwedel, S. Lorenzen, C., & Wegner, J. (2009). *Particle sedimentation patterns in the eastern Fram Strait during 2000–2005: Results from the Arctic long-term observatory HAUSGARTEN*. *Deep-Sea Res. Pt. I*, 56(9), 1471-1487.
- Bauerfeind, E. et al., 2014. *Inorganic nutrients measured on water bottle samples at HAUSGARTEN during POLARSTERN cruise ARK-XXIII/2*. Alfred Wegener Institute, Helmholtz Center for Polar and Marine Research, Bremerhaven.
- Beszczynska-Möller, A., Fahrbach, E., Schauer, U., & Hansen, E. (2012). *Variability in Atlantic water temperature and transport at the entrance to the Arctic Ocean, 1997–2010*. *ICES J. Mar. Sci.*, 69(5), 852-863.
- Bourke, R. H., Tunnicliffe, M. D., Newton, J. L., Paquette, R. G., & Manley, T. O. (1987). *Eddy near the Molloy Deep revisited*. *J. Geophys. Res.-Oceans (1978–2012)*, 92(C7), 6773-6776.
- Buckley, J. R., Gammelsrød, T., Johannessen, J. A., Johannessen, O. M., & Røed, L. P. (1979). *Upwelling: oceanic structure at the edge of the Arctic ice pack in winter*. *Science*, 203(4376), 165-167.
- Cherkasheva, A., Bracher, A., Melsheimer, C., Köberle, C., Gerdes, R., Nöthig, E. M., Bauerfeind, E., & Boetius, A. (2014). *Influence of the physical environment on polar phytoplankton blooms: a case study in the Fram Strait*. *J Marine Syst*, 132, 196-207.
- Clayton, S., Nagai, T., & Follows, M. J. (2014). *Fine scale phytoplankton community structure across the Kuroshio Front*. *J. Plankton Res.*, 36(4), 1017-1030.
- de Steur, L., Hansen, E., Gerdes, R., Karcher, M., Fahrbach, E., & Holfort, J. (2009). *Freshwater fluxes in the East Greenland Current: A decade of observations*. *Geophys. Res. Lett.*, 36(23).
- Degerlund, M., & Eilertsen, H. C. (2010). *Main species characteristics of phytoplankton spring blooms in NE Atlantic and Arctic waters (68–80 N)*. *Estuaries and coasts*, 33(2), 242-269.
- Doney, S. C. (2006). *Oceanography: Plankton in a warmer world*. *Nature*, 444(7120), 695-696.
- Dumont, D., Kohout, A., & Bertino, L. (2011). *A wave-based model for the marginal ice zone including a floe breaking parameterization*. *J Geophys. Res.-Oceans.* (1978–2012), 116(C4).
- Edler L. (1979). *Recommendations on methods for marine biological studies in the Baltic Sea. Phytoplankton and chlorophyll*. *Baltic Marine Biologists Publication* 5, 1-38.
- Ekman, V. W. (1905). *On the influence of the earth's rotation on ocean currents*. *Ark. Mat. Astron. Fys.*, 2, 1-53.

- Evans, C. A., O'Reilly, J. E., O'Reilly, J. E., & Thomas, J. P. (1987). *A handbook for the measurement of chlorophyll a and primary production (Vol. 8)*. Texas A&M University.
- Fennel, W., & Johannessen, O. M. (1998). *Wind forced oceanic responses near ice edges revisited*. *J. Marine Syst.*, 14(1), 57-79.
- Franks, P. J. (1992). *Phytoplankton blooms at fronts: patterns, scales, and physical forcing mechanisms*. *Rev. Aquat. Sci.*, 6(2), 121-137.
- Gammelsrod, T., Mork, M., & Roed, L. P. 1975. *Upwelling possibilities at an ice edge*. *Marine Science Communication Journal*, 1(2), 115-145.
- Häkkinen, S. (1986). *Coupled ice-ocean dynamics in the marginal ice zones: Upwelling/downwelling and eddy generation*. *J. Geophys. Res.-Oceans (1978–2012)*, 91(C1), 819-832.
- Haine, T. W., & Marshall, J. (1998). *Gravitational, symmetric, and baroclinic instability of the ocean mixed layer*. *J. Phys. Oceanogr.*, 28(4), 634-658.
- Johannessen, J. A., Johannessen, O. M., Svendsen, E., Shuchman, R., Manley, T., Campbell, W. J., & Van Leer, J. (1987). *Mesoscale eddies in the Fram Strait marginal ice zone during the 1983 and 1984 Marginal Ice Zone Experiments*. *J. Geophys. Res.-Oceans (1978–2012)*, 92(C7), 6754-6772.
- Johannessen, O. M., Johannessen, J. A., Morison, J., Farrelly, B. A., & Svendsen, E. A. S. (1983). *Oceanographic conditions in the marginal ice zone north of Svalbard in early fall 1979 with an emphasis on mesoscale processes*. *J. Geophys. Res.-Oceans (1978–2012)*, 88(C5), 2755-2769.
- Johannessen, O. M., Campbell, W. J., Shuchman, R., Sandven, S., Gloersen, P., Johannessen, J. A. & Haugan, P. M. (1992). *Microwave study programs of air-ice-ocean interactive processes in the seasonal ice zone of the Greenland and Barents Seas*. *Microwave Remote Sensing of Sea Ice*, 261-289.
- Johannessen, O. M., Sandven, S., Budgell, W. P., Johannessen, J. A., & Schuchman, R. A. (1994). *Observation and simulation of ice tongues and vortex pairs in the marginal ice zone*. *The Polar Oceans and their role in shaping the global environment*, 109-136.
- Josberger, E. G. (1987). *Bottom ablation and heat transfer coefficients from the 1983 Marginal Ice Zone Experiments*. *J. Geophys. Res.-Oceans (1978–2012)*, 92(C7), 7012-7016.
- Kattner, G., & Becker, H. (1991). *Nutrients and organic nitrogenous compounds in the marginal ice zone of the Fram Strait*. *J. Marine Syst.*, 2(3), 385-394.
- Kwok, R., Cunningham, G. F., Wensnahan, M., Rigor, I., Zwally, H. J., & Yi, D. (2009). *Thinning and volume loss of the Arctic Ocean sea ice cover: 2003–2008*. *J. Geophys. Res.-Oceans (1978–2012)*, 114(C7).
- Lapeyre, G., & Klein, P. (2006). *Impact of the small-scale elongated filaments on the oceanic vertical pump*. *J. Marine. Res.*, 64(6), 835-851.
- Lee, C. M., & Eriksen, C. C. (1996). *The subinertial momentum balance of the North Atlantic subtropical convergence zone*. *J. Phys. Oceanogr.*, 26(9), 1690-1704.
- Lee, C. M., Cole, S., Doble, M., Freitag, L., Hwang, P., Jayne, S., Jeffries, M. Krishfield, R., Maksym, T., & Maslowski, W. (2012). *Marginal ice zone (MIZ) program: science and experiment plan*. (No. APL-UW-1201). WASHINGTON UNIV SEATTLE APPLIED PHYSICS LAB.

- Lee, Z., Weidemann, A., Kindle, J., Arnone, R., Carder, K. L., & Davis, C. (2007). *Euphotic zone depth: Its derivation and implication to ocean-color remote sensing*. *J. Geophys. Res.-Oceans* (1978–2012), 112(C3).
- Legal, C., Klein, P., Treguier, A. M., & Paillet, J. (2007). *Diagnosis of the vertical motions in a mesoscale stirring region*. *J. Phys. Oceanogr.*, 37(5), 1413-1424.
- McManus, M. A., & Woodson, C. B. (2012). *Plankton distribution and ocean dispersal*. *J. Exp. Biol.*, 215(6), 1008-1016.
- MIZEX Group (1986). MIZEX East 83/84: *The summer marginal ice zone program in the Fram Strait/Greenland Sea*. *Eos*, 67(23).
- Neumann, G., & Pierson, W. J. (1966). *Principles of physical oceanography* (Vol. 545). Englewood Cliffs, NJ: Prentice-Hall, 210.
ISBN 10: 0137097417
- Nicolaus, M., Katlein, C., Maslanik, J., & Hendricks, S. (2012). *Changes in Arctic sea ice result in increasing light transmittance and absorption*. *Geophys. Res. Lett.*, 39(24).
- Niebauer, H. J. (1982). *Wind and melt driven circulation in a marginal sea ice edge frontal system: a numerical model*. *Cont. Shelf Res.*, 1(1), 49-98.
- Niebauer, H. J., & Alexander, V. (1985). *Oceanographic frontal structure and biological production at an ice edge*. *Cont. Shelf Res.*, 4(4), 367-388.
- Niebauer, H. J., & Smith, W. O. (1989). *A numerical model of mesoscale physical-biological interactions in the Fram Strait marginal ice zone*. *J. Geophys. Res.-Oceans* (1978–2012), 94(C11), 16151-16175.
- Niebauer, H. J. (1991). *Bio-physical oceanographic interactions at the edge of the Arctic ice pack*. *J. Marine Syst.*, 2(1), 209-232.
- Nihoul, J. C. (Ed.). (1986). *Marine interfaces ecohydrodynamics* (Vol. 42). Elsevier Oceanography Series, Elsevier, Amsterdam-Oxford-New York-Tokyo, 670.
ISBN: 978-0-444-42626-0
- Paquette, R. G., Bourke, R. H., Newton, J. F., & Perdue, W. F. (1985). *The East Greenland polar front in autumn*. *J. Geophys. Res.-Oceans* (1978–2012), 90(C3), 4866-4882.
- Prairie, J. C.; Sutherland, K. R.; Nickols, K. J.; Kaltenberg, A. M. (2012) *Biophysical interactions in the plankton: A cross-scale review*. *Limnol. Oceanogr.: Fluids and Environments* 2(1):121-145.
- Quadfasel, D., Gascard, J. C., & Koltermann, K. P. (1987). *Large-scale oceanography in Fram Strait during the 1984 Marginal Ice Zone Experiment*. *J. Geophys. Res.-Oceans* (1978–2012), 92(C7), 6719-6728.
- Redfield, A.C.; Ketchum, B.H.; Richards, F.A., (1963). *The influence of organisms on the composition of seawater*. In: "The Sea", M.N. Hill (ed.); Wiley, Interscience, New York, pp. 26-77.
- Rienecker, M. M., Suarez, M. J., Gelaro, R., Todling, R., Bacmeister, J., Liu, E., Bosilovich, M., Schubert, S., Takacs, L., Kim, G.-K., Bloom, S., Chen, J., Collins, D., Conaty, A., da Silva, A., Gu, W., Joiner, J., Koster, R., Lucchesi, R., Molod, A., Owens, T., Pawson, S., Pegion, P., Redder, C.R., Reichle, R., Robertson, F.R., Ruddick, A.G., Sienkiewicz, M., & Woollen, J. (2011). *MERRA: NASA's modern-era retrospective analysis for research and applications*. *J. Clim.*, 24(14), 3624-3648.
- Røed, L. P., & O'Brien, J. J. (1983). *A coupled ice-ocean model of upwelling in the marginal ice zone*. *J. Geophys. Res.-Oceans* (1978–2012), 88(C5), 2863-2872.

- Schmidt, W. (1917). *Wirkungen der ungeordneten Bewegung im Wasser der Meere und Seen*. Annalen der Hydrographie und maritime Meteorologie, 45, 367-381.
- Skogen, M. D., Budgell, W. P., & Rey, F. (2007). *Interannual variability in Nordic seas primary production*. ICES J. Mar. Sci., 64(5), 889-898.
- Skreslet, S. (1988) *Buoyancy in Phaeocystis pouchetii (Hariot) Lagerheim*. J. Exp. Mar. Biol Ecol., 119(22):157-166.
- Slagstad, D., and T. A. McClimans (2005) *Modeling the ecosystem dynamics of the Barents sea including the marginal ice zone: I. Physical and chemical oceanography*. J. Mar. Syst., 58(1-2):1-18.
- Slagstad, D., Ellingsen, I. H., & Wassmann, P. (2011). *Evaluating primary and secondary production in an Arctic Ocean void of summer sea ice: an experimental simulation approach*. Prog. Oceanogr., 90(1), 117-131.
- Smayda, T. J. (1970) *The suspension and sinking of phytoplankton in the sea*. Oceanogr. Mar. Biol. Ann. Rev. 8:353-414.
- Smith, D. C., J. H. Morison, J. A. Johannessen, & N. Untersteiner (1984), *Topographic generation of an eddy at the edge of the East Greenland Current*, J. Geophys. Res.-Oceans, 89(C5), 8205–8208.
- Smith, S. L., Smith, W. O., Codispoti, L. A., & Wilson, D. L. (1985). *Biological observations in the marginal ice zone of the East Greenland Sea*. J. Mar. Res., 43(3), 693-717.
- Smith, W. O., Baumann, M. E., Wilson, D. L., & Aletsee, L. (1987a). *Phytoplankton biomass and productivity in the marginal ice zone of the Fram Strait during summer 1984*. J. Geophys. Res.-Oceans (1978–2012), 92(C7), 6777-6786.
- Smith, W. O. (1987b). *Phytoplankton dynamics in marginal ice zones*. Oceanog. Mar. Biol., 25, 11-38.
- Smith, W. O., & Sakshaug, E. (1990). Polar Phytoplankton (Chapter 9). Polar oceanography, Part B: Chemistry, biology, and geology, *Academic Press Ltd., London*, 477.
ISBN: 0-12-653032-7
- Spreen, G., Kaleschke, L., & Heygster, G. (2008). *Sea ice remote sensing using AMSR-E 89-GHz channels*. J. Geophys. Res.-Oceans (1978–2012), 113, C02S03.
- Squire, V. A., & Moore, S. C. (1980). *Direct measurement of the attenuation of ocean waves by pack ice*. Nature, 283, 365 – 368.
- Sterner, R. W., Andersen, T., Elser, J. J., Hessen, D. O., Hood, J. M., McCauley, E., & Urabe, J. (2008). *Scale-dependent carbon: nitrogen: phosphorus seston stoichiometry in marine and freshwaters*. Limnol. Oceanogr., 53(3), 1169-1180.
- Thiede, J., Pfirman, S., Schenke, H. W., & Reil, W. (1990). *Bathymetry of Molloy Deep: Fram Strait between Svalbard and Greenland*. Mar. Geophys. Res., 12(3), 197-214.
- Thomas, L. N., & Lee, C. M. (2005). *Intensification of ocean fronts by down-front winds*. J. Phys. Oceanogr., 35(6), 1086-1102.
- Thomas, L. N., Taylor, J. R., Ferrari, R., & Joyce, T. M. (2013). *Symmetric instability in the Gulf Stream*. Deep-Sea Res. Pt. II, 91, 96-110.
- Wadhams, P., & Squire, V. A. (1983). *An ice-water vortex at the edge of the East Greenland Current*. J. Geophys. Res.-Oceans (1978–2012), 88(C5), 2770-2780.
- Wassmann, P. (2002) *Seasonal C-cycling variability in the open and ice-covered waters of the Barents Sea*. J. Marine Syst., 38 (1):1-7.

- Wassmann, P., et al. (2006) *Modelling the ecosystem dynamics of the Barents Sea including the marginal ice zone II. Carbon flux and interannual variability*. *J. Mar. Syst.* 59(1-2):1-24.
- Wassmann, P., & M. Reigstad. (2011). *Future Arctic Ocean seasonal ice zones and implications for pelagic-benthic coupling*. *Oceanography*, 24(3):220–231, <http://hdl.handle.net/10037/3910>
- Wenzhöfer, F., Asendorf, V., Bauerfeind, E., Bienhold, C., Hagemann, J., Hasemann, C., Hüttich, D., Janssen, F., Lalande, C., Lehmenhecker, S., Lochthofen, N., Nowald, N., Ratmeyer, V., Rehage, R., Reuter, R., Reuter, M., Schewe, I., Seiter, C., Soltwedel, T., Tardeck, F., Wulff, T., Zarrouk, M., (2014). *HAUSGARTEN 2013 - Cruise No. MSM29 - June 23 - July 12, 2013 - Tromsø (Norway) - Tromsø (Norway)*, Berichte von DFG Senatskommission für Ozeanographie, Bremen.
- Wulff, T., Bauerfeind, E., Hagemann, J., Hasemann, C., Koch, B. P., Lehmenhecker, S., Wurst, M., Klages, M. (2015). *Collecting Water Samples with AUV "PAUL". Sample Safety, Sample Purity and Exemplary Results of Field Measurements*. *Methods in Oceanography*. (submitted)
- Wulff, T., Lehmenhecker, S., Bauerfeind, E., Hoge, U., Shurn, K., & Klages, M. (2013). *Biogeochemical research with an Autonomous Underwater Vehicle: Payload structure and Arctic operations*. In *OCEANS-Bergen, 2013 MTS/IEEE* (pp. 1-10). IEEE.
- Wulff, T., Lehmenhecker, S., & Hoge, U. (2010). *Development and operation of an AUV-based water sample collector*. *Sea Technology*, 51(12), 15-19.
- Wulff, U. & Wulff, T. (2015). *Correcting Navigation Data of Shallow-Diving AUV in Arctic*. *Sea Technology*, 56(3), 27-30
- Zhang, Y., Bellingham, J. G., Ryan, J. P., & Godin, M. A. (2015). *Evolution of a physical and biological front from upwelling to relaxation*. *Cont. Shelf Res.*, 108, 55-64.
- Zhang, Y., Bellingham, J. G., Ryan, J. P., Kieft, B., & Stanway, M. J. (2013). *Two-dimensional mapping and tracking of a coastal upwelling front by an autonomous underwater vehicle*. In *Oceans-San Diego, 2013* (pp. 1-4). IEEE.

10 Conclusion

Within the framework of this thesis, an AUV was deployed to analyze the interaction between physics, chemistry and biology (“ecohydrodynamic”). Achieving the goal of collecting high resolution data in the MIZ with an AUV was a stepwise process. In a chronological order various sensors and supporting systems had to be integrated into the vehicle first. In a second step, maneuvers, procedures and data correction algorithms to conduct surface water measurements were developed. In a third and last step, dedicated studies to unravel the MIZ’s ecohydrodynamics were conducted.

The MIZ of the Fram Strait is an extremely dynamic environment with numerous processes occurring on different spatial and temporal scales. AUV dives can collect high resolution data, yet they merely provide a short and small glimpse of the conditions along the ice. Hence, it might be difficult to transfer the findings of this thesis onto MIZs in general.

10.1 Objective I: Scientific

Identification of key physical, chemical and biological parameters that define the productivity of the MIZ.

10.1.1 Physical parameters

The results of 2013 suggest that stratification is one of the key physical factors affecting the MIZ’s productivity as the distribution of phytoplankton (presented in [section 9.4.3.2](#), indicated by chlorophyll *a*) strongly correlates with the isopycnals. This finding is in agreement with [Cherkasheva et al. \(2014\)](#) where stratification was identified to be the most

important factor affecting primary production in the Fram Strait. Yet, for the MIZ and a meltwater layer, the statement can be more specific. A meltwater front is characterized by a change in salinity and temperature with density of sea water being rather dependent on salinity than on temperature. Thus, salinity is the underlying parameter governing the stratification along the MIZ and eventually affect its productivity.

There is also a temporal component associated to stratification as stratified waters can prevent nutrients from being resupplied – eventually terminating phytoplankton growth by nutrient depletion when the water column is not mixed.

Additionally, it is well known that the availability of light plays a crucial role for under ice production and can even be limiting ([Smith et al., 1987b](#); [Nicolaus et al., 2012](#)). However, PAR data, which have been recorded below a solid ice cover using *PAUL*’s float maneuver, are missing due to a payload malfunction in 2012. Consequently, the euphotic depth could not be determined. Data of the under ice dive of 2010 (conducted at a constant depth) indicate significant shading by the ice, yet shading below a solid ice cover could not be quantified in terms of light penetration depth.

To summarize this, the following factors were identified to be key physical parameters that affect the productivity of a MIZ:

- Gradient in salinity
- Period the salinity gradient is maintained
- Availability of light

10.1.2 Chemical parameters

Within the group of dissolved inorganic nutrients (nitrate, nitrite, phosphate, ammonium, silicate), nitrate is relatively easy to measure *in-situ*. Comparing a dive in the MIZ (2013) and an open water dive (2012), the distribution of nitrate is patchier at the MIZ. The steepest nitrate gradients are closely associated to regions of enhanced stratification, indicating that the stratification prevented nitrate and other nutrients from being resupplied. In some regions, nitrate was almost completely depleted. Hence, it was most likely limiting phytoplankton growth although melting sea ice tends to enhance possible limitation of biological activity (Tovar-Sánchez et al., 2010).

Measuring CO₂ in the water column was another objective of this thesis, as it also represents a nutrient and thus affects primary production. Furthermore it influences the water's pH value and causes ocean acidification (Orr et al., 2005; Engel et al., 2013; Low-Décarie et al., 2014). However, applied techniques turned out to be unsuitable. The response time of the implemented CO₂ sensor was within the range of minutes – making it impossible to conduct small scale water column studies as the AUV moves at speeds of 1.5 m s⁻¹. Determining CO₂ by conventional methods (measuring total alkalinity and dissolved inorganic carbon from PAUL's water samples) resulted in highly variable values. It is uncertain if these values represented real gradients or if they are due to measurement errors. As a consequence, no statement can be given on the relevance of CO₂.

To summarize this, the following factors were identified to be key chemical parameters that affect the productivity of a MIZ:

- Nitrate concentration

10.1.3 Biological parameters

Data of 2013 indicate that high phytoplankton concentrations can reduce the light penetration depth due to enhanced turbidity. As a consequence, less light is available and the euphotic depth is reduced – making it easier for organisms to sink below it. Additionally, the accumulation of phytoplankton can also result in an increased self-shading which can reduce production (e.g. Shigesada & Okubo, 1981). However the results suggest self-shading due to phytoplankton accumulation, PAUL's dive only provided a “snapshot” and the effects of this phenomenon on productivity could not be observed *in-situ*.

Furthermore, the chlorophyll *a* distribution measured in 2013 suggests that phytoplankton communities might be divided by the buoyancy of the species or even individuals. This approach remained speculative in section 9.4.3.2, yet there are clear indications that phytoplankton and water movements are at least partly decoupled, probably by active buoyancy control (Arrieta et al., 2015).

Although it was not investigated within the framework of this thesis, the productivity of the MIZ also depends on the composition of the plankton community, the activity of grazers and the mortality of primary producers. However, PAUL's water samples were not analyzed with regard to plankton species as the two water intakes of PAUL's sample collector are rather small (2 x 21 cm²). Especially with regard to bigger zooplankton species, samples would not have been representative.

Recent studies also state that the composition of the phytoplankton community is important. The phytoplankton itself determines the underwater light spectrum as light is partitioned according to the respective pigments abundant in the

10.2 Objective I: Technological

phytoplankton community (Lewandowska et al., 2015). As the availability of specific wavelengths might affect phytoplankton growth, the composition of the community is relevant.

To summarize this, the following factors were identified to be key biological parameters that affect the productivity of a MIZ:

- Plankton concentration
- Buoyancy control of phytoplankton
- Composition of plankton community
- Predator and grazer pressure

Review, testing and integration of existing biogeochemical sensors.

10.2.1 Payload set-up

In order to identify key parameters affecting the ecologic system of the MIZ, setting up the vehicle's payload section was a crucial milestone. As of the finalization of this thesis, *PAUL* is able to measure nine independent physical, chemical, and biological parameters and to collect water samples (see section 5). The weight, the dimensions and the electrical integration of the instruments made it necessary to redesign the vehicle's payload section completely (in 2010/11). The redesign included 1) designing new buoyancy modules to be able to trim the vehicle, 2) structural set-up of the payload section and 3) electrical set-up (power supply + data recording).

The buoyancy modules were specifically optimized for the vehicle's internal shape. Thus, very little space remained unused. The structural set up allows easy access to the water samples and it allows new instruments to be integrated in the vehicle on short notice. The position of the sample collector changed significantly. The water supply lines were shortened by over 1.2 m and the flow velocity through the sample collector was increased. Thus, the water in the sample containers is exchanged quicker. For the electrical set-up, the newly developed payload control computer (PCC) proved to be a reliable instrument. Electrical energy is centrally distributed via the PCC and data are recorded with a temporal resolution of 1 Hz. Generally, the investigations presented in this thesis would not have been possible without this successful redesign.

10.2.2 Sensors

Prior to the acquisition of a sensor, different instruments were compared by means of the manufacturers' data sheets. The trade study included characteristics of scientific relevance (e.g. response time), as well as engineering characteristics such as dimensions, data transfer or power consumption. Implemented sensors turned out to be suitable, yet intense testing was conducted in case of the CO₂ sensor.

The smaller sensors, the two fluorometers (chlorophyll *a*, CDOM) and the PAR sensor, proved to be simple, robust and reliable. The power consumption of these instruments is low and negligible for typical durations of AUV missions. Thus, little effort had to be put into their integration and operation.

The medium size sensor, a dissolved oxygen sensor of the type SBE 43 (Sea Bird Electronics), was selected as it features a well-known electrochemical measuring principle (Clark electrode), low power consumption and a fast response time. The response time increases with lower water temperatures, yet it was faster than optical sensors when it was selected in 2011. In general, the SBE 43 dissolved oxygen sensor performed well, yet there is a clear trend towards optical sensors. Thus, this sensor will be exchanged in the future.

Integration of the two bigger sensors (nitrate, CO₂) was complex, as especially the CO₂ sensor has a high power consumption of about 15 W during its initial heating phase. The CO₂ sensor turned out to be unsuitable for AUV operations. The main problem is its measuring principle detecting gaseous CO₂ by the absorption of infrared radiation. Thus, the sensor needs a dry gas circuit which is separated from the water by means of a semipermeable membrane. The transit time through this membrane increases the sensor's response time – making it impossible to

Detect steep CO₂ gradients at typical AUV speeds of 1.5 m s⁻¹. Additionally, the transit time through the membrane also depends on water temperature and pressure. A correction algorithm to compensate for this time delay is available, yet it was developed for slowly ascending ARGO floats (Fiedler et al., 2013). As the speed of the sensor through the water column is the crucial parameter to correct the data and as ascend velocities of a floating AUV and an ARGO float are comparable, developing the float maneuver was partly driven by the goal to apply this algorithm. However, as there was no support from the sensor's manufacturer, implementing the correction algorithm could not be realized within the framework of this thesis.

The nitrate sensor performed well, yet first deployments indicated that an *in-situ* calibration using PAUL's water samples was necessary. Calculated nitrate values were unrealistically high. Although the exact reason is unknown, it is likely caused by cross-sensitivity of the sensor. Nitrate is detected by the absorption of ultraviolet light. In decreasing order of importance, the UV-spectrum between 210 – 230 nm is mainly determined by bromide, nitrate and organic matter (Ogura & Hanya, 1966). Correction methods with regard to bromide cross sensitivity have been investigated by Zielinski et al. (2007) and Sakamoto et al. (2009). To apply the correction method, the complete absorption spectrum needs to be recorded. However, in the AUV, the nitrate sensor's signals are transmitted as analog voltage signals. Thus, the signals represent pre-processed nitrate values containing no information on the absorption spectra. To be able to record the entire spectrum, communication between the sensor and the PCC needs to be digitalized – making an *in-situ* calibration obsolete and saving sample material.

10.2.3 Water Sample Collector

The sample collector is an exceptional instrument as it is an in-house development and only few vehicles worldwide are able to conduct sample return missions. *PAUL*'s sample collector can collect 22 samples á 220 ml. Due to this comparably small volume and depending on the intended combination of analyses, optimized sample processing to provide sufficient sample material for each analytical method is crucial. For example, dividing each sample into fractions to measure dissolved inorganic nutrients (DIN), dissolved inorganic carbon (DIC), total alkalinity (TA) and chlorophyll *a*, as it was done in 2012, was only possible applying an optimized and well-trained procedure.

The safety of the samples with regard to physical or chemical contamination was verified in [section 8.4.1](#) and [section 8.4.2](#). Results indicated that the samples are safely stored and water cannot ingress into the sample containers as long as they do not encounter high external overpressure.

External overpressure was avoided by the AUV operator (taking the deepest sample first and then proceed towards the surface). Chemically, longer residence times in the sample containers and contact to particular laboratory equipment can slightly change the composition of the samples. However, the effect is small and samples were processed within the shortest possible time span after the dive. Additionally, samples were always processed in cooled laboratories (4°C) – minimizing the diffusion coefficient of chemical compounds which might transit from the sample collector's materials into the sample.

Although the sample collector has performed well, some of the samples are normally lost due to an insufficient sealing of the sample containers. With certain sample containers showing this malfunction more frequent than others, the malfunction is likely subject of low manufacturing precision, rather than a major design flaw.

10.3 Objective II: Scientific

Study of ecologically relevant meso- and submesoscale transport processes in the MIZ.

Wind driven vertical transports related to ice are well known, yet processes occurring on small scales have rarely been observed and investigated. Applying new observation techniques such as AUVs, submesoscale processes featuring dimensions smaller than 5 km, can be investigated. *PAUL*'s data of 2013 indicate the presence of submesoscale processes superimposing a mesoscale phenomenon. The mesoscale transport processes are associated to an ice tongue roughly 70 km in length that drifted through the study area (section 9.4.2.1). Atmospheric forcing and the drift of the tongue most likely caused vertical transport processes in the wake of the ice tongue. Although *PAUL*'s dive area was not directly located in the wake area, studies indicate that these processes can affect extensive areas (Fennel & Johannessen, 1998). We suggest that the elevated nitrate values which were detected by *PAUL* in the euphotic zone in 2013 (section 9.4.3.1) result from this "wake-upwelling". This process is most likely able to stimulate productivity as the affected area is huge (Fig. 9-8) and nutrients seem to be kept in the euphotic zone for several days. The submesoscale process superimposing wake-upwelling was related to the meltwater

front. Down-front wind conditions stimulated frontogenesis. Although direct measurements of the water currents using an ADCP were not possible, the results clearly indicate the presence of a frontogenetic ageostrophic secondary circulation (ASC). Frontogenetic processes and associated ASCs have not been observed at a meltwater front before.

Measurement results and visual observations indicate that characteristics of a meltwater front and the characteristics of the ice field are not closely related. Thus, horizontal cross-front gradients (temperature, salinity, density) would remain steep, regardless if the meltwater front is associated to a closed ice cover with a sharp ice edge or an ice field slowly "dispersing" towards the open ocean. This suggests that basic preconditions to stimulate ASCs are frequently given along the Fram Strait's ice edge. Due to the steep horizontal density gradient across a meltwater front, an ASC could cause high vertical velocities. However, the ecological relevance of this process is unclear, yet it might be limited. Due to the low depth of the meltwater front (~15 m), the penetration depth of ASC-related vertical transports might be low as well. Mixing processes might be confined to the euphotic zone which is usually nutrient depleted. Thus, the total nutrient inventory would remain unchanged.

10.4 Objective II: Technological

Development of methods to resolve the surface water stratification.

AUV operations in the vicinity of an ice cover always include a high risk for the vehicle – especially when it has to approach the ice to investigate the surface layer.

As a consequence, the float maneuver was developed to be able to approach the surface / the ice slowly. With *PAUL* being trimmed a little less dense than water, the thruster is deactivated and the vehicle drifts towards the surface. Ascent velocities depend on the vehicle's trim, yet usually were between 10 – 20 cm s⁻¹. These slow movements affect the vehicle's navigation system negatively (the dive shown in [section 7](#) illustrates the negative effect of the maneuver), yet problems could be solved and the float maneuver comprises significant advantages in terms of vehicle safety:

Compared to an undulating way of driving (“sawtooth” or “zig-zag”), floating makes it easier for the operator to estimate the depth where the vehicle peaks and starts to descend again. Between the reactivation of the thruster and the vehicle finally descending, *PAUL* drifted about 2 – 2.5 m further up. Knowing these values, the mission planning can be adjusted and safety margins (minimal vertical distance to the ice) can be minimized.

As the vehicle drifts upwards in an almost horizontal attitude (*PAUL*'s nose was usually pitched down by 3 – 5°) the vehicle needs to rotate over a smaller angle and can start its descent quicker.

Conducting a “sawtooth” maneuver the vehicle would always cover a certain horizontal distance while changing its depth – probably leaving the

range of a ship-bound underwater tracking system quickly. In contrast, the vehicle ascends almost vertically when executing the float maneuver. Consequently, more vertical profiles can be recorded without leaving a certain range around the ship.

Apart from these technological issues, the float maneuver proved to be suitable to achieve the scientific goal of mapping the stratification. *PAUL* crosses the water layers with minimal disturbance – providing a detailed picture of the upper water column. It is an additional benefit of the float maneuver that the vehicle's PAR sensor has a stable, vertical orientation when *PAUL* ascends. Although the raw PAR data are corrected by means of the vehicle's motion sensor data (see [section 5.6.2.2](#)), this stable vertical orientation keeps the measurement error small by default. Thus, the underwater light field is exactly recorded.

As mentioned in [section 10.2.2](#), developing the float maneuver was partly driven by the fact that ascent velocities of *PAUL* and an ARGO float are comparable. Hence, the algorithm to correct the data of the CO₂ sensor according to [Fiedler et al. \(2013\)](#) is applicable. Although not achieved within the framework of this thesis, this remains one of the key objectives for the future.

In the course of *PAUL*'s Arctic deployments, exact information on the drift of the ice turned out to be highly important to conduct AUV missions in the MIZ. The flying drone described in [section 6](#) proved to be a valuable tool to achieve this task. However, the particular drone described in [section 6](#) was remotely controlled and thus its range of operation was limited by the pilot's visual range. To overcome this limitation, autonomous long-range drones are currently developed in the course of project ROBEX (see [section 11.4](#)).

11 Outlook

11.1 Wake Upwelling

Under the assumption that the conclusions of [section 9](#) are correct, ecologically relevant upwelling can occur in the wake of drifting ice tongues. This is of particular importance for the Fram Strait as ice structures extending from the main ice edge have been observed before ([Wadhams & Squire, 1983](#)). Especially in the region covered by AWI's deep sea observatory HAUSGARTEN, around the Molloy Deep depression, these ice structures appear to be a common feature ([Fig. 11-1](#)).

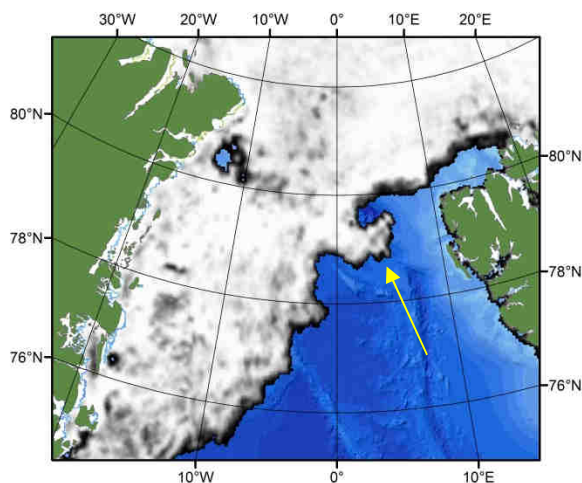


Fig. 11-1. Exemplary ice tongue (yellow arrow) in the Molloy Deep region (July 3rd, 2011)

Most likely, the frequent occurrence of the ice structures in this region is related to the quasi stationary, cyclonic eddy in the vicinity of the Molloy Deep ([Fig. 11-2](#), [Bourke et al., 1987](#)).

As a consequence, the Molloy Deep region features two processes, both able to increase the nutrient concentrations at the surface for days, maybe even weeks. Firstly, the cyclonic rotation of the eddy causes upwelling in its center

(e.g. [Smith, 1987a](#)). Secondly, “wake-upwelling” according to [section 9](#) might occur.

Within the framework of this thesis, a short study investigating the summer MIZ (June – September) of the year 2011 was conducted using satellite images. For roughly one third of the period, ice structures extending from the MIZ at the Molloy Deep region were present. These structures are prone to atmospheric forcing.

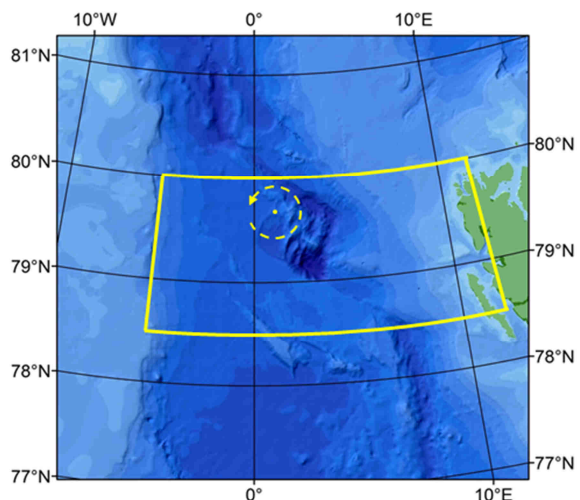


Fig. 11-2. Area of the deep sea observatory HAUSGARTEN in the Fram Strait indicated by a yellow frame (78.5 - 80 °N and 5 °W - 12 °E). The yellow circle northwest of the Molloy Deep illustrates location, diameter and direction of rotation of the quasi stationary cyclonic eddy. Center of the eddy is located at 79°40' N and 001 °E. The diameter is 60 km (according to [Bourke et al., 1987](#)).

With regard to nutrient supply, their impact needs a) to be distinguished from other processes (e.g. eddy-driven upwelling) and b) to be quantified by future investigations (MIZ in June 2011: [Fig. 11-3](#), July – September: see [Appendix](#)).

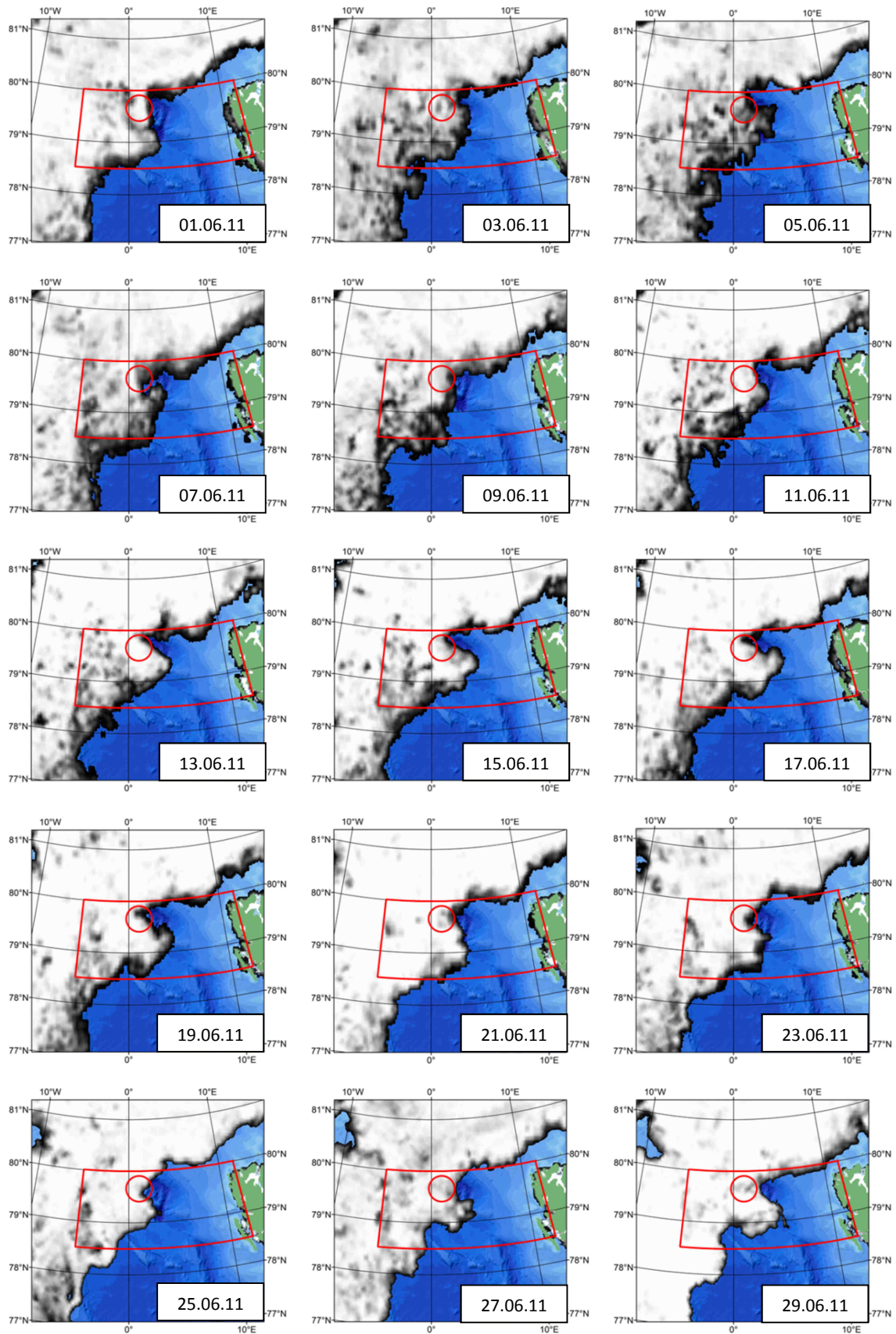


Fig. 11-3. Ice edge in the Fram Strait in June 2011. Red frame: HAUSGARTEN area, red circle: Molloy Deep eddy.

11.2 Frontogenesis

Applying currently available data, the question whether frontogenesis (Thomas & Lee, 2005) can occur along a melt water front cannot be answered finally. To further investigate this phenomenon, resilient calculations of the water column's stability and the Potential Vorticity (PV) are necessary. Especially determining PV values is crucial as PV follows a conservation law and can only be changed at the surface (Thomas, 2005). Thus, PV can be used as an indicator for present or past vertical transport processes. However, direction and speed of a water flow must be known to calculate PV. In case of the meltwater front this results in monitoring the upper water column (from the surface to the depth of the meltwater layer, roughly 15 m depth) by means of an Acoustic Doppler Current Profiler (ADCP)

Ship based ADCPs are mostly unsuitable for this task as they normally work with comparably low frequencies to achieve a longer range. Thus the vertical resolution of these devices is relatively coarse.

Additionally, as these devices are attached to the lower side of a vessel's hull and as there is a "blank zone" in front of an ADCP's head where no measurements can be taken, surface waters are most likely lost for analysis (e.g. R/V *Merian* in 2013: 75 kHz ADCP, vertical resolution: 8 m, 1st usable cell between 23 – 31 m water depth, max. depth of the melt water layer: 15 m). Hence, AUV-based ADCP measurements, with the ADCP being installed in an upward looking configuration, appear to be a promising option. Within the framework of the infrastructure program FRAM (FRontiers in Arctic Monitoring) the integration of a 300 kHz ADCP into *PAUL* is currently in progress (Fig. 11-4).

However, measuring water currents by means of an AUV-based ADCP are not free of problems (Fong & Jones, 2006). As an ADCP determines water velocities and flow directions with respect to its own orientation, its own state of motion must precisely be known in order to correct the data subsequently.



Fig. 11-4. PAUL's payload section with the newly integrated 300 kHz ADCP on the left side of the image. First integration test in April 2015.

As the vehicle has to operate close to the surface to measure surface currents it will most likely be unable to establish “bottom-lock”. Thus, *PAUL*’s navigation accuracy is reduced and it is a subject to current research efforts to evaluate if ADCP measurements are possible at all.

Apart from physical parameters, *PAUL*’s dives of 2013 also showed that measuring biological parameters needs to be extended. Regarding the results of section 9, the composition of the phytoplankton community along a meltwater front needs to be analyzed. The formation of zones with different phytoplankton concentrations could not be explained (Fig. 11-5). Thus, the approach of phytoplankton movements being partly decoupled from water movements by active buoyancy control remained speculative. However, investigating the species directly is only possible by taking water samples. To collect water samples at these spots, currently applied dive plans must be modified. Additionally, post-dive procedures and sample processing must be altered as well, as conserving phytoplankton samples for community

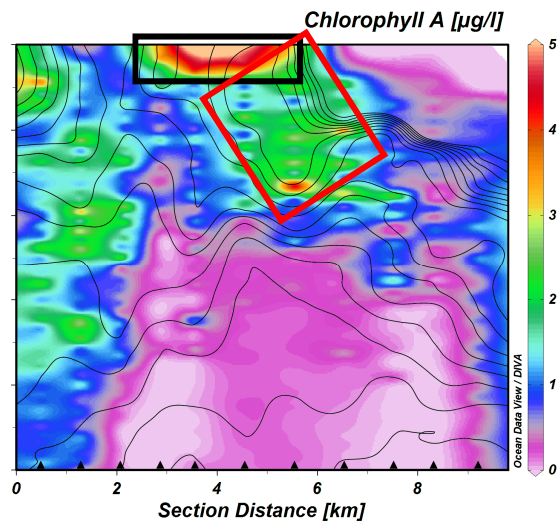


Fig. 11-5. Accumulation zone (black) and Subduction zone (red) illustrated by means of elevated chlorophyll *a* concentrations

analyses has not been part of the standard “repertoire”. In the future it is also planned to implement an “intelligent sampling” capability into *PAUL*’s payload control software. Applying this technique, *PAUL* would be able to collect samples autonomously – for example triggered by a fluorescence value exceeding a certain threshold.

11.3 Vehicle Tracking

To fully understand the physics of a MIZ it is crucial to cope with the dynamics of this region. From both a technical and a scientific point of view, the main challenge is to monitor various parameters simultaneously and to measure steep vertical and horizontal gradients. Hence, precise georeferencing is crucial. As it was shown in [section 7](#), AUV navigation data need to be corrected by tracking the vehicle. As tracking is done acoustically and thus depends on the

propagation of sound waves in the water, it can for example be affected by turbulences induced by a ship's propeller. To extend the range of underwater tracking, sectors providing optimal conditions around R/V *Polarstern* and *PAUL* were identified by [Wulff U.](#) ([Fig. 11-6, unpublished](#)). The results will enter future dive planning and operators will try to keep "green" sectors of both *Polarstern* and *PAUL* overlapping.

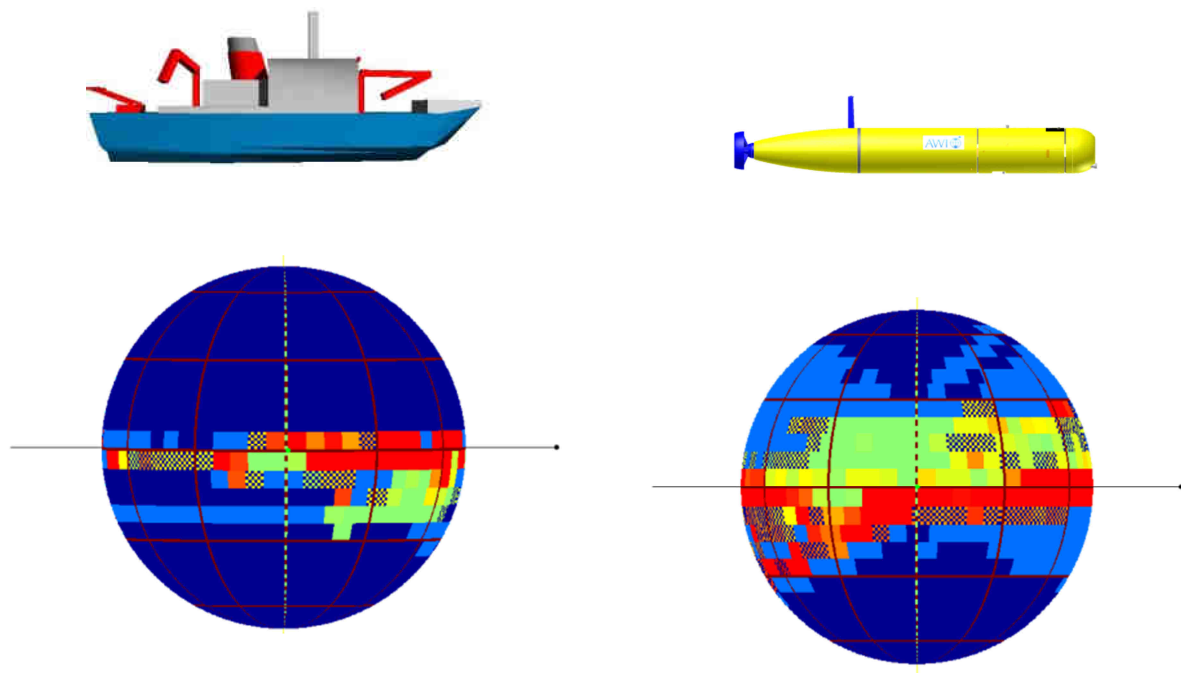


Fig. 11-6. Spherical body around *Polarstern* and *PAUL* showing sectors suitable for acoustic tracking (green) or unsuitable (red). Exemplary results for the starboard side of *Polarstern* and *PAUL*. Dark blue indicates no data.

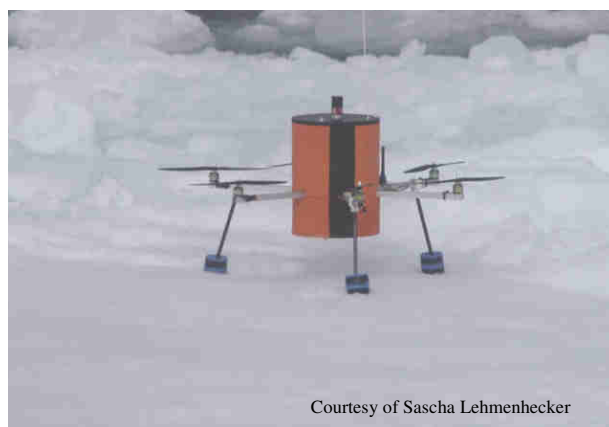
11.4 Observation concept in the MIZ

In the MIZ, atmosphere, ice, and ocean interact with each other. As a consequence, operating only an AUV is insufficient and studies must be complemented by additional data, especially surface data. Investigations described in [section 9](#), included data gathered by satellites (wind, sea surface temperature, ice concentration), the support vessel (wind, surface PAR intensity, ADCP, salinity) and models (wind) to obtain a picture as holistic as possible. These available data sources cover key parameters of the oceanographic and atmospheric part of the system “MIZ”. However, small scale data on the cryosphere are missing. Important data such as the exact drift direction of the ice are either unavailable or their quality is insufficient. As described in [section 6](#), first steps towards collecting detailed cryosphere data were accomplished at AWI in 2011 and 2012 (flying drone, [Fig. 11-7](#)).

Within the framework of project ROBEX (Robotic Exploration of Extreme Environments)

the approaches of 2011 and 2012 have been carried on. Within ROBEX, the design team UAV (Unmanned Aerial Vehicle) was founded in spring 2014. Here, AWI cooperates with the German Aerospace Center (DLR) and the University of Würzburg to develop two different types of autonomous drones dedicated to ice investigations: The Exploration UAV and the Landing UAV.

The Exploration UAV is supposed to provide an overview of the ice field by means of special imaging or mapping systems. Thus, the composition of the ice field and its surface roughness, which eventually determines the momentum exchange between atmosphere and ice, will be investigated. Small structures (< 5 km) such as ice vortices, not visible on satellite images, yet indicating high regional dynamics, will become identifiable. The Landing UAV is supposed to land on the ice and monitor its drift. Apart from this, the Landing UAV will also measure the light intensity on the ice.



Courtesy of Sascha Lehmenhecker

Fig. 11-7. The flying drone of 2012 prior to lift off after having spent 6 h on the ice.

Both vehicles are intended to carry out their respective missions autonomously – including an autonomous landing on the support vessel. Eventually, operating these UAVs is part of a greater observation concept aiming at monitoring all relevant parameters simultaneously.

Fig. 11-8 gives an overview of the entire concept and the instruments involved. Realizing this concept is currently in progress with first test having been accomplished in summer 2015 within the framework of Arctic expedition ARK 29/2 (July – August 2015, R/V *Polarstern*).

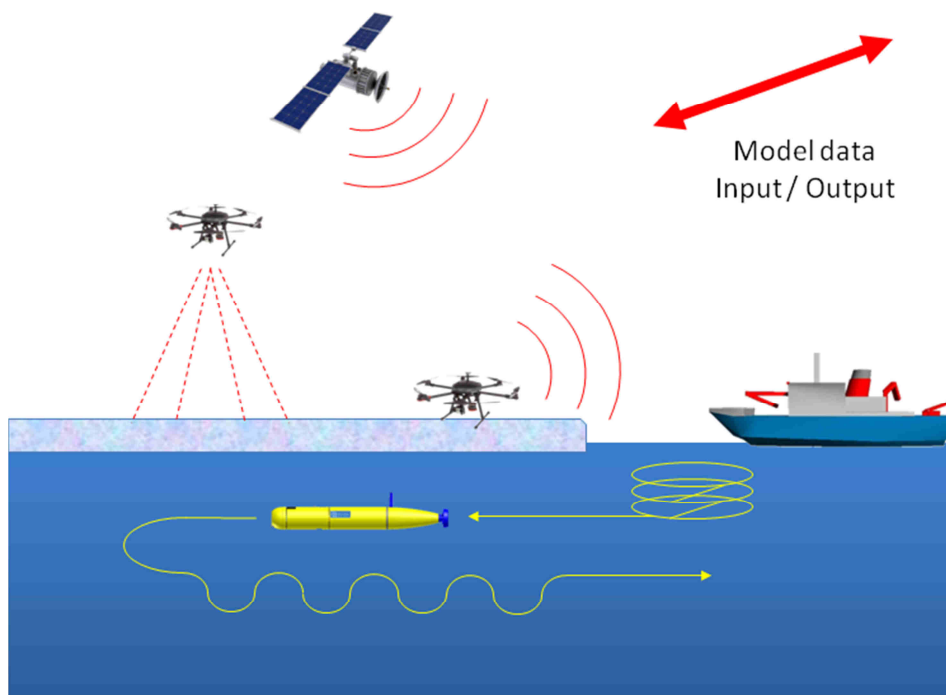
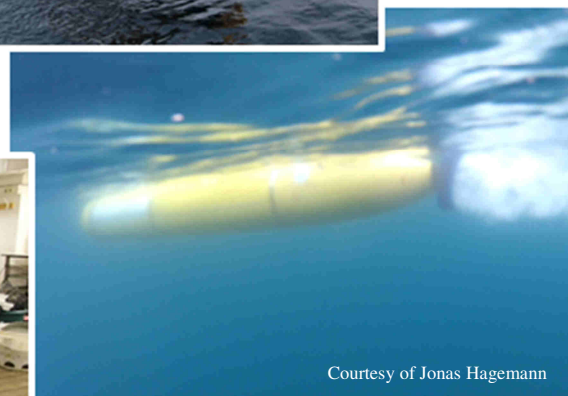


Fig. 11-8. Future observation concept for the MIZ. The AUV provides physical, chemical and biological data of the water column. Two flying drones collect cryospheric data such as images of the ice’s surface or direction and speed of the ice’s drift. A support vessel collects surface data such as wind, and large scale hydrographic data. Satelliet data are used to obtain a large scale environmental picture (e.g. ice conditions, wind or sea surface temperature). Data of ice-ocean models will be used to prepare the dives and the dives will also provide data to further improve the models.

Final statement

New technologies and methods to observe the MIZ will provide new insights into fast, small-scale processes which – so far – might have only been known on a theoretical level. New methods will improve our ability to observe all kinds of phenomena by providing high-resolution data.

Especially in marginal ice zones, with their dynamics and their large number of processes, using new technologies such as autonomous robots is not just a useful way to collect data, it might be the only way to understand the complex interactions of these remarkable regions.



Acknowledgements

In the first place I would like to thank the members of my thesis committee, Antje Boetius, Oliver Zielinski and Michael Klages who were always on hand with help and advice through the last years. In particular I would like to thank Antje for becoming my supervisor in 2010 after I had gone through an “eventful” phase of my PhD. It was Antje who initially defined the objectives and provided a structure for this thesis.

Apart from the members of my thesis committee I would like to specifically thank the following people: Sascha Lehmenhecker for his help with electronic equipment and his remarkable ability to deal with all kind of problems on short notice, Eduard Bauerfeind for patiently filling an engineer’s head with biological stuff and having changed my vision when looking on the sea (former times: water, today: plankton blooms), Wilken-Jon von Appen for his great support in struggling with the hurdles of physical oceanography, Jonas Hagemann for spending hours in the cold store processing AUV water samples with me and – last but not least – Uwe Wulff who, apart from being my dad, has become an AUV freelancer eventually publishing a father + son article (Wulff & Wulff, 2015).

Big thanks for numerous “AWI life hacks” to all my other colleagues: Thomas Soltwedel, Normen Lochthofen, Christiane (“Pitty”) Hasemann, Frank Wenzhöfer, Ulrich Hoge, Renate Degen, Ingo Schewe, Melanie Bergmann, Johannes Lemburg, Tim Küber, Janine Ludszuweit, Corinna Kanzog, Martina Wilde, Annabel Ledrich, Torben Gentz, Roi Martinez und Michael Schlüter. I will attend our coffee break more often...

I also like to acknowledge the “silent heroes”: People in the administration, the purchase department the workshop, caretakers, etc. who constantly contribute to the good working conditions at AWI.

I also would like to thank my friends Dirk, Stefan, Christin, Julia, Remo, Dennis, Renate, Benny and Katrin for frequently lowering my stress level and just having a nice time!

My parents Elvira and Uwe, my brother Steffen, my aunt Anne and my (almost) sister-in-law Tina: Thank you for having you as a family and that you shared the good and also the bad moments of the last years. Mannheim has always been a “safe haven” for me. Mum, Dad, I will not forget this!

1L5471

References

- Aagaard, K., & Greisman, P. (1975). *Toward new mass and heat budgets for the Arctic Ocean*. J. Geophys. Res., 80(27), 3821-3827.
- AMAP (2012). Arctic Climate Issues 2011: *Changes in Arctic Snow, Water, Ice and Permafrost*. In: SWIPA 2011 Overview Report. Arctic Monitoring and Assessment Programme (AMAP), Oslo. xi + 97pp. <http://www.amap.no/documents/doc/the-arctic-marine-foodweb/937>
ISBN: 978-82-7971-073-8
- Arndt, C. E., & Lønne, O. J. (2002). *Transport of bioenergy by large scale Arctic ice drift*. In: Ice in the Environment: Proceedings of the 16th IAHR International Symposium on Ice. Dunedin, New Zealand (pp. 382-390).
- Arrigo, K. R., Perovich, D. K., Pickart, R. S., Brown, Z. W., van Dijken, G. L., Lowry, K. E., Mills, M. M., Palmer, A. M., Balch, W. M., Bahr, F., Bates, N. R., Benitez-Nelson, C., Bowler, B., Brownlee, E., Ehn, J. K., Frey, K. E., Garley, R., Laney, S. R., Lubelczyk, L., Mathis, J., Matsuoka, A., Mitchell, B. G., Moore, G. W. K., Ortega-Retuerta, E., Pal, S., Polashenski, C. M., Reynolds, R. A., Schieber, B., Sosik, H. M., Stephens, M., & Swift, J. H. (2012). *Massive phytoplankton blooms under Arctic sea ice*. Science, 336(6087), 1408-1408.
- Arrigo, K. R., Brown, Z. W., & Mills, M. M. (2014). *Sea ice algal biomass and physiology in the Amundsen Sea, Antarctica*. Elementa: Science of the Anthropocene, 2(1), 000028.
- Auel, H., & Hagen, W. (2002). *Mesozooplankton community structure, abundance and biomass in the central Arctic Ocean*. Mar. Biol., 140(5), 1013-1021.
- Auel, H., Klages, M., & Werner, I. (2003). *Respiration and lipid content of the Arctic copepod Calanus hyperboreus overwintering 1 m above the seafloor at 2,300 m water depth in the Fram Strait*. Mar. Biol., 143(2), 275-282.
- Barber, D. G., Hop, H., Mundy, C. J., Else, B., Dmitrenko, I. A., Tremblay, J. E., Ehn, J. K., Assmy, P., Daase, M., Candlish, L. M., & Rysgaard, S. (2015). *Selected physical, biological and biogeochemical implications of a rapidly changing Arctic Marginal Ice Zone*. Prog. Oceanogr. (accepted).
- Bauerfeind, E., Bodungen, B. V., Arndt, K., & Koeve, W. (1994). *Particle flux, and composition of sedimenting matter, in the Greenland Sea*. J. Marine Syst., 5(6), 411-423.
- Bauerfeind, E., Nöthig, E. M., Beszczynska, A., Fahl, K., Kaleschke, L., Kreker, K., Klages, M., Soltwedel, T., Lorenzen, C., & Wegner, J. (2009). *Particle sedimentation patterns in the eastern Fram Strait during 2000–2005: Results from the Arctic long-term observatory HAUSGARTEN*. Deep-Sea Res. Pt. I, 56(9), 1471-1487.
- Beszczynska-Möller, A., Fahrbach, E., Schauer, U., & Hansen, E. (2012). *Variability in Atlantic water temperature and transport at the entrance to the Arctic Ocean, 1997–2010*. ICES J. Mar. Sci., fss056.
- Bergmann, M., Dannheim, J., Bauerfeind, E., & Klages, M. (2009). *Trophic relationships along a bathymetric gradient at the deep-sea observatory HAUSGARTEN*. Deep-Sea Res. Pt. I, 56(3), 408-424.
- Birnbaum, G., & Lüpkes, C. (2002). *A new parameterization of surface drag in the marginal sea ice zone*. Tellus A, 54(1), 107-123.

- Boetius, A., Albrecht, S., Bakker, K., Bienhold, C., Felden, J., Fernández-Méndez, M., Hendricks, S., Katlein, C., Lalande, C., Krumpen, T., Nicolaus, M., Peeken, I., Rabe, B., Rogacheva, A., Rybakova, E., Somavilla, R., & Wenzhöfer, F. (2013). *Export of algal biomass from the melting Arctic sea ice*. *Science*, 339(6126), 1430-1432.
- Bourke, R. H., Tunnicliffe, M. D., Newton, J. L., Paquette, R. G., & Manley, T. O. (1987). *Eddy near the Molloy Deep revisited*. *J. Geophys. Res.-Oceans* (1978–2012), 92(C7), 6773-6776.
- Carmack, E., Barber, D., Christensen, J. H., Macdonald, R., Rudels, B., and Sakshaug, E.: *Climate variability and physical forcing of the food webs and the carbon budget on panarctic shelves*, *Prog. Oceanogr.*, 72, 145–181
- Cherkasheva, A., Bracher, A., Melsheimer, C., Köberle, C., Gerdes, R., Nöthig, E. M., Bauerfeind, E., & Boetius, A. (2014). *Influence of the physical environment on polar phytoplankton blooms: a case study in the Fram Strait*. *J. Mar. Syst.*, 132, 196-207.
- Coachman, L. K., & Aagaard, K. (1988). *Transports through Bering Strait: Annual and interannual variability*. *J. Geophys. Res.-Oceans* (1978–2012), 93(C12), 15535-15539.
- Comiso, J. C. (2003). *Large-scale characteristics and variability of the global sea ice cover. Sea ice: an introduction to its physics, chemistry, biology and geology*, In: Thomas, D. N. and Dieckmann, G. S. (ed.), *Sea Ice – An Introduction to its Physics, Chemistry, Biology and Geology*, Blackwell Science Ltd. 112-142. ISBN 0-632-05808-0
- Degerlund, M., & Eilertsen, H. C. (2010). *Main species characteristics of phytoplankton spring blooms in NE Atlantic and Arctic waters (68–80 N)*. *Estuar. Coasts*, 33(2), 242-269.
- Deser, C., Walsh, J. E., & Timlin, M. S. (2000). *Arctic sea ice variability in the context of recent atmospheric circulation trends*. *J. Climate*, 13(3), 617-633.
- Doney, S. C. (2006). *Oceanography: Plankton in a warmer world*. *Nature*, 444(7120), 695-696.
- Dumont, D., Kohout, A., & Bertino, L. (2011). *A wave-based model for the marginal ice zone including a floe breaking parameterization*. *J. Geophys. Res.-Oceans* (1978–2012), 116(C4).
- Engel, A., Borchard, C., Piontek, J., Schulz, K. G., Riebesell, U., & Bellerby, R. (2013). *CO2 increases 14C-primary production in an Arctic plankton community*. *Biogeosciences* (BG), 10(3), 1291-1308.
- Fahrbach, E., Meincke, J., Østerhus, S., Rohardt, G., Schauer, U., Tverberg, V., & Verduin, J. (2001). *Direct measurements of volume transports through Fram Strait*. *Polar Res.*, 20(2), 217-224.
- Falk-Petersen, S., Hop, H., Budgell, W. P., Hegseth, E. N., Korsnes, R., Løyning, T. B., Ørbæk, J. B., Kawamura, T. & Shirasawa, K. (2000). *Physical and ecological processes in the marginal ice zone of the northern Barents Sea during the summer melt period*. *J. Mar. Syst.*, 27(1), 131-159.
- Feltham, D. L., Untersteiner, N., Wettlaufer, J. S., & Worster, M. G. (2006). *Sea ice is a mushy layer*. *Geophys. Res. Lett.*, 33(14).
- Fennel, W., & Johannessen, O. M. (1998). *Wind forced oceanic responses near ice edges revisited*. *J. Mar. Syst.*, 14(1), 57-79.
- Ferguson, J., Pope, A., Butler, B., & Verrall, R. (1999). *Theseus AUV-two record breaking missions*. *Sea Technology*, 40(2), 65-70.

- Fernández-Méndez, M., Katlein, C., Rabe, B., Nicolaus, M., Peeken, I., Bakker, K., Flores, H., & Boetius, A. (2015). *Photosynthetic production in the central Arctic Ocean during the record sea-ice minimum in 2012*. *Biogeosciences*, 12(11), 3525-3549.
- Fiedler, B., Fietzek, P., Vieira, N., Silva, P., Bittig, H. C., & Körtzinger, A. (2013). *In situ CO₂ and O₂ measurements on a profiling float*. *J. Atmos. Ocean. Tech.*, 30(1), 112-126.
- Fong, D. A. & Jones, N. L. (2006). *Evaluation of AUV-based ADCP measurements*. *Limnol. Oceanogr.-Meth.*, 4(3), 58-67
- Francois, R. E., & Nodland, W. E. (1972). *Unmanned Arctic research submersible (UARS) system development and test report*. APL-UW 7219, Applied Physics Laboratory, University of Washington.
- Friedlaender, A. S., Halpin, P. N., Qian, S. S., Lawson, G. L., Wiebe, P. H., Thiele, D., & Read, A. J. (2006). *Whale distribution in relation to prey abundance and oceanographic processes in shelf waters of the Western Antarctic Peninsula*. *Mar. Ecol.-Prog. Ser.*, (317), 297-310
- Gammelsrod, T., Mork, M., & Roed, L. P. 1975. *Upwelling possibilities at an ice edge*. *Mar. Sci. Commun.*, 1(2), 115-145.
- Gascard, J. C., Kergomard, C., Jeannin, P. F., & Fily, M. (1988). *Diagnostic study of the Fram Strait marginal ice zone during summer from 1983 and 1984 Marginal Ice Zone Experiment Lagrangian observations*. *J. Geophys. Res.-Oceans* (1978–2012), 93(C4), 3613-3641.
- Gosselin, M., Levasseur, M., Wheeler, P. A., Horner, R. A., & Booth, B. C. (1997). *New measurements of phytoplankton and ice algal production in the Arctic Ocean*. *Deep-Sea Res. Pt. II*, 44(8), 1623-1644.
- Tucker, W. B., Gow, A. J., & Weeks, W. F. (1987). *Physical properties of summer sea ice in the Fram Strait*. *J. Geophys. Res.-Oceans* (1978–2012), 92(C7), 6787-6803.
- Gradinger, R. R., & Baumann, M. E. M. (1991). *Distribution of phytoplankton communities in relation to the large-scale hydrographical regime in the Fram Strait*. *Mar. Biol.*, 111(2), 311-321.
- Gradinger, R., & Ikävalko, J. (1998). *Organism incorporation into newly forming Arctic sea ice in the Greenland Sea*. *J. Plankton Res.*, 20(5), 871-886.
- Gradinger, R. (1999). *Integrated abundance and biomass of sympagic meiofauna in Arctic and Antarctic pack ice*. *Polar Biol.*, 22(3), 169-177.
- Gradinger, R., Bluhm, B., & Iken, K. (2010). *Arctic sea-ice ridges—Safe heavens for sea-ice fauna during periods of extreme ice melt?*. *Deep-Sea Res. Pt. II*, 57(1), 86-95.
- Guest, P. S., & Davidson, K. L. (1987). *The effect of observed ice conditions on the drag coefficient in the summer East Greenland Sea marginal ice zone*. *J. Geophys. Res.-Oceans* (1978–2012), 92(C7), 6943-6954.
- Guest, P. S., Glendening, J. W., & Davidson, K. L. (1995). *An observational and numerical study of wind stress variations within marginal ice zones*. *J. Geophys. Res.-Oceans* (1978–2012), 100(C6), 10887-10904.
- Gupta, M., Barber, D. G., Scharien, R. K., & Isleifson, D. (2014). *Detection and classification of surface roughness in an Arctic marginal sea ice zone*. *Hydrol. Process.*, 28(3), 599-609.
- Haas, C., Hendricks, S., Eicken, H., & Herber, A. (2010). *Synoptic airborne thickness surveys reveal state of Arctic sea ice cover*. *Geophys. Res. Lett.*, 37(9).

- Häkkinen, S. (1986). *Coupled ice-ocean dynamics in the marginal ice zones: Upwelling/downwelling and eddy generation*. J. Geophys. Res.-Oceans (1978–2012), 91(C1), 819-832.
- Hansen, E., Gerland, S., Granskog, M. A., Pavlova, O., Renner, A. H. H., Haapala, J., Løyning, T. B., & Tschudi, M. (2013). *Thinning of Arctic sea ice observed in Fram Strait: 1990–2011*. J. Geophys. Res.-Oceans, 118(10), 5202-5221.
- Hayes, D. R., & Morison, J. H. (2002). *Determining turbulent vertical velocity, and fluxes of heat and salt with an autonomous underwater vehicle*. J. Atmos. Ocean. Tech., 19(5), 759-779.
- Hop, H., Falk-Petersen, S., Svendsen, H., Kwasiński, S., Pavlov, V., Pavlova, O., & Søreide, J. E. (2006). *Physical and biological characteristics of the pelagic system across Fram Strait to Kongsfjorden*. Prog. Oceanogr., 71(2), 182-231.
- Hunt Jr, G. L., Stabeno, P., Walters, G., Sinclair, E., Brodeur, R. D., Napp, J. M., & Bond, N. A. (2002). *Climate change and control of the southeastern Bering Sea pelagic ecosystem*. Deep-Sea Res. Pt. II., 49(26), 5821-5853.
- Inoue, J., Hori, M. E., Enomoto, T., & Kikuchi, T. (2011). *Intercomparison of surface heat transfer near the Arctic marginal ice zone for multiple reanalyses: A case study of September 2009*. Sola, 7, 57-60.
- Jakobsson, M., Mayer, L., Coakley, B., Dowdeswell, J. A., Forbes, S., Fridman, B., Hodnesdal, H., Noormets, R., Pedersen, R., Rebesco, M., Schenke, H. W., Zarayskaya, Y., Accettella, D., Armstrong, A., Anderson, R. M., Bienhoff, P., Camerlenghi A., Church, I., Edwards, M., Gardner, J. V., Hall, J. K., Hell, B., Hestvik, O., Kristoffersen, Y., Marcussen, C., Mohammad, R., Mosher, D., Nghiem, S. V., Pedrosa, M. T., Travaglini, P. G. & Weatherall, P. (2012). *The international bathymetric chart of the Arctic Ocean (IBCAO) version 3.0*. Geophys. Res. Lett., 39(12).
- Johannessen, J. A., Johannessen, O. M., Svendsen, E., Shuchman, R., Manley, T., Campbell, W. J., Josberger, E.G., Sandven, S., Gascard, C., Olaussen, T., Davidson, K. & Van Leer, J. (1987). *Mesoscale eddies in the Fram Strait marginal ice zone during the 1983 and 1984 Marginal Ice Zone Experiments*. J. Geophys. Res.-Oceans (1978–2012), 92(C7), 6754-6772.
- Johannessen, O. M., Johannessen, J. A., Morison, J., Farrelly, B. A., & Svendsen, E. A. S. (1983). *Oceanographic conditions in the marginal ice zone north of Svalbard in early fall 1979 with an emphasis on mesoscale processes*. J. Geophys. Res.-Oceans (1978–2012), 88(C5), 2755-2769.
- Johannessen, O. M., Johannessen, J. A., Sandven, S., & Davidson, K. L. (1986). *Preliminary results of the Marginal Ice Zone Experiment (MIZEX) summer operations*. The Environment of the Nordic Seas, edited by B. Hurdle, 665-679.
- Jónsson, S., Foldvik, A., & Aagaard, K. (1992). *The structure and atmospheric forcing of the mesoscale velocity field in Fram Strait*. J. Geophys. Res.-Oceans (1978–2012), 97(C8), 12585-12600.

- Klenke, M., & Schenke, H. W. (2002). *A new bathymetric model for the central Fram Strait*. *Mar. Geophys. Res.*, 23(4), 367-378.
- Kohout, A. L., & Meylan, M. H. (2008). *An elastic plate model for wave attenuation and ice floe breaking in the marginal ice zone*. *J. Geophys. Res.-Oceans* (1978–2012), 113(C9).
- Kwok, R., Cunningham, G. F., & Pang, S. S. (2004). *Fram Strait sea ice outflow*. *J. Geophys. Res.-Oceans* (1978–2012), 109(C1).
- Kwok, R., Cunningham, G. F., Wensnahan, M., Rigor, I., Zwally, H. J., & Yi, D. (2009a). *Thinning and volume loss of the Arctic Ocean sea ice cover: 2003–2008*. *J. Geophys. Res.-Oceans* (1978–2012), 114(C7).
- Kwok, R., & Rothrock, D. A. (2009b). *Decline in Arctic sea ice thickness from submarine and ICESat records: 1958–2008*. *Geophys. Res. Lett.*, 36(15).
- Kunz, C., Murphy, C., Camilli, R., Singh, H., Bailey, J., Eustice, R., ... & Willis, C. (2008, September). *Deep sea underwater robotic exploration in the ice-covered arctic ocean with AUVs*. In *Intelligent Robots and Systems, 2008. IROS 2008. IEEE/RSJ International Conference* (pp. 3654-3660). IEEE.
- Lalande, C., Bauerfeind, E., & Nöthig, E. M. (2011). *Downward particulate organic carbon export at high temporal resolution in the eastern Fram Strait: influence of Atlantic Water on flux composition*. *Mar. Ecol-Prog. Ser.*, 440, 127-136.
- Lange, M. A., Ackley, S. F., Wadhams, P., Dieckmann, G. S., & Eicken, H. (1989). *Development of sea ice in the Weddell Sea*. *Ann. Glaciol.*, 12, 92-96.
- Lee, S. H., Joo, H. M., Liu, Z., Chen, J., & He, J. (2012). *Phytoplankton productivity in newly opened waters of the Western Arctic Ocean*. *Deep-Sea Res. Pt. II*, 81, 18-27.
- Lee, Z., Weidemann, A., Kindle, J., Arnone, R., Carder, K. L., & Davis, C. (2007). *Euphotic zone depth: Its derivation and implication to ocean-color remote sensing*. *J. Geophys. Res.-Oceans* (1978–2012), 112(C3).
- Lehmenhecker, S., & Wulff, T. (2013). *Flying drone for AUV under-ice missions*. *Sea Technology*, 55(2), 61-64.
- Lemke, P., & Manley, T. O. (1984). *The seasonal variation of the mixed layer and the pycnocline under polar sea ice*. *J. Geophys. Res.-Oceans* (1978–2012), 89(C4), 6494-6504.
- Lewandowska, A. M., Striebel, M., Feudel, U., Hillebrand, H., & Sommer, U. (2015). *The importance of phytoplankton trait variability in spring bloom formation*. *ICES J. Mar. Sci.*, fsv059.
- Loeng, H. (1991). *Features of the physical oceanographic conditions of the Barents Sea*. *Polar Res.*, 10(1), 5-18.
- Loose, B., Schlosser, P., Perovich, D., Ringelberg, D., Ho, D. T., Takahashi, T., Irchter-Menge, J., Reynolds, C. M., McGillis, W. R., & Tison, J. L. (2011). *Gas diffusion through columnar laboratory sea ice: Implications for mixed-layer ventilation of CO₂ in the seasonal ice zone*. *Tellus B*, 63(1), 23-39.
- Low-Décarie, E., Fussmann, G. F., & Bell, G. (2014). *Aquatic primary production in a high-CO₂ world*. *Trends Ecol. Evol.*, 29(4), 223-232.
- Lønne, O. J., & Gulliksen, B. (1991a). *On the distribution of sympagic macro-fauna in the seasonally ice covered Barents Sea*. *Polar Biol.*, 11(7), 457-469.

- Lønne, O. J., & Gulliksen, B. (1991b). *Sympagic macro-fauna from multiyear sea-ice near Svalbard*. *Polar Biol.*, 11(7), 471-477.
- Lu, K., Weingartner, T., Danielson, S., Winsor, P., Dobbins, E., Martini, K., & Statscewich, H. (2015). *Lateral mixing across ice meltwater fronts of the Chukchi Sea shelf*. *Geophys. Res. Lett.*, 42(16), 6754-6761.
- Lüpkes, C., & Birnbaum, G. (2005). *Surface drag in the Arctic marginal sea-ice zone: a comparison of different parameterisation concepts*. *Bound.-Lay. Meteorol.*, 117(2), 179-211.
- Lytle, V. I., & Ackley, S. F. (1996). *Heat flux through sea ice in the western Weddell Sea: convective and conductive transfer processes*. *J. Geophys. Res.-Oceans* (1978–2012), 101(C4), 8853-8868.
- Manley, T. O., Hunkins, K. L., & Muench, R. D. (1987). *Current regimes across the East Greenland Polar Front at 78°40' north latitude during summer 1984*. *J. Geophys. Res.-Oceans* (1978–2012), 92(C7), 6741-6753.
- Maslanik, J. A., Fowler, C., Stroeve, J., Drobot, S., Zwally, J., Yi, D., & Emery, W. (2007). *A younger, thinner Arctic ice cover: Increased potential for rapid, extensive sea-ice loss*. *Geophys. Res. Lett.*, 34(24).
- Maslowski, W., Marble, D., Walczowski, W., Schauer, U., Clement, J. L., & Semtner, A. J. (2004). *On climatological mass, heat, and salt transports through the Barents Sea and Fram Strait from a pan-Arctic coupled ice-ocean model simulation*. *J. Geophys. Res.-Oceans* (1978–2012), 109(C3).
- Maykut, G. A., & Untersteiner, N. (1971). *Some results from a time-dependent thermodynamic model of sea ice*. *J. Geophys. Res.*, 76(6), 1550-1575.
- McEwen, R., Thomas, H., Weber, D., & Psota, F. (2005). *Performance of an AUV navigation system at Arctic latitudes*. *IEEE J. Oceanic. Eng.*, 30(2), 443-454.
- McMinn, A., & Hegseth, E. N. (2004). *Quantum yield and photosynthetic parameters of marine microalgae from the southern Arctic Ocean, Svalbard*. *J. Mar. Biol. Assoc. UK*, 84(05), 865-871.
- McPhail, S. D., Furlong, M. E., Pebody, M., Perrett, J. R., Stevenson, P., Webb, A., & White, D. (2009, May). *Exploring beneath the PIG Ice Shelf with the Autosub3 AUV*. In *OCEANS 2009-EUROPE* (pp. 1-8). IEEE.
- McPhee, M. G., Morison, J. H., & Nilsen, F. (2008). *Revisiting heat and salt exchange at the ice-ocean interface: Ocean flux and modeling considerations*. *J. Geophys. Res.-Oceans* (1978–2012), 113(C6).
- Michel, C., Legendre, L., Therriault, J. C., Demers, S., & Vandeveld, T. (1993). *Springtime coupling between ice algal and phytoplankton assemblages in southeastern Hudson Bay, Canadian Arctic*. *Polar Biol.* 13(7), 441-449.
- MIZEX Group (1986). *MIZEX East 83/84: The summer marginal ice zone program in the Fram Strait/Greenland Sea*. *Eos*, 67(23).
- Morison, J. H., & McPhee, M. G. (1998). *Lead convection measured with an autonomous underwater vehicle*. *J. Geophys. Res.-Oceans* (1978–2012), 103(C2), 3257-3281.
- Muench, R. D., LeBlond, P. H., & Hachmeister, L. E. (1983). *On some possible interactions between internal waves and sea ice in the marginal ice zone*. *J. Geophys. Res.-Oceans* (1978–2012), 88(C5), 2819-2826.

- Mumm, N., Auel, H., Hanssen, H., Hagen, W., Richter, C., & Hirche, H. J. (1998). *Breaking the ice: large-scale distribution of mesozooplankton after a decade of Arctic and transpolar cruises*. *Polar Biol.*, 20(3), 189-197.
- Nicolaus, M., Gerland, S., Hudson, S., Haapala, J., Hanson, S., Palo, T., & Perovich, D. K. (2008). *Seasonality of Spectral Albedo and Transmission of Sea Ice in the Transpolar Drift, Arctic Ocean*. In AGU Fall Meeting Abstracts (Vol. 1, p. 0504).
- Nicolaus, M., Katlein, C., Maslanik, J., & Hendricks, S. (2012). *Changes in Arctic sea ice result in increasing light transmittance and absorption*. *Geophys. Res. Lett.*, 39(24).
- Niebauer, H. J. (1982). *Wind and melt driven circulation in a marginal sea ice edge frontal system: a numerical model*. *Cont. Shelf Res.*, 1(1), 49-98.
- Niebauer, H. J. (1988). *Effects of El Nino-Southern Oscillation and North Pacific weather patterns on interannual variability in the subarctic Bering Sea*. *J. Geophys. Res.-Oceans* (1978–2012), 93(C5), 5051-5068.
- Niebauer, H. J., & Smith, W. O. (1989). *A numerical model of mesoscale physical-biological interactions in the Fram Strait marginal ice zone*. *J. Geophys. Res.-Oceans* (1978–2012), 94(C11), 16151-16175.
- Niebauer, H. J. (1991). *Bio-physical oceanographic interactions at the edge of the Arctic ice pack*. *J. Marine Syst.*, 2(1), 209-232.
- Noethig, E. M., Bracher, A., Engel, A., Metfies, K., Niehoff, B., Peeken, I., Bauerfeind, E., Cherkasheva, A., Gaebeler-Schwarz, S., Hardge, K., Kiliyas, E., Kraft, A., Kidane, Y. M., Lalande, C., Piontek, J., Thomisch, K., Wurst, M., (2015). *Plankton Ecology during summer in the Fram Strait – A compilation of long-term and short-term observations*, *Polar Res.* (accepted).
- Nomura, D., Yoshikawa-Inoue, H., Toyota, T., & Shirasawa, K. (2010). *Effects of snow, snowmelting and refreezing processes on air-sea-ice CO₂ flux*. *J. Glaciol.*, 56(196), 262-270.
- Ogura, N., & Hanya, T. (1966). *Nature of ultra-violet absorption of sea water*. *Nature* 212, 758
- Orr, J. C., Fabry, V. J., Aumont, O., Bopp, L., Doney, S. C., Feely, R. A., Gnanadesikan, A., Gruber, N., Ishida, A., Joos, F., Key, R. M., Lindsay, K., Maier-Reimer, E., Matear, R., Monfray, P., Mouchet, A., Najjar, R. G., Plattner, G.-K., Rodgers, K. B., Sabine, C. L., Sarmiento, J. L., Schlitzer, R., Slater, R., Totterdell, I. J., Weirig, M.-F., Yamanaka, Y. & Yool, A. (2005). *Anthropogenic ocean acidification over the twenty-first century and its impact on calcifying organisms*. *Nature*, 437(7059), 681-686.
- Peralta-Ferriz, C., & Woodgate, R. A. (2015). *Seasonal and interannual variability of pan-Arctic surface mixed layer properties from 1979 to 2012 from hydrographic data, and the dominance of stratification for multiyear mixed layer depth shoaling*. *Prog. Oceanogr.*, 134, 19-53.
- Perovich, D. K., Tucker, W. B., & Krishfield, R. A. (1989). *Oceanic heat flux in the Fram Strait measured by a drifting buoy*. *Geophys. Res. Lett.*, 16(9), 995-998.

- Perovich, D. K., Grenfell, T. C., Light, B., & Hobbs, P. V. (2002). *Seasonal evolution of the albedo of multiyear Arctic sea ice*. *J Geophys. Res.-Oceans* (1978–2012), 107(C10), SHE-20.
- Poltermann, M. (2001). Arctic sea ice as feeding ground for amphipods—food sources and strategies. *Polar Biology*, 24(2), 89-96.
- Polyakov, I. V., Walsh, J. E., & Kwok, R. (2012). *Recent changes of Arctic multiyear sea ice coverage and the likely causes*. *B. Am. Meteorol. Soc.*, 93(2), 145-151.
- Popova, E. E., Yool, A., Coward, A. C., Aksenov, Y. K., Alderson, S. G., De Cuevas, B. A., & Anderson, T. R. (2010). *Control of primary production in the Arctic by nutrients and light: insights from a high resolution ocean general circulation model*. *Biogeosciences*, 7(11), 3569-3591.
- Post, E., Bhatt, U. S., Bitz, C. M., Brodie, J. F., Fulton, T. L., Hebblewhite, M., Kerby, J., Kutz, S. J., Stirling, I., & Walker, D. A. (2013). *Ecological consequences of sea-ice decline*. *Science*, 341(6145), 519-524.
- Prinsenberg, S. J., & Peterson, I. K. (2011). *Observing regional-scale pack-ice decay processes with helicopter-borne sensors and moored upward-looking sonars*. *Ann. Glaciol.*, 52(57), 35-42.
- Rand, K. M., Whitehouse, A., Logerwell, E. A., Ahgeak, E., Hibpshman, R., & Parker-Stetter, S. (2013). *The diets of polar cod (*Boreogadus saida*) from August 2008 in the US Beaufort Sea*. *Polar biology*, 36(6), 907-912.
- Rey, F., Noji, T. T., & Miller, L. A. (2000). *Seasonal phytoplankton development and new production in the central Greenland Sea*. *Sarsia*, 85(4), 329-344.
- Richardson, K., Markager, S., Buch, E., Lassen, M. F., & Kristensen, A. S. (2005). *Seasonal distribution of primary production, phytoplankton biomass and size distribution in the Greenland Sea*. *Deep-Sea Res. Pt. I*, 52(6), 979-999.
- Roach, A. T., Aagaard, K., Pease, C. H., Salo, S. A., Weingartner, T., Pavlov, V., & Kulakov, M. (1995). *Direct measurements of transport and water properties through the Bering Strait*. *J. Geophys. Res.-Oceans* (1978–2012), 100(C9), 18443-18457.
- Rösel, A., & Kaleschke, L. (2012). *Exceptional melt pond occurrence in the years 2007 and 2011 on the Arctic sea ice revealed from MODIS satellite data*. *J. Geophys. Res.-Oceans* (1978–2012), 117(C5).
- Rothrock, D. A., Zhang, J., & Yu, Y. (2003). *The arctic ice thickness anomaly of the 1990s: A consistent view from observations and models*. *J. Geophys. Res.-Oceans* (1978–2012), 108(C3).
- Røed, L. P., & O'Brien, J. J. (1983). *A coupled ice-ocean model of upwelling in the marginal ice zone*. *J. Geophys. Res.-Oceans* (1978–2012), 88(C5), 2863-2872.
- Rudels, B., Anderson, L. G., & Jones, E. P. (1996). *Formation and evolution of the surface mixed layer and halocline of the Arctic Ocean*. *J. Geophys. Res.-Oceans* (1978–2012), 101(C4), 8807-8821.
- Rudels, B., Björk, G., Nilsson, J., Winsor, P., Lake, I., & Nohr, C. (2005). *The interaction between waters from the Arctic Ocean and the Nordic Seas north of Fram Strait and along the East Greenland Current: results from the Arctic Ocean-02 Oden expedition*. *J. Mar. Syst.*, 55(1), 1-30.

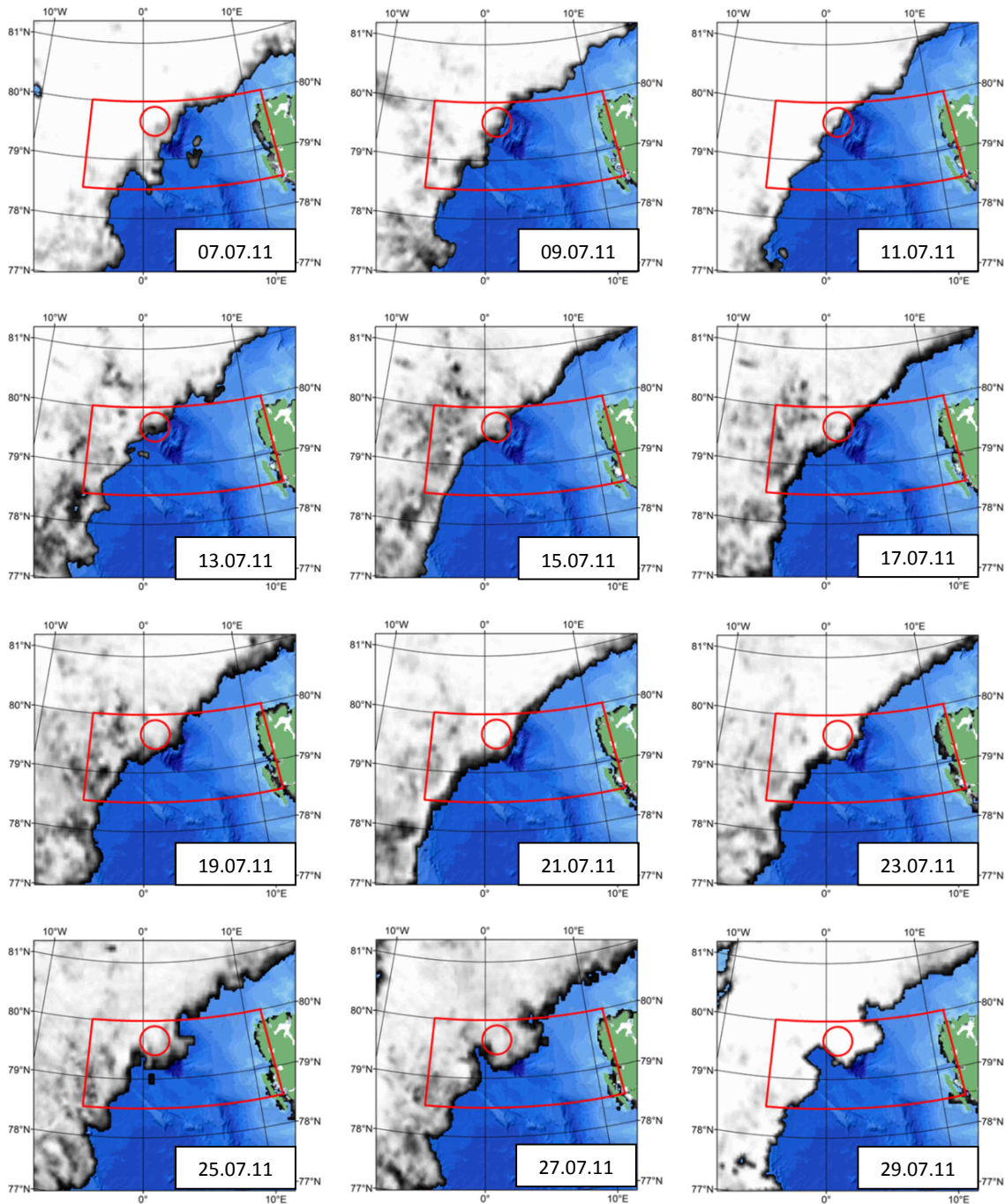
- Sakamoto, C. M., Johnson, K. S., & Coletti, L. J. (2009). *Improved algorithm for the computation of nitrate concentrations in seawater using an in situ ultraviolet spectrophotometer*. *Limnol. Oceanogr.*, 7(1), 132-143.
- Schauer, U., Fahrbach, E., Osterhus, S., & Rohardt, G. (2004). *Arctic warming through the Fram Strait: Oceanic heat transport from 3 years of measurements*. *J. Geophys. Res.-Oceans* (1978–2012), 109(C6).
- Schauer, U., Beszczynska-Möller, A., Walczowski, W., Fahrbach, E., Piechura, J., & Hansen, E. (2008). *Variation of measured heat flow through the Fram Strait between 1997 and 2006*. In *Arctic–Subarctic Ocean Fluxes* (pp. 65-85). Springer Netherlands. ISBN: 978-90-481-7721-9
- Schlichtholz, P., & Houssais, M. N. (1999). *An inverse modeling study in Fram Strait. Part I: dynamics and circulation*. *Deep-Sea Res. Pt. II*, 46(6), 1083-1135.
- Schulze, L. M., & Pickart, R. S. (2012). *Seasonal variation of upwelling in the Alaskan Beaufort Sea: Impact of sea ice cover*. *J. Geophys. Res.-Oceans* (1978–2012), 117(C6).
- Semiletov, I. P., Pipko, I. I., Repina, I., & Shakhova, N. E. (2007). *Carbonate chemistry dynamics and carbon dioxide fluxes across the atmosphere–ice–water interfaces in the Arctic Ocean: Pacific sector of the Arctic*. *J. Marine Syst.*, 66(1), 204-226.
- Shaffer, G. (1994). *Role of the Bering Strait in controlling North Atlantic*. *Nature*, 367, 354-357.
- Shigesada, N., & Okubo, A. (1981). *Analysis of the self-shading effect on algal vertical distribution in natural waters*. *J. Math. Biol.*, 12(3), 311-326.
- Sjøberg, B., & Mork, M. (1985). *Wind-induced stratified ocean response in the ice edge region: An analytical approach*. *J. Geophys. Res.-Oceans* (1978–2012), 90(C4), 7273-7285.
- Slagstad, D., & McClimans, T. A. (2005). *Modeling the ecosystem dynamics of the Barents Sea including the marginal ice zone: I. Physical and chemical oceanography*. *J. Marine Syst.*, 58(1), 1-18.
- Slagstad, D., Ellingsen, I. H., & Wassmann, P. (2011). *Evaluating primary and secondary production in an Arctic Ocean void of summer sea ice: an experimental simulation approach*. *Prog. Oceanogr.*, 90(1), 117-131.
- Smedsrud, L. H., Sirevaag, A., Kloster, K., Sorteberg, A., & Sandven, S. (2011). *Recent wind driven high sea ice area export in the Fram Strait contributes to Arctic sea ice decline*. *The Cryosphere*, 5(4), 821-829.
- Smetacek, V., & Nicol, S. (2005). *Polar ocean ecosystems in a changing world*. *Nature*, 437(7057), 362-368.
- Smith, D. C., & Morison, J. H. (1993). *A numerical study of haline convection beneath leads in sea ice*. *J. Geophys. Res.-Oceans* (1978–2012), 98(C6), 10069-10083.
- Smith, S. L., Smith, W. O., Codispoti, L. A., & Wilson, D. L. (1985). *Biological observations in the marginal ice zone of the East Greenland Sea*. *J. Mar. Res.*, 43(3), 693-717.
- Smith, W. O. (1987a). *Phytoplankton dynamics in marginal ice zones*. *Oceanogr. Mar. Biol.*, 25, 11-38.
- Smith, W. O., Baumann, M. E., Wilson, D. L., & Aletsee, L. (1987b). *Phytoplankton biomass and productivity in the marginal ice zone of the Fram Strait during summer 1984*. *J. Geophys. Res.-Oceans* (1978–2012), 92(C7), 6777-6786.

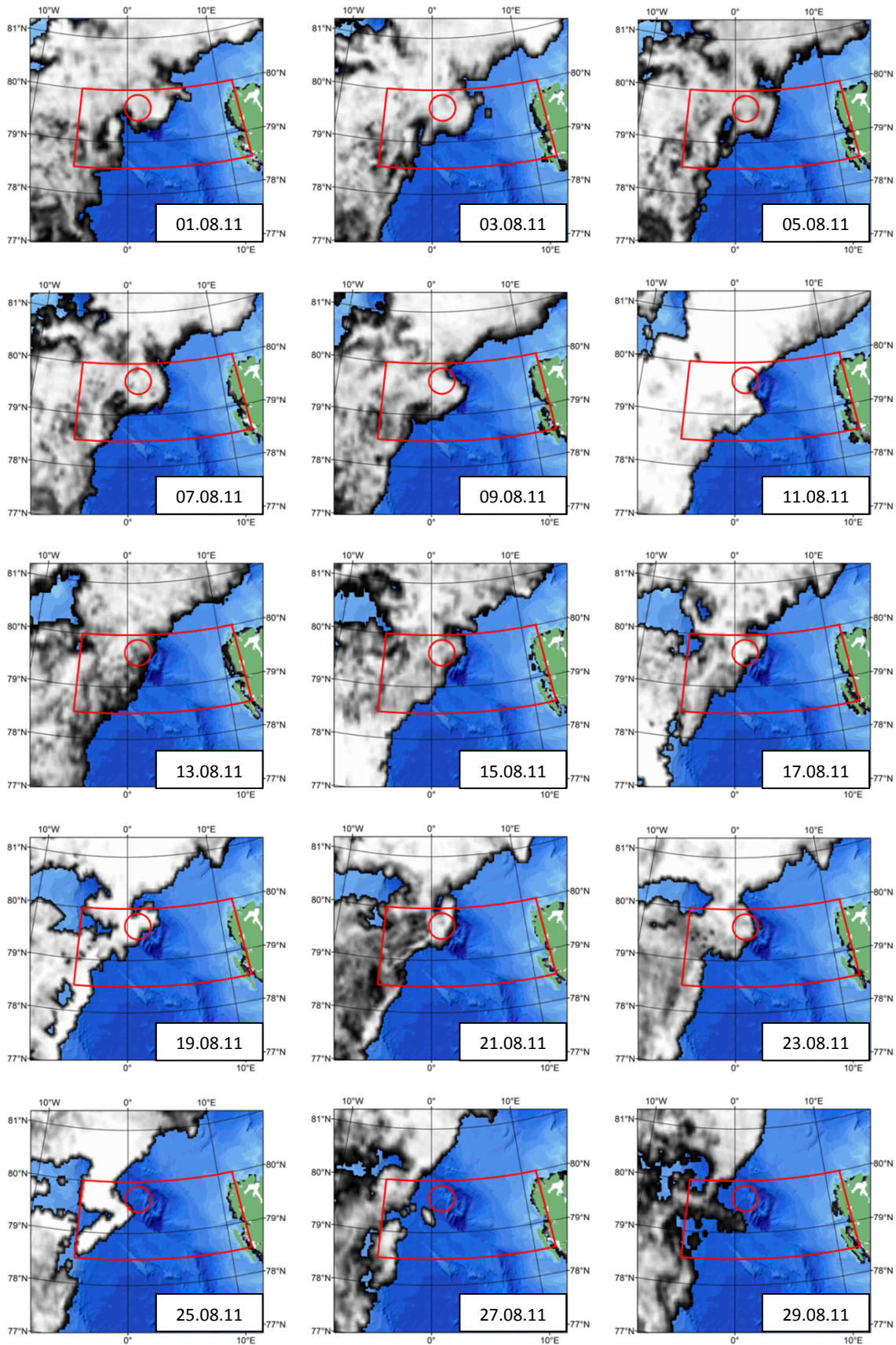
- Smith, W. O., Codispoti, L. A., Nelson, D. M., Manley, T., Buskey, E. J., Niebauer, H. J., & Cota, G. F. (1991). *Importance of Phaeocystis blooms in the high-latitude ocean carbon cycle*. *Nature*, 352, 514-516
- Soltwedel, T., Jaeckisch, N., Ritter, N., Hasemann, C., Bergmann, M., & Klages, M. (2009). *Bathymetric patterns of megafaunal assemblages from the arctic deep-sea observatory HAUSGARTEN*. *Deep-Sea Res. Pt. I*, 56(10), 1856-1872.
- Søreide, J. E., Leu, E. V. A., Berge, J., Graeve, M., & Falk-Petersen, S. T. I. G. (2010). *Timing of blooms, algal food quality and Calanus glacialis reproduction and growth in a changing Arctic*. *Glob. Change Biol.*, 16(11), 3154-3163.
- Spies, A. (1987). *Phytoplankton in the marginal ice zone of the Greenland Sea during summer, 1984*. *Polar Biol.*, 7(4), 195-205.
- Squire, V. A., & Moore, S. C. (1980). *Direct measurement of the attenuation of ocean waves by pack ice*. *Nature*, 283, 365-368
- Steele, M. (1992). *Sea ice melting and floe geometry in a simple ice-ocean model*. *J. Geophys. Res.-Oceans* (1978–2012), 97(C11), 17729-17738.
- Stirling, I. (1997). *The importance of polynyas, ice edges, and leads to marine mammals and birds*. *J. Marine Syst.*, 10(1), 9-21.
- Stroeve, J. C., Serreze, M. C., Holland, M. M., Kay, J. E., Malanik, J., & Barrett, A. P. (2012). *The Arctic's rapidly shrinking sea ice cover: a research synthesis*. *Climatic Change*, 110(3-4), 1005-1027.
- Taylor, R. L., Semeniuk, D. M., Payne, C. D., Zhou, J., Tremblay, J. É., Cullen, J. T., & Maldonado, M. T. (2013). *Colimitation by light, nitrate, and iron in the Beaufort Sea in late summer*. *J. Geophys. Res.-Oceans*, 118(7), 3260-3277.
- Thiede, J., Pfirman, S., Schenke, H. W., & Reil, W. (1990). *Bathymetry of Molloy Deep: Fram Strait between Svalbard and Greenland*. *Mar. Geophys. Res.*, 12(3), 197-214.
- Thomas, L. N. (2005). *Destruction of potential vorticity by winds*. *J. Phys. Oceanogr.*, 35(12), 2457-2466
- Thomas, L. N. & Lee, C. M., (2005). *Intensification of ocean fronts by down-front winds*. *J. Phys. Oceanogr.*, 35(6), 1086-1102
- Tovar-Sánchez, A., Duarte, C. M., Alonso, J. C., Lacorte, S., Tauler, R., & Galbán-Malagón, C. (2010). *Impacts of metals and nutrients released from melting multiyear Arctic sea ice*. *J. Geophys. Res.-Oceans* (1978–2012), 115(C7).
- Tremblay, J. É., & Gagnon, J. (2009). *The effects of irradiance and nutrient supply on the productivity of Arctic waters: a perspective on climate change*. In: *Influence of climate change on the changing Arctic and sub-Arctic conditions* (pp. 73-93). Springer Netherlands. ISBN: 978-1-4020-9459-0
- Tremblay, J. É., Anderson, L. G., Matrai, P., Coupel, P., Bélanger, S., Michel, C., & Reigstad, M. (2015). *Global and regional drivers of nutrient supply, primary production and CO₂ drawdown in the changing Arctic Ocean*. *Prog. Oceanogr.* (in press)
- Untersteiner, N. (1988). *On the ice and heat balance in Fram Strait*. *J. Geophys. Res.-Oceans* (1978–2012), 93(C1), 527-531.
- Van Angelen, J. H., Van den Broeke, M. R., & Kwok, R. (2011). *The Greenland Sea Jet: A mechanism for wind-driven sea ice export through Fram Strait*. *Geophys. Res. Lett.*, 38(12).
- Vinje, T. E. (1977). *Some observations from Nimbus-6 data collecting platforms in polar seas*. In *Joint IAGA/IAMAP Assembly*.

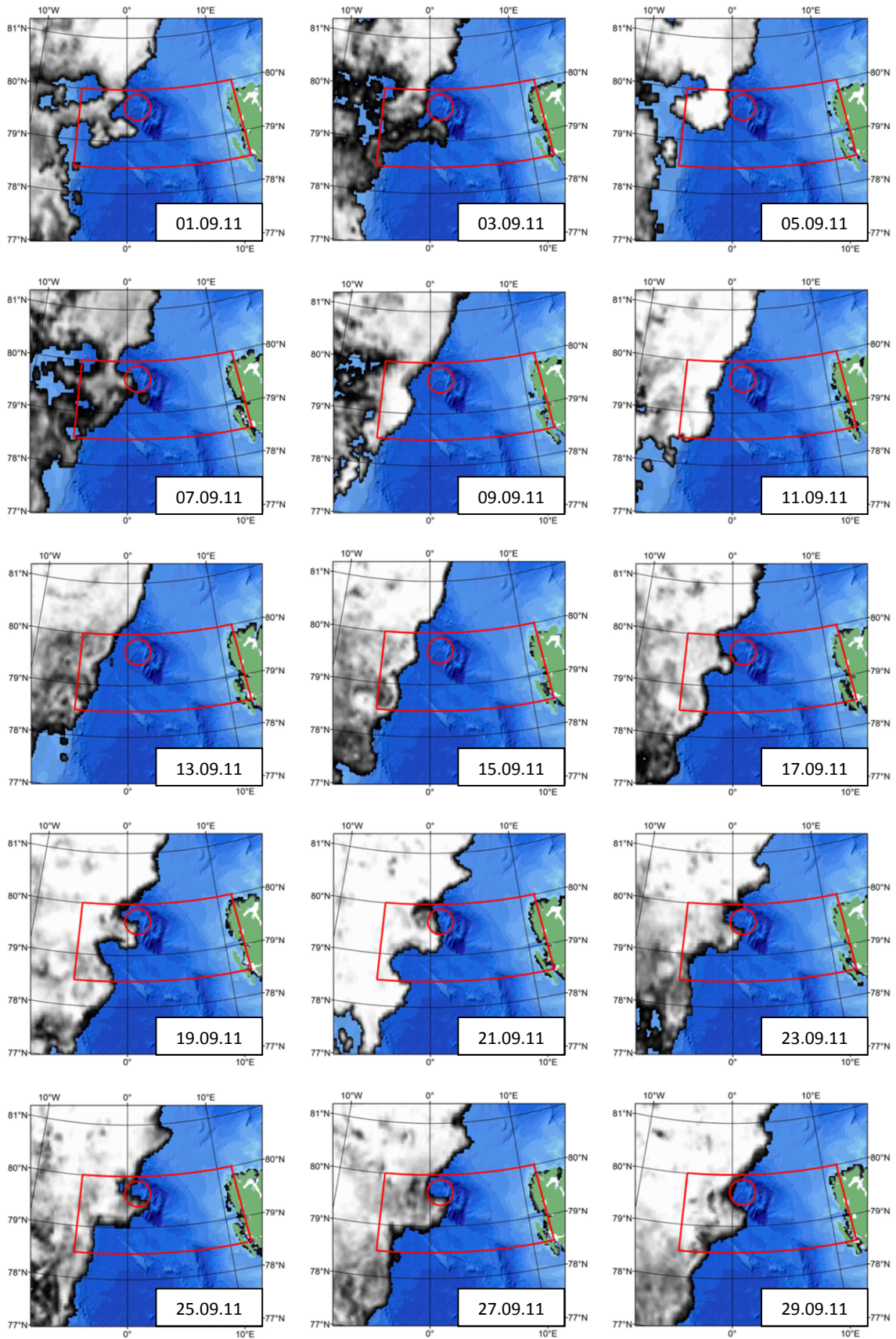
- Volk, T., & Hoffert, M. I. (1985). *Ocean carbon pumps: Analysis of relative strengths and efficiencies in ocean-driven atmospheric CO₂ changes*. In: *The Carbon Cycle and Atmospheric CO₂: Natural Variations Archean to Present* (pp. 99-110). American Geophysical Union, 1985
ISBN: 0-87590-060-7
- von Appen, W. J., Schauer, U., Somavilla, R., Bauerfeind, E., & Beszczynska-Möller, A. (2015). *Exchange of warming deep waters across Fram Strait*. *Deep-Sea Res. Pt. I*, 103, 86-100.
- Wadhams, P. (1983). *Sea ice thickness distribution in Fram Strait*. *Nature* 305, 108-111.
- Wadhams, P., & Squire, V. A. (1983). *An ice-water vortex at the edge of the East Greenland Current*. *J. Geophys. Res.-Oceans* (1978–2012), 88(C5), 2770-2780.
- Wadhams, P., Wilkinson, J. P., & Kaletzký, A. (2004). *Sidescan sonar imagery of the winter marginal ice zone obtained from an AUV*. *J. Atmos. Ocean Tech.*, 21(9), 1462-1470.
- Wadhams, P., Squire, V. A., Goodman, D. J., Cowan, A. M., & Moore, S. C. (1988). *The attenuation rates of ocean waves in the marginal ice zone*. *J. Geophys. Res.-Oceans* (1978–2012), 93(C6), 6799-6818.
- Wadhams, P., Wilkinson, J. P., & McPhail, S. D. (2006). *A new view of the underside of Arctic sea ice*. *Geophys. Res. Lett.*, 33(4).
- Wassmann, P., Reigstad, M., Haug, T., Rudels, B., Carroll, M. L., Hop, H., Gabrielsend, G. W., Falk-Petersen, S., Denisenko, S. G., Arashkevich, E., Slagstad, D. & Pavlova, O. (2006). *Food webs and carbon flux in the Barents Sea*. *Prog. Oceanogr.*, 71(2), 232-287.
- Wassmann, P., Duarte, C. M., Agusti, S., & Sejr, M. K. (2011). *Footprints of climate change in the Arctic marine ecosystem*. *Glob. Change Biol.*, 17(2), 1235-1249.
- Werner, I., & Auel, H. (2005). *Seasonal variability in abundance, respiration and lipid composition of Arctic under-ice amphipods*. *Mar. Ecol.-Prog. Ser.*, 292, 251-262.
- Williams, T. D., Bennetts, L. G., Squire, V. A., Dumont, D., & Bertino, L. (2013). *Wave-ice interactions in the marginal ice zone. Part 1: Theoretical foundations*. *Ocean Modelling*, 71, 81-91.
- Wulff, T., Lehmenhecker, S., & Hoge, U. (2010). *Development and operation of an AUV-based water sample collector*. *Sea Technology*, 51(12), 15-19.
- Zielinski, O., Fiedler, B., Heuermann, R., Kortzinger, A., Kopiske, E., Meinecke, G., & Munderloh, K. (2007, June). *A new nitrate continuous observation sensor for autonomous sub-surface applications: Technical design and first results*. In *OCEANS 2007-Europe* (pp. 1-4). IEEE.

Appendix

Following images show the constant presence of ice tongues in the HAUSGARTEN area within the months July (starting at July 7th), August and September of 2011.







Versicherung an Eides statt

Ich, Thorben Wulff, wohnhaft Obere Bürger 20, 27568 Bremerhaven, Mat.-Nr.: 2451908,

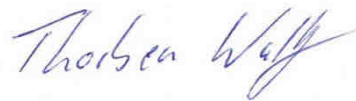
versichere an Eides Statt durch meine Unterschrift, dass ich die vorstehende Arbeit selbständig und ohne fremde Hilfe angefertigt und alle Stellen, die ich wörtlich dem Sinne nach aus Veröffentlichungen entnommen habe, als solche kenntlich gemacht habe, mich auch keiner anderen als der angegebenen Literatur oder sonstiger Hilfsmittel bedient habe und die zu Prüfungszwecken beigelegte elektronische Version der Dissertation mit der abgegebenen gedruckten Version identisch ist.

Ich versichere an Eides Statt, dass ich die vorgenannten Angaben nach bestem Wissen und Gewissen gemacht habe und dass die Angaben der Wahrheit entsprechen und ich nichts verschwiegen habe.

Die Strafbarkeit einer falschen eidesstattlichen Versicherung ist mir bekannt, namentlich die Strafandrohung gemäß § 156 StGB bis zu drei Jahren Freiheitsstrafe oder Geldstrafe bei vorsätzlicher Begehung der Tat bzw. gemäß § 161 Abs. 1 StGB bis zu einem Jahr Freiheitsstrafe oder Geldstrafe bei fahrlässiger Begehung.

Bremerhaven, 24.10.16

Ort, Datum



Thorben Wulff